THREE-DIMENSIONAL FINITE ELEMENT MODEL FOR STRUCTURAL CONCRETE SUBJECTED TO IMPACT LOADINGS

By

Abdellah Thabet *BSc, MSc*

Submitted for the Degree of

Doctor of Philosophy

at Heriot-Watt University

Department of Civil and Offshore Engineering

January 1994.

To my family

Contents

List of Tables

List of Figures

Acknowledgements

This thesis describes the work carried out by the author in the Department of Civil and Offshore Engineering at Heriot-Watt University under the supervision of David Haldane. I am greatly indebted to David Haldane for suggesting the subject of my research, and for his continued guidance, stimulation and invaluable advice throughout the duration of the research period. I am also particularly grateful to him for his patient reviews of the thesis, which undoubtedly improved its quality and readability.

Thanks are due to the United Kingdom Atomic Energy Authority (UKAEA), particularly John Broadhouse and Allan Neilson for making available the elastic concrete code. Thanks are also extended to Allan Neilson for allowing me to use the software package TAURCON for the data post-processing.

Finally, I express my gratitude to all members of staff in the Department of Civil and Offshore Engineering, particularly Professor A.D Edwards for invaluable discussions and advice during the formulation of the concrete model.

Abstract

This thesis describes the development of a non-linear finite element concrete model for the analysis of reinforced concrete members under the action of impact loadings. The model uses a triaxial stress formulation which is based on a four parameter failure criterion combined with the incremental form of the theory of plasticity. The behaviour of the concrete under compressive stresses is simulated using an elastic-plastic mixed strain hardening model which is accompanied by a crushing failure. The influence of the loading rate on the concrete is introduced by modifying the level of the yield and loading surfaces. In tension a smeared crack model has been used together with a tension softening model for the retained post-cracking stresses and an aggregate interlock model is used for the reduction in the shear stresses. Failure of the concrete is either by cracking or crushing depending on the value of a crushing coefficient, the value of which is a function of the three stress invariants. The reinforcing bars are represented by tensile stiffeners which are smeared in the appropriate directions over the element cross section. Perfect bonding is assumed between the concrete and the reinforcement representation. The reinforced concrete model formulation is coded and integrated into the finite element source code DYNA3D. The model has been used to analyse the behaviour of plain concrete specimens, reinforced concrete beams and a portal frame under the action of impact loadings. The accuracy of the analytical results was assessed by comparing them with the published results from laboratory test programmes.

Chapter 1

INTRODUCTION

1.1 BACKGROUND

Impact events occur in a wide variety of circumstances, they can be part of a planned process ranging from the striking of a nail with a hammer to the use of equipment in the construction industry to drive piles. Impact events may also be unplanned such as accidental collisions involving aircraft, buses, cars, trains, dropped objects, etc. There is an increasing acceptance that some structures must be designed to resist impact loadings as well as static loadings because of the concern of the general public with respect to safety.

Clearly impact is a large field of study, which can involve simple objects e.g. a nail, to complex structural systems such as those used in the protection of nuclear power plants. The materials involved include concrete, metals, ceramics, polymer

composites, etc.

An impact event can be defined as the collision of two or more solid objects. During the collision, the contact between the bodies is localised and of short duration. The pressure acting on the contact surfaces of the bodies is high and quickly propagates as stress waves through all the bodies involved. It can also result in the displacement of a large quantity of material around the impact region.

In the present investigation particular attention is focused on the effects impact loadings have on structural concrete members. This essentially consists of an event in which a mass (impactor) is allowed to fall onto structural concrete members. These occurrences can be found, for example, during landing of airplanes on a concrete runway, driving of concrete piles, in the progressive collapse of concrete structures and the effect of dropped objects on concrete structures.

The contact pressure transmitted to the concrete by the impactor is dependent on the mass, rigidity and shape of the impactor, the contact velocity, and the mass and form of the concrete structure. A full description of an impact event, taking all these factors into account, is one of considerable complexity.

The prediction of the behaviour of a concrete structure when it is subjected to

impact loading is also of considerable complexity. During an impact event concrete structures have been observed to react both locally and globally. The local response of the structure to impact loading may result in one of a number of failure mechanisms such as surface crushing, concrete plug and scabbing as shown in Figure 1.1. The time scale during which these mechanisms develop is of the same order of magnitude as the time taken for a stress wave to propagate through the thickness of the member. Thus this type of failure normally occurs within microseconds of the initiation of the impact. The global deformation normally results in a flexural failure which occurs relatively late during the impact event.

The methods of analysis which are commonly used in the design of concrete members subjected to impact loadings evaluate the local and global responses of the member separately. The local response is determined using empirical formula derived from the results of laboratory and prototype tests whereas the global deformation is calculated using vibration models. These simplified analytical approaches are not considered to be sufficiently accurate for the evaluation of the safety of concrete members subjected to impact loadings. This is because the concrete members behave in a continuous manner and the global response of the member is very much influenced by its local response to impact loading.

The methods normally used to determine the response of a member subjected to impact loading may be broadly classified as follows:

(1) laboratory or field testing leading to empirical formula;

(2) simplified analytical solutions such the vibration method and the spring-mass system;

(3) advanced numerical approaches such as the finite element method.

1.2 ASSESSMENT PROCESSES

1.2.1 Laboratory or Field Studies

A method of assessment based on either laboratory or field studies, in which the actual response of the member is measured, is considered to be fundamental to the understanding of the behaviour of a structural concrete member under the action of impact loadings. In the case of impact loading assessment the concrete members are subjected to a rate of loading which is higher than the normal static loading rate i.e. a stress increase rate which is higher than 1 N/mm^2sec, which corresponds to a strain rate of approximately 30×10^{-6} $1/sec$ [1].

This approach is mainly adopted in investigations into the magnitude of global variables such as the variation in the load carrying capacity with respect to deflection, the reactions at the supports, the development of the crack patterns and the resulting modes of failure of the member.

The success of such investigations is dependent on observations and on the accurate measurement of the parameters being examined which in turn requires the use of sophisticated equipment which is both highly responsive and accurate in the sampling and storage of the data from the test. It is also dependent on the methods which are used in the interpretation of the measurements which have to take into account the inevitable scatter in these measurements.

The laboratory based investigations are normally performed on a single member i.e. a beam, a column or a plate from a concrete structure. Laboratory based investigations into the behaviour of structural concrete members such as pressure vessels, offshore structures and dams are occasionally undertaken. They are difficult to perform because of the facilities and the sophistication and extent of the equipment required. Such tests are normally very expensive to undertake.

Empirical formula are derived from the test results which are then used to predict the damage inflicted on the structural members including perforation, penetration, scabbing, cracking and spalling. A detailed review of these empirical formula can be found elsewhere [1, 2].

1.2.2 Analytically Based Approaches

The second approach involves the adoption of simplified analytical relationships for the design of structural concrete members subjected to dynamic loading. The

theoretical assumptions on which the analytical relationships are based mean that they can only be used as an initial approximation for the prediction of the contact load and the resulting impact behaviour of the structural member.

Analytical approaches used in the design of concrete members to resist impact are of three types:

(1) The first analytical approach, the most used by engineers, is mainly based on the results obtained from a static solution. In the case of the design of a concrete member subjected to dynamic loadings, the loads are replaced by approximate equivalent static loads. Impact factors are normally introduced to take into account the rate (speed) at which the load is applied. An impact factor can be defined as the ratio of the dynamic deflection to the static deflection [3]. Once the equivalent static load (commonly referred to as the dynamic load) has been determined the approach involves the use of static equations of equilibrium to calculate, for example, the deflections along the length of a beam.

(2) The second type of analytical approach has been based on assumptions relating to the masses and deformations of the objects involved. This approach is commonly referred to as "*the beam impact problem*" [4, 5]. This approach can be sub-divided as follows.

(a) The mass of the target is considered to be massive compared to the mass of the impactor. The movement of the target can then be assumed to be limited to the local deformations in the impact zone.

(b) The displacement of the target is taken into account. The target is modelled as a concentrated mass, which reduces the problem to that of an impact between two masses.

(c) The target is assumed to vibrate under the action of the impact load.

(3) The third type of analytical approach, which may be regarded as being more representative of the impact phenomenon, uses mechanical models of spring-mass systems [1, 6] to simulate an impact event between a structural member and an impactor. The structural member and the impactor are modeled as two colliding masses. A spring is used between the two masses to model the reaction forces of the deformed bodies after contact. This approach can be used to predict the contact force and describe the resulting impact behaviour such as the concrete plug which develops during an impact event [6].

1.2.3 Finite Element Approach

The analytical approaches described in the previous Section, particularly the approach in which either the vibrations of the target or spring-mass system is considered thus requiring the use of complex mathematical formulations to solve the problem, are considered to be approximate and therefore incomplete. This is because the members are modelled using the assumptions that they behave as a single degree of freedom system and that the influence of the local response of the member on its global response is insignificant.

It is believed that the local response to impact loading does have a significant influence on the overall global deformation of the member e.g. the occurrence of a shear failure under impact loading may adversely affect the integrity of the member.

In order to solve a complete impact problem without using the assumptions which separate the local and the global deformations of the member, numerical approaches such as the finite element method can be considered to be more appropriate.

In recent years many researchers have studied the strength of concrete members using numerical analysis. Several different approaches have been used but in recent times they have focused on the finite element method. The majority of

the finite element models used in the analysis of structural concrete members are based on a two-dimensional idealisation. Little work has been reported on the use of three-dimensional idealisations. The advantage of using three-dimensional finite elements is two fold. Firstly, it avoids the need to justify the simplifications involved in transforming a three dimensional body into a two or even one dimensional simulation. Additionally, there is a need for a considerable amount of time and effort to be spent in the interpretation of the output data resulting from such simplifications. In three dimensional finite element analysis the boundaries of the model follow as close as possible the actual boundaries of the member. The loads applied to the structure are also modelled as close as possible to the real case. The second reason concerns the modelling of the material. The adoption of triaxial stress conditions means that all the passive but critical effects in the assessment of the material strength can be taken into account. Normally, they are difficult to model in two or one dimensional models e.g. the dilation of concrete and the variation in the concrete strength due to the presence of transverse stresses i.e. confinement.

The numerical solution of the contact-impact problem for ductile materials such as steel has been solved and implemented into three-dimensional advanced finite element codes such as DYNA3D [7]. The analysis of a concrete structure subjected to impact loadings is generally complex due to the many non-linearities involved. The degree of complexity leads to the question of the significance of

the different factors which contribute to the non-linear behaviour of reinforced concrete such as:

(1) The non-linear load-deformation response and the difficulties involved in forming suitable constitutive relationships in the case of multiaxial stress conditions.

(2) The occurrence of tensile cracking at relatively low load levels followed by a progressive loss of strength over the cross section of the concrete member under increasing load.

(3) The difficulties in formulating failure criteria for a range of stress conditions.

(4) Treatment of the reinforcement and the interaction between the concrete and the reinforcement which form the composite system.

(5) The formulation of the sensitivity relationship for concrete with respect to the rate of loading.

In order to obtain a meaningful set of results from the finite element approach all the difficulties highlighted above must be addressed as well as several other important parameters which govern the behaviour of reinforced concrete under such conditions.

1.3 OBJECTIVES

The need for a three-dimensional finite element code capable of simulating the behaviour of a range of concrete members subjected to impact loadings is widely acknowledged. It would provide a valuable tool for the determination of the behaviour of complex structural concrete systems, particularly in the context of safety evaluations.

The principal objective of this programme of research was the development of such a three-dimensional finite element code. In order to achieve this objective a new material model to be used in the analysis of concrete members was developed in which the material non-linearity is solved using the theory of plasticity. The integration of the model into a widely accepted finite element code and the subsequent validation of the model using the results from a number of published investigations into the behaviour of structural concrete members subjected to impact loading has been addressed.

In order to satisfy the principal objective detailed above the investigation was undertaken as follows:

(1) a critical review of the work published on the linear and non-linear behaviour of concrete;

(2) the adoption of a three-dimensional stress solution to formulate the concrete

material;

(3) the formulation of the material non-linear behaviour using the theory of plasticity;

(4) the integration of a three dimensional smeared cracking model into the stress formulation;

(5) the integration of shear transfer effects and tension softening into the stress formulation;

(6) the incorporation of the resulting algorithm into the three-dimensional finite element code DYNA3D;

(7) the analysis of a number of plain and reinforced concrete members in order to assess the accuracy of the model which has been developed.

This research work can be considered to be a step forward towards a complete solution of the impact problem with respect to reinforced concrete structures. This is because the solution procedure adopted in this work simulates the impact event as close as possible to the actual one i.e. with no geometrical or material simplifications. The contribution of this work towards this complete solution is in the triaxial material formulation of the elastic-plastic fracture model. The formulation of the model simulates several features which characterize the concrete behaviour such cracking, crushing and mixed cracking and crushing. The development of three dimensional finite element algorithm using the derived formulation and its incorporation for the first time in the finite element code DYNA3D.

1.4 CONTENTS OF THE THESIS

Chapter 2:

In this Chapter, the mechanical properties of plain concrete subjected to uniaxial, biaxial and triaxial loading conditions are discussed. The Chapter addresses the subject in three Sections:

(1) the behaviour of concrete subjected to static loadings;

(2) the behaviour of concrete subjected to impact loadings;

(3) the importance of each property of concrete on the formulation of the mathematical model.

Chapter 3:

A review of the published constitutive models for concrete. The concrete models have been divided into four main types:

(1) equivalent uniaxial models;

(2) non-linear elastic and variable modulii based models;

(3) concrete models based on endochronic theory;

(4) plasticity based concrete models.

Also in this Chapter, the elastic-plastic fracture model for concrete in compression and the smeared crack model for concrete in tension, which has been used in this investigation, have been described.

Chapter 4:

This Chapter is concerned with the finite element modelling of concrete structures and the numerical procedures used in the implementation of the elastic plastic formulation.

(1) The underlying concepts of the finite element method and the derivation of the governing equations of equilibrium using the principle of virtual displacements are presented in this Chapter. The eight node isoparametric brick element which has been used to model concrete has been discussed. The smeared representation for the reinforcing bars is also described.

(2) The explicit central difference method which is used to solve the equations of equilibrium is described.

(3) The underlying concept used in the calculation of the contact force during an impact between two bodies is discussed briefly.

Chapter 5:

In this Chapter the listing of the code and detailed flow charts of the algorithms used in the development of the three-dimensional elastic-plastic concrete model are given. The integration of the concrete model in a general purpose finite element analysis code DYNA3D is also discussed. The input data required for the newly developed concrete model is also discussed in detail.

Chapter 6:

In order to examine the accuracy of the concrete model which has been developed for the analysis of the behaviour of plain concrete, two plain concrete test specimens subjected to static and impact loadings have been solved. The finite element solutions have been compared with the published results obtained from the laboratory tests.

In this Chapter the analysis is further extended in order to assess the sensitivity of the concrete model to a number of material parameters.

Chapter 7:

This Chapter addresses the analysis of reinforced structural members subjected to impact loadings. Two types of reinforced concrete member i.e. eighth scale and full size reinforced concrete members, were analysed using the model developed for reinforced concrete in this investigation. The finite element solutions are compared with the published results obtained from the laboratory tests.

Chapter 8:

Finally, Chapter 8 summarises the conclusions drawn from this investigation and is followed by detailed recommendations for future research.

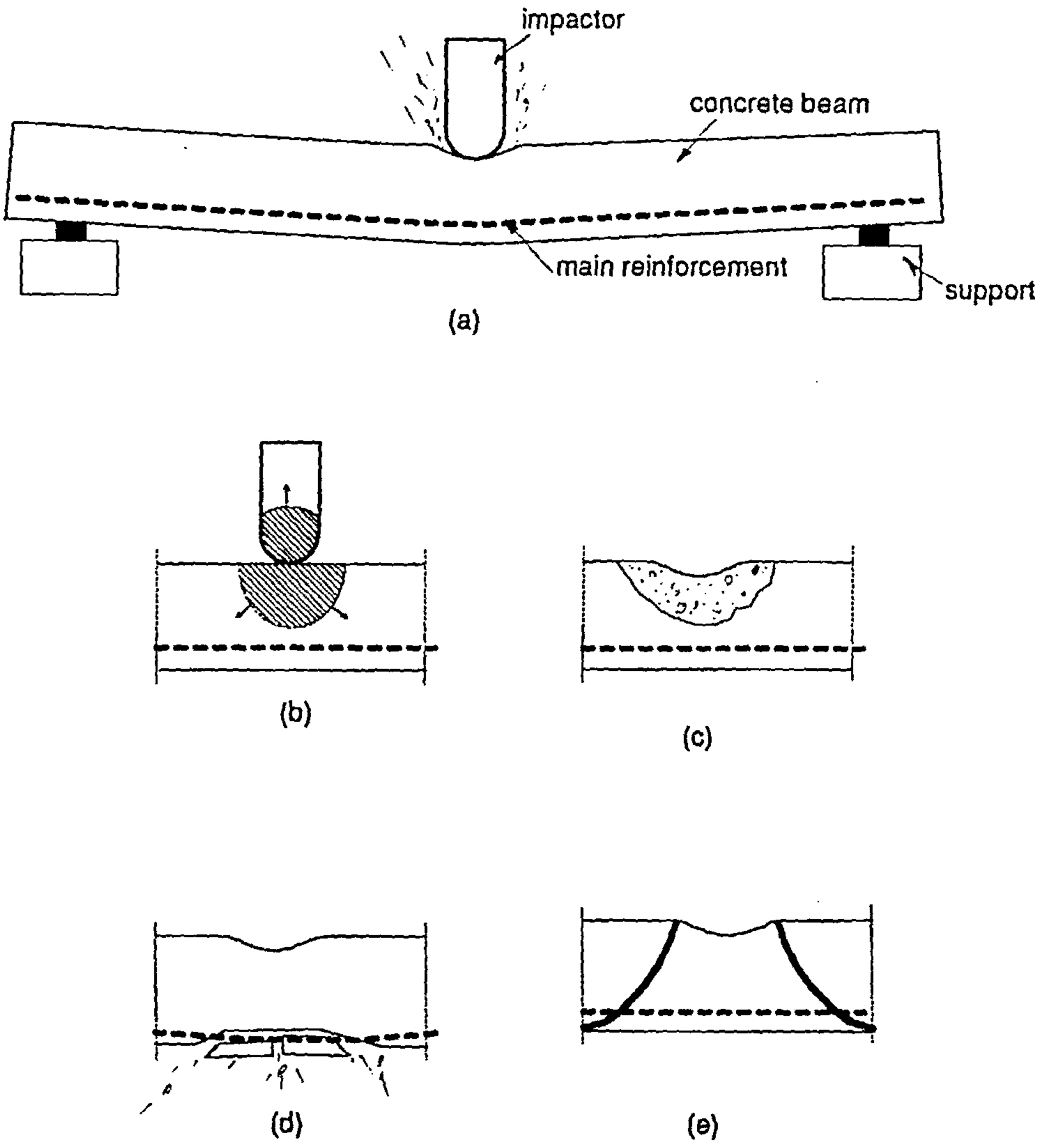

Figure 1.1: Contact-impact problem involving a concrete beam

(a) global response

(b) impact generated stress waves

(c) local crushing and spalling in the contact zone

(d) local effect of scabbing

(e) formation of the concrete plug

Chapter 2

MECHANICAL BEHAVIOUR OF CONCRETE

2.1 INTRODUCTION

Despite the widespread use of concrete as a construction material, knowledge of its precise physical properties and behaviour under various stress conditions is still under investigation. The difficulties in understanding the behaviour of concrete at the material level is due mainly to its complex heterogeneous structure. In order to be able to explain the behaviour of concrete under load even in the case of standard test specimens used for quality control purposes e.g. cubes, cylinders, etc, a knowledge of its internal structure at the microscopic level is essential and is also required as input in the constitutive modelling of concrete at the macroscopic level.

Concrete is a composite material consisting of different types and sizes of aggregate particles embedded in a mortar paste matrix. The structure of concrete is therefore heterogeneous. At the microscopic level, there are micro-cracks at the interfaces between the aggregates and the mortar. Voids with or without water which form due to bleeding and shrinkage effects can also be observed close to the coarse aggregate particles. Incorrect casting can lead to segregation with the heavier aggregate particles tending to sink in the shutter. Thus, segregation also introduces heterogeneity into the structure of the concrete.

Coarse aggregate particles normally consist of natural gravels or crushed particles of rock, typically ranging in size from 2 mm up to 40 mm. The volume fraction of the coarse aggregates in concrete mixes is generally of the order of 0.3-0.6. The aggregates are bonded together primarily by the mortar matrix.

A mortar is composed of fine aggregates, less than 2 mm, and cement paste. The cement paste bonds the fine aggregate particles together. In a normal mortar the volume fraction of fine aggregates is approximately 0.5.

The cement paste can be considered to be made up of unhydrated cement particles embedded in a hydrated cement paste matrix. The hydrated cement paste is highly porous with a porosity of approximately 30 percent. The hydrated cement

paste is considered to be a rigid matrix which binds the unhydrated cement, the fine and coarse aggregates together.

The pores in the hydrated cement paste are formed in the early stages of the production of concrete and are almost filled with water. The air content of the cement paste will increase with time due to evaporation of the mix water and the formation of newly hydrated cement paste. Despite the high porosity of the cement paste, the permeability coefficient with respect to water is considerably less than the corresponding values for several types of rock.

The hydration of cement will take place continuously over a long period of time so long as water is present in the concrete. Micro-cracks, which develop during this period of time can close either partly or completely. It is also widely recognised that the strength of concrete continues to increase over a period of years, although the paste has stiffened into its final structural form, four to six hours after the addition of the water to the mix.

The mixing process has a significant influence on the physical behaviour of the hardened concrete. The process of hydration and curing of the cement paste results in the development of incompatible strains in the matrix resulting in the formation of micro-cracks before any load has been applied [8] as shown in Figure 2.1. As will be discussed later this phenomenon has been found to be

very significant in the evaluation of the mechanical behaviour of concrete. The existence of micro-cracks will be regarded as an inherent property of the concrete.

2.2 RESPONSE TO STATIC LOADINGS

2.2.1 Introduction

The three most significant characteristics which are present in concrete are:

(1) a large number of bond micro-cracks which exist at the interfaces between the aggregates (generally found near the larger aggregate particles) and the mortar;

(2) the high porosity of the cement paste, approximately 30 percent, (these pores are filled with water and/or air);

(3) the presence of air and/or water voids at all dimensional levels above the molecular level.

Each of the above characteristics has a significant influence on the mechanical behaviour of concrete when subjected to loading. At low stress levels the existence and propagation of the bond micro-cracks which are caused by an increase

in the bond/tension forces between the aggregates and the mortar is the most important factor which determines the mechanical behaviour of the concrete.

During loading the concrete as a whole deforms, the incompatibility in the strains between the aggregates and the mortar matrix becomes significant which leads to further breakdown in the internal structure of the concrete. This breakdown is the result of bridging between existing cracks even after cracks encounter crack-arrests (aggregates) as shown Figure 2.1. At the macroscopic level the process of breakdown is accompanied by both loss of stiffness and the development of permanent deformations. At the structural member level, breakdown appears in the form of cracks and possibly slip at the aggregate-cement paste interfaces.

Again many of the micro-cracks (bond cracks) in concrete are caused by segregation, shrinkage, or thermal expansion in the mortar and therefore, exist even before any load has been applied. Concrete does not fail solely because of the presence of these micro-cracks. As the applied loading is increased these micro-cracks propagate and new cracks form in the mortar because of the differences in stiffness between the aggregates and the mortar (aggregates are stiffer than mortar). Experimental studies by Hsu and Slate [8] show that the measured aggregate-mortar bond strength in tension is approximately 33 to 67 percent of the tensile strength of the mortar depending on the aggregate type. Therefore, the primary reason for the low tensile strength of concrete is the low bond

strength in tension of the aggregate-mortar interface. Shah and Chandra [9] have demonstrated.that increasing the size of the aggregate reduces the bond strength in tension and increases the volume dilation.

At high stress levels in compression, the break up and collapse of voids and pores in the mortar becomes an important factor in the behaviour of concrete. In tension the voids and pores in the paste accentuate crack propagation and stress concentrations.

One of the measures of the quality of a concrete which is frequently used by engineers is the cube crushing strength. The strength of concrete in a member is variable and is dependent on the state of stress in the member. For example:

(1) under compressive confinement conditions concrete can safely carry loads that induce stresses which are considerably higher than its cube crushing strength;

(2) in the presence of tensile confinement concrete will fail even although the stress at any point is less than the cube strength.

The stress conditions highlighted above, which can be considered as extremes, and intermediary stress conditions can occur continuously during the actual loading

of concrete members:

(1) If a concrete member is prevented from expanding laterally the compressive stress which is induced by the load applied to the member may exceed the cube crushing strength. Such restraints can be generated by the confining effect of the steel reinforcement or by the surrounding concrete, for example, when a localised compressive load is applied to a large concrete block.

(2) Even larger stress levels can be achieved if transverse compressive stresses are applied to a member which is loaded in compression. Examples of this can be found in prestressed concrete structures. In the case of the presence of transverse tensile stress conditions the member is likely to fail before the compressive stresses in the member reach the cube crushing strength. Failure stresses of this magnitude can occur in slabs subjected to flexural deformation and volume expansion, for example, in-plane tensile loadings resulting from the effects of temperature.

The examples above have shown how the strength of concrete is affected by the nature of the stress conditions developed within a member, therefore, strength in this context cannot simply be limited to a constant cube crushing strength. In order to examine the variation in strength at each point in a concrete member a strength function is used. Such a strength function is commonly referred to as a

failure or strength criterion.

The derivation of a suitable failure criterion is dependent on obtaining information on the strength and deformation properties of concrete. This information is usually obtained from testing plain concrete specimens under specific loading conditions. There are two standard tests which are used to investigate the variations in strength of a concrete member:

(1) Uniaxial tests.

(2) Multiaxial tests.

A careful study of the large number of papers which have been published on the strength of concrete subjected to different stress conditions has led to the present understanding of the behaviour of concrete under the action of simple uniaxial and complex multiaxial loading conditions.

It is difficult, if not impossible, to judge (evaluate) the quality of the published results with respect to the strength of concrete under any state of stress mainly because all the information required is not given about the test arrangement and procedures. However it is recognised that the variation in the concrete strength is dependent on a number of parameters which are related to the test specimens themselves and the interfaces between the test specimens and the testing machine. The principal parameters which are influential in such tests are summarised below.

(1) Test specimen size:

The test specimen must have adequate dimensions in order to ensure that it is representative of the concrete as a whole. The minimum specimen dimensions need to be several times greater than the maximum aggregate size. On the other hand, excessive specimen length can result in failure due to instability, whereas insufficient specimen length may allow the stress perturbation at the interfaces with testing machine to affect the stress distribution in the central portion of the specimen. The orientation of the test specimen during casting and the method of curing can also significantly influence the test results.

(2) Testing machines and loading platens:

The primary requirement of the testing machine is to enable the test specimens to be loaded in such a manner that a stable failure can be obtained. In this context a stable failure is believed to be a failure which occurs without any sudden change in the load carrying capacity of the test specimen. In order to achieve a stable failure, it is necessary to control the deformation of the test specimen and also to use a stiff testing machine [10, 11].

A stable failure can also be affected by the procedure employed to load the test specimens, for example, the frictional forces at the interfaces between

the test specimen and the loading platens must be reduced in order to prevent them from having a significant influence on the results. A number of techniques have been employed to achieve this and can be broadly described as follows:

(a) Loading through solid platens.

(b) Loading through brush platens.

(c) Loading through fluid cushions.

Low frictional forces which can develop between the loaded surfaces of a test specimen and the platens of the testing machine can result in a brittle failure of the test specimen and can also lead to increased scatter in the test results. This is due to the presence of the weak regions randomly located in the concrete i.e. regions containing micro-cracks. On the other hand, if larger frictional forces are developed on the loaded surfaces of the test specimen a ductile failure can be obtained.

High frictional forces can be developed on the platen surfaces of a test specimen if loading is applied through dry rigid platens. This test arrangement results in ductile failure i.e. the strength and deformation of the test specimen are higher than those obtained when test specimen is loaded through either brush platens or fluid cushions [12].

It can be argued, therefore, that when test specimens are loaded through dry rigid platens the test results may be of questionable value.

However, it is obvious that there are cases where results have been carefully and reliably obtained. These results have been examined and subsequently used by many researchers. They have also formed the basis for several approaches to stress analysis and have been used in evaluations of the strength of concrete using mathematical models. Although, they do not exactly reflect the stress conditions present in structural concrete members they can be considered to act as a good reference for the behaviour of concrete under stress conditions similar to those developed in a concrete member.

2.2.2 Uniaxial Stress Conditions

(1) Uniaxial Compressive Test Results:

Uniaxial compressive stress-strain curves can be obtained by loading in compression, for example, standard concrete specimens such as 150 mm or 100 mm cubes or 150 mm diameter $\times$ 300 mm high [13] cylinders.

Typical stress-strain curves obtained from such uniaxial compressive tests are shown in Figures 2.2, 2.3 and 2.4. Figure 2.2(a) describes the variation in the axial strain in terms of compressive stress. Figure 2.2(b) shows the variation in the lateral strain in terms of compressive stress. Figure 2.3 describes the variation in the volumetric strain, where $\epsilon_v = \epsilon_1 + \epsilon_2 + \epsilon_3$, in terms of compressive stress.

In Figure 2.4, several uniaxial stress-strain curves are given for concretes with a range of compressive strengths f'_c .

A description of the general behaviour of concrete under uniaxial compressive stresses can be deduced from the above plots:

(1) At stress levels up to approximately 30 percent of the maximum uniaxial compressive strength f'_c the material behaves almost linear elastically as shown in Figure 2.2. At this level of deformation the cracks present in the concrete before loading remain almost unchanged. This has been linked to the balance of energy present in the concrete specimen which in this case is less than the energy required to create new cracks.

(2) At a stress level above 30 percent of the uniaxial compressive strength the concrete begins to soften. The stress-strain curve shows a gradual increase in curvature up to about 75 percent of the maximum compressive strength. In the stress range from 30 to 75 percent of f'_c, the bond cracks begin to increase in length, width and number until a level of strain is reached at which the cracks in the mortar start to initiate and extend around the aggregates. At the same time other bond cracks continue to grow slowly. The material is fractured gradually as bridging between the bond cracks develops to form continuous crack patterns. The cracks tend to lie approximately in a direction parallel to the direction of the applied load. This type of material

behaviour is considered to be non-linear. If unloading of the concrete occurs at this stage the non-linear behaviour can be easily noted from the residual deformation present in the stress-strain curve. If subsequent re-loading of the concrete takes place a characteristic hysteresis loop is formed in the stress-strain curve, as shown in Figure 2.2(c).

The specimen initially decreases in volume to reach a minimum value at a stress level of approximately 75 percent of the maximum uniaxial compressive strength. The reduction in the volume of the concrete is then reversed and subsequently a maximum volumetric expansion of the test specimen is reached as shown in Figure 2.3. This level of stress is considered to be the level at which the concrete starts to experience most of its permanent deformation i.e. degradation [14].

(3) Above 75 percent of the uniaxial compressive stress, the rate of increase in stress decreases until it reaches a peak value of f'_c where the largest cracks have reached their critical length. Additional cracks open and propagate at an increasing rate and the resistance of the test specimen to the applied loading becomes unstable where even if the load is held constant complete collapse occurs. Beyond the peak level, the load carrying capacity of the test specimen decreases and the stress-strain curve starts to descend until a crushing failure occurs at the ultimate strain value [15].

(4) The shape of the stress-strain curves for normal and high strength concretes are similar. However for high strength concrete the curve continues to behave in a linear manner up to a higher stress level than that for normal strength concrete as well as exhibiting a higher stiffness. The peak stress occurs, for all types of concrete, at a strain value close to 2000 micro-strain. The descending branch of the stress-strain curve tends to fall more sharply than the corresponding curve for the lower strength concrete as shown in Figure 2.4.

The modulus of elasticity of concrete is highly dependent on its compressive strength, f'_c, the higher the compressive strength the higher the values of the modulus of elasticity as shown in Figure 2.4. The value of E can be calculated using a number of relationships given in Codes of Practice. For example the following empirical relationship is given in BS8110:

$$E = 5.5\sqrt{f_{cu}/\gamma_m}\ kN/mm^2$$

Poisson's ratio of concrete has been observed to remain approximately constant, ranging from 0.15-0.2 [13], for stresses up to 80 percent of the uniaxial compressive strength of concrete. The magnitude of Poisson's ratio starts to increase above this level of stress. In the case where a crushing failure in the concrete is

being approached the value for Poisson's ratio is in excess of 0.5, [16]

(2)Uniaxial Tensile Test Results:

Although concrete is not normally designed to resist direct tension, a knowledge of its tensile strength is of value in estimating the load at which cracking will develop. Hughes and Chapman [17] and Peterson [10] investigated the tensile strength of concrete and were able to obtain the complete tensile stress-strain curve for concrete, including the portion of the curve beyond the point at which the peak stress is reached.

The mechanical behaviour of concrete under the action of uniaxial tensile loading has many similarities with its corresponding behaviour under uniaxial compressive loading. A typical uniaxial tensile stress-strain curve for concrete is shown in Figure 2.5. At a stress level of approximately 70 percent of the uniaxial tensile strength the material is almost linear elastic. The propagation of the micro-cracks which are distributed across the test specimen is negligible. Above this level the bond micro-cracks start to grow. The pattern of growth of these cracks is such that they follow the path which requires the least amount of energy to break the bonds between the mortar matrix and the aggregate particles, (i.e. through the weakest zone in the mortar). The increased non-linearity of the stress-strain curve starts to develop because of the reduction in the strength of the test specimen resulting from the opening of initial cracks in the material, and followed by the

complete collapse of the concrete due to the development of continuous cracks. The strength of the specimen at this stage drops to its lowest value as shown by the stress-strain curve in Figure 2.5.

The direction of crack propagation under uniaxial tensile loading is at right angles to the direction of the applied stress. The failure in tension is caused by the formation of a limited number of bridging cracks which is not the case under uniaxial compressive stress conditions where more extensive bridging of cracks have been observed because of the compressive nature of the deformation. This is the reason why the cracks which usually develop under compressive stress conditions run parallel to the direction of the applied load.

The tensile strength can be expressed in terms of the compressive strength of concrete cylinders. Hughes and Chapman [17] and Johnson [18] have conducted several investigations and found that the ratio between uniaxial tensile and compressive strengths ranges from 0.05 to 0.1. Johnson [18] also found that the type of aggregate influences the tensile strength of concrete.

It can be concluded from the above discussion that below 70 percent of the maximum tensile strength level crack propagation may be assumed to be relatively stable and the stress-strain relationships are linearly elastic.

2.2.3 Multiaxial Stress Conditions

(1) Biaxial Stress Conditions

In general there are two types of test specimens which have been used in biaxial tests. One is a hollow cylinder in which lateral loadings are applied radially and vertical loading is applied to the end faces. The resulting flow of stress is biaxial. The problem with such a test is that the tangential stresses are computed using elastic relationships. Elastic behaviour as is widely accepted is not expected to occur in concrete at or near maximum stress conditions. Other types of test specimens which have been used have been in the form of either cubes or slabs.

Concrete slabs are the most popular type of test specimens for experimental investigations into the behaviour of concrete under biaxial stress conditions. Stress-strain curves for biaxial compression-compression, compression-tension and tension-tension stress combinations have been obtained by Kupfer and Hilsdorf [19] using $200 \times 200 \times 50\ mm$ slabs. Tasuji et al [20] used $127 \times 127 \times 13\ mm$ slabs for similar loading combinations and in general confirmed the results which have been published previously [19].

A large number of papers address the behaviour of plain concrete under biaxial stress conditions. Among these Kupfer and Hilsdorf [19], Rosenthal and Gucklich [21], Nelissen [22] and Tasuji et al [20] have all investigated the influence of a

wide spectrum of loadings, including tests under biaxial tensile stress conditions, on the behaviour of concrete.

A description of the general behaviour of concrete under biaxial stress conditions can be deduced from the results obtained from the above investigations:

(1) Figure 2.6 shows a typical biaxial compression-compression relationship for concrete [19], and for comparison purposes, a uniaxial compression curve for the same concrete has been included. Kupfer and al [19] found an increase of 25 percent in compressive strength for a biaxial stress combination where $\sigma_1/\sigma_2 = 0.5$. They also found an increase of approximately 16 percent in the compressive strength for a stress combination where $\sigma_1/\sigma_2 = 1$. The compressive strength has been found to decrease under biaxial compression-tension in an almost linear manner as the applied tensile stress is increased, as shown in Figure 2.7. The strength under biaxial tension-tension is almost identical to that of the uniaxial tensile strength of concrete, as shown in Figure 2.8. This is in contrast to the findings of Tasuji et al [20] where a definite increase in the biaxial tensile strength of concrete compared with its uniaxial tensile strength was found. However, Rosenthal and Glucklich [21] found that the magnitude of the tensile strength of concrete under biaxial tensile stress conditions was less than the magnitude obtained under uniaxial stress conditions.

(2) The relative deformation of concrete under biaxial stresses is dependent on whether the stress combination is of either a compressive or a tensile type. For uniaxial and biaxial compression stresses the average maximum compressive strain is approximately 3000 micro-strain and the average maximum tensile strain induced varies from approximately 2000 to 3500 micro-strain. The deformation is greater under biaxial compression-compression than in the case of uniaxial compression stress conditions as shown in Figure 2.6.

In biaxial compression-tension, the magnitude of the relative deformation at failure decreases as the tensile stress increases as shown in Figure 2.7.

In uniaxial and biaxial tension, the average value of the relative deformation at failure ranges between 25 and 80 micro-strain as shown in Figure 2.8.

(3) For biaxial compression the volumetric strains $\Delta V/V = \epsilon_1 + \epsilon_2 + \epsilon_3$ for various ratios σ_1/σ_2 are shown in Figure 2.9. Up to a stress of 35 percent of the maximum strength, volumetric strain and applied stress are approximately proportional. If the stress increases beyond this value the volume reduction variation is not proportional to the applied stress and the minimum volume is reached at approximately 95 percent of the maximum strength. On continued straining, the volume variation of the specimen is reversed

(increased) and eventually reaches positive values of $\Delta V/V$. This increase in volume is due to the progressive growth of the major micro-cracks in the concrete.

(4) Failure in the concrete occurs as a result of tensile splitting along a fracture surface at right angles to the direction of the maximum tensile stress.

These results can be illustrated in the form of a failure envelope for biaxial stress as shown in Figure 2.10 where the linear elastic and the non-linear behaviour together with the failure envelopes are shown.

(2) Triaxial Stress Conditions:

In investigations into the behaviour of concrete under triaxial loading conditions cubes and cylinders have been mainly used by researchers. Cylindrical shaped specimens are used when constant principal stresses are applied to the lateral surface of the test specimen in addition to an axial stress which is varied independently. The advantages of using a cylinder is that axial and lateral deformations can be measured using strain gauges bonded to the lateral surface of the test specimens. Additionally the disturbance introduced in the central part of the test specimen by the friction present at the end faces is negligible for cylinders with height to diameter ratios equal to or greater than 2.0.

The limitations present when cylindrical specimens are used is that the transverse principal stresses must always be equal. In order to vary the three principal stresses independently a cube must be used. Furthermore the testing machine must be equipped with three pairs of loading platens and be capable of applying axial loads along the three orthogonal directions independently. The tests are usually carried out using pressure cells. Therefore only a triaxial compression or a triaxial tension test can be performed. True triaxial tests have been carried out by Krishnaswamy [23], Mills and Zimmerman [24], Launay and Gachon [25] and Van Mier and Vonk [26] using cubes in which all the principal stresses were varied independently.

Experimental test data relating to the triaxial stress-strain behaviour of plain concrete containing several levels of confinement [27] have been reported. Typical stress-strain curves including those for high levels of confining stresses are shown in Figure 2.11. These curves show that the strength of concrete under triaxial compression increases significantly when transverse stresses are present. The higher the stresses resisted by the concrete the higher is the deformation experienced (up to 5.0 percent of the axial relative deformation). This is because under higher triaxial compressive stresses, the possibility of breakdown in bonds within the material is reduced and the failure is due to the crushing of the cement paste. The majority of the deformation of the test specimen under triaxial compression is due to an inelastic reduction in the volume or compaction of the

concrete under stress. The curve in Figure 2.12 shows the inelastic reduction of the concrete as a function of the volumetric stresses.

In the case of transverse tensile stresses the strength of concrete is reduced considerably depending on the magnitude of these stresses. It has been shown by Newman and Vile [28] and by Taylor [29] that a small tensile stress combined with a compressive stress can drastically reduce the strength of concrete to a value below the biaxial compressive strength.

Recently, Kotsovos [30] investigated the stress-strain behaviour of concrete in the presence of transverse stresses. The variation in the peak axial compressive stress sustained by concrete specimens with respect to confining stresses is shown in Figure 2.13. It is interesting to note in Figure 2.13 that a small confining pressure of about 10 percent of the uniaxial compressive strength is sufficient to increase the loading capacity of the test specimen by as much as 50 percent. While a small lateral tensile stress of the order of 5 percent of the uniaxial compressive strength is sufficient to reduce the concrete strength by 50 percent. This implies that the presence of small transverse stresses within a structural concrete member in the path of the applied stresses will have a significant effect on the carrying capacity of the member.

The heterogeneous nature of concrete means that the distribution of the internal

stresses can never be uniform even under uniform boundary conditions. For example, a cylindrical shaped specimen develops triaxial stress conditions even if it is subjected to uniform uniaxial loading conditions since there will always be a build-up of internal transverse stresses. The internal transverse stresses develop as a result of the reactions to the deformations which take place within the concrete involving the aggregates, voids and micro-cracks.

One of the requirements of the transverse stresses is to resist, for example, the volume dilation of the concrete and this is analogous to the application of a confining pressure. The effect of resisting the volume dilation results in an increase in the strength of the dilated region if the secondary stresses are compressive. If the secondary stresses are tensile stresses the dilation will increase and the strength of the surrounding region will be reduced.

On this basis a concrete failure is unlikely to occur in regions where compressive stresses are highest. Instead, failure will occur in the adjacent regions, where the compressive stress may be significantly smaller, but where the lateral tensile stresses are present. This implies that concrete fails in tension, never in compression.

It was shown earlier that an infinite number of stress combinations can occur in a concrete member during loading with the extremes ranging from pure triaxial

compression-compression-compression to pure triaxial tension-tension-tension in which the principal stresses are equal. These two extremes and intermediary cases can be built into a single envelope. Results obtained from laboratory tests for concrete subjected to multiaxial stress conditions have indicated that at failure concrete has an almost regular envelope (surface) which can be a function of the principal stresses if the concrete is assumed to be an isotropic material, Gerstle et al [12].

This is only an approximation because during loading, it is known that micro-cracks will grow which results in the material becoming anisotropic. The concrete failure envelope is shown in Figure 2.14. In the case of increasing volumetric compressive stresses, along the axis in which $\sigma_1 = \sigma_2 = \sigma_3$, the deviatoric (shear) plane, which is perpendicular to this axis tends towards a geometrical limit which has a circular cross section. For smaller volumetric stresses the cross sections are non circular convex and reduce towards a triangular shape in the tensile zone. A general mathematical representation of the failure surface expressed in terms of a strength criterion is discussed in Chapter 3.

True triaxial tests conducted by Launay and Gachon [25] produced information on the limit of elasticity, the crack initiation, and failure of concrete, as shown in Figure 2.15.

2.2.4 Conclusions

An understanding of the structure and behaviour of concrete at the microscopic level is essential in the development of mathematical models. It has been concluded that concrete is heterogeneous at the structural level of the material, however, it can be assumed to be homogeneous at the dimensional level of normal structural concrete members. The variations in material strength and deformation of concrete specimens under static uniaxial and multiaxial loading conditions have been described in detail in the literature.

The results obtained from standard concrete test specimens do not exactly reflect the stress conditions present in structural concrete members. Nevertheless, in the mathematical modelling of the behaviour of concrete using the finite element method, they can be regarded as a useful reference for studying the behaviour of concrete under certain stress conditions which have a similarity with those developed in structural concrete members

2.3 RESPONSE TO IMPACT LOADINGS

2.3.1 Introduction

In the previous Section it has been shown that the strength of concrete is dependent on the growth of micro-cracks within its internal structure. The propagation of the cracks follow the weakest path in the structural concrete member. It can

be very easily deduced that cracking in concrete is time dependent and that the non-linear response is dependent on the time allowed for these cracks to form and propagate.

If a concrete specimen is subjected to a rate of loading which is higher than normal static loading rates, then it is anticipated that the concrete specimen will behave and fail in a different manner to that experienced under static loading. The formation of the cracks under higher rates of loading is more spontaneous and is dependent on the intensity of the rate of loading. The path followed by the cracks is dependent on the loading rate and their development can be influenced as follows:

(1) The propagation of the cracks will follow the shortest route through the weakest paths in the internal structure of the concrete.

(2) The propagation of the cracks breaks through any crack arrestors represented mainly by the surfaces of the aggregates.

(3) The cracks propagate through the aggregate particles.

In the above scenarios, the presence of the micro-cracks is still important but

no longer plays a major part in the failure and therefore in the strength of the concrete specimen. The rate or the speed at which the loading is applied is now the most influential factor. This is because each of the mechanisms highlighted above requires a specific loading intensity to occur, for example, to fracture the aggregates it is necessary to develop a stress which exceeds the strength of the aggregates.

Two extremes, in terms of strength, can be developed in a concrete specimen depending on the rate at which the load is applied; the lowest magnitude which corresponds to the strength developed under static loading conditions and the highest magnitude which corresponds to the strength of the aggregate particles used in the concrete mix.

It is the aim of this Section to present and to review the most significant published research work in this area. It is also important to compare the different changes which take place in the mechanical properties e.g. the strength, stress-strain relationships i.e the secant modulus, between concrete specimens subjected to static and high loading rates. These issues are important in the formulation of mathematical models which are used to simulate the behaviour of the material in a numerical analysis.

2.3.2 Concrete Properties at High Strain Rates

Several reviews of the work undertaken on the influence of impact loadings on the properties of concrete have been published by Atchely and Furr [31], Mainstone [32] and Banthia and Pigeon [33]. A thorough review has been published by a CEB Task Group [1] and Bischoff and Perry [34, 35].

(1) Uniaxial Compressive Strength

It was found that the mechanical properties of concrete depend on the rate at which it is stressed. For example Green [36] used a ballistic pendulum to assess the impact behaviour of concrete using $100 \times 100 \times 100\ mm$ cubes and $100 \times 100 \times 508\ mm$ beams made from the same concrete mix. The impact strength of concrete was determined from the response of the test specimen to a number of repeated blows. This criterion was adopted because the study was initiated in relation to the failure of concrete during the driving of piles. The resistance of the test specimens to such loadings was found to increase with the rate at which the compressive loading was applied. It was also noted and that the size and shape of the aggregates had an influence on the resistance of the concrete to impact loading. No clear relationship was found between the rupture modulus of the beams and the impact strength of the test specimens. It was concluded that the modulus of rupture was not a good guide to the impact strength of concrete.

Atchely and Furr [31] conducted impact tests under compressive loading on plain

concrete cylinders (152.4 mm diameter $\times$ 308.8 mm long) using a rigid drop hammer. It was concluded that the compressive strength of concrete and the energy absorbed increased as the rate of loading was increased and there was evidence that this will reach a constant value under higher rates of loading. It was also observed that an increase in the secant modulus and ductility of the concrete with increasing rates of loading took place.

Goldsmith et al [37] used the Hopkinson pressure bar technique to propagate dynamic stress pulses through normal concrete and epoxy concrete composite test specimens. They concluded that the role of the aggregates was far more important under impact loadings than the role of the bonding material.

Hughes and Gregory [38] recognised the effect of both the stiffness of the testing machine and the size of the test specimen on the results from impact tests. Consequently they impacted large concrete cubes and prisms, (102 mm cubes and 244 $\times$ 102 $\times$ 102 mm prisms) using a large drop hammer apparatus. The test was carried out using the low friction pads developed by Hughes and Bahramian [39] to reduce the effect of platen friction. The reported average rate of straining was between 13 and 44.5 sec^{-1}. Also the strain increased almost linearly with respect to time. The average ratio of impact to static strength was found to be approximately 1.9. It was concluded that of all the individual and independent parameters involved aggregate plays the most important role in the resistance of

concrete to compressive impact loadings. There was no build up of frictional force during loading when the low friction pads were used, and therefore the typical cones of unbroken concrete were not formed, instead cracks developed parallel to the axis of the applied loading. A very small cone was reported by Green [36] to have developed at the contact face under the impact loading but it was immediately followed by a crack running parallel to the loading axis.

Later, Sparks and Menzies [40] also noted the importance of the stiffness of the aggregates on the impact resistance of concrete and concluded that a reduction in the aggregate stiffness increases the sensitivity of concrete to the rate of compressive loading.

Contrary to the findings of Atchely and Furr [31], Hughes and Watson [41] reported a decrease in the strain at maximum strength with an increase in the rate of compressive loading and that the decrease in strain at maximum strength depended on the aggregate type. They attributed this to the absence of creep effects (increase in strain under sustained loading) when high rates of loading were used. They also observed that aggregate failures were more frequent under impact loadings than under static loads which may have been due to the influence of the speed at which the cracks developed. At failure, the cracks are forced to propagate through a relatively stiffer region i.e. the aggregate particles, instead of changing direction upon reaching the surface of the aggregate particles (crack

arrest), and then running towards a region of weaker material i.e. the cement paste. They also suggested that the test results are influenced by secondary effects such as stress wave reflections.

Curbach and Eibl [42] recognized the effect of the stress wave on the results when they tested extra long plain concrete cylinders (100 *mm* diameter × 1800 *mm* long) using a rigid drop hammer. The axial strains and displacements were measured at a distance of 300 *mm* from the point of impact. They then used a stress wave theory to determine the stresses. The results from this investigation are shown in Figure 2.16. In particular, they reported an appreciable increase in ductility at the maximum strength level with respect to the rate of loading which contradicts the early observations reported by Hughes and Watson [41]. They also reported that the initial secant modulus is rate dependent and found that the initial secant modulus measured in the impact test is 1.63 times the corresponding value under static loading conditions. This result contradicts the findings of Ahmad and Shah [43] who found that the initial secant modulus remained unchanged for plain concrete under increasing rates of loading. A similar conclusion was also reached by Suaris and Shah [44] but further work in this area is considered to be necessary. However, Ahmad and Shah [43] found that for both plain and confined concrete there was an increase in the tangent modulus of elasticity and in the strength.

Perry and Bischoff [45] have tested concrete cylinders (101.6 *mm* diameter × 254 *mm* long) using a rigid drop hammer. The axial and lateral stress-strain relationships for a number of test specimens have been obtained. The axial and lateral strain values were determined using strain gauges bonded to the lateral surface of the test specimen. The stresses were measured using a loadcell located at the base of the test specimen. The difference in time between the stress and strain measurements was taken into consideration during the processing of the data. The stress-strain curves which have been reported have shown an average increase of 55 percent over the static cylinder strength.

Summary:

The direct compression tests have shown that the impact strength of concrete increases up to a maximum value as the rate of loading increases. The increase in strength in compression was found to be dependent on the rate at which the impact load is applied and to a great extent on the quality of the concrete. Figure 2.17 shows the effect of the concrete quality, which is defined in terms of the static compressive strength [35], on the variation in compressive strength under increasing strain rates. The type of aggregates used was also found to have an influence on the magnitude of the impact compressive strength.

(2) Uniaxial Tensile Strength:

Zielinski et al [46] conducted an extensive investigation into the fracture of concrete and mortar under uniaxial impact tensile loadings using the split Hopkinson bar technique. The results indicated that the impact tensile strength was higher than the corresponding static value and that the impact strains at the maximum stress were larger than the corresponding static strains. Figure 2.18 shows static and impact stress-strain diagrams for mortar, micro-concrete and normal concrete under tensile loading.

(3) Multiaxial Loading:

A universal triaxial impact test arrangement and test procedure for concrete specimens capable of applying a predefined strain rate and strain path has yet to be developed. Only a limited number of investigations into the response of concrete subjected to biaxial stress conditions at different rates of loading have been reported in the literature and it seems that the difficulties in conducting such studies is associated with the failure to develop a suitable testing machine and recording system.

Mlakar et al [47] studied concrete under dynamic tensile-compression loading using hollow cylinders (330.2 *mm* outside diameter × 25.4 *mm* wall thickness × 660.4 *mm* high) subjected to axial compression and internal pressure. They reported an increase in the impact stress component with increasing strain rates whereas the strain at peak stress was found to be independent of the loading rate

(no change in the strain at peak stress was found compared to the static strain value).

However, Zielinski [48] reported that the increase in tensile strength under biaxial compression-impact tension is similar to that under uniaxial tension. These results confirmed the observations made by Takeda and Tachikawa [49] which were based on results obtained from dynamic multiaxial tests on concrete cylinders.

The only study related to shear at high strain rates has been reported by Takeda et al [50], who found that the shear strain decreases after reaching a peak shear stress at high rates of loading. They have attributed this to the speed at which shear cracks develop. The speed of the development of the shear cracks was found to increase with the rate of loading. These results are in agreement with those obtained by Mlakar et al [47] but contradict the findings of John and Shah [51].

Figure 2.19 summarises the behaviour of concrete under different loading conditions. Essentially, the sensitivity of the tensile strength to the loading rate is higher than that for the compressive strength. The sensitivity of flexural strength to the loading rate lies between that for the compressive and tensile strengths. This implies that the sensitivity of concrete to the loading rate is primarily related to the effect of strain rate on cracking.

2.3.3 Conclusions

(1) The results from investigations into the influence of loading rate on the behaviour of concrete have been obtained primarily by subjecting concrete specimens to flexural and to unconfined direct tension or compression loadings.

(2) The direct compression tests have shown that the impact strength of concrete increases up to a maximum value as the rate of loading increases. The increase in strength in compression was dependent on the rate at which the impact load is applied and to a great extent on the concrete quality. The type of aggregates used was also found to have an influence on the magnitude of the impact compressive strength.

(3) A similar finding was reported for both flexural and direct tensile loadings but the reasons for the greater increase in the tensile strength were thought to be due to the cracks which develop through zones of higher toughness. This is because the cracks have no time to find the weakest path through the material and extensive cracking takes place throughout the volume of the stressed concrete material.

It should, however, be noted that the level of experimental investigations remains very basic and tends to concentrate on obtaining an understanding of the behaviour of concrete under uniaxial stress conditions. Even so, there is a large scatter in the results which have been published mainly relating the ductility and the variation in the initial secant modulus of the material to increasing rates of loading. On the other hand there is only a limited amount of data available from investigations into the behaviour of concrete under multiaxial loadings.

2.4 CONCLUSIONS

The principal conclusions which emerge from this review are that the behaviour of concrete under static uniaxial and multiaxial loading conditions has been defined and is generally accepted. The behaviour of concrete under such loadings can be reproduced for a specific concrete mix using accepted testing techniques and standard concrete specimens. The most important points relating to the design and mathematical modelling of structural members are as follows:

(1) Damage to concrete occurs continuously during loading and is initiated at very low strain levels. The damage to the concrete is progressive and time dependent. Its nature and severity is very much dependent on the loading conditions. This is not surprising as concrete is inherently heterogeneous with micro-cracks present within its structure before external loadings are applied.

(2) The strength and deformation of concrete under static uniaxial loading conditions are different to those obtained under multiaxial loading conditions, but the pattern of behaviour is similar. The most important point is that under multiaxial loading conditions, the compressive strength of concrete increases as the magnitude of the compressive transverse stresses increase and decrease sharply when transverse tensile stresses are present under triaxial stress conditions. Therefore, if the effects of the transverse (secondary) stresses are not included the modelling of concrete can be both unsafe and inefficient.

(3) The understanding of the behaviour of concrete under impact loading is limited. The reported experimental investigations remain basic. They have tended to concentrate on developing an understanding of the behaviour of concrete under uniaxial stress conditions. Even so, the results which have been obtained contain a large scatter, particularly with respect to ductility and the variation in the secant modulus of concrete. However, the most important feature which has been observed is that the strength of concrete increases as the rate of loading increases. The increase in strength depends very much on the characteristic of the constituents of the concrete mix e.g. cement paste matrix, aggregate particles, etc.

(4) The investigation of the behaviour of concrete under multiaxial loadings has been very limited because of the practical difficulties in conducting either a general biaxial or a triaxial impact test with predetermined strain rates and strain paths. The principal difficulties lie in the development of the required experimental apparatus and test procedures. Even under uniaxial impact loading conditions many of the experimental results are difficult to compare. Future research in this field is widely recognised as being required.

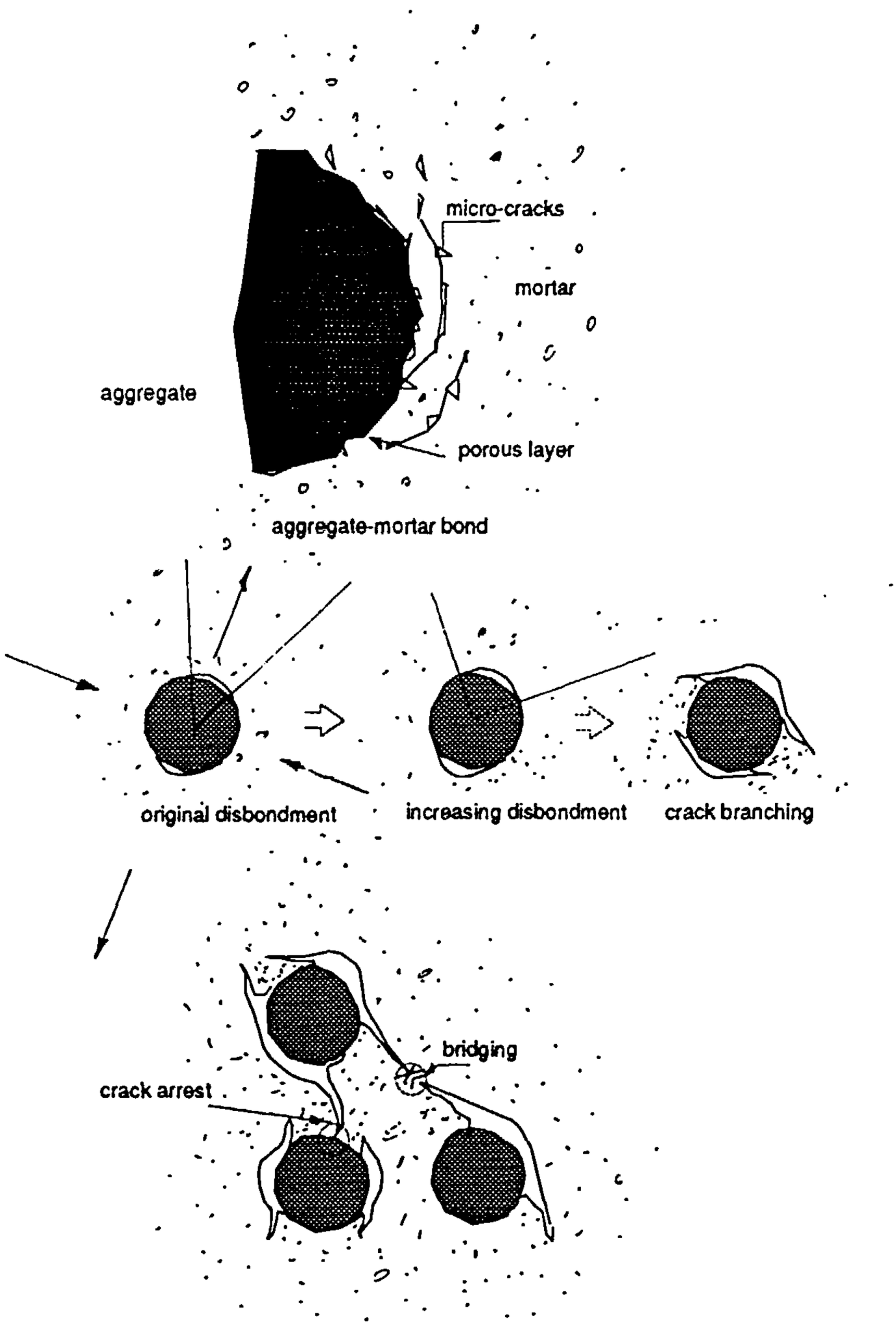

Figure 2.1: Damage Mechanism at microscopic level in concrete (after DiTommaso et al [52])

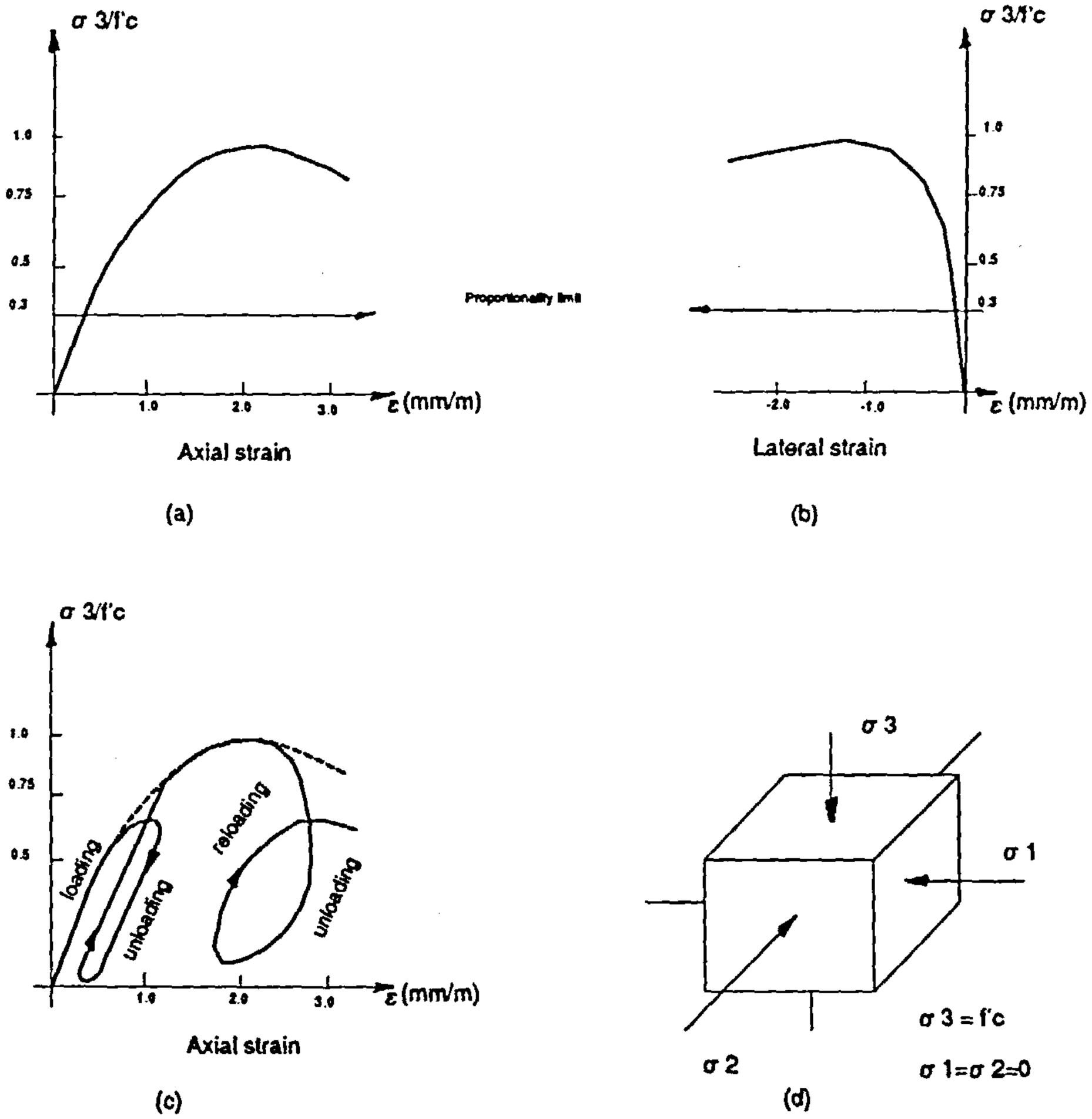

Figure 2.2: Concrete stress-strain curves under uniaxial compression

(a) Axial stress-strain curve

(b) Stress-lateral strain curve

(c) Axial stress-strain curve with loading, unloading and re-loading

f'_c is the maximum uniaxial compressive strength

σ is the axial stress

ϵ is the strain

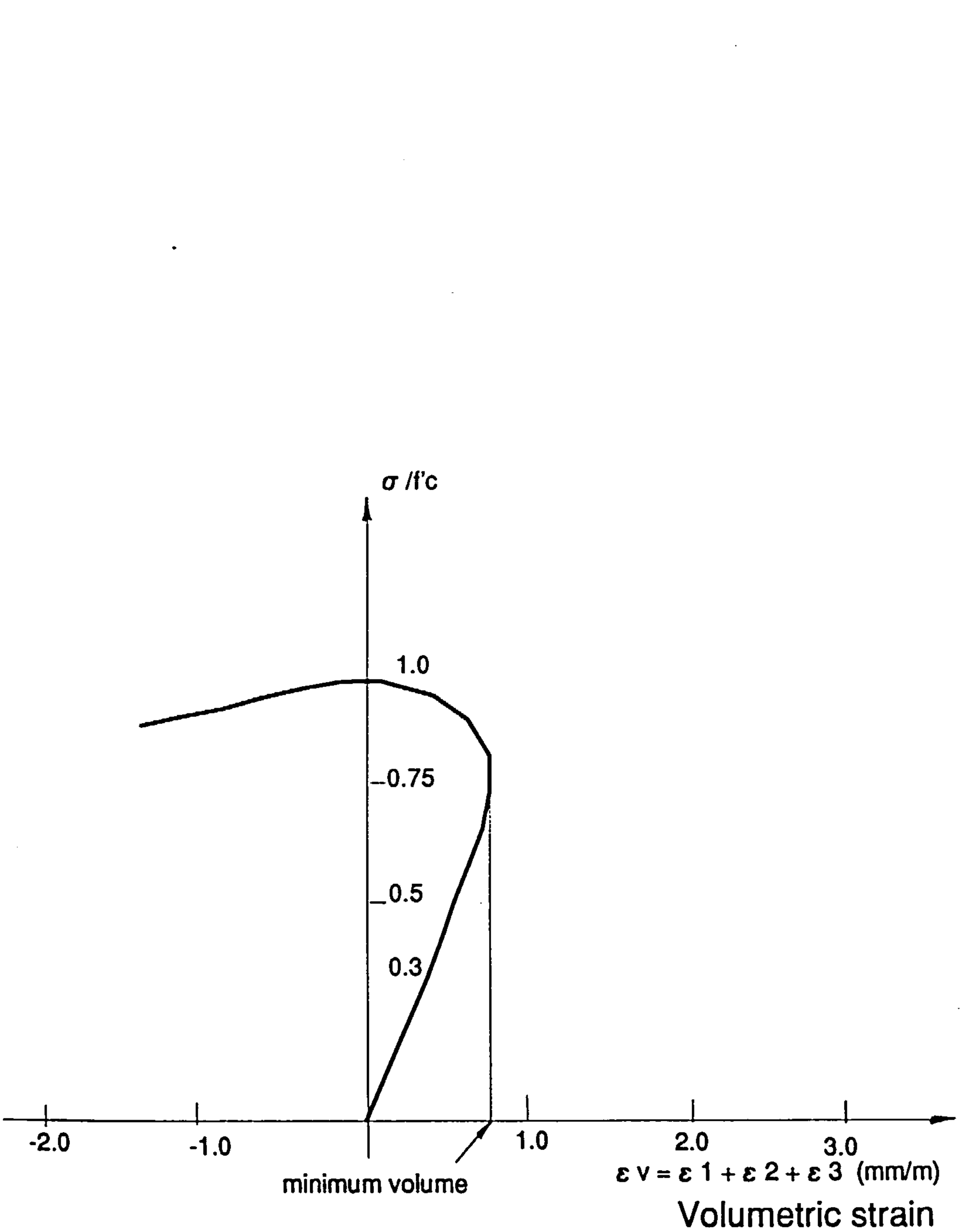

Figure 2.3: Concrete stress/volumetric strain curve

f'_c is the maximum uniaxial compressive strength

σ is the axial stress

ϵ_1, ϵ_2 and ϵ_3 are the three principal strains

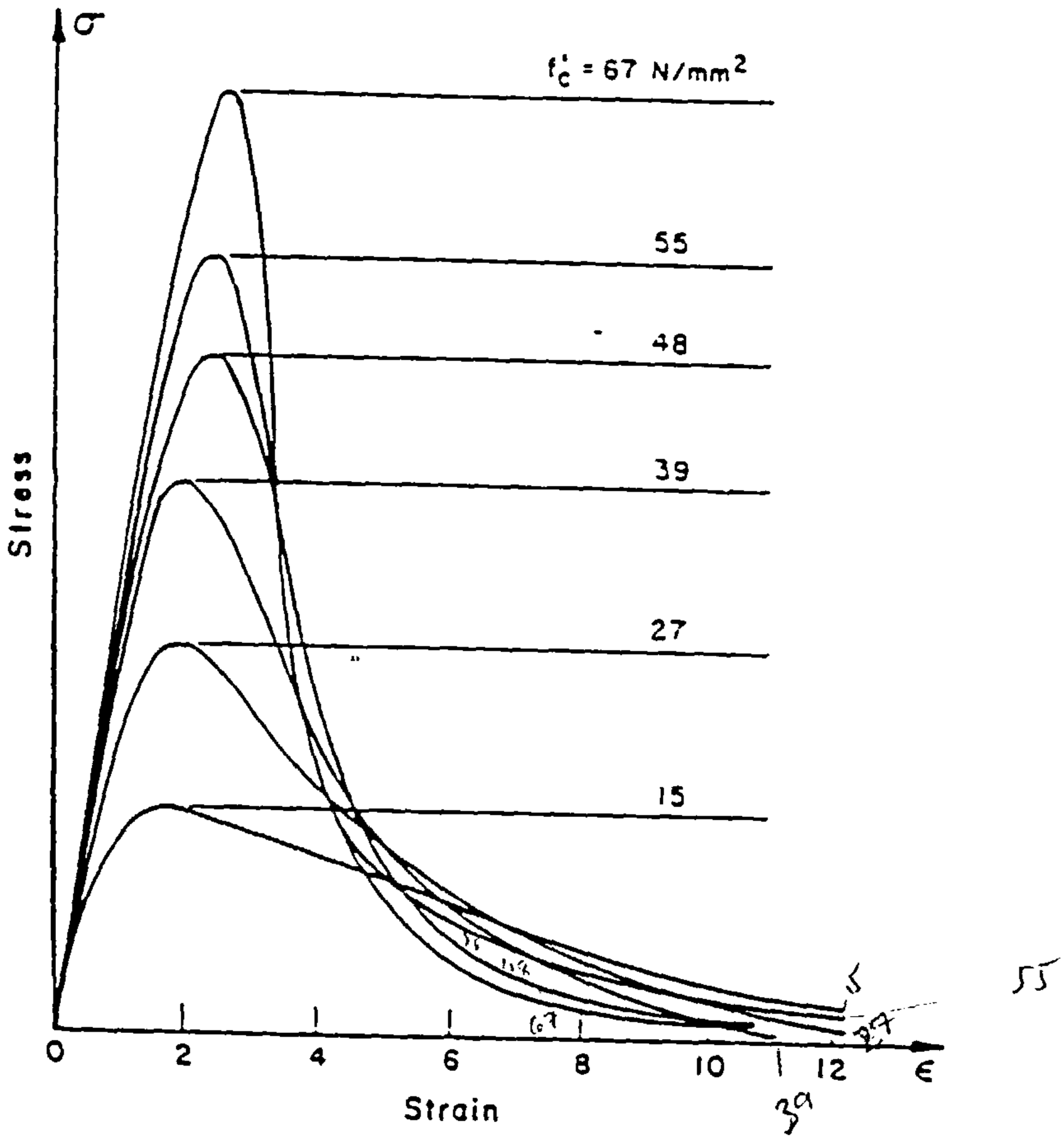

Figure 2.4: Complete stress-strain curves for normal and high strength concrete under uniaxial compression (reported in [27])

f'_c is the maximum uniaxial compressive strength

σ is the axial stress

ϵ is the strain

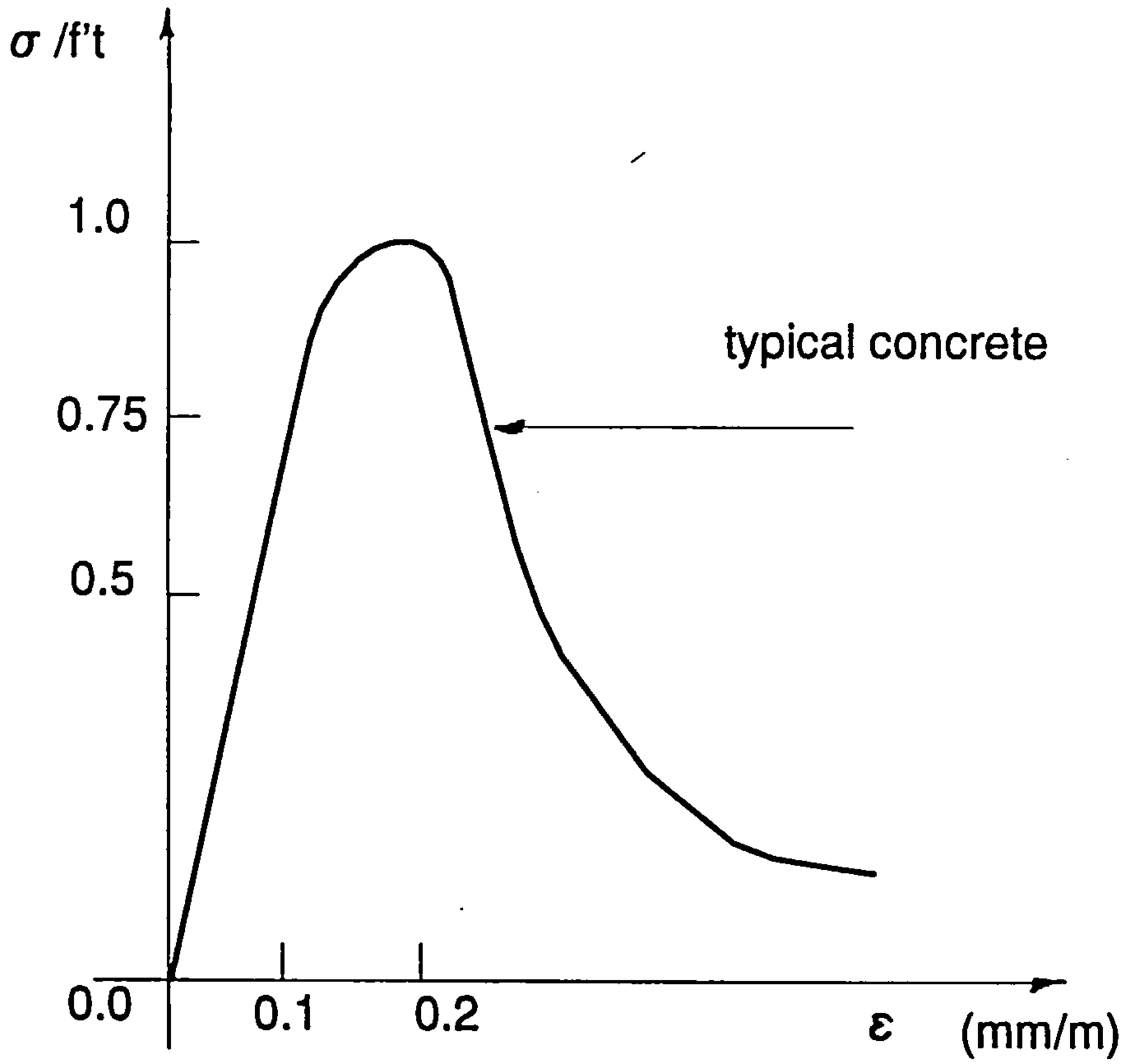

Figure 2.5: Uniaxial tensile stress-strain curve

f_t' is the maximum uniaxial tensile strength

σ is the axial stress

ϵ is the strain

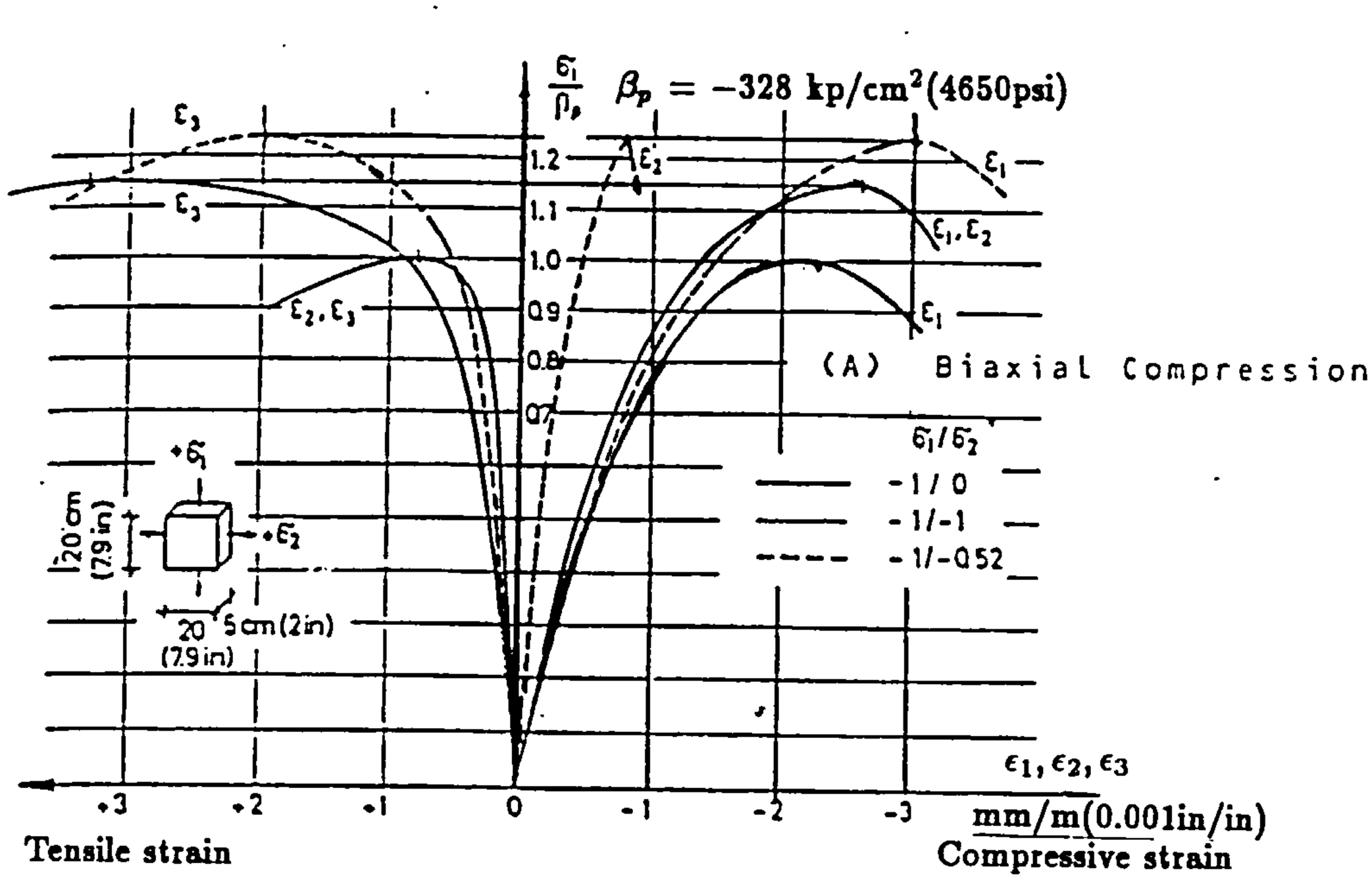

Figure 2.6: Stress-strain curves for concrete under biaxial compression-compression (after Kupfer et al [19])

β_p is the maximum uniaxial compressive strength

σ_1 is the axial stress

σ_2 is the lateral stress

$\epsilon_{1,2,3}$ are the strains in the cube

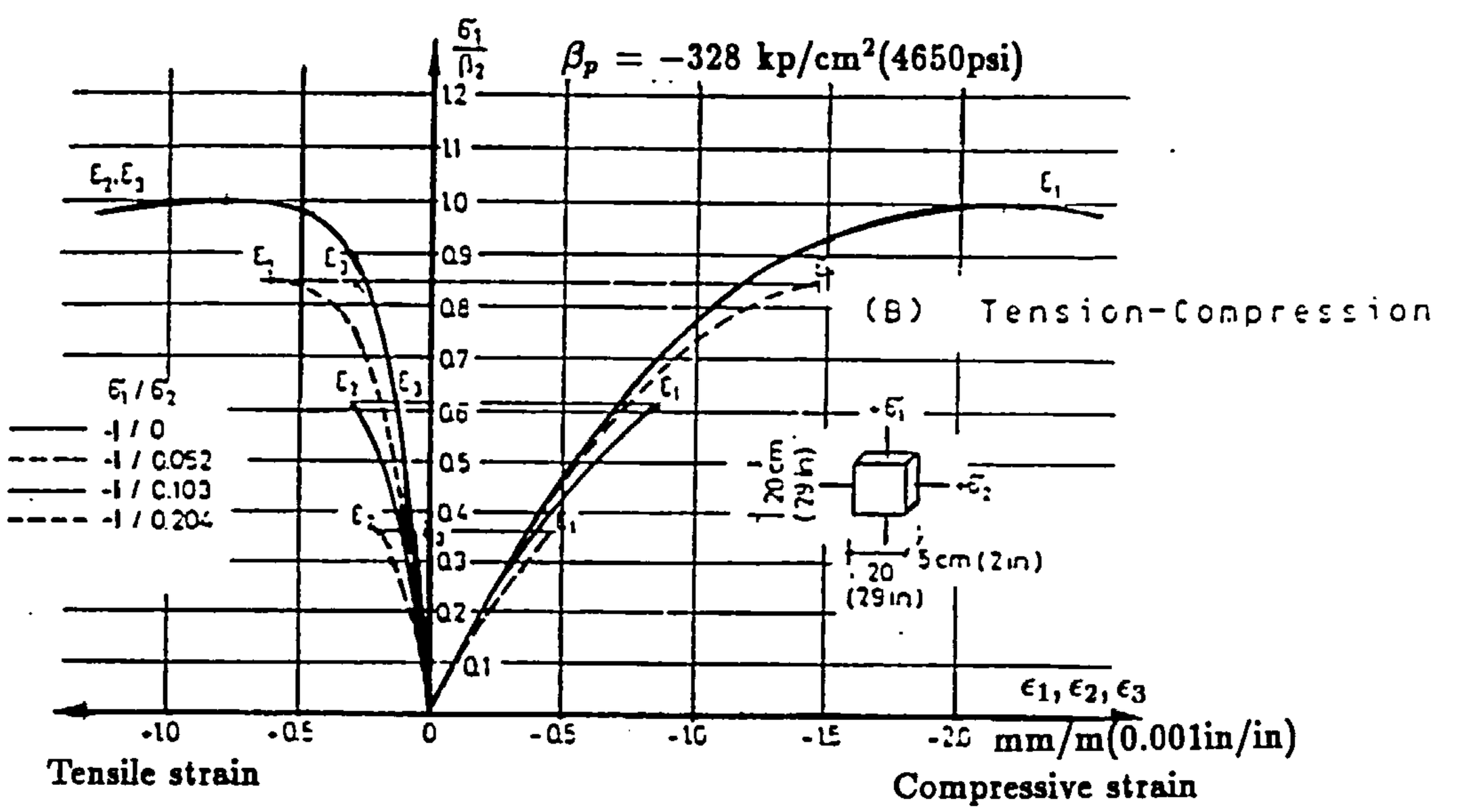

Figure 2.7: Stress-strain curves for concrete under biaxial compression-tension (after Kupfer et al [19])

β_p is the maximum uniaxial compressive strength

σ_1 is the axial stress

σ_2 is the lateral stress

$\epsilon_{1,2,3}$ are the strains in the cube

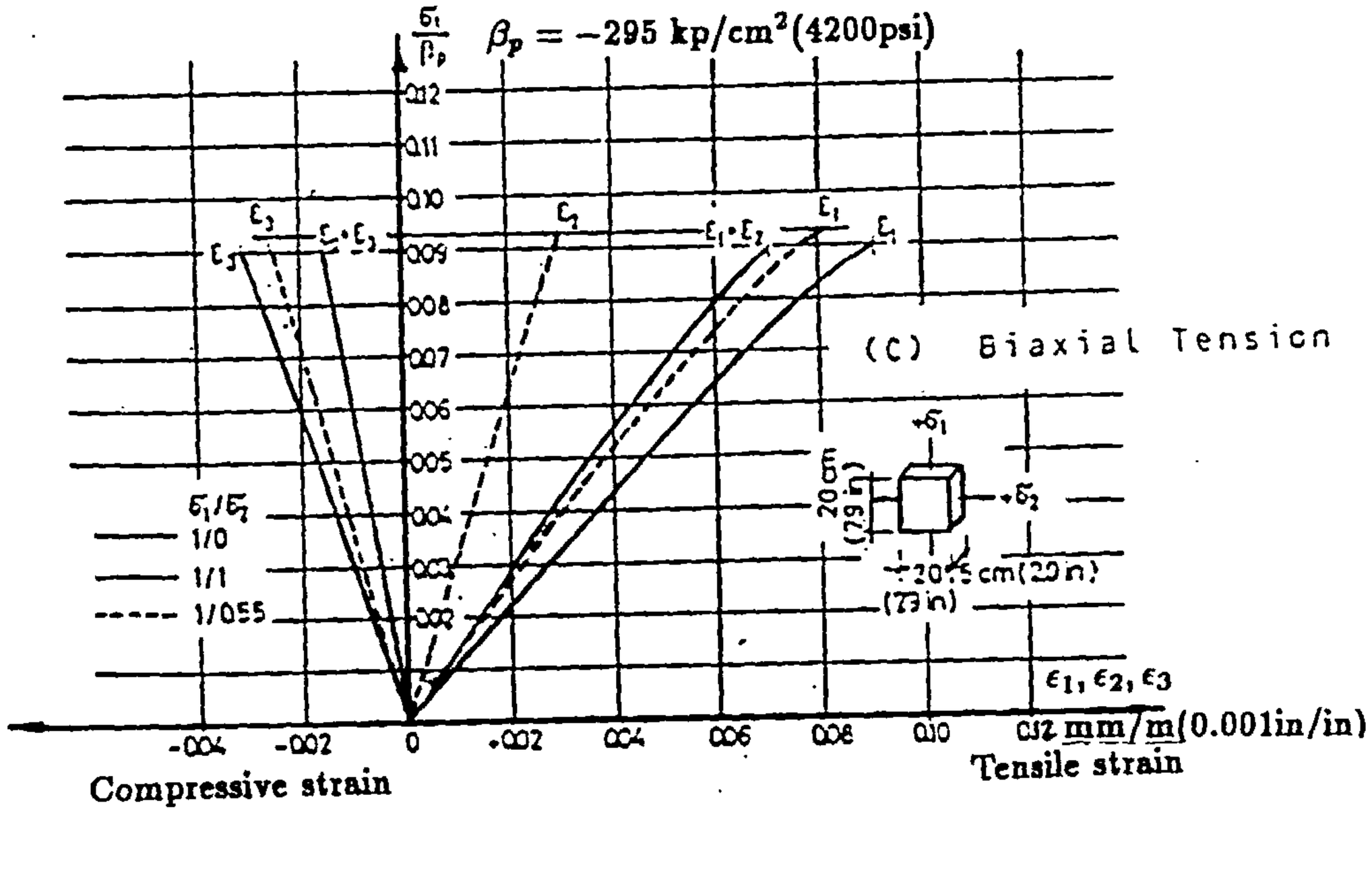

Figure 2.8: Stress-strain relationships for concrete under biaxial tension-tension (after Kupfer et al [19])

β_p is the maximum uniaxial compressive strength

σ_1 is the axial stress

σ_2 is the lateral stress

$\epsilon_{1,2,3}$ are the strains in the cube

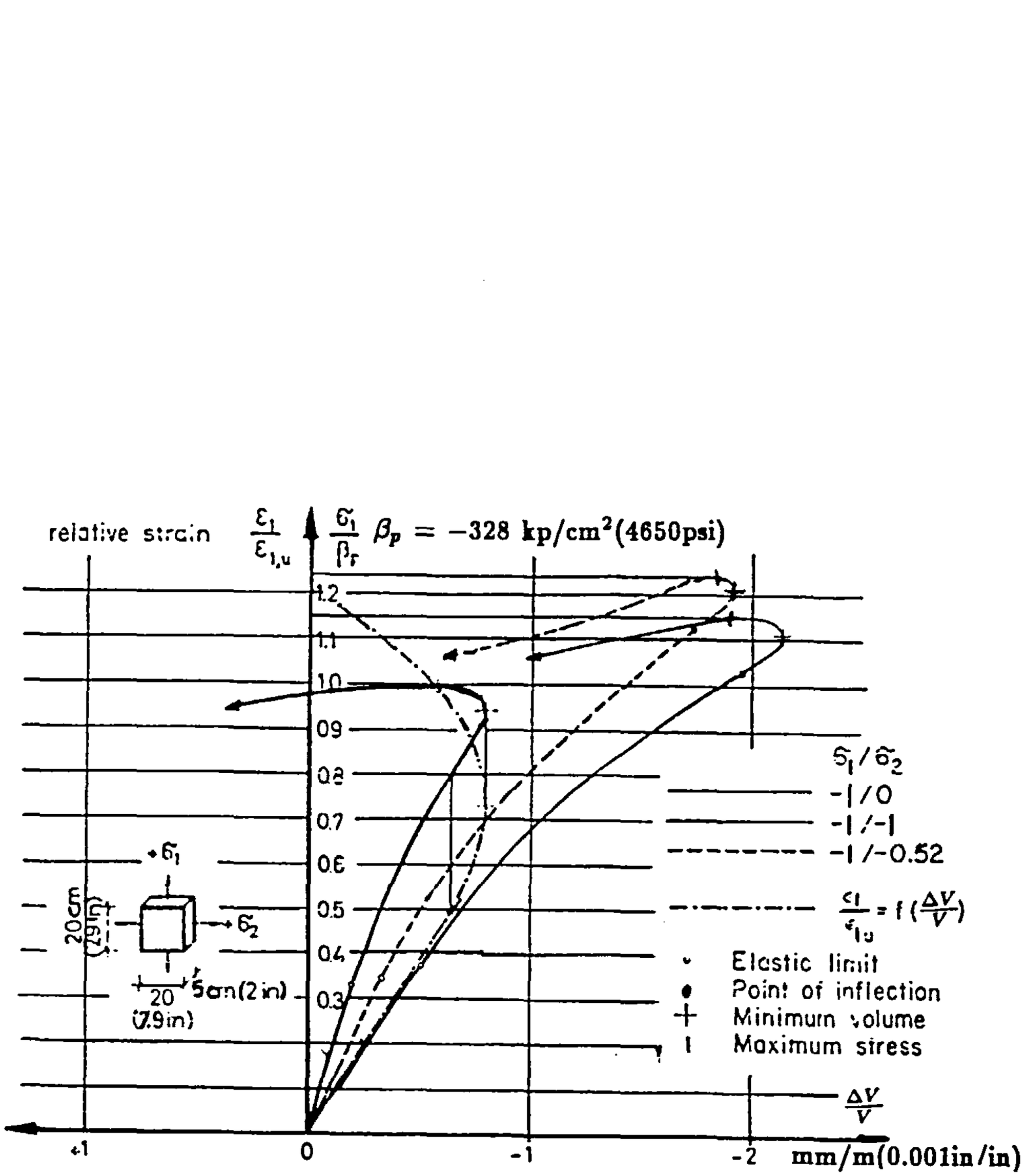

Figure 2.9: Volumetric strain for concrete under biaxial compression (after Kupfer et al [19])

β_p is the maximum uniaxial compressive strength

$\sigma_{1,2,3}$ are the axial stresses

ϵ_1 is the strain in the cube

ϵ_{1u} is the strain at failure

$\Delta V/V$ is equal to $\epsilon_1 + \epsilon_2 + \epsilon_3$

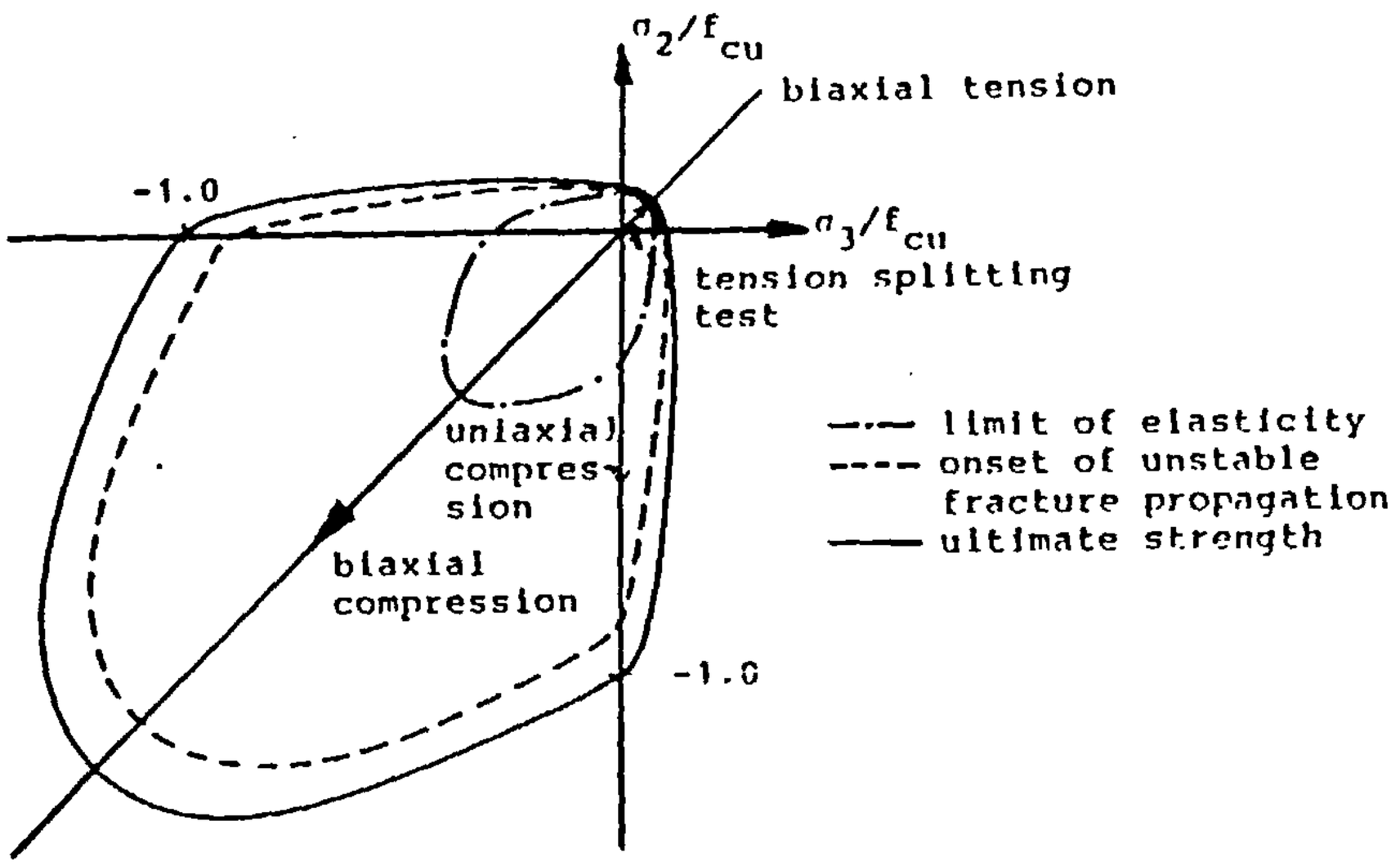

Figure 2.10: Stresses at the elastic and failure limits for concrete under biaxial stress conditions (after Kupfer et al [19])

f_{cu} is the maximum uniaxial compressive strength

$\sigma_{2,3}$ are axial stresses

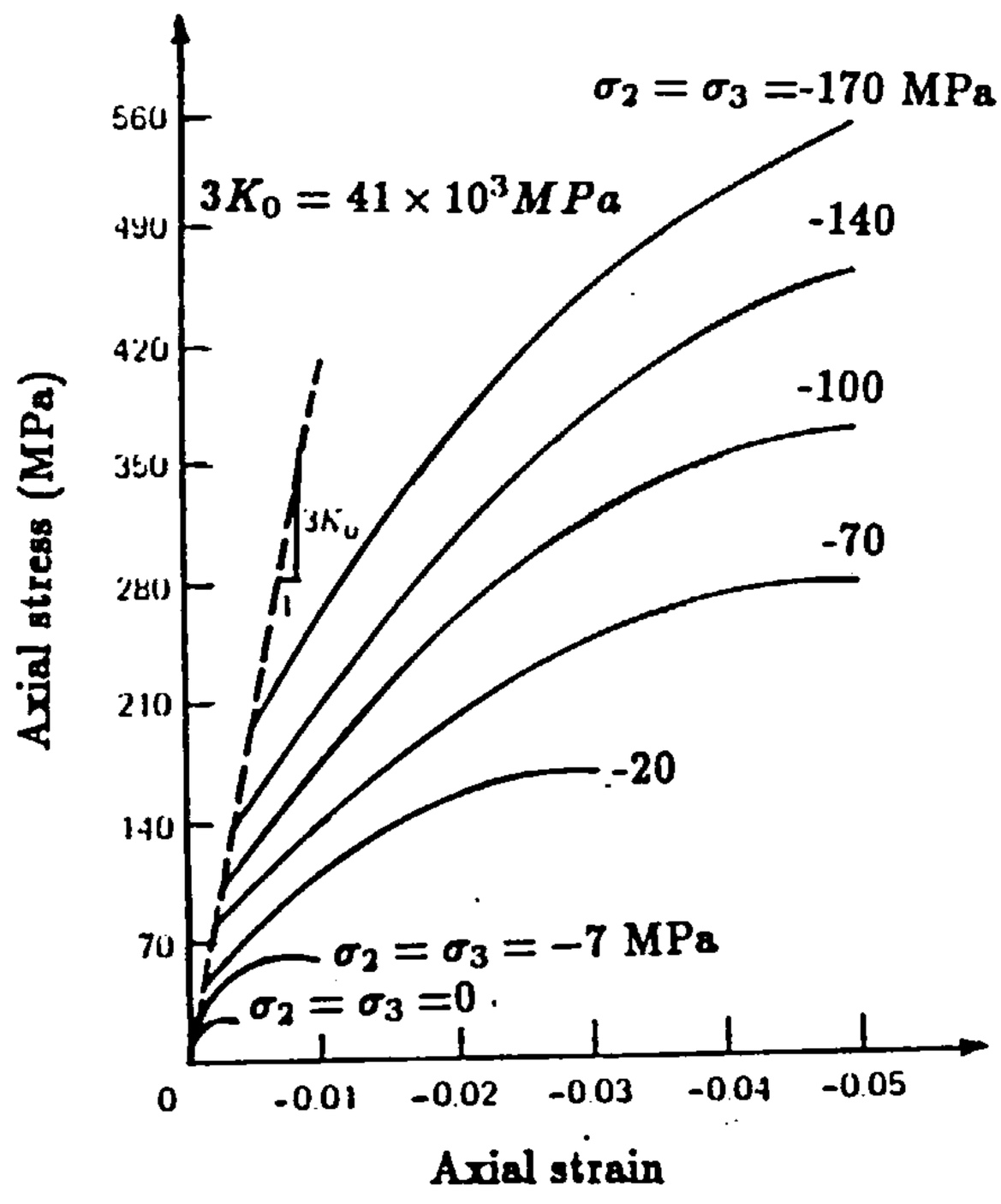

Figure 2.11: Triaxial stress-strain curves for concrete (reported by Chen [27])

σ_1 is the axial stresses

$\sigma_2 = \sigma_3$ the lateral compressive pressure

$3K_0 = E_0/(1-2\nu) = 41.0GPa$

where K_0, E_0 and ν are the Bulk and Young's modulii and Poisson's ratio respectively.

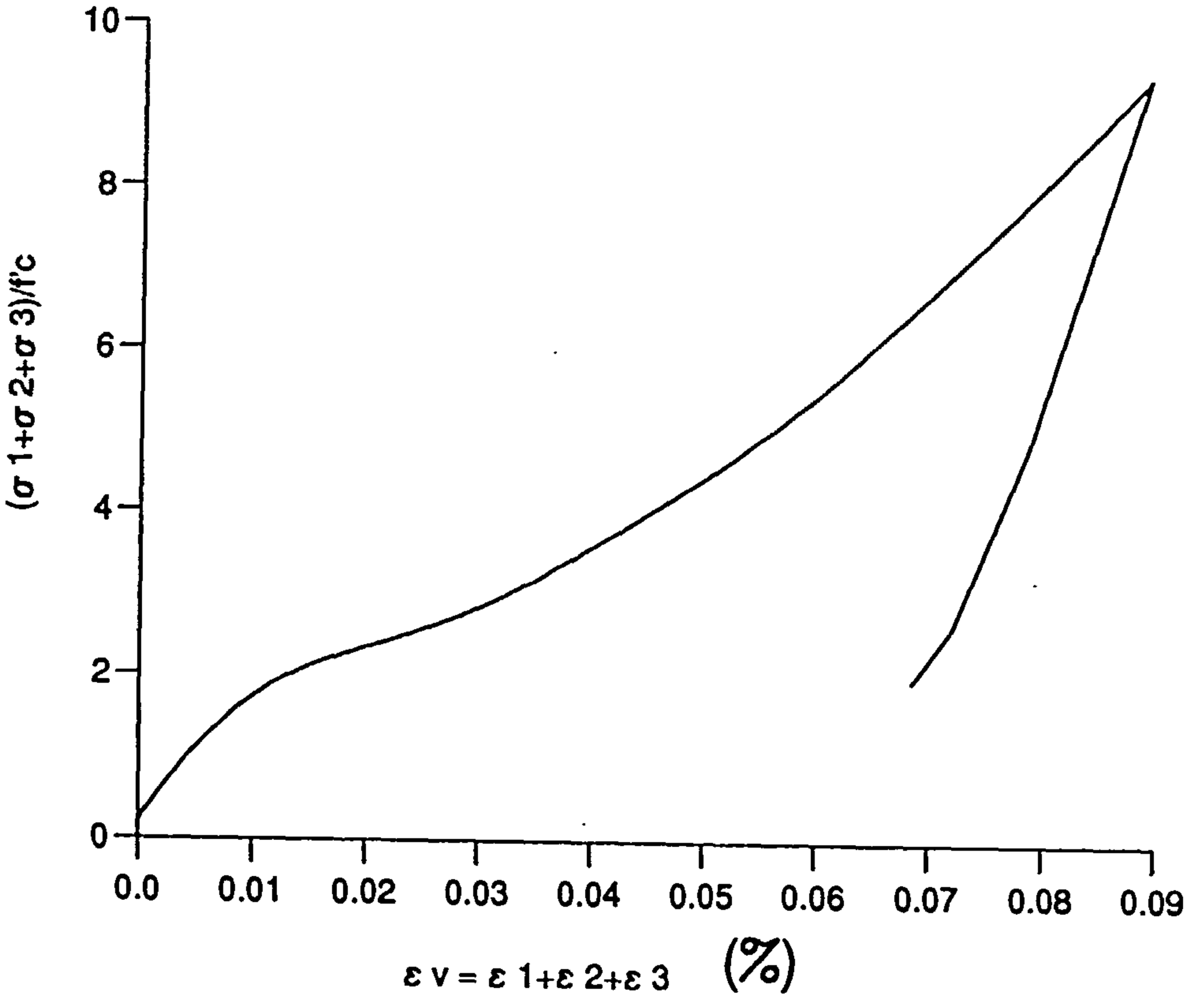

Figure 2.12: Concrete compaction curve

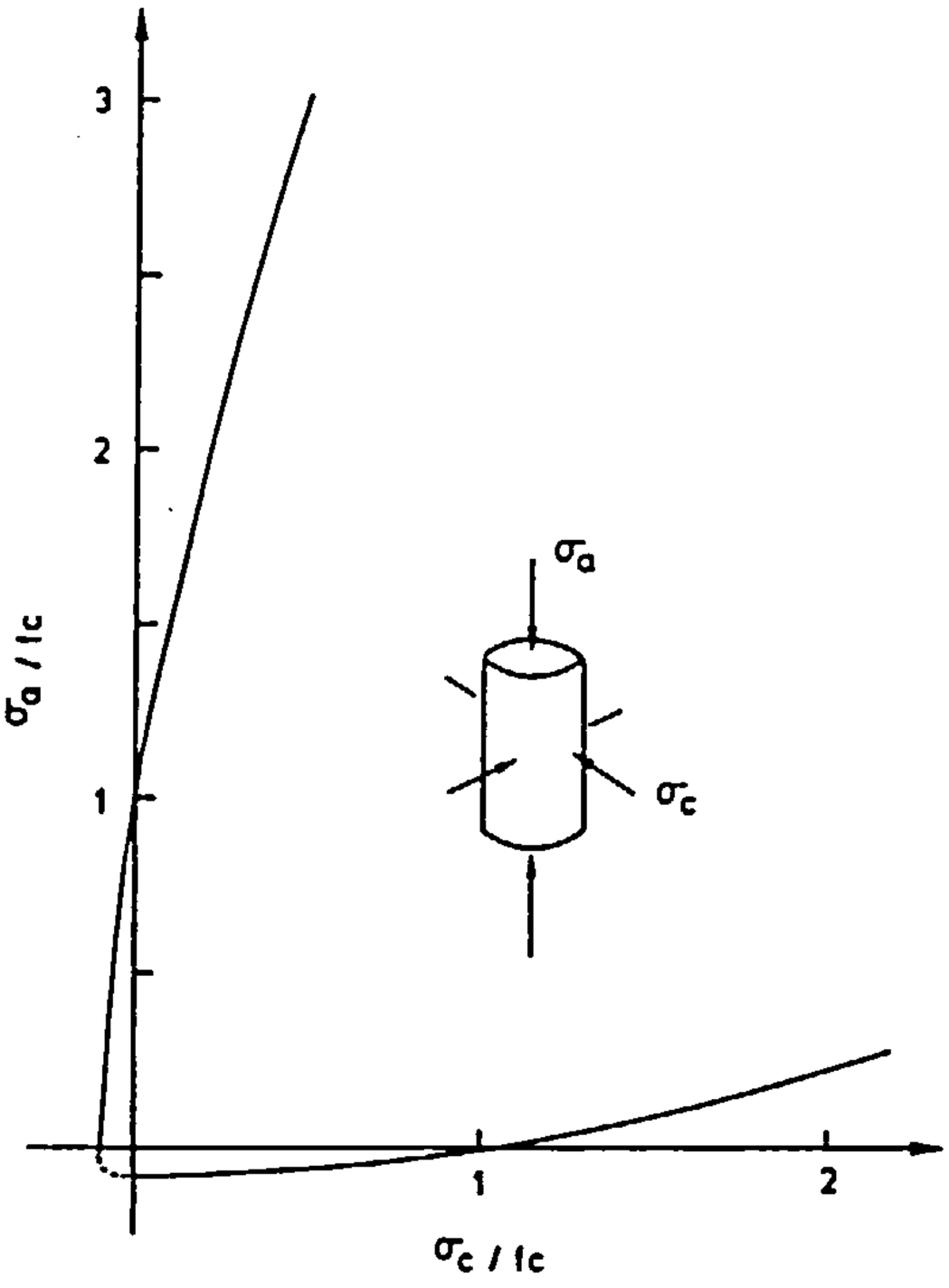

Figure 2.13: Failure envelope for concrete under triaxial stresses (after Kotsovos [30])

f_c is the maximum uniaxial compressive strength

σ_a is the axial stress

σ_c is the lateral pressure

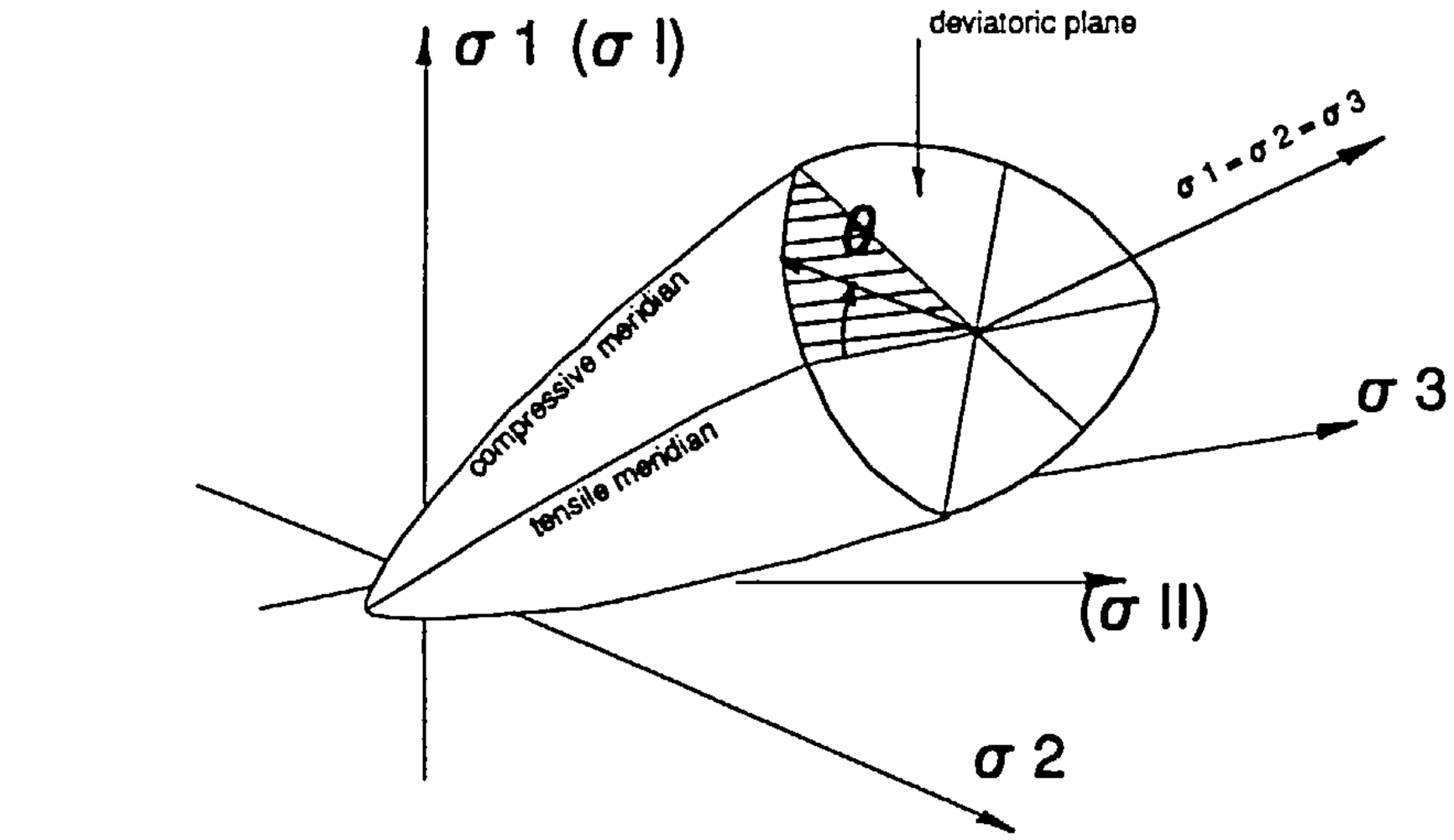

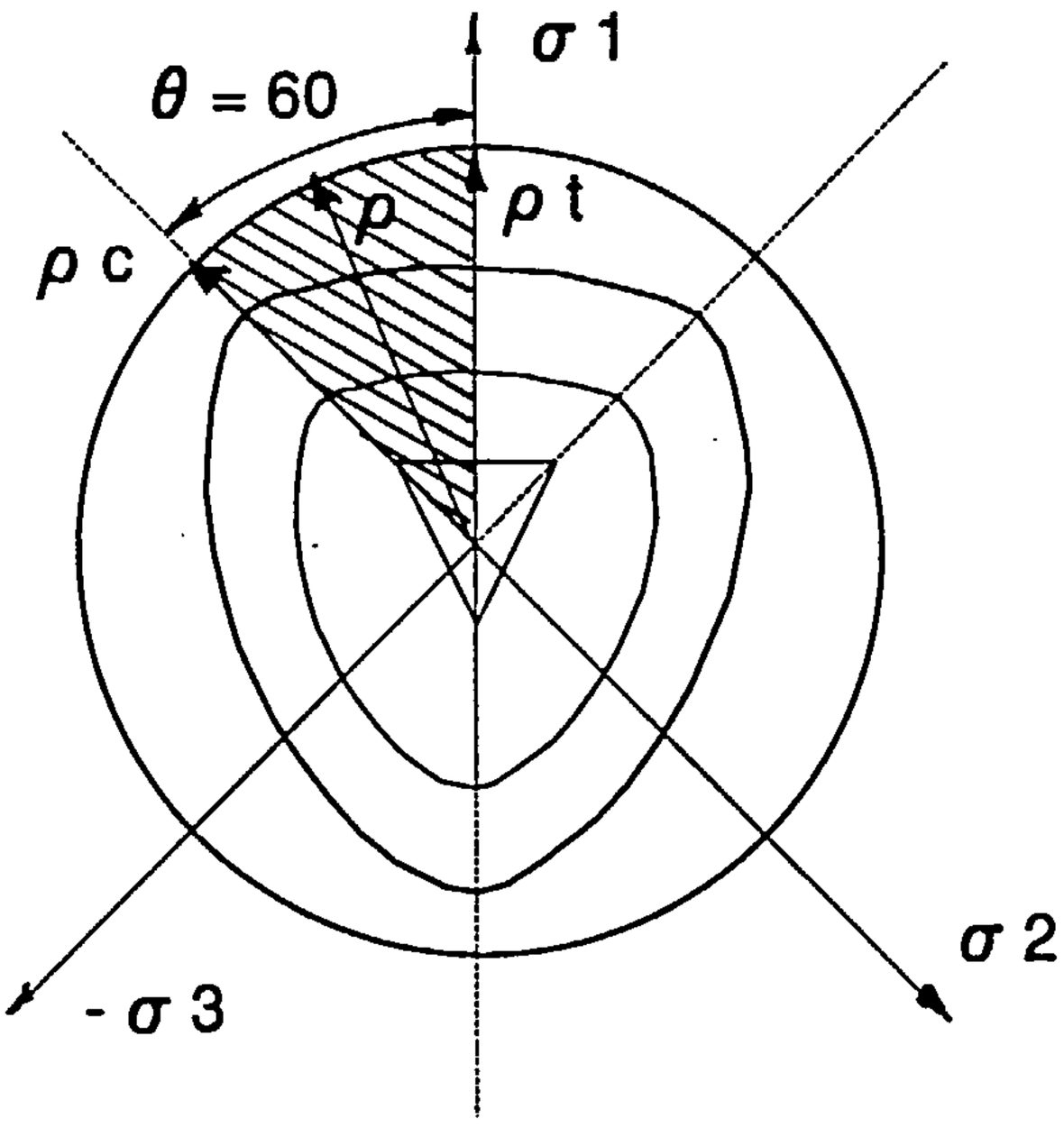

Figure 2.14: Failure surface in three-dimensional stress space

σ_1, σ_2 and σ_3 are the principal stresses

σ_I and σ_{II} are the principal stresses for two dimensional representation

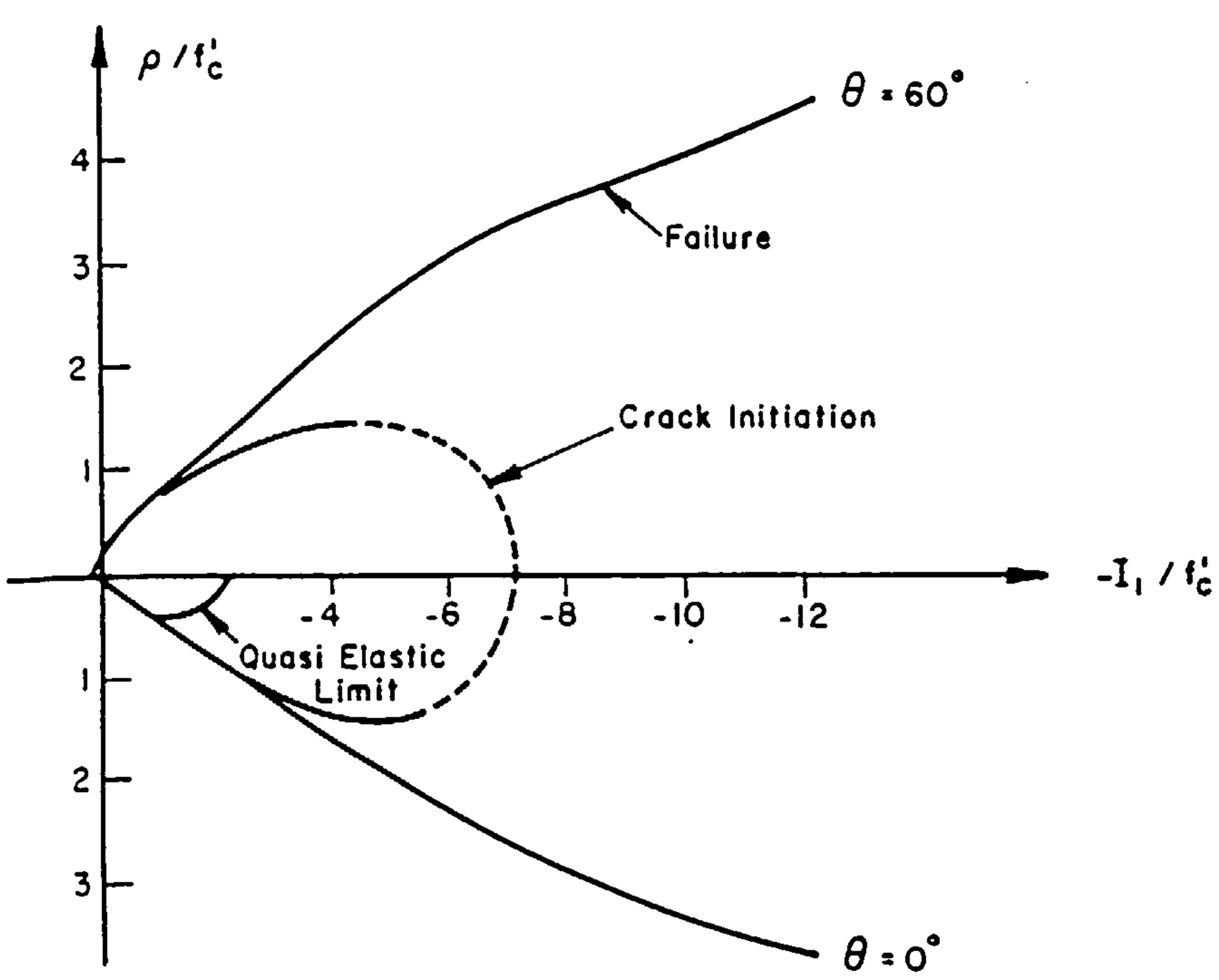

Figure 2.15: Experimentally obtained failure and crack initiation curve (after Launay and Gachon [25, 53])

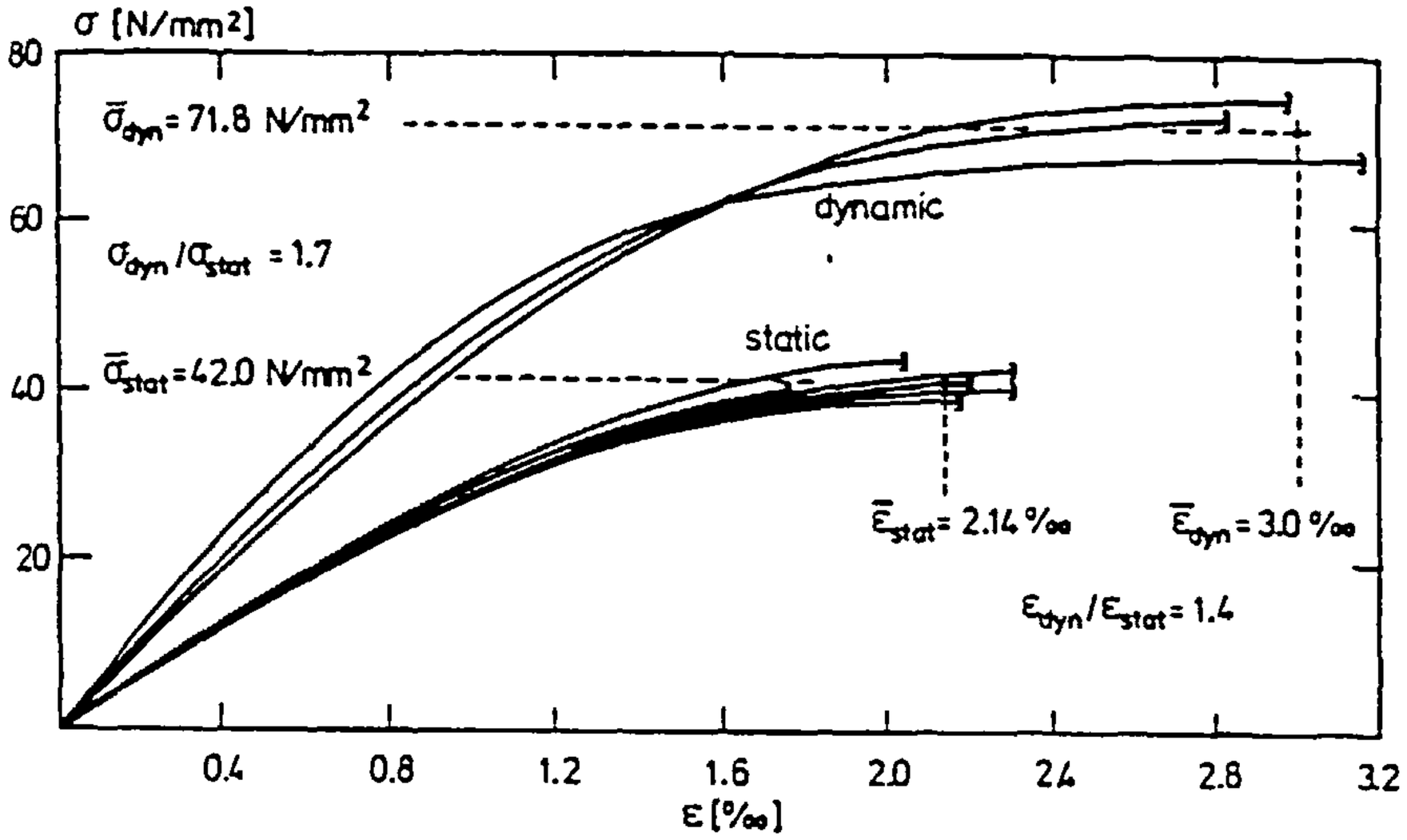

Figure 2.16: Dynamic and static stress-strain curves for concrete (after Curbach and Eibl [42])

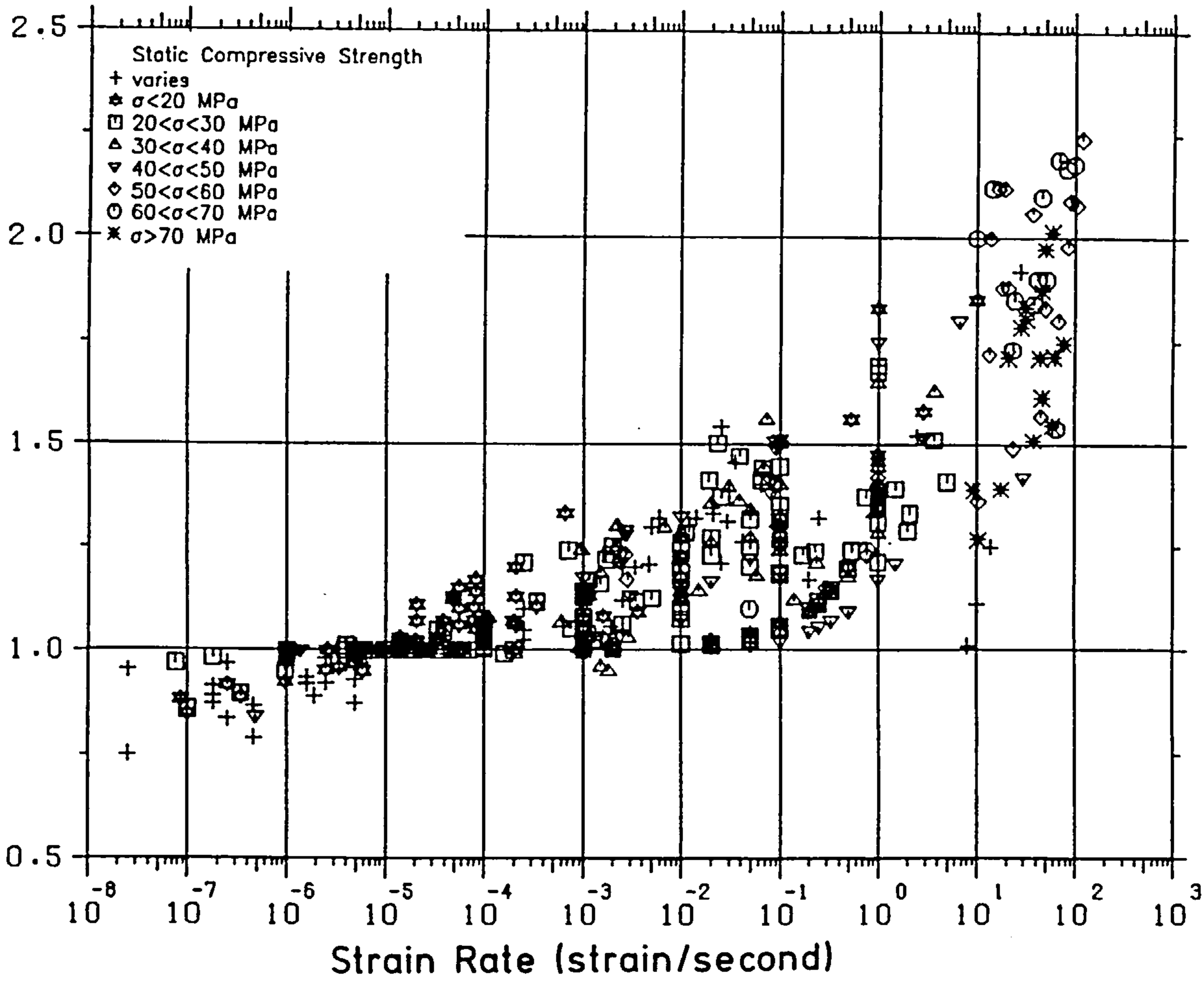

Figure 2.17: Effect of concrete quality on the strain-rate influence (after Bischoff and Perry [35])

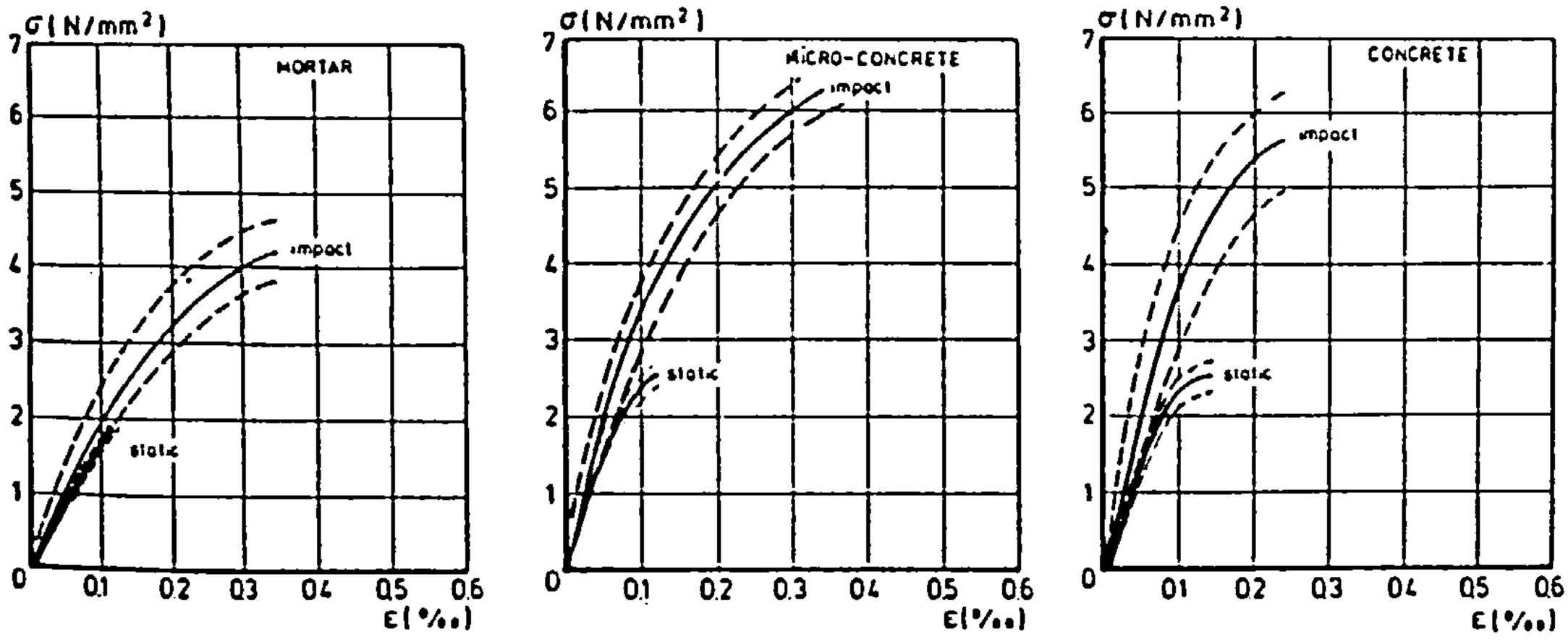

Figure 2.18: Static and impact tensile stress-strain curves for mortar, micro-concrete and concrete under tensile loading (after Zielinski [46])

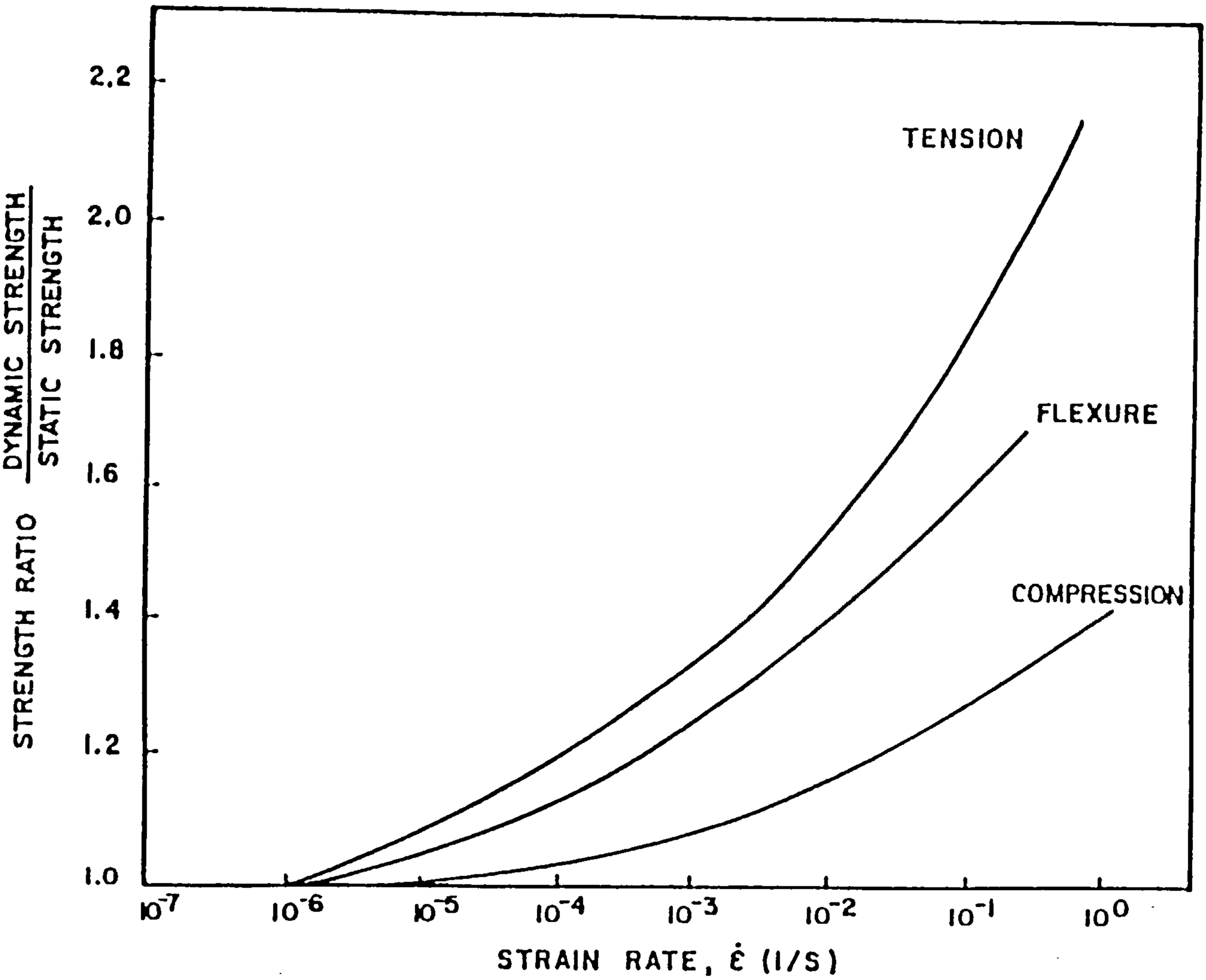

Figure 2.19: Strain rate behaviour of plain concrete in different simple response modes (after Suaris and Shah [44])

Chapter 3

CONCRETE CONSTITUTIVE RELATIONS

3.1 INTRODUCTION

The finite element method has emerged during the last twenty years as a powerful tool in the analysis of structural concrete members under complex loading conditions. One of the main routines which is required by the finite element method is the material constitutive relationships which are used to model the behaviour of concrete within a structure.

In this Chapter, special emphasis is given to the constitutive relationships for plain concrete. However, the interaction between the concrete and the reinforcing bars embedded within it is taken into account in a discrete representation.

The relationships which model the reinforcing bars and the interaction between concrete and the reinforcing bars are discussed in Chapter 4.

The variables used in this Chapter are defined in Appendix A.

In Chapter 2, it was accepted that concrete has a heterogeneous structure. Depending on the dimensional level at which concrete is to be studied several possibilities for constitutive modelling exist. Standard test specimens used for quality control testing i.e. cubes and cylinders, often have dimensions which require microscopic modelling. Thus, coarse aggregates, mortar and the bond interfaces within the material are modelled as separate entities. In general, however, concrete members are of such dimensions that constitutive modelling at the macroscopic level is sufficient. In order to comply with the selection of a macroscopic constitutive model, the smallest dimension of the finite elements into which the structural concrete member is subdivided should be several times larger than the size of the largest aggregate particle. At this scale the material structure of the concrete can be considered to have, before loading, isotropic and homogeneous properties i.e. aggregate particles, pores, micro-cracks are assumed to be sufficiently well distributed in the concrete finite element.

The test results have indicated that concrete under load experiences very complex changes from isotropic to anisotropic material behaviour involving cracking

which leads to non-linear stress-strain relationships. These changes in the material behaviour of the concrete can also be influenced by the loading conditions.

The development of a material model for concrete which simulates all the aspects of the behaviour of concrete is extremely difficult and unified constitutive relations for the use in numerical analysis have not yet been developed. However, many of the factors which are involved in linear and non-linear behaviour can be modelled reasonably well. A routine which is designed to model the behaviour of concrete within a finite element code should be capable of replicating the following effects:

(1) Stress-strain constitutive relationships for the elastic and inelastic behaviour of plain concrete up to failure.

(2) A failure criterion which is capable of simulating the variation in strength of plain concrete under the action of different stress states.

(3) A cracking model which takes account of the change in the concrete from an isotropic to an anisotropic material after failure.

(4) A post maximum strength constitutive relationship in which the cracked

concrete material undergoes softening and loss of strength after maximum strength has been reached under the action of different stress conditions.

The above requirements are discussed in the following Sections

3.2 STRESS-STRAIN CONSTITUTIVE MODELS

The stress-strain constitutive relationships for the elastic and inelastic behaviour of concrete can be modelled using a number of different theories e.g.

(a) non-linear elastic relationships;

(b) endochronic theory;

(c) plasticity theory;

(d) fracture, damage and stochastic approaches.

A detailed discussion of these approaches has already been published [27, 53, 54, 55] and a comprehensive review of several models based on the use of these approaches in the finite element analysis of reinforced concrete structures has also been published [56, 57, 58]. In the following Section, the underlying concepts and limitations of each approach will be discussed.

3.2.1 Non-Linear Elastic Models

The non-linear elastic models use stress-strain variations in the form of relationships which include either the tangent or the secant modulii within the framework of the theory of elasticity. In general two types of approaches have been used to formulate the non-linear elastic models i.e.

(1) Hyperelastic models which are total formulations expressed in terms of secant stress-strain relationships.

(2) Hypoelastic models which are incremental formulations expressed in terms of tangent stress-strain relationships.

Hyperelastic Models:

An elastic material is defined by its total reversibility. This means that after loading and subsequent unloading the material follows the same path along the stress-strain curve. This also means that after one cycle of loading and re-loading the material is identical to that before the initial loading and that the mechanical external work done will be regained if the load is removed.

It can be deduced that the stress-strain relationships must be formulated such that there is a one to one correspondence between stress and strain i.e. the current state of stress depends only on the current state of strain and not on the history of the deformation of the material. This direct dependency of stress on

strain is referred to as a Cauchy type response in the theory of elasticity [53, 59].

$$\sigma_{ij} = D^0_{ijkl}\epsilon_{kl} \tag{3.1}$$

where σ_{ij} and ϵ_{kl} are the total stress and the total strain tensors respectively. D_{ijkl} is a six by six matrix which describes the stiffness of the material. D_{ijkl} is a symmetric matrix for all elastic materials, see Section 3.5.4.

Equation 3.1 results in a one to one relation between the actual states of stress and strain and it can be defined as a secant formulation.

Another approach which can be used to describe this direct dependency of stress on strain is to express the stresses as gradients of an energy function W [27, 59, 53]. The energy function W can be derived as a function of the strain invariants I'_1, I'_2 and I'_3. The definition of the strain invariants is given in Appendix A. The strain invariance property is restricted only to materials which have an initial isotropic structure. Let the energy function, W, be a polynomial and that the initial strain-free state corresponds to the stress-free state, then the following expression is valid:

---

[0]General tensorial notation is adopted

$$\sigma_{ij} = \frac{\partial W}{\partial \epsilon_{ij}} \tag{3.2}$$

The material defined by Equation 3.2 can also be described in terms of strains which are derived as gradients of the complementary energy function Γ which is a function of the stress invariants I_1, I_2 and I_3 i.e.

$$\epsilon_{ij} = \frac{\partial \Gamma}{\partial \sigma_{ij}} \tag{3.3}$$

The material which has stress-strain relationships defined by either Equation 3.2 or Equation 3.3 is referred to as a hyperelastic material.

The hyperelastic stress-strain relationships have been used by many researchers to analyse the behaviour of concrete under biaxial and triaxial stress conditions despite the fact that the predicted concrete deformation is irreversible and path-independent. In the earlier application of the finite element method to problems in structural concrete, simplified forms of the hyperelastic stress-strain relationships were used. Basically the stress-strain relationships were simple extensions of the linear elasticity method. Among the many proposed hyperelastic stress-strain models, Nilson [60] modelled concrete in compression using equivalent uniaxial stress-strain relationships similar to the relationship initially proposed by Saenz [61]. At ultimate strength, the concrete has a constant horizontal tangent modulus.

The biaxial effects on the stresses are computed with a stress dependence on orthotropic relationships. The concrete in tension was given a linear variation between the stress and strain up to the failure point.

Another approach which has been used to model a hyperelastic material uses the decomposition of the stress and strain states into volumetric and deviatoric components as a function of the bulk and shear modulii as follows:

$$\begin{aligned} \sigma_{oct} &= 3K_s\epsilon_{oct} \\ \tau_{oct} &= 2G_s\gamma_{oct} \end{aligned} \tag{3.4}$$

The volumetric and deviatoric values are also known as the octahedral normal and deviatoric stresses (σ_{oct}, τ_{oct}) and strains ($\epsilon_{oct}, \gamma_{oct}$). K_s and G_s are the secant bulk and shear modulii. The total stress state is obtained by adding each of the stress components as reported by Kupfer et al [62], for biaxial stress-strain formulations and Cedolin [63] for triaxial stress-strain formulations.

The hyperelastic stress-strain models are attractive because they are simple to formulate and to integrate into finite element codes. However, they seem to predict only a limited deformation in the concrete. For example, they are well known to have a deficiency in modelling the volumetric dilation of the concrete. This may be the reason why for example the concrete model proposed by Cedolin et al [63] only agrees with the test results below a certain level of the compressive

stress. This level of compressive stress is approximately equal to the level at which concrete starts to experience dilation.

The hyperelastic stress-strain formulation may be suitable for concrete in tension because the stress-strain variation is almost linear elastic up to the failure point. Therefore, if a tensile failure is the predominant non-linearity in a loaded structural concrete member the total stress-strain models can be used. However, accurate modelling of the cracks which occur in concrete members is required [27, 64].

Hypoelastic Models:

The hypoelastic model is used to describe the behaviour of the materials in which the state of stress depends on the current state of strain and the stress path followed to reach that state. In an incremental stress-strain model, the stress and strain increments are related through the tangential material stiffness i.e.

$$d\sigma_{ij} = D_{ijkl} d\epsilon_{kl} \tag{3.5}$$

Integration of Equation 3.5 with respect to time gives the total stress in the material.

$$\sigma_{ij} = \sigma^{i}_{ij} + \int D_{ijkl} \frac{\partial \epsilon_{kl}}{\partial t} dt \tag{3.6}$$

The relationship obtained indicates that the hypoelastic material is stress path dependent. σ_{ij}^{i} is the initial state of the stress which should be added to the current state of stress.

A number of isotropic and orthotropic hypoelastic models have been developed and utilised in finite element formulations for the analysis of concrete members. The formulation uses two types of scalar functions to relate the stress to the strain i.e. the variable tangent modulus and the variable bulk and shear modulii.

In the simplest of the approaches the isotropic linear elastic formulation is used but Young's modulus is replaced with a variable tangent modulus. The variable tangent modulus should comply with the values obtained from experimental investigations. Liu et al [65] used this type of model on the basis of the results obtained from earlier work [60] and developed a biaxial stress-strain law for plain concrete which includes the effect of the presence of confinement and micro-cracks. They suggested a simpler segmented envelope for biaxial compression. The failure envelope is inside the compression zone and in a way can be further approximated to a square allowing a constant 20 percent increase in strength above the value of the uniaxial compressive strength f_c' for biaxial compression-compression stress conditions.

Tasuji et al [66] extended the work of Liu et al [65] using the results from experimental investigations into the biaxial loading of plain concrete [20], to obtain an improved formulation for the general stress-strain relationships which describe the behaviour of plain concrete in biaxial compression-compression, biaxial compression-tension and biaxial tension-tension.

Darwin and Pecknold [67] proposed an incremental form of the orthotropic formulation which is again based on the concept of equivalent uniaxial strain in two dimensions, where the biaxial effect on the concrete is represented by equivalent uniaxial stress-strain curves for each of the principal stress axes. The model has been found to be capable of modelling the behaviour of concrete under cyclic loading as well as quasi-static loading.

More sophisticated models based on the decomposition of the stress and strain into the octahedral normal and deviatoric components have been formulated. However, the models are based on non-linear tangent bulk and shear modulii as follows:

$$\begin{aligned} d\sigma_{oct} &= 3K_t d\varepsilon_{oct} \\ d\tau_{oct} &= 2G_t d\gamma_{oct} \end{aligned} \tag{3.7}$$

where K_t and G_t are the tangent bulk and shear modulii respectively which are determined from experimental test results. The total stress state is deduced by

adding each of the stress increments which are equal to the combination of the normal and the deviatoric stress increments.

Palaniswamy and Shah [68] proposed a constitutive relationship based on the use of two concrete properties i.e. the bulk modulus and Poisson's ratio. These two material properties are considered to be a function of the invariants of the stress which were fitted to the test results.

Several other concrete models have been formulated and used by researchers. They have used different forms of the variations into the modulii in order to make the models more flexible in fitting the available data. For example, Phillips and Zienkiewicz [69] modelled the deformation of concrete subjected to compressive stresses using a constant tangent bulk modulus, K_t, and a variable tangent shear modulus, G_t, as a function of the second stress invariant, J_2. They also justify the use of a constant tangent modulus by the lack of available data.

The models which have been found to be the most effective in duplicating the behaviour concrete at the material level as opposed to the structural level appears to be those which utilise the three invariants of the stress (strain) tensor i.e. a full three-dimensional representation of the failure envelope [70, 71, 72].

Kotsovos and Newman [70] have used results from multiaxial tests [12] and decomposed the internal stresses into octahedral normal and deviatoric stresses and strains. They found that the volumetric deformation changes are a function of the normal and deviatoric stresses whereas the deviatoric deformation (volumetric distortion) changes are only a function of the deviatoric stress. They have consequently derived mathematical expressions for the variation in the bulk and shear modulii with respect to these stresses. A correction function that takes into account the volume changes which occur under deviatoric stresses was also determined and included in the expression below:

$$\sigma_{ij} = 2G\epsilon_{ij} + \frac{(3K - 2G)}{3}\epsilon_{kk} - \sigma_{oct} \tag{3.8}$$

The term σ_{oct} reduces the volumetric stresses which occur at a given strain due to internal cracking and dilation. σ_{oct} is a function of the octahedral shear stress and is found from tests. The values predicted using this model agree very closely with the experimental results for concrete under axisymmetric stress states.

Gerstle [72] proposed another form of octahedral stress-strain relationships for general multiaxial stress conditions which replicate earlier test results [12, 73]. The concrete material behaviour is modelled using three variable modulii. The

octahedral stress increments are related by the following constitutive relationships:

$$d\varepsilon_{oct} = \frac{d\sigma_{oct}}{3K(\sigma_{oct})} + \frac{d\tau_{oct}}{H(\sigma_{oct})}$$

$$d\gamma_{oct} = \frac{d\tau_{oct}}{2G(\tau_{oct})}$$

The three modulii K, G, and H are the tangent values which are related and dependent on either the current stresses or strains. The formulation tries to capture the variation in the internal stress previously observed [70], where a coupling modulus H is introduced which takes into account the fact that deviatoric stress causes volume changes prior to failure. This is actually the same argument used in the model developed for concrete by Kotsovos and Newman [70].

The variable modulii developed by Gerstle [72] appear to predict the response of concrete satisfactorily.

Ottosen [71, 74], used another form of the equivalent stress-strain relationship to model the multiaxial behaviour of plain concrete. In this model, the analysis is defined by introducing a non-linear index to satisfy a four parameter failure criterion in the three directions. The advantage of using the non-linear index apparently arises from the ability to permit the calculation of the tangent modulus at peak stresses for the three loading directions. The peak stress under uniaxial conditions is equal to the compressive strength of the concrete. However, under multiaxial stress conditions the compressive strength of concrete varies with

the state of the secondary transverse stresses, therefore the tangent modulii also varies with the stress conditions.

To correct and obtain the peak stress using the appropriate tangent modulus along the three directions, a surface in the stress space is used in which the principal stresses are substituted on the failure surface. The more compressive stress is increased while the other two remain constant until the failure criteria is satisfied in the three directions.

In the case of dynamic loadings the variable modulus formulations have been used in several studies. For example, Berriaud et al [75] have used variable modulii under biaxial stress conditions. The variation in the bulk modulus was approximated to a bilinear variation and the shear modulus was approximated to a trilinear variation. The concrete model has been used to investigate the behaviour of concrete members subjected to impact loading. They concluded that under high loading rates the concrete undergoes strain hardening in compression and in order to duplicate such a phenomenon it must be taken into account in the formulation. The two curves used by Berriaud et al [75] are shown in Figure 3.1.

To investigate the behaviour of concrete members subjected to impact loadings,

To investigate the behaviour of concrete members subjected to impact loadings,

Gupta and Seaman [76, 77] have used the theory of plasticity to model the concrete behaviour. They have used two yield surfaces to model the concrete behaviour under compressive and shearing stresses and a tensile fracture criterion to model the concrete behaviour under tensile stress. Broadhouse and Neilson [78] and Fleischer et al [79] have used a variable bulk modulus combined with a failure criterion. The stress calculations use a relationship similar to the one given by Equation 3.8. Typical approximations of the variations in the octahedral stress σ_{oct} with respect to the volumetric changes (expansion) ϵ_{oct} of the concrete material are shown in Figure 2.12. However, the shear modulus has been assumed to have a linear elastic variation. The approximation made in using a linear constant shear modulus may be justified by the type of failure which characterizes a structural concrete member subjected to impact loading.

Summary:

The non-linear elastic models are simple to use, and can usually predict the stress-strain response reasonably accurately if a broad data base for the concrete under investigation is available. However, their applicability is restricted to only particular types of stress conditions. This is because the material properties are determined from test results from concrete specimens which are normally recorded as the maximum stress is approached. The material properties of the concrete are then applied to concrete members which have different shapes and dimensions to the test specimens used to determine the material properties.

Nevertheless, it seems that all the restrictions do not cause major drawbacks in the utilisation of the non-linear models in the finite element analysis of concrete members. This is probably due to the fact that, even near the ultimate load, only a small portion of the concrete is subjected to a high compressive stress, and the majority of the non-linear behaviour is controlled by cracking of the concrete and yielding of reinforcing bars in tension.

The majority of the elasticity based concrete models have been developed and used primarily to represent the behaviour of concrete under static loadings. However, only a few of the elasticity based models have been found to be capable of modelling the behaviour of concrete under dynamic loadings, as well as static loadings, for example, the incremental orthotropic model developed by Pecknold and Darwin [67].

3.2.2 Endochronic Theory

Models based on the endochronic theory show promise since they attempt to model the influence of internal damage on the concrete material in a continuous manner without recourse to a yield condition or hardening rules.

The endochronic theory was initially developed to describe the mechanical behaviour of metals [80, 81]. The endochronic theory was originally based on visco-plastic formulations, supplemented by a new internal variable i.e. a pseudo-time scale referred to as intrinsic time. Constitutive equations in either integral or differential form are used to describe aspects of the behaviour of metals including strain hardening, loading, unloading and re-loading. The theory does not require specific definitions for the yield function, subsequent loading functions or hardening rules as is the case in the theory of plasticity. Bazant and Bhat [82] and Bazant and Shieh [83] have adopted and extended the endochronic approach to describe the behaviour of concrete. They derived an incremental form of the theory and later refined it to model the material behaviour of concrete under load.

Although the endochronic theory has been attacked, it seems that some phenomena like the influence of the loading history upon the variations in the stress-strain relationships, as well as the concrete strain rate dependency, are very well represented by this model. This is especially true for reinforcing steel.

It should however be emphasised that modelling concrete using the endochronic theory requires the determination of a large number of constants [84] so that the hardening, softening and dilation behaviour can be defined. In this context it can be concluded that the endochronic theory is more reliant on results obtained from tests on concrete specimens than any other approach.

On the other hand, a reduced number of constants are required in the concrete model based on the theory of plasticity and this is linked to the postulated rule for elastic-plastic material with work hardening. This approach is described in the following Sections.

3.2.3 Plasticity Based Models

Introduction :

Concrete experiences linear and non-linear deformations under compressive stress conditions. These deformations can be observed in the stress-strain variations shown in Figure 3.2. The curve can be assumed to develop in three stages i.e. (I) before yielding, (II) during the plastic flow stage, and (III) after failure.

(I) During this loading stage the material behaves in an almost linear manner until it reaches a yield point. The yield point is usually considered to be a fraction of the peak strength of the concrete under investigation [27].

(II) In this stage, the material is progressively damaged by internal cracking. The deformation is considered to be non-linear since after unloading only a portion of the total strain is recovered. This deformation is permanent, as shown in Figure 2.2(c) and is considered to occur as the result of strain

hardening.

(III) In recent years the stress-strain relationship in this stage has been under extensive investigation in order to determine whether it describes a physical property of the concrete material or other effects related to the test procedure. It has been argued by Kotsovos [85, 86] and by Van Mier [87, 26] that the descending branch of the curve shown in Figure 3.2 does not represent a property of the concrete material. It merely describes secondary testing effects resulting from the interaction between the testing machine and the test specimen. This is not the case according to Bazant [54] who has argued that strain softening does exist in concrete and other non homogeneous materials and that it is reproduceable in laboratory tests if the appropriate loading conditions are present. It was also noted that strain softening can only be observed on small concrete specimens loaded in compression as well as tension or shear, and using a sufficiently stiff testing machine. However more recent work [26] indicated that a less rigorous point of view must be taken. Although the structural effects on softening were found to be very pronounced, some of the observations on the post maximum strength response were attributed to material behaviour as well.

Stages II and III of the stress-strain curve are considered to represent a non-linear response which is due to plastic hardening and softening of the material. This

type of non-linear behaviour of concrete can be analysed using plastic formulations.

Several theories of plasticity can be formulated for use in the finite element method e.g. the deformation theory of plasticity, the incremental theory of plasticity and the theory of progressive fracture of solids.

Deformation Theory of Plasticity:

In the deformation theory of plasticity, the total strain tensor is used in the calculation of the stress tensor. The total strain tensor is decomposed into elastic and plastic components. The plastic component of the strain is calculated using scalar functions and hardening parameters. The deformation theory of plasticity has not been used for concrete in its classical form but in a modified form such as the rigid perfectly plastic models.

Incremental Theory of Plasticity:

The incremental theory of plasticity is based on three fundamental assumptions:

(1) The existence of an initial yield surface, loading surfaces and a failure surface.

(2) The formulation of an appropriate flow rule that specifies the stress-strain relationship in the plastic range.

(3) The formulation of suitable hardening rules that describe the evolution of loading surfaces between the initial yield and the failure surfaces.

When these assumptions are defined the elastic and plastic stress-strain relationships can then be established in incremental form. Unlike the deformation theory of plasticity the decomposition of the total strain into elastic and plastic components is made at increment level i.e.

$$d\varepsilon = d\varepsilon^E + d\varepsilon^P \tag{3.9}$$

where $d\varepsilon$ is the strain increment, $d\varepsilon^E$ and $d\varepsilon^P$ are the elastic and plastic strain increments respectively. The elastic component is recovered upon unloading while the plastic component remains as a permanent deformation in the material as shown in Figure 3.3.

One of the assumptions required in the formulation of the incremental or flow theory of plasticity is the existence of the loading function, f, which is dependent on the current stress conditions and a number of other variables such as the hardening parameters. The loading function is used in order to distinguish between loading involving plastic deformation and elastic unloading. The loading function provides the initial plastic yield surface and also the failure surface. The initial yield surface is identified by:

$$f = f(\sigma_{ij}, h) = 0 \tag{3.10}$$

The material at the level of the initial yield surface starts to experience plastic deformation. Below this level the material is assumed to behave in a linear elastic manner. f is a mathematical expression which is a function of stress and a property of the material, h, which determines the hardening. h is normally determined experimentally.

The loading functions can be interpreted as surfaces in the stress space. The sign of f is chosen so that interior points with respect to the surface i.e. $f < 0$ represents stress states for which the next increment of stress will cause purely elastic behaviour. When the points have a stress state which is on the yield surface, such that $f = 0$, a subsequent increment of stress may cause either purely elastic behaviour or lead to plastic deformation depending on the direction of the stress tensor increment. The available choices in the deformation of the material are shown in Figure 3.4 (b). It is evident from the above that elastic loading or unloading occurs when:

$$f \leq 0 \quad and \quad \frac{\partial f}{\partial \sigma_{ij}} d\sigma_{ij} < 0 \tag{3.11}$$

Alternatively, the material behaviour is accompanied by plastic deformation:

$$f = 0 \quad and \quad \frac{\partial f}{\partial \sigma_{ij}} d\sigma_{ij} > 0 \tag{3.12}$$

Various geometrical forms of the loading functions, f, have been proposed [27, 53, 55, 57]. In the triaxial principal stress space these surfaces can be divided into two categories, open and closed loading surfaces. Among the open loading surfaces is the Von Mises yield surface, which corresponds to a pure octahedral shear dependence. To account for the limited tensile capacity of concrete, the Von Mises surfaces are usually combined with a separate tensile failure surface i.e. the maximum stress surface or the tension cut off surface.

In the Drucker-Prager surface, the octahedral shear is linearly dependent on the octahedral normal stress. It can be looked upon as a modified Mohr-Coulomb surface. The latter has been used frequently as failure surfaces for concrete. The former surface has also frequently been used to model the behaviour of soils. There are two shortcomings of the Drucker-Prager surface when applied to concrete i.e. the linear relation between the octahedral shear and the octahedral normal stress and the independence of the third deviatoric stress invariant (θ). Experimental investigations have shown that the octahedral normal and shear stress relationships in the triaxial failure surface are curved, as shown in Figure 2.14.

Refinement of the Drucker-Prager surface has been proposed by Bresler and Pister [88] and Chen and Chen [89] where it has been assumed that there is a parabolic dependence between the octahedral normal and shear stresses. The deviatoric

plane is kept independent of the third deviatoric stress invariant i.e. a circular cross section in the deviatoric plane.

In the three-parameter surface proposed by Argyris et al [90], the surface retains the linearity between the octahedral normal and shear stresses but the deviatoric sections of the surface have non-circular forms i.e. the surface is dependent on the deviatoric stress invariants.

Four and five parameter failure surfaces have been developed [74, 91, 92]. The models have both a curved relationship between the octahedral normal and shear stresses ($\sigma_{oct} - \tau_{oct}$) as well as a non-circular cross section in the deviatoric plane i.e. θ-dependence. These models reproduce all the important features of the tri-axial failure surface of concrete and are in reasonable close agreement with the experimental data.

Before reaching the above failure surface,f, concrete passes through the onset of linear deformation which is given by the initial yield surface. It can be noted from experimental evidence, as shown in Figure 2.15, that the initial loading surface should be closed. The various closed loading surfaces which have been developed were based on this observation. They have been developed essentially to investigate the behaviour of soil-like materials. The formulation, therefore, includes pronounced compaction properties. The closed initial surface may be true for the

initial yield surface but the failure surface should be open as demonstrated by test results, as shown in Figures 2.13 and 2.14.

The evolution of a loading surface, f, during plastic deformation is described by specifying an appropriate flow rule. In the plastic range, the stress-strain relationships are established with the introduction of the plastic-potential function, g. The plastic strain increment vector is assumed to be proportional to the stress gradients of the plastic potential function, as follows:

$$d\varepsilon^P = d\lambda \frac{\partial g}{\partial \sigma_{ij}} \tag{3.13}$$

where $d\lambda$ is a positive scalar factor of proportionality. Equation 3.13 is known as the flow rule since it governs the progression of plastic deformation after the material has yielded. The gradient $\partial g/\partial \sigma$ defines the direction of the plastic strain increment vector and the length is determined by the factor $d\lambda$. When the the plastic potential function is assumed to be similar to the loading surface such as $f \equiv g$, Equation 3.13 becomes

$$d\varepsilon^P = d\lambda \frac{\partial f}{\partial \sigma_{ij}} \tag{3.14}$$

Elastic Perfectly Plastic Material Behaviour:

An elastic perfectly plastic material is defined by a material which shows elastic behaviour up to certain level of strength at which point the strain increases at constant stress. This level of strength is called the yield point for uniaxial stress

conditions and the yield surface for multiaxial stress conditions. The yield surface depends only on the state of stress and the effect of strain hardening is omitted from the constitutive relationships for the material. In the uniaxial representation the stress-strain curve beyond the initial yield point is approximated by a horizontal straight line with a constant stress level in compression as shown in Figure 3.4(a).

The elastic perfectly plastic stress-strain relationships have been used to model the behaviour of concrete in compression but with a limited amount of ductility i.e. the concrete fractures upon reaching its ultimate strain value. In the case of dynamic events such as impacts the influence of the loading rate can be taken into account by increasing the yield level in accordance with the rate of loading.

The concept of perfect plasticity has been used as a basis of the limit analysis techniques where the collapse load of a concrete member is determined. Although the concept does not represent the behaviour of concrete because of the yield plateau which is in conflict with the softening behaviour of concrete and the post maximum strength effects in general. It has led to a simple and practical procedure for the determination of the peak resisting capacity of different structural concrete members.

Elastic Plastic With Strain Hardening :

In the perfectly elastic plastic formulation only the initial yield surface is developed and remains fixed in the stress space i.e. $f \leq 0$ as shown in Figure 3.4(b). If as a result of a subsequent stress increment the loading at a point in the concrete is allowed to move outside the initial yield surface then f may take values greater than zero i.e. $f > 0$. The new response of the material beyond the yield surface is required to be specified. This response is called strain hardening plasticity and it is determined as a function of the current values of stress and strain and the hardening rules.

The hardening rules define the evolution of the loading surfaces in the stress space between the initial yield and failure surfaces therefore they must model all the loading surfaces. The hardening rules reflect the disturbance of the structure of the material due to the growth of internal micro-cracks up to the failure point and beyond.

Since no experimental work was available for the evaluation of the loading function, the progression for concrete in the stress space up to failure is generally based on hardening rules developed from mathematical functions which fit the concrete non-linear stress-strain curve. The hardening rules which are usually adopted in the incremental theory of plasticity [93, 27] are based on rules proposed earlier [94, 95]. They are as follows:

(1) Isotropic expansion which assumes that the loading surfaces grow uniformly without distortion as plastic flow takes place beyond the initial yield surface.

(2) Kinematic hardening expansion which assumes that during plastic deformation, the loading surfaces translate as a rigid body in space, maintaining the size, shape and the orientation of the initial yielding surface.

(3) The mixed hardening expansion is a combination of isotropic and kinematic hardening expansions. This is general strain hardening in which the loading surface experiences translation and uniform expansion, while it retains its original shape.

The choice of hardening rule appears to depend on the type of loading conditions which are applied to the member. Isotropic hardening should be used in the case of proportional loading but under dynamic loading conditions mixed isotropic and kinematic models should be used [93]. Furthermore the influence of the loading rate on the concrete can be taken into account during the calculation of the loading surfaces i.e. in the form of the hardening parameter, h.

Plasticity based models have been used extensively to describe the behaviour of concrete since Chen and Chen [89] set up a general framework for this type of modelling. These include the models developed by Owen and Figueiras [96] and Cervera and Hinton [97]. In these models, the formulation assumes elastic plastic behaviour with hardening effects up to the ultimate strength followed by

a perfectly plastic response until the failure surface is reached. Recently more refined approaches based on plastic-fracturing theory have been developed and used in modelling the post maximum strength response of concrete. They include the model developed by Hsieh et al [91]. Other researchers including, Chen and Schnobrich [98], Fardis et al [99], Vermeer and De Borst [100], Han and Chen [53], Glemberg et al [101] and Chen and Buyukosturk [102] have used the theory of plasticity to model concrete. These models differ from each other in the shape of the failure and the yield surfaces and in the hardening and flow rules.

3.2.4 Fracture, Damage and Stochastic Based Models

The behaviour characterised by the previous approaches is an approximation of the actual behaviour of concrete under load. The non-linear elastic and endochronic models rely very much on results obtained from laboratory tests on concrete specimens. Plastic analysis can be considered to be discontinuous because it is formulated in stages of loading but it represents a good concept for the modelling of the behaviour of a concrete member. This is because the theory of plasticity relies less on test results therefore, the uncertainties in the properties of reinforced concrete members are eliminated. On the other hand, it was concluded in Chapter 2, that concrete under load undergoes continuous degradation. For example, the elastic modulus and hence the stiffness of the concrete decrease with increased loading. This type of behaviour is considered to be due to the development of micro-cracking. Thus, an ideal material model would be a model

which uses a progressive fracture concept such as the model which has been proposed by Dougill [103, 104]. This ideal material is shown in Figure 3.5(b) which defines elastic perfectly elastic behaviour. Upon unloading, the material returns to its initial stress-free and strain-free states. No plastic strain occurs, since the degradation in stiffness is mainly due to cracking. This type of degradation of the concrete is different from hardening and softening behaviour and cannot be interpreted within the framework of the theory of plasticity. The model has been improved [53] after recognizing the difference between cracking and plastic flow, to a model referred to either as fracturing theory or damage theory.

A material exhibiting both plasticity and progressive stiffness degradation behaviour is shown in Figure 3.5(c). Concrete falls into this category, particularly in its softening range. To account for both types of behaviour, a combined theory referred to as the plastic-fracturing theory was proposed by Bazant and Kim [105].

Models based on damage theory are relatively new particularly for concrete. They are based on the concept that damage occurs as permanent degradation of the material under deformation. A damage parameter is introduced as a scalar or vectorial function for this degradation process which is, in comparison with fracture mechanics, a continuous and global process and not a degradation process which is only due to the presence of cracks.

Another method formulates the fracture process within the matrix of concrete using a stochastic formulation. In this case concrete is modelled as a group of n elements with two or three different relationships representing random behaviour. As the failure of concrete under compression is also governed by its resistance to the tensile stresses under multiaxial stress conditions, the relationships are applicable to both compression and tension.

3.2.5 Summary

The following conclusions are based on the above descriptions:

(1) The hyperelastic models are the simplest approaches to concrete modelling.

These models have been found not to be capable of modelling the behaviour of concrete near or at its failure point in compression.

(2) The hypoelastic models based on the concept of variable modulii are a good fit for the results from a number of tests i.e. uniaxial, biaxial and triaxial data under proportional loading. Non-linear elasticity models based on a variable bulk modulus have recently been used in the analysis of concrete members subjected to dynamic loading. However, it has been suggested [1], that in general they are not suitable for the analysis of a concrete member subjected to impact or impulsive loadings because very little non-linear deformation is captured. A similar statement can be made for the hyperelastic models.

(3) The endochronic theory is considered to be a powerful approach through the concept of intrinsic (endochronic) time which is used to measure the extent of damage of the internal structure of the concrete when it is deformed. However, the approach involves many functions and constants which are obtained by complicated curve fitting procedures in order to obtain at a successful solution.

(4) The increment theory of plasticity almost satisfies the non-linear behaviour of concrete including loading and unloading. Although, the resulting solution is considered to be discontinuous because it is iterated in discontinuous stages of loading it still represents a good concept in the modelling of structural concrete. This is because the theory of plasticity relies less on test results and therefore, the uncertainties in the properties of reinforced concrete members are avoided.

Furthermore, if the increment theory of plasticity is combined with the following features it can be considered to satisfy the basic behaviour of concrete as a material when subjected to loading:

(1) a failure criterion that replicates the variation in strength under multiaxial stress conditions;

(2) a model which takes account of the degradation in the concrete strength after failure.

Rate effects can be introduced by using a non-associated potential function which describes the effect of the speed of loading on the concrete or by introducing a hardening parameter which takes this effect into account.

3.3 CRACKING MODELS

It has been shown earlier that the propagation of a fracture constitutes a major nonlinear factor in the behaviour of concrete. The modelling of fractured concrete has also been found by several researchers to play an important role in the stability of the solution in the finite element analysis of reinforced concrete members.

The fracture of concrete may be classified as crushing or cracking. Under compressive stresses, the crushing type of fracture is characterised by progressive degradation of the internal structure of the material. Crushing is assumed to occur when the compression deformation capacity of the material is exceeded. In the case of multiaxial loading, the ultimate deformation level is usually modelled by the failure function envelopes, f, in either stress or strain space. At the point at which concrete is crushed all the stresses are released completely and the concrete loses its stiffness in all directions.

The cracking type of fracture is governed by tensile stress and it is characterised by propagation of the existing micro-cracks and the subsequent formation of bridges between these cracks which results in the development of a failure plane. On the

formation of a crack the concrete experiences partial loss of stiffness in the plane of failure which is usually modelled by gradually releasing the normal and the shear stresses across the failure plane. In the case of triaxial stress conditions, the cracked element is able to carry stress under biaxial or uniaxial stress conditions. Eventual complete loss of the concrete element occurs when cracks form in all three directions.

The initiation of a crack in the concrete is generally modelled after a fracture criterion has been violated. Several types of fracture criterion are used, these are the maximum principal stress criterion, the maximum principal strain criterion and the dual criterion which is determined as a function of both the maximum principal stress and strain as follows:

$$\sigma_1 \geq 0 \tag{3.15}$$

$$\varepsilon_1 \leq 0$$

A crack is assumed to form in a plane normal to the principal stress where the stress has exceeded a limiting value of the tensile strength of the concrete. After cracking the material stiffness decreases progressively. A number of approaches have been used to describe the loss in stiffness after the concrete element has cracked (post-cracking behaviour of the concrete) [57]. They can be described as a function of the release of strength or energy. These approaches are described in the following Section.

3.4 POST CRACKING MODELS

Earlier post cracking models were based on an elastic brittle criterion. The concrete is linear elastic in tension until the principal stress at a Gauss integration point exceeds the tensile strength, f_t', of the material. At that point, all of the first principal stress is released i.e. perfectly brittle response as shown in Figure 3.6(a). The element does not provide any resistance at right angles to the direction of the crack, however, a fraction of the shear strength is retained along the crack plane. Although numerical instability is thought to arise from the sudden change in equilibrium resulting from the sudden stress release, the method has been adopted and has given good results over a wide range of problems [27, 106, 107].

To remedy the above instability and bring about a smoother numerical response a second strength criteria has been developed. A plastic fracturing model as shown in Figure 3.6(b) has been developed, which assumes that once the principal stress exceeds the tensile strength of the material, a crack forms, however the material at that point retains a residual stress equal to that strength. It thus represents elastic perfectly plastic behaviour in tension except that the stiffness perpendicular to the crack is set to zero. Suzuki and Chen [108] claim to have used this model successfully.

Cracking in plain and reinforced concrete members is believed not to be a perfectly brittle response or a response with a plateau strength because experimental evidence has shown that the stresses normal to the cracked plane are gradually released as the crack width increases. This type of behaviour is shown in Figure 3.6(c). To model this gradual release of stresses a fracture energy criterion has been proposed by Bazant and Cedolin [109, 110] in which the principles of fracture mechanics have been applied to concrete as a material. The basis of the approach is that during loading concrete is damaged progressively and hence energy is dissipated and cracks (smeared or discrete) propagate as a function of the rate of the release of energy during the damage process. Many of the characteristics of the internal behaviour of a structural concrete member such as post-maximum strength effects on the concrete strength, bond slip between the concrete and the reinforcement have been included using this method. However, in all the cases studied the method has in every way invalidated the approaches based on the release of the concrete strength using the elastic brittle criterion. Bazant and Cedolin [111] stated that post-cracking based on the release of the concrete strength are correct if accurate relationships for the cracked concrete element are implemented.

The post-cracking response of concrete after a crack has formed is usually modelled in the finite element method using either the tension stiffening concept or the strain softening concept.

3.4.1 Tension Stiffening

Concrete is a weak material in tension, therefore steel reinforcing bars are placed in the tensile zone so that the strength of the concrete member can be enhanced. At ultimate loading the reinforced concrete member cracks after the tensile strength of the concrete is reached. The number and severity of the cracks are controlled by the size, position and orientation of the steel bars. Near the crack the concrete strength is decayed to zero and the steel bars carry all the tensile forces. However, a proportion of the tensile forces is transferred back to the concrete between the cracks as a result of bond between the steel bars and the concrete. The ability of the concrete to retain some of the tensile forces is called tension stiffening but it diminishes as the distance from the steel bars increases.

Tensile stiffening was introduced by Lin and Scordelis [112] and Gilbert and Warner [113] who proposed a descending branch to the stress-strain curve beyond the peak tensile strength. The tension stiffening models can be considered to be relevant to the smeared crack element representation because of the effect of the loss in stiffness resulting from a fracture in the concrete. The fracture is spread over a finite concrete area where some stiffness would, in fact, exist. This stiffness gives the descending branch of the stress-strain curve which has been modelled using linear, bilinear and non-linear relationships by many researchers [97, 114, 115].

3.4.2 Strain Softening

The stress-strain relationship for concrete test specimens under tensile stress conditions is mainly controlled by the propagation of the micro-cracks after failure has occurred. Additional deformation in the test specimen will be concentrated near the crack tips i.e. the deformation is localized around the fracture zone. The strength of the concrete at the fracture zone gradually decreases as the strain increases. This type of behaviour in the concrete results in the development of the descending part of the stress-strain curve. At a distance from the crack tips the concrete undergoes unloading as the crack forms. Peterson [10] has proposed the use of a stress-crack width relationship for concrete in the fracture zone, as shown in Figure 3.7, and a stress-strain relationship remote from the fracture zone to model the strain softening. This type of model has been used successfully in several studies [10, 78, 116]

3.4.3 Shear Retention

Suidan and Schnobrich [117] have found in the finite element analysis of reinforced concrete members that when the stiffness is reduced after the formation of a crack at the sampling stress point no shear is retained along the crack then the reliability of the results obtained is questionable. Later, experimental evidence revealed that there is a rapid fall in the value of the shear modulus after cracking [118].

The shear retention (transfer of shear forces across the crack) takes place once a crack plane has formed. The texture of the surface of the crack plane is an important parameter. This is because there may be constraints present along the crack surface which prevent the separated sections of the concrete member from moving apart thus the surface is capable of transferring some shear force. Aggregate particles which are present in the contact surfaces will normally provide the necessary restraints. It has been estimated that in an inclined fractured surface cracked concrete can still transfer an average of approximately 50% of the shear because of the relative movement between the surfaces of the structural concrete member.

The following approaches have been used to take account of shear retention in a post maximum strength model:

(1) The amount of shear which should be retained is proportional to the shear modulus which is equal to βG, where $0.1 < \beta < 0.6$. A value of $\beta = 0.4$ has been recommended [119].

(2) Another method of including shear transfer in a cracked region has been proposed in which a variable shear retention is used. Cedolin and dei Poli [63] put forward a linear relationship as a function of the maximum principal tensile strain.

(3) Shear transfer can also be included in the calculation of the strength of a

cracked concrete element using a relationship between the size of the aggregate particles and the crack width. This relationship is called aggregate interlock. The amount of shear which can be retained is expressed in terms of aggregate interlock relationships defined by the curve shown in Figure 3.8.

(4) In another study Kotsovos et al [120] found that high shear retention causes a local weakening of the concrete at a given crack and thus suggested that the aggregate interlock concept may be questionable. Later in three dimensional analysis Kotsovos et al [86] used a value of $\beta = 0.1$ in order to eliminate this effect.

3.4.4 Finite Element Representation of Cracks

In the application of the finite element approach to fracture problems, two basic forms of crack formulation are available. The first and the most obvious is the discrete crack formulation, which follows the propagation of one or more specific cracks through a member. There are three basic implementations of the discrete crack formulation, all of which influence the layout of the finite element mesh. The earliest approach allowed cracks to propagate between elements in a fixed mesh (topology). In other words when the appropriate failure criterion for the initiation of cracks in the concrete element was satisfied, connecting nodes were disconnected so that adjacent elements can separate, as shown in Figure 3.9(a).

Indeed in some early applications to concrete, not only was the layout of the finite element mesh fixed, but the inter-element crack positions were predefined [121].

The second approach used the development of singular elements to model the singularity at the crack tip. Different devices were used e.g. an additional singular shape function (e.g. 1/r), or a degenerated isoparametric element [122, 123]. The singular element can be used either with an inter-element approach or when a crack is allowed to propagate across an element. The latter requires redefinition of the finite element mesh topology since elements are subdivided after the propagation of a crack. This concept led to the development of the third approach which is based on adaptive refinement.

The application of the discrete crack modelling approach to concrete members has generally involved a fracture associated with a single crack in the analysis of the behaviour of structure such as pressure vessels or in the analysis of the bond forces between the reinforcing bars and the concrete. The major drawback of the approach is associated with the selection of the single crack to be included in the model.

Furthermore, it is inappropriate to decide a priori which crack is going to be critical during the loading of a structural concrete member in order to reduce the number of cracks to be modelled. In any case, it is the crack pattern which

determines the response of the concrete member, and not necessarily the presence of a single crack.

The second basic crack formulation uses a smeared or continuous crack approach which assumes that once the cracking criterion has been satisfied a number of cracks open at the appropriate angles over an area around the integration points. The number of cracks is dependent on the points used in the integration of the solution. Figure 3.9(b) shows two finite elements with one and nine integration points. If only one integration point is used, the smeared crack covers the entire element, whereas when nine integration points are used, the crack formed covers a discrete zone around the integration point, as shown in Figure 3.9(b).

Once a crack is deemed to have opened the stresses are transformed in the direction of the cracked plane and the stiffness at right angles to the crack is either reduced or eliminated. Therefore, the smeared crack approach is based on the inability of the concrete material to carry tensile loads normal to a crack plane. This inability to transmit stresses is taken into account by changing the material properties such as the elasticity matrix D from an expression defining isotropic material behaviour to one defining anisotropic material behaviour.

The primary advantages of the smeared crack formulation are that it is relatively inexpensive in terms of computer processing time compared to the discrete crack

formulations particularly those which use the adaptive approach. The smeared or continuous crack approach is mainly criticised for the lack of detailed information provided on the crack pattern in a coarse finite element mesh. However, these artificial cracks can give a good overview of the crack pattern, which is often all that is required. In addition, as Bazant [111] has pointed out, better resolution can be obtained by refining the mesh topology using an appropriate strategic approach.

It is interesting to note that the basis of the smeared crack approach is to allow the occurrence of as many cracks as possible. This idea is in agreement with the approach adopted in numerical analysis because an exact numerical integration of the stiffness of an element is found with the number of Gauss points required for the order of that element. Furthermore the Gauss points are generally the stress sampling points at which cracks are presumed to form. Therefore the higher the order of the element the greater is the accuracy of the numerical integration and hence the improvement in the smearing of the pattern of cracks. For example a constant strain element allows one cracked point, a bilinear element four cracked points and a parabolic element a maximum of nine cracked points. In two dimensions two cracks can open at any point, in three dimensions up to three cracks can open at any point as shown in Figure 3.9(c). A full integration of the eight node solid element will result in a possible 12 cracks.

However, multiple cracked elements have been reported to generate a higher degree of nonlinearity. Gupta and Akbar [124], Baker and Edwards [125] have found that multi-cracking in four node and eight node isoparametric elements increases the degree of nonlinearity which gave rise to erratic results and even unstable behaviour. They argue that the angles of the principal stresses at the sampling points generate too much nonlinearity for a stable solution. Gupta and Akbar [124] and Baker [119] used reduced integration for bilinear and linear elements for concrete and reported excellent results for the bending and shear deformations. Crisfield [126] and Baker [119] did, however, express concern that reduced integration could give rise to spurious mechanisms (hourglass modes). Later Gonzalez Vidosa et al [86] appeared to obtain better results using under-integrated 20 node solid elements in a nonlinear elastic analysis.

On the other hand, May and Al-Ramadhani [127] have studied the effect of integration on the stability of cracked eight node isoparametric elements. They have reported [124, 125] similar spurious deformations before the ultimate capacity of the concrete member was reached. They then proposed five and three by three integration points to eliminate the spurious modes in the cracked concrete elements.

More work is needed in this area of numerical analysis because other research work [128, 129] has demonstrated that spurious deformations can occur even if the finite elements are fully integrated. It has been claimed [128, 129] that

the spurious deformations were triggered by the presence of the strain softening capability in the formulation for the concrete.

3.4.5 Concluding Remarks

In view of the above discussion and the uncertainties associated with the specification of the material properties which were discussed in Chapter 2, relatively simple constitutive models expressed in terms of the available uniaxial properties of concrete will be developed. The new model will use a triaxial stress formulation which is based on a four parameter failure criterion combined with the incremental theory of plasticity.

The stress-strain relationship for concrete in compression will be modelled using an elastic-plastic strain hardening model accompanied by fracture of the material at the ultimate strength. The direction and magnitude of the plastic straining will be governed by the normality condition of an associated flow rule and isotropic and kinematic hardening rules.

In tension, the concrete will be assumed to be elastic until cracking takes place. Cracking of the concrete will be controlled by the maximum stress criterion. Up to three orthogonal cracks will be allowed to form at the sampling points. Closing and reopening of the cracks will be permitted in this formulation in order to simulate the subsequent modal deformations which occur as the member vibrates.

Failure will be determined using a crushing coefficient function of the three invariants of the stress tensor. The complete model can be described to have an elastic-plastic fracture formulation

3.5 CONCRETE MODEL ADOPTED

Introduction

The formulation of the elastic-plastic fracture model for concrete which has been developed for this investigation is described in this Section. The concrete stress-strain relationship is assumed to be linear elastic until a stress combination reaches the initial yield surface. The initial yield surface has a similar geometrical shape to the failure surface but reduced in size. The failure surface adopted for this investigation is a four parameter failure criterion [91]. Incremental stress-strain relationships are developed as a function of a strain hardening model and a flow rule in order to define the plastic behaviour of the concrete between the initial yield surface and the failure surface.

Failure of the concrete is determined using a crushing coefficient which is based on a dual criterion. Three different modes of failure can be identified by the crushing coefficient i.e. cracking, crushing and mixed cracking, and crushing modes. The failure of the concrete is represented by three dimensional smeared cracking.

After failure the concrete undergoes stress release. Figure 3.10 shows the idealisation of the elastic-plastic fracture model in terms of uniaxial stress conditions.

In the following Sections the principal parameters involved in the derivation of the concrete model are discussed.

3.5.1 Failure Surface

Concrete as a material can be assumed to be a homogeneous and to have isotropic behaviour at the macroscopic level. This implies that the concrete strength envelope (failure surface), can be defined using a mathematical function in which the variables are independent of the choice of the coordinate system i.e. the stress invariants. In the case of triaxial stress conditions, the failure surface is dependent on three invariants of the stress. Equation A.5 in Appendix A has been written in terms of the Haigh-Westergarrd coordinate system as follows:

$$f(\xi, \rho, cos3\theta) = 0 \tag{3.16}$$

where

$$\begin{aligned} \xi &= \frac{1}{3} I_1 \\ \rho &= \sqrt{2J_2} \\ cos3\theta &= \frac{3\sqrt{3}}{2} \frac{J_3}{J_2^{3/2}} \end{aligned} \tag{3.17}$$

Equation 3.16 describes a surface which represents an envelope of all the stress conditions that can be reached by incremental elastic deformations. It can be noted from the geometry of the failure surface in the deviatoric plane that there is a form of symmetry. It is then sufficient to describe the failure surface by a parabolic sector of the surface while the other sectors are known because of symmetry, as shown in Figure 2.14. The parabolic portion is defined in this case between $\theta = 0$ and $\theta = 60^0$ for principal stress conditions given by $\sigma_1 > \sigma_2 > \sigma_3$. The parabola will have all the characteristics of the envelope along the octahedral axis. It varies from almost a straight line for the case when the octahedral stress is zero to a circular arc for high compressive octahedral stresses. The intermediate shape is given by the function below:

$$f(\xi, \rho, \theta) = a\rho^2 + \lambda(\theta)\rho + d\xi + 1 = 0 \tag{3.18}$$

$$\lambda(\theta) = bcos\theta + c \tag{3.19}$$

The expressions for the parabola in Equations 3.18 and 3.19 are defined by four constants a, b, c and d which are determined from the results of tests on a specific concrete.

Equation 3.18 can be written in terms of the stress invariants I_1, J_2, and J_3 by using the expression in Equation 3.17 as well as the relationship between ρ and J_2 found in the equation for the first principal stress σ_1 i.e.

$$\sigma_1 = \frac{1}{\sqrt{3}}\xi + \sqrt{\frac{2}{3}}\rho cos\theta$$

$$\rho cos\theta = (\sqrt{3/2}\sigma_1 - I_1/\sqrt{6})$$

Equation 3.18 will then have the following form:

$$A\frac{J_2}{f_c'^2} + B\frac{\sqrt{J_2}}{f_c'} + C\frac{\sigma_1}{f_c'} + D\frac{I_1}{f_c'} - 1 = 0 \qquad (3.20)$$

In Equation 3.20 σ_1 is the maximum principal stress with a positive stress value representing a tensile stress. A, B, C and D are four new material constants which are functions of the constants a, b, c and d in Equation 3.18. f_c' is the uniaxial compressive strength of the concrete under consideration.

Initial Yield and Loading Surfaces:

In these elastic-plastic formulations the initial yield surface has a similar shape to the failure surface but reduced in size. The material constants therefore remain the same, except that the limiting values are those which define the onset of nonlinear deformation. The region below the initial yield surface for the concrete is formulated using linear elastic stress-strain relationships. For stress conditions above the initial yield surface concrete experiences permanent deformation and

the stress-strain relationships must then be changed from linear elastic to plastic.

In order to construct plastic stress-strain relationships in an incremental form the following characteristics must be defined:

(a) a loading surface which determines the current state of plasticity in the material;

(b) strain hardening rules which determine the evolution of the loading surfaces;

(c) a flow rule which determines the direction of the plastic deformation.

The function which defines the loading surfaces is determined assuming that the plastic potential function, f, in Equation 3.14, has a similar form to the initial yield surface. A specific form of the loading function, f, for concrete may be expressed as follows:

$$f(\overline{\sigma}_{ij}, \tau) = \frac{A\overline{J}_2}{\tau(\epsilon_P^i)} + B\sqrt{\overline{J}_2} + C\overline{\sigma}_1 + D\overline{I}_1 - \tau_(\epsilon_P^i) = 0 \qquad (3.21)$$

where the stress invariants are:

$$\overline{I}_1 = \overline{\sigma}_{ii} \qquad (i = 1,2,3)$$

$$\overline{J}_2 = \tfrac{1}{2}\overline{s}_{ij}\overline{s}_{ij} \qquad (i = 1,2,3 \text{ and } j = 1,2,3)$$

in which

$$\overline{\sigma}_{ij} = \sigma_{ij} - \alpha_{ij}$$

$$\overline{s}_{ij} = s_{ij} - \alpha_{ij} + \frac{1}{3}\delta_{ij}\alpha_{ij}$$

where s_{ij} is the deviatoric stress tensor, $\overline{\sigma}_1$ is the maximum principal value of the stress tensor σ_{ij} and δ_{ij} is Kronocker delta where:

$$\delta_{ij} = 1 \text{ for } i = j \text{ and } \delta_{ij} = 0 \text{ for } i \neq j$$

α_{ij} is the tensor which characterizes the translation of the centre of the loading surface as shown in Figure 3.11. $\tau(\epsilon_p^i)$ is an isotropic hardening function. ϵ_p^i is the equivalent plastic strain due to isotropic hardening.

Figure 3.11 shows the initial yield surface, the evolution phases of the loading surface and the failure surface for biaxial stress conditions. To model the behaviour of concrete under cyclic loading and unloading conditions, the movement of the loading surface is allowed to follow a mixed hardening model. The failure surface encloses all the loading surfaces and serves as the upper bound surface. The initial yield surface is the lower bound for the subsequent loading surfaces. The failure surface remains unchanged during the entire loading process. During plastic deformation, the loading surface expands and changes its shape from the initial yield surface to the final shape which either coincides with or intercepts the failure surface. Each loading surface is characterized by the strain hardening

intensity.

3.5.2 Strain Hardening in Concrete

Concrete strain hardening occurs after the stress conditions have reached the plastic zone. In the present investigation, a mixed strain hardening model is adopted because the concrete model is intended to be used for reinforced concrete members subjected to dynamic loading conditions. Mixed strain hardening implies that isotropic and kinematic hardening relations are required which allow the loading surfaces to expand and to translate from the original initial yield surface until they intercept the failure surface. The failure surface is fixed in the principal stress space at some distance from the initial yield surface.

The loading surfaces defined by Equation 3.21 are continuous. Taking advantage of the condition of consistency of the function f the equivalence below is true:

$$f(\overline{\sigma}_{ij}, \tau) = 0 \qquad \Rightarrow \qquad df(\overline{\sigma}_{ij}, \tau) = 0$$

The shapes of the loading surfaces remain unchanged during their expansion and translation in the stress space, as shown in Figure 3.11. Thus, the differential of the function which gives the initial yield surface and the differential of the current loading surface are equal, hence:

$$\frac{\partial f(\overline{\sigma}_{ij}, \tau)}{\partial \overline{\sigma}_{ij}} = \frac{\partial f(\sigma_{ij}, \tau)}{\partial \sigma_{ij}}$$

The complete differential of Equation 3.21 can now be explicitly written as follows:

$$\begin{aligned} df(\overline{\sigma}_{ij}, \tau) &= 0 \\ \frac{\partial f}{\partial \sigma_{ij}} d\sigma_{ij} + \frac{\partial f}{\partial \sigma_{ij}} d\alpha_{ij} + \frac{\partial f}{\partial \tau} d\tau &= 0 \end{aligned} \tag{3.22}$$

Equation 3.22 is used to determine $d\lambda$ the positive scalar constant which defines the flow rule i.e. Equation 3.14. The explicit formula for $d\lambda$ is given at the end of this Section. The effect of the kinematic and the isotropic hardening is determined by letting the plastic strain increment $d\varepsilon_{ij}^{P}$ be divided into a linear combination of a plastic strain due to the isotropic hardening strain $d\varepsilon_{ij}^{i}$ and a plastic strain due to the kinematic hardening strain $d\varepsilon_{ij}^{k}$ as follows:

$$d\varepsilon_{ij}^{P} = d\varepsilon_{ij}^{i} + d\varepsilon_{ij}^{k} \tag{3.23}$$

$$= M d\varepsilon_{ij}^{P} + (1 - M) d\varepsilon_{ij}^{P} \tag{3.24}$$

where M is a material parameter which defines the isotropic hardening effects. The indices i and k in Equation 3.23 indicate the isotropy and kinematic effects respectively. The parameter M governs the type of hardening as is clearly shown in Equation 3.24 i.e. if $M = 1$ then the material experiences pure isotropic hardening. If $M = 0$, the hardening experienced in the material is pure kinematic. A value between 0.0 and 1.0 invokes mixed hardening. The amount of isotropic or kinematic hardening strain produced in any material under any stress conditions is relatively difficult to determine. Nevertheless, it is translated by the value given to M. Values of M equal to either 0.15 or 0.20 have been recommended

by Axelsson and Samuelsson [93] for metals using a curve fitting procedure. No corresponding data for the determination of a value for M for concrete has been reported in the literature.

$d\lambda$ is calculated from Equation 3.22 and is determined using the following three steps:

(1) The first term $(\partial f/\partial\sigma)d\sigma$ is obtained using the total strain increment, Equation 3.9, which is taken to be the sum of the elastic increment and the plastic increment as follows:

$$\frac{\partial f}{\partial\sigma}d\sigma = \frac{\partial f}{\partial\sigma}D(d\varepsilon - d\lambda\frac{\partial f}{\partial\sigma}) \tag{3.25}$$

(2) In order to obtain the kinematic hardening model which is valid for the stress space, Ziegler [95] derived the following relationships:

$$\begin{aligned} d\alpha &= du(\sigma - \alpha) \\ &= du\overline{\sigma} \\ &= cd\varepsilon^k\overline{\sigma} \\ &= c(1-M)d\varepsilon^P\overline{\sigma} \end{aligned} \tag{3.26}$$

In the case of a smooth loading surface the strain increment is linear in the stress space and therefore:

$$
\begin{aligned}
d\varepsilon^P &= \sqrt{d\varepsilon^P d\varepsilon^P} \\
d\varepsilon^P &= d\lambda \sqrt{\frac{\partial f}{\partial \sigma}\frac{\partial f}{\partial \sigma}} \\
d\varepsilon^P &= d\lambda R
\end{aligned} \tag{3.27}
$$

where:

$$
R = \sqrt{\frac{\partial f}{\partial \sigma}\frac{\partial f}{\partial \sigma}}
$$

Substitution of Equation 3.27 in Equation 3.26 gives the relation for kinematic hardening and as a result the second term in Equation 3.22 is defined as follows:

$$
\frac{\partial f}{\partial \sigma} d\alpha = \frac{\partial f}{\partial \sigma} c(1-M) d\lambda R \bar{\sigma} \tag{3.28}
$$

(3) The last term in Equation 3.22 is obtained by differentiating Equation 3.21 with respect to the effective stress increment τ which is a fraction of the plastic strain increment associated with isotropic hardening. It can be noted from Equation 3.24 that the isotropic hardening is related to the effective plastic strain as follows:

$$
d\varepsilon^i = M d\varepsilon^P
$$

Now the effective plastic stress corresponding to the effective plastic strain is:

$$d\tau = \overline{H} M d\varepsilon^P \tag{3.29}$$

$$d\tau = \overline{H} M \sqrt{d\varepsilon^P d\varepsilon^P}$$

$$d\tau = \overline{H} M d\lambda \sqrt{\frac{\partial f}{\partial \sigma}\frac{\partial f}{\partial \sigma}}$$

where $\overline{H}$ is the plastic tangent modulus which is obtained from the stress-strain curve for the concrete under investigation. $\overline{H}$ determines the shape of the stress-strain curve and the non-linear behaviour experienced by the concrete. The differential of Equation 3.21 with respect to τ is then

$$\frac{\partial f}{\partial \tau} d\tau = \frac{\partial f}{\partial \tau} \overline{H} M d\lambda R \tag{3.30}$$

The explicit form of Equation 3.22 is given below from which $d\lambda$ is obtained:

$$\frac{\partial f}{\partial \sigma} D(d\varepsilon - d\lambda \frac{\partial f}{\partial \sigma}) + \frac{\partial f}{\partial \sigma} c(1-M) d\lambda R\overline{\sigma} - \frac{\partial f}{\partial \tau} \overline{H} M d\lambda R = 0 \tag{3.31}$$

Hence,

$$d\lambda = \frac{\frac{\partial f}{\partial \sigma} D d\varepsilon}{(\frac{\partial f}{\partial \sigma})^T D \frac{\partial f}{\partial \sigma} + Rc(1-M)\frac{\partial f}{\partial \sigma}\overline{\sigma} - R\overline{H} M \frac{\partial f}{\partial \tau}}$$

3.5.3 Flow Rule

In the incremental form of plasticity a flow rule must be defined so that the plastic strain increment can be determined for a given stress increment. Concrete has been found to exhibit volumetric deformation changes as a function not only of the normal stresses but also of the deviatoric stresses [12, 73]. Therefore, the directions of the plastic stresses are not always perpendicular to the loading surface for the current stress conditions. However, the associated flow rule which defines a plastic stress increment normal to the current loading surface has been widely applied in concrete models because it is relatively easy to formulate. This approach is adopted in the model which has been developed in this investigation.

The only component which has not yet been defined in Equation 3.14 is the normal to the current loading surface i.e. the gradient of which is $\partial f/\partial \sigma$. It is obtained by applying the chain rule of differentiation to the loading function given by Equation 3.21 with respect to the components of the stress tensor as follows:

$$\frac{\partial f}{\partial \sigma} = \frac{\partial f}{\partial I_1}\frac{\partial I_1}{\partial \sigma} + \frac{\partial f}{\partial J_2}\frac{\partial J_2}{\partial \sigma} + \frac{\partial f}{\partial cos3\theta}\frac{\partial cos3\theta}{\partial \sigma} \tag{3.32}$$

After differentiation for all the variables and algebraic manipulation the terms of Equation 3.32 are obtained:

$$\frac{\partial f}{\partial I_1} = B'/f_c$$

$$\frac{\partial f}{\partial J_2} = \frac{\partial}{\partial J_2}\left(\frac{AJ_2}{f_c^2} + \frac{\lambda\sqrt{J_2}}{f_c}\right)$$

$$\frac{\partial f}{\partial cos3\theta} = \frac{C'}{3}\frac{\sqrt{J_2}}{f_c}\frac{sin\theta}{sin(3\theta)}$$

and

$$\frac{\partial I_1}{\partial \sigma} = \{\, 1 \;\; 1 \;\; 1 \;\; 0 \;\; 0 \;\; 0 \,\}^T$$

$$\begin{aligned}\frac{\partial J_2}{\partial \sigma} &= \frac{\partial J_2}{\partial s_x}\frac{\partial s_x}{\partial \sigma} + \frac{\partial J_2}{\partial s_y}\frac{\partial s_y}{\partial \sigma} + \frac{\partial J_2}{\partial s_z}\frac{\partial s_z}{\partial \sigma} \\ &+ \frac{\partial J_2}{\partial \sigma_{xy}}\frac{\partial \sigma_{xy}}{\partial \sigma} + \frac{\partial J_2}{\partial \sigma_{yz}}\frac{\partial \sigma_{yz}}{\partial \sigma} + \frac{\partial J_2}{\partial \sigma_{zx}}\frac{\partial \sigma_{zx}}{\partial \sigma}\end{aligned}$$

$$\frac{\partial cos3\theta}{\partial \sigma} = \frac{\partial cos3\theta}{\partial J_3}\frac{\partial J_3}{\partial \sigma} + \frac{\partial cos3\theta}{\partial J_2}\frac{\partial J_2}{\partial \sigma}$$

Details of the derivation of the terms in Equation 3.32 are given in Appendix B

3.5.4 Incremental Stress-Strain Relations

The total strain increment is given by Equation 3.9. The plastic strain increment $d\varepsilon^P$ is obtained using the scalar constant $d\lambda$ and the gradient $\partial f/\partial\sigma$ which have both been defined in the previous Sections. According to Hooke's law, the stress is determined by:

$$\begin{aligned} d\sigma &= D d\varepsilon^E \\ d\sigma &= D(d\varepsilon - d\varepsilon^P) \\ d\sigma &= D(d\varepsilon - d\lambda\frac{\partial f}{\partial\sigma}) \end{aligned} \tag{3.33}$$

The explicit form of the elastic-plastic stress-strain relation is obtained by utilising the expression for $d\lambda$ in Equation 3.33 as follows:

$$d\sigma = \{D - \frac{D\frac{\partial f}{\partial\sigma}\frac{\partial f}{\partial\sigma}D^T}{(\frac{\partial f}{\partial\sigma})^T D\frac{\partial f}{\partial\sigma} + Rc(1-M)\frac{\partial f}{\partial\sigma}\overline{\sigma} - R\overline{H}M\frac{\partial f}{\partial\tau}}\}d\varepsilon \tag{3.34}$$

or

$$d\sigma = D^{EP} d\varepsilon \tag{3.35}$$

The plastic stress-strain relationship D^{EP} in Equation 3.35 is a symmetric six by six matrix, 36 components, but only 21 components are derived explicitly. The

derivation of D^{EP} is given in detail in Appendix B

$\overline{H}$ and c are two material constants. They are always related to the results from the standard concrete test specimens normally used in quality control tests. The method of calculation for $\overline{H}$ and c is given in detail in Appendix C.

D is the elasticity matrix and D may be expressed as a function of the bulk modulus K and the shear modulus G or Young's modulus E and Poisson's ratio ν:

$$D = \begin{bmatrix} K+\frac{4}{3}G & K-\frac{2}{3}G & K-\frac{2}{3}G & 0 & 0 & 0 \\ K-\frac{2}{3}G & K+\frac{4}{3}G & K-\frac{2}{3}G & 0 & 0 & 0 \\ K-\frac{2}{3}G & K-\frac{2}{3}G & K+\frac{4}{3}G & 0 & 0 & 0 \\ 0 & 0 & 0 & G & 0 & 0 \\ 0 & 0 & 0 & 0 & G & 0 \\ 0 & 0 & 0 & 0 & 0 & G \end{bmatrix}$$

where

$$K = \frac{E}{3(1-2\nu)}$$

$$G = \frac{E}{2(1+\nu)}$$

3.5.5 Determination of the Constants for the Concrete Model

The failure criterion required the properties of the concrete under consideration to be determined in order to simulate its behavioural characteristics. Hsieh et al [91] put forward for the case of static loading, the four stress conditions required to define the values of the constants A, B, C and D

(1) Uniaxial compressive strength $\sigma_3 = -f'_c$ $\quad$ ($\sigma_1 = \sigma_2 = 0$)

(2) Uniaxial tensile strength $\sigma_1 = f'_t = 0.1 f'_c$ $\quad$ ($\sigma_2 = \sigma_3 = 0$)

(3) Biaxial compressive strength $\sigma_2 = \sigma_3 = f'_{bc} = 1.15 f'_c$ $\quad$ ($\sigma_1 = 0$)

A graphical representation in the biaxial principal stress plane of Equation 3.20 and the corresponding laboratory based data reported by Kupfer [19] are shown in Figure 2.6.

(4) The results from the test conducted by Mills and Zimmerman [24] are shown in the σ_{oct}/f'_c, τ_{oct}/f'_c coordinate system in Figure 3.12. Only the compressive ($\theta = 60^0$) and the tensile ($\theta = 0$) meridians are shown. The point (σ_{oct}/f'_c, τ_{oct}/f'_c) = (-1.95,1.6) was used for the fourth condition to determine the constants of the failure criterion. The point (σ_{oct}/f'_c, τ_{oct}/f'_c) = (-1.95,1.6) corresponds in fact to the triaxial stress state combination: σ_1

$= \sigma_2 = 0.8f'_c$ and $\sigma_3 = 4.2f'_c$.

A system of four equations was developed with four unknowns using the above conditions. The solution of the system of equations gave values for A, B, C and D of 2.0108, 0.9714, 9.1412 and 0.2312 respectively.

The four parameter failure criterion, which was defined by Equation 3.20 and the four constants, satisfied all the requirements with respect to the variation of the concrete strength in the principal stress space.

In the case where the four conditions above are not applicable, the four constants A, B, C, and D must be calculated.

On the other hand to determine the extent to which the shape of strain hardening has developed a tangent modulus, $\overline{H}$, for the stress-strain curve of the concrete under consideration is required. At least three points are needed, the first point must start at the initial yield stress and the last point must coincide with the strength of the concrete in compression. Figure 3.10 shows the position of a set of three points on the curve.

The effect of the rate of loading on concrete is taken into consideration using the properties of test specimens obtained under the same rate of loading. The test

specimens are used to determine the constants and the hardening parameters for the concrete.model in the same manner as they are used in the case of static loadings. In the case where such test specimens are not available empirical formula are employed to determine the data required. For example the compressive stresses and the corresponding strain values can be calculated knowing the static values and the rate of straining which is to be applied. Details of these empirical formulae have been published previously [1]. The relationships used to determine the hardening parameters are detailed in Appendix C.

3.5.6 Smeared Crack Model

Failure Criterion:

The magnitudes of the tensile and compressive load carrying capacities of concrete elements are different. The stress in a concrete element under load can fall into one of a number of stress combinations such as compression-compression-compression compression-compression-tension, tension-tension-tension, etc. In this model, the initiation of cracking is controlled by a crushing coefficient α which is used to identify the type of failure. The concept of the crushing coefficient is based on the consideration of a dual criterion i.e. the stress and strain criteria are combined to define the pure cracking and the pure crushing zones within the range of the possible stress combinations [91].

The dual criterion is defined for triaxial stress conditions in terms of the stress

invariants I_1, J_2, and $cos\theta$.

(1) The pure cracking mode is identified by assuming that the maximum principal stress must be tensile or zero. The following condition must be satisfied:

$$\sigma_1 > 0 \tag{3.36}$$

The principal stress σ_1 can be obtained as a function of the stress invariants, then Equation 3.36 can take the following form:

$$\sqrt{J_2}cos\theta + \frac{1}{2\sqrt{3}}I_1 > 0 \qquad (0 \leq \theta \leq 60^0) \tag{3.37}$$

(2) The pure crushing mode is identified by assuming that the maximum principal strain is compressive i.e. less then zero, hence:

$$\begin{aligned} \varepsilon_1 &< 0 \\ \sigma_1 - \nu(\sigma_2 + \sigma_3) &< 0 \end{aligned} \tag{3.38}$$

In terms of the stress invariants, Equation 3.38 takes the following form:

$$\sqrt{J_2}cos\theta + \frac{I_1}{2\sqrt{3}}\frac{1-2\nu}{1+\nu} < 0 \qquad (0 \leq \theta \leq 60^0) \tag{3.39}$$

Combining Equations 3.37 and 3.39 a crushing coefficient α is defined as follows:

$$\alpha = -\frac{I_1}{2\sqrt{3}\sqrt{J_2}cos\theta} \qquad (0 \leq \theta \leq 60^0) \tag{3.40}$$

The failure modes are then identified as:

(1) Pure cracking, $\alpha < 1$;

In the case of pure cracking the stress condition is on the tensile meridian

and $\theta = 0$, as shown in Figure 2.14.

(2) Pure crushing, $\alpha > \frac{(1+\nu)}{(1-2\nu)}$;

In the case of pure crushing the stress condition is on the compressive meridian and $\theta = 60^0$.

(3) Mixed mode of failure, $1 \leq \alpha \leq \frac{(1+\nu)}{(1-2\nu)}$.

The stress condition for this type of failure lies inside the boundary defined by the tensile and compressive meridians and the condition where $0 \leq \theta \leq 60^0$

The boundaries of the three failure modes are defined by Poisson's ratio ν. For example a typical value of 0.2 for Poisson's ratio results in the following range of failure modes:

(a) $\alpha \leq 1$ corresponds to pure cracking;

(b) $1 > \alpha > 2$ corresponds to a mixed type of failure;

(c) $\alpha \geq 2$ pure crushing failure mode.

It should be emphasised that in obtaining the crushing coefficient (α), a linear elastic stress-strain relationship has been used, which is described by Equation 3.38. This is an entirely consistent procedure for a linear elastic concrete in tension or linear compressive stress states. However, concrete in the compressive

zone is formulated using the theory of plasticity. In such a case the crushing coefficient may not apply immediately before crushing, and the procedure is utilised only as an approximation of the actual behaviour.

Considering the crushing coefficient (α), it is possible to compute the extent of the compressive and tensile failures for a finite element, and to locate geometrically the two fractions in the element.

After the failure criterion has been violated the principal stresses and their cosine directors are calculated for the concrete element. If the maximum principal stress, σ_1, exceeds the critical tensile stress the first crack is assumed to form. The critical tensile stress for different stress combinations is calculated as follows:

(1) Pure cracking, $\alpha < 1$ and $\sigma_1 \geq \sigma_2 \geq \sigma_3$

$$\sigma_i = \sigma_{cr} = f_t \qquad i = 1,2,3 \tag{3.41}$$

(2) Mixed mode of failure, $1 \leq \alpha \leq \frac{(1+\nu)}{(1-2\nu)}$. The tensile strength decreases linearly in the following form:

(a) Tension-tension-compression stress conditions $\sigma_1 \geq \sigma_2 > 0, \sigma_3 \leq 0$

$$\sigma_i = \sigma_{cr} = f_t(1 + \sigma_3/f_c') \qquad i = 1,2 \tag{3.42}$$

(b) Tension-compression-compression stress conditions $\sigma_1 > 0, \sigma_3 \leq \sigma_2 \leq 0$

$$\sigma_i = \sigma_{cr} = f_t(1 + \sigma_2/f_c')(1 + \sigma_3/f_c') \tag{3.43}$$

where σ_{cr} is the cracking stress.

These equations simulate the fact that compression in one direction will tend to initiate cracking in the other and thus reduces the tensile capacity of the material.

After the onset of cracking has been reached, as determined by the magnitude of the maximum principal stress, the crack width corresponding to the principal stress is calculated by multiplying the normal strain by a characteristic length *cl*.

$$w_1 = (\varepsilon_1 l_1^2 + \varepsilon_2 m_1^2 + \varepsilon_3 n_1^2 + \varepsilon_4 l_1 m_1 + \varepsilon_5 m_1 n_1 + \varepsilon_6 l_1 n_1) cl \qquad (3.44)$$

where w_1 is the crack width in direction 1. l_1, m_1 and n_1 are the cosine directors which define the maximum principal stress σ_1. ε_i, where $i = 1 - 6$ are the strain components of the concrete element. *cl* is the current critical length of the concrete element which is calculated as follows:

$$cl = V^{\frac{1}{3}}$$

where V is the volume of concrete represented by the integration point. For one integration point, it is equal to the current volume of the concrete element.

If the calculated crack width exceeds a given critical width i.e. $w_1 \geq w_{cr}$ the crack is assumed to be fully open. The concrete finite element isotropic property is changed to an anisotropic one by setting to zero the dominant principal stress and any other newly developed tensile stress in the direction which is perpendicular to the crack plane.

If a second crack initiates at a later stage of the loading, the analysis of the stress orientation is transformed to a two dimensional problem. New cosine directors are defined for the plane which is perpendicular to the first principal stress σ_1. The magnitude of the new principal stresses $\sigma_2^{'}$ and $\sigma_3^{'}$ are calculated from the original principal stresses σ_2 and σ_3 and the current shear stress τ_{23}. Thus,

$$\sigma_i^{'} = \frac{\sigma_2 + \sigma_3}{2} \pm \sqrt{\frac{(\sigma_2 - \sigma_3)^2}{2} + \tau_{23}^2} \qquad i = 2,3$$

The failure plane corresponding to the second crack is perpendicular to the direction of the second principal stress $\sigma_2^{'}$. The cosine directors of this plane are determined as a function of the angle between the new principal stresses, $\sigma_2^{'}$ and $\sigma_3^{'}$, and the global cosine directors. A second crack width, w_2, is determined in a similar form to Equation 3.44.

$$w_2 = (\varepsilon_1 l_2^2 + \varepsilon_2 m_2^2 + \varepsilon_3 n_1^2 + \varepsilon_4 l_2 m_2 + \varepsilon_5 m_2 n_2 + \varepsilon_6 l_2 n_2) cl \qquad (3.45)$$

In the current model, a maximum of three cracks are allowed to form in the element because only one integration point is used to calculate the stiffness of

the eight node element. In the case of triaxial tensile stress conditions, a third crack may occur when the third principal stress, σ_3', exceeds the uniaxial tensile strength f_t and the crack width w_3 is calculated in a similar manner to Equation 3.44 using the appropriate cosine directors.

Strain Softening:

In the finite element modelling of plain concrete, a post cracking model is used to simulate the fact that the concrete member after cracking is still able to play an active role in the stiffness of the concrete element. The stresses in the cracked element are modified to take account of the post maximum strength of the cracked concrete. The stresses responsible for the cracks are decoupled from the stress(es) in the uncracked direction and decayed to zero as a function of the current crack width. A linear relationship between the stress normal to the crack and the crack width is used to model the progressive decay of the tensile stress perpendicular to the crack plane [10, 116]. The form of the stress decay is as follows:

$$\sigma_t(w) = f_t(1 - \frac{w}{w_{cr}}) \qquad 0 < w < w_{cr} \tag{3.46}$$

$$= 0 \qquad w \geq w_{cr} \tag{3.47}$$

where w_{cr} is the critical crack width value at which cracks in the concrete finite element are deemed to be fully open. Figure 3.7 shows the variation in $\sigma_t(w)$ with respect to the crack width.

The stresses in the uncracked directions are calculated using appropriate plane stress formulations in the case where only one crack is fully formed or using uniaxial formulations in the case where two cracks are fully formed. In addition a correction is made for the contribution from Poisson's ratio from the stress decay increment. For example, if direction one is cracked and has been incremented in the post maximum strength process by $d\sigma_1$ the stress in directions two and three are calculated as follows:

$$\sigma_2' = \sigma_2 + (\frac{E}{(1-\nu)^2} d\varepsilon_2' + \frac{E\nu}{(1-\nu)^2} d\varepsilon_3') + \frac{\nu}{1-\nu} d\sigma_1$$

$$\sigma_3' = \sigma_3 + (\frac{E\nu}{(1-\nu)^2} d\varepsilon_2' + \frac{E}{(1-\nu)^2} d\varepsilon_3') + \frac{\nu}{1-\nu} d\sigma_1$$

If the concrete element has cracked in directions 1 and 2 and it has been incremented by $d\sigma_1$ and $d\sigma_2$ then the uncracked stress is obtained using the following uniaxial formulations:

$$\sigma_3' = \sigma_3 + E d\varepsilon_3' + \nu(d\sigma_1 + d\sigma_2) \tag{3.48}$$

where σ_1', σ_2' and σ_3' are the stresses in the cracked concrete element and σ_1, σ_2 and σ_3 are the three principal stresses and $d\varepsilon_1', d\varepsilon_2'$ and $d\varepsilon_3'$ are the normal strain increments.

Closing and reopening of the cracks at the sampling points may occur as a result of the new loading increment and the redistribution of the stresses in the cracked

element. For a closing crack, the element is considered to be able to resist only compressive and shear stresses. Crack closing and re-opening follows a secant path, as shown in Figure 3.7. The residual compressive stress is calculated using a linear relationship between the crack width increment and the secant modulus.

Shear Transfer:

As well as modifying the stresses in the cracked direction, it is necessary to consider the shear capacity in the cracked region. The shear transfer in the cracked element is assumed to be dependent only on aggregate interlock. The two methods which can be used in the new concrete model, are as follows:

(1) The amount of shear which should be retained is a proportion of the shear modulus and equal to βG, where β is a value which is required to be specified.

(2) The shear retention factor is included using a relationship between aggregate size and crack width. The amount of shear that should be retained follows an aggregate interlock function defined by the curve in Figure 3.8 which represents a measurement of the crack shear stiffness with respect to the crack width of the inclined surface. The proportion of the shear stress which will be retained is as follows:

$$S(w) = 1 \qquad w = 0 \tag{3.49}$$

$$= \frac{(a-w)^2}{a^2} \qquad 0 < w < a \tag{3.50}$$

$$= 0 \qquad w = a \tag{3.51}$$

where w and a are the current crack width and the aggregate size respectively.

3.6 CONCLUSIONS

A new non-linear concrete model suitable for the three dimensional analysis of concrete members subjected to impact loading has been formulated. The model has used a triaxial stress formulation which was based on a four parameter failure criterion combined with the incremental theory of plasticity.

The stress-strain relationship for concrete in compression has been modelled using an elastic-plastic strain hardening model accompanied by fracture of the material at ultimate strength. The direction and magnitude of the amount of plastic straining is governed by the normality condition of an associated flow rule and isotropic and kinematic hardening rules.

In tension, the concrete is assumed to be elastic until cracking takes place. Cracking of the concrete is controlled by the maximum stress criterion. A smeared crack

model has been used together with a tension softening model which was based on a bilinear approximation of the relationship between the stress normal to the crack and its width. A model for the reduction in the shear stress was based on either a direct reduction in the shear stress or a reduction based on a parabolic relationship between the crack width and the size of the aggregate particles. Up to three orthogonal cracks are allowed to form at the sampling points. Closing and reopening of the cracks is permitted in this formulation in order to simulate the eventual modal deformations as the member vibrates.

Failure of the concrete is determined using a crushing coefficient which is based on a dual criterion. Three different modes of failure can be identified by the crushing coefficient i.e. cracking, crushing and mixed cracking and crushing modes.

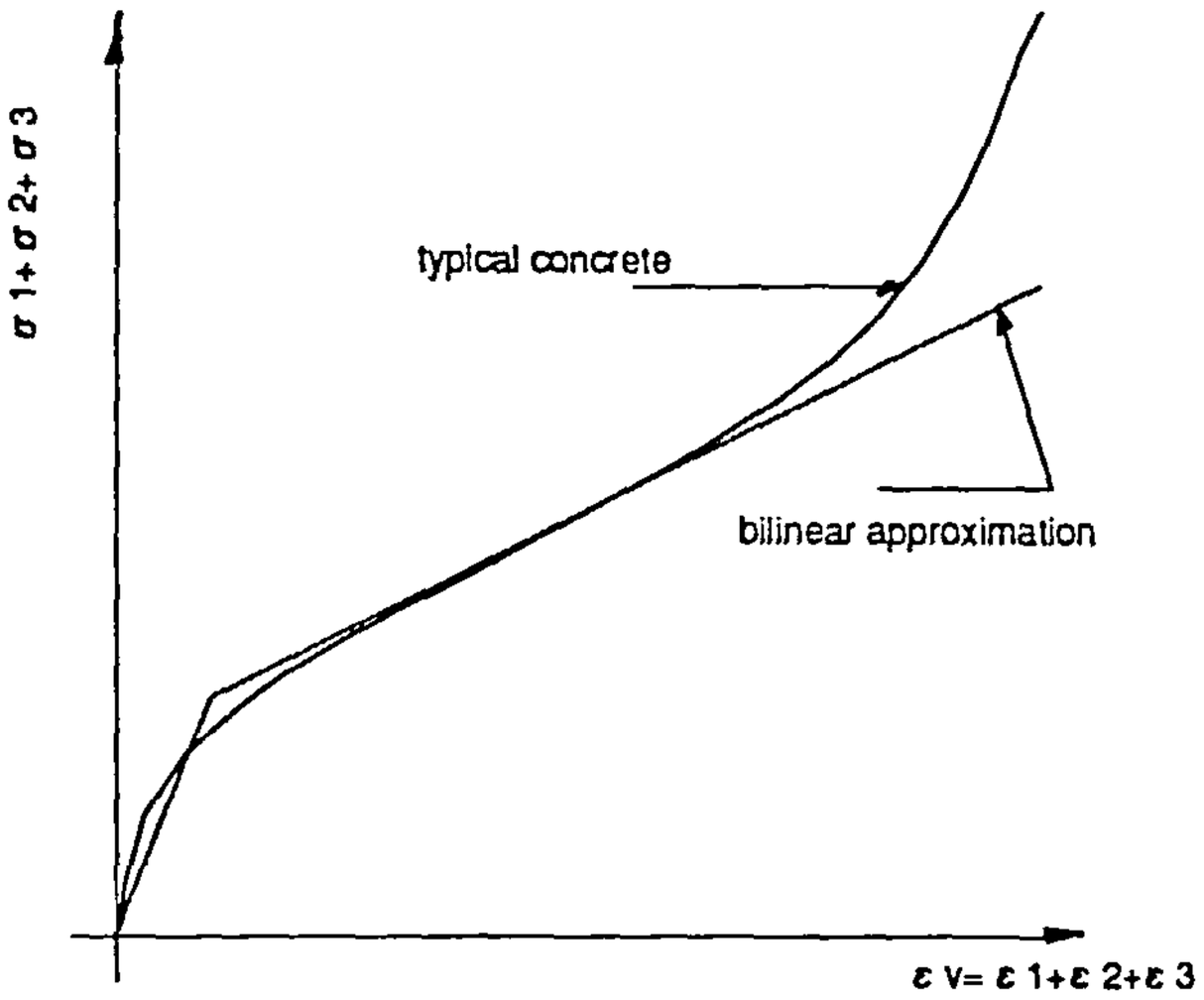

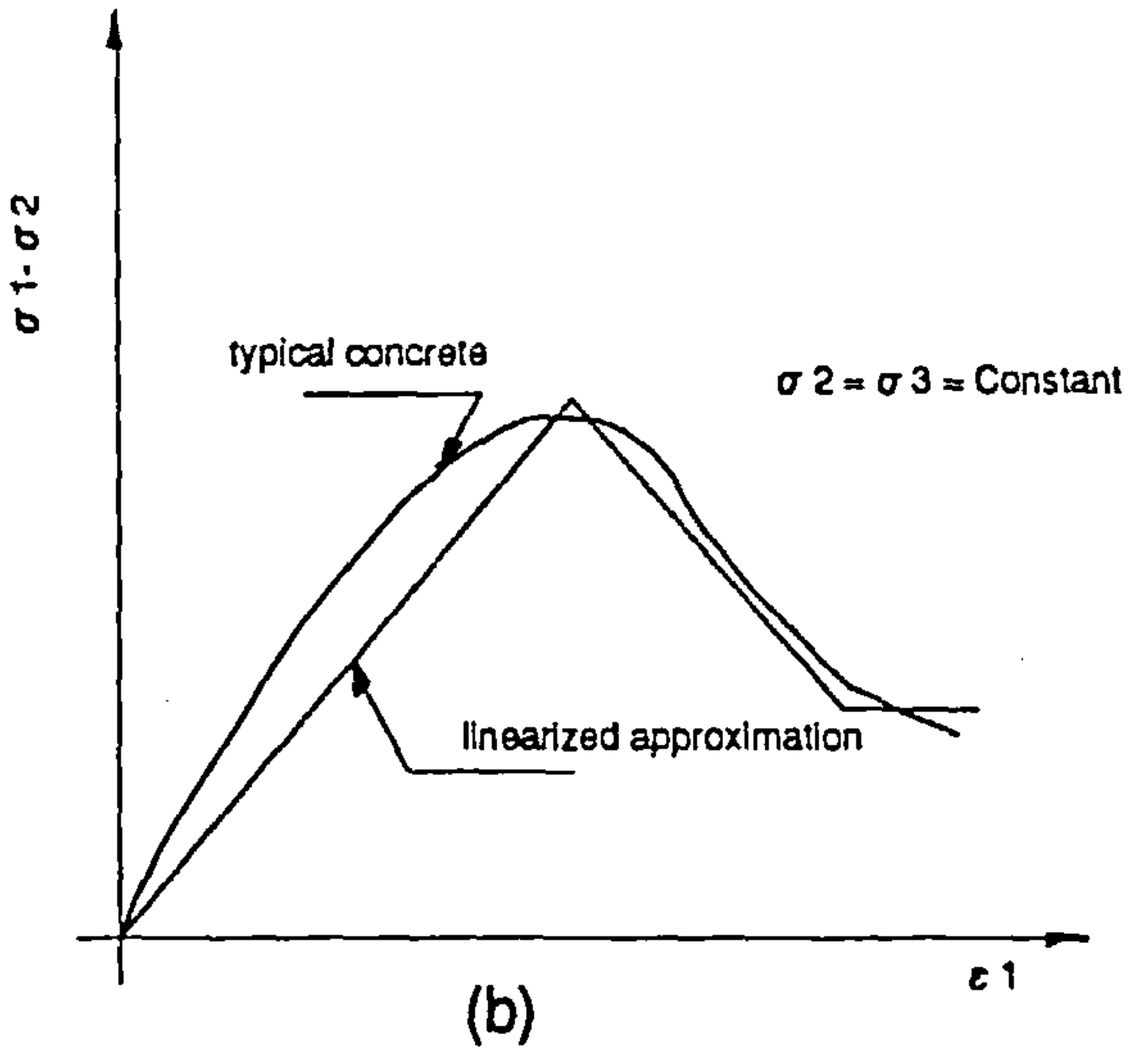

Figure 3.1: Approximation of the octahedral and deviatoric variations

(a) bilinear relationship between the octahedral stress and strain

(b) trilinear relationship between the deviatoric stress and strain

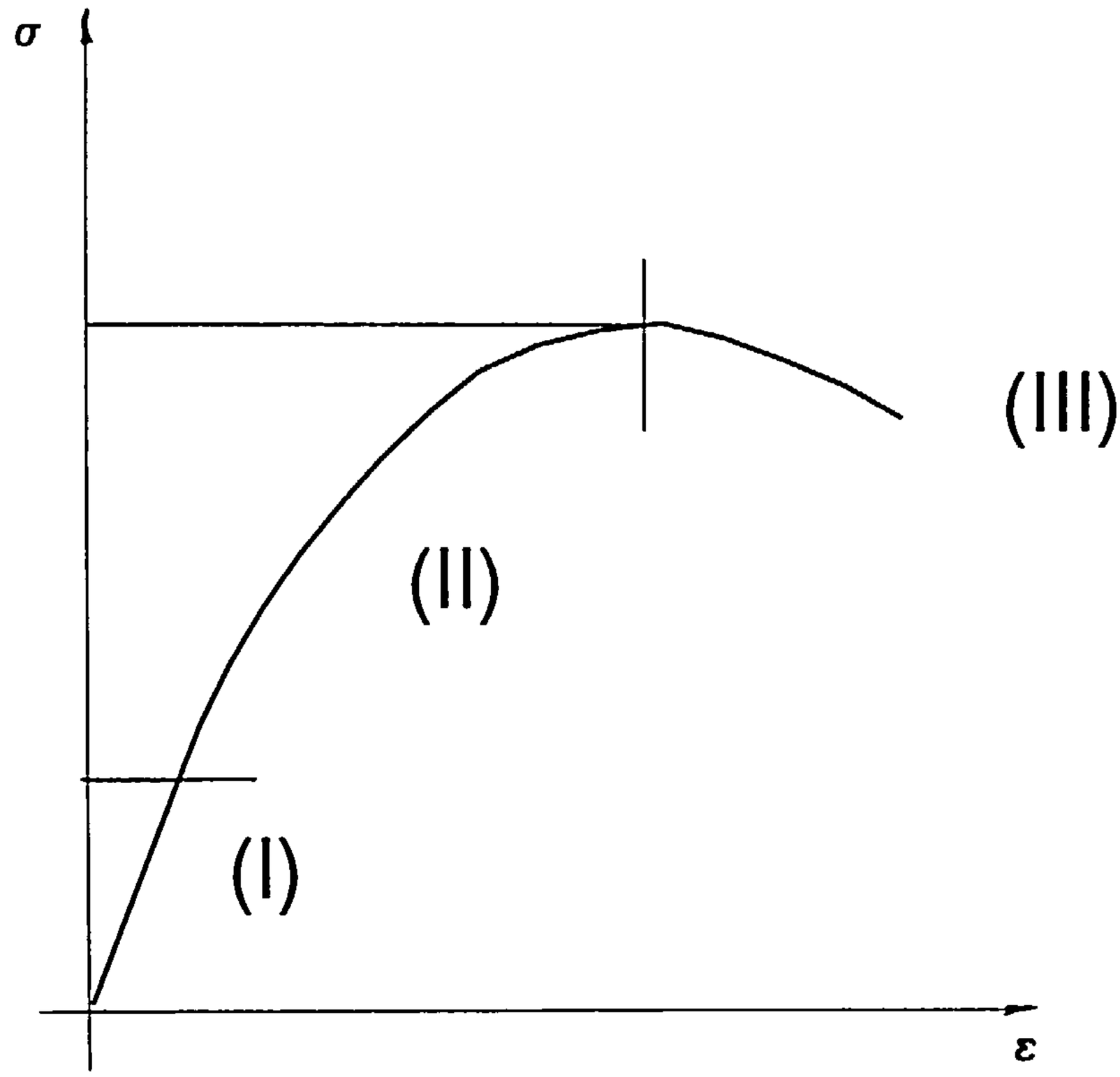

Figure 3.2: Typical uniaxial compressive stress-strain curve for plain concrete

(I) linear elastic variation between stress and strain

(II) plasticity with strain hardening up to the peak strength

(III) concrete strain softening until failure

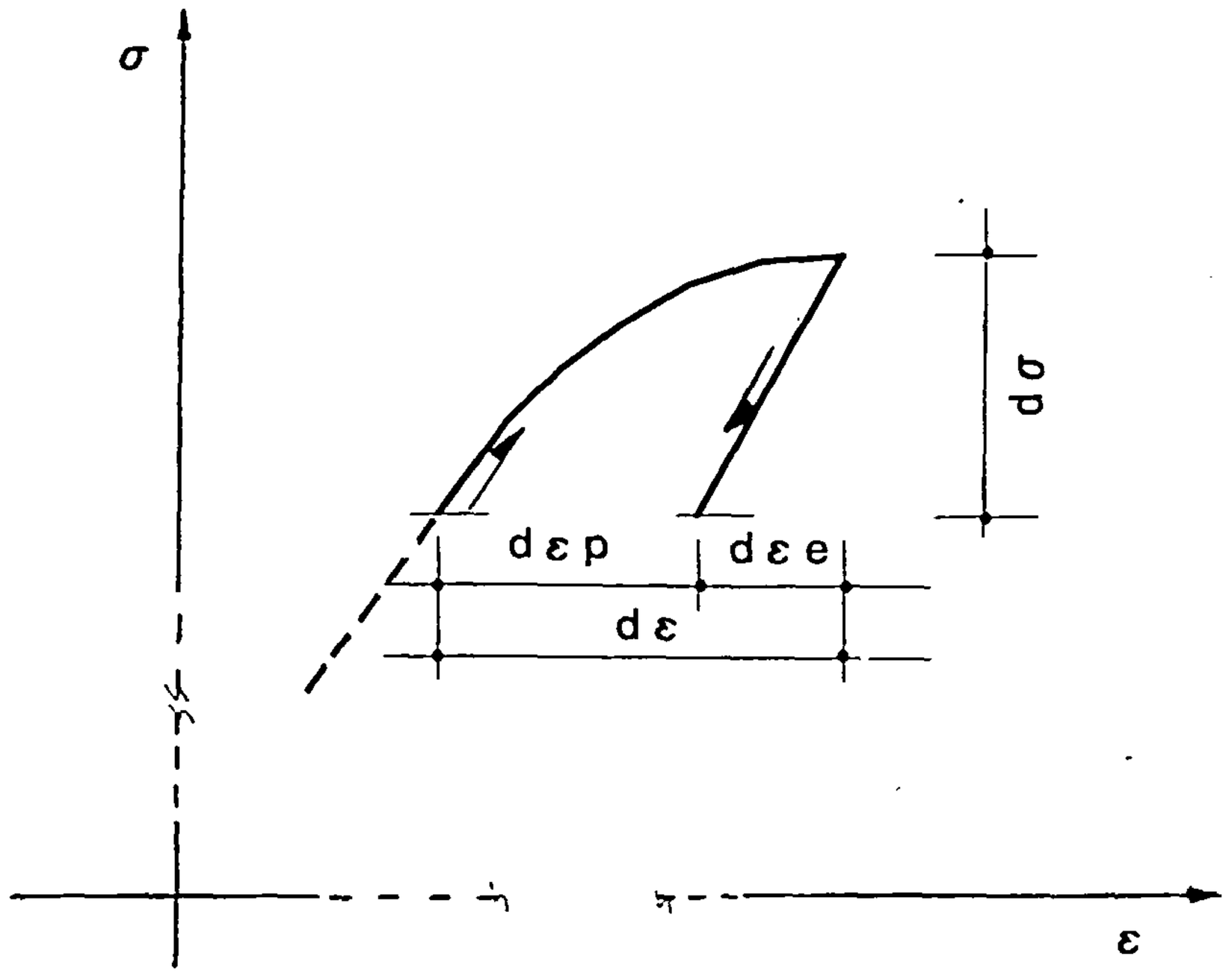

Figure 3.3: Elastic and plastic components of the strain increment

$d\sigma$ and $d\varepsilon$ are the stress and strain increments

$d\varepsilon$e and $d\varepsilon$p are elastic and plastic components of the strain increments

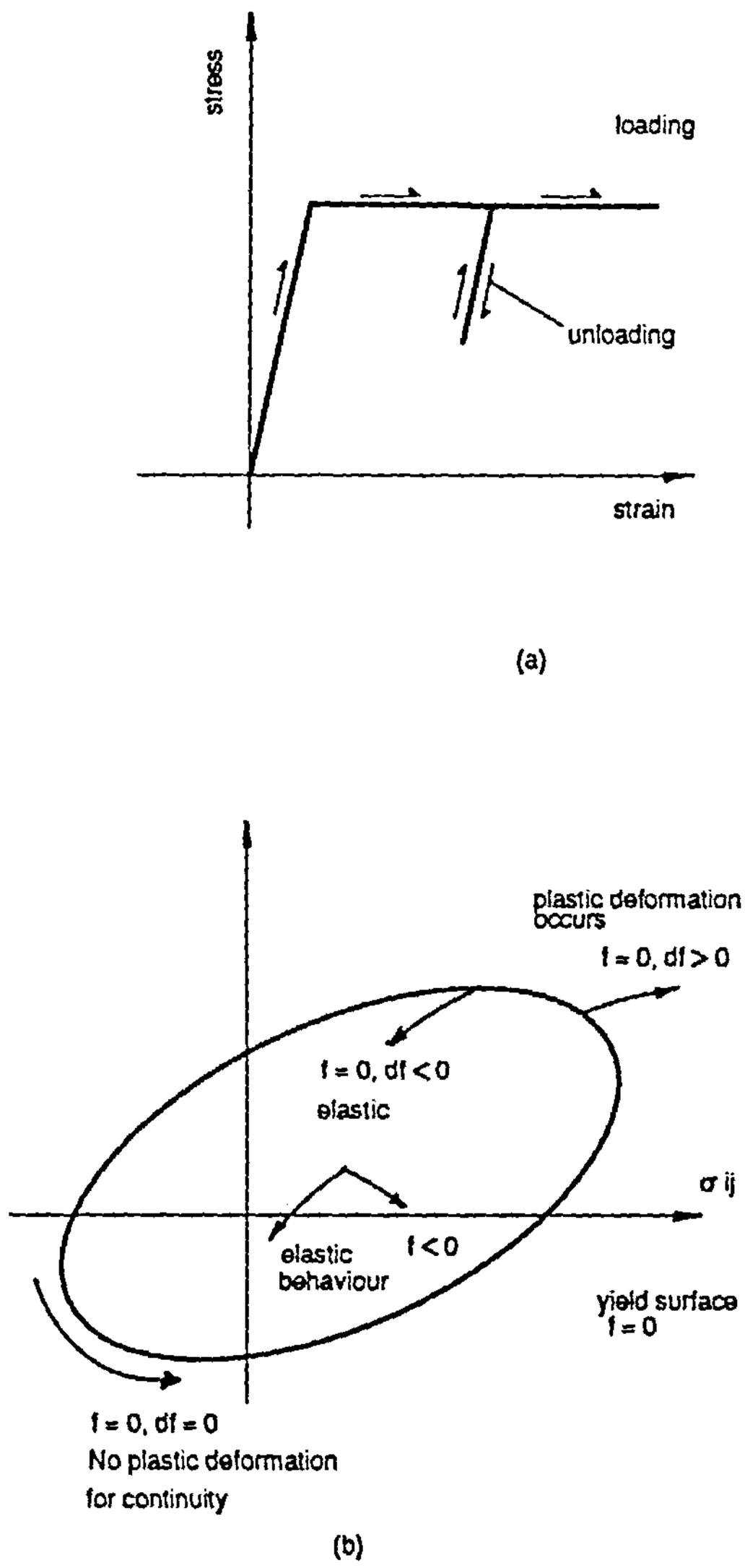

Figure 3.4: Elastic-perfectly plastic material representation

(a) uniaxial stress-strain relation

(b) Geometry representation of yield surface and criterion of loading and unloading

$$df = \partial f / \partial \sigma_{ij} d\sigma_{ij}$$

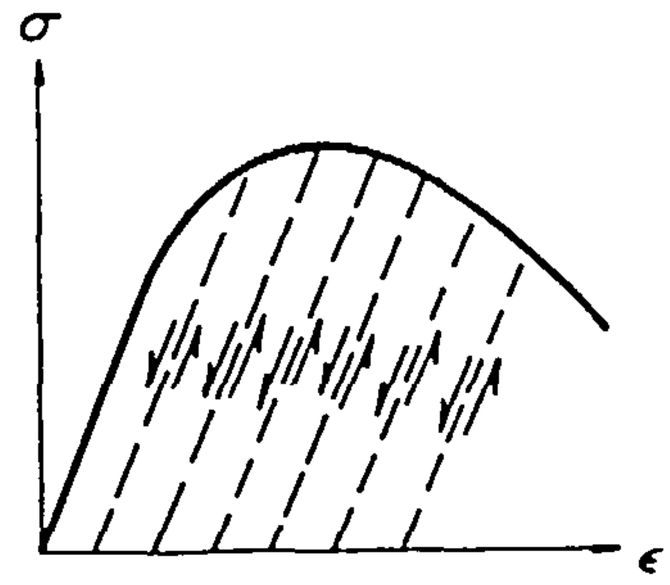

(a)

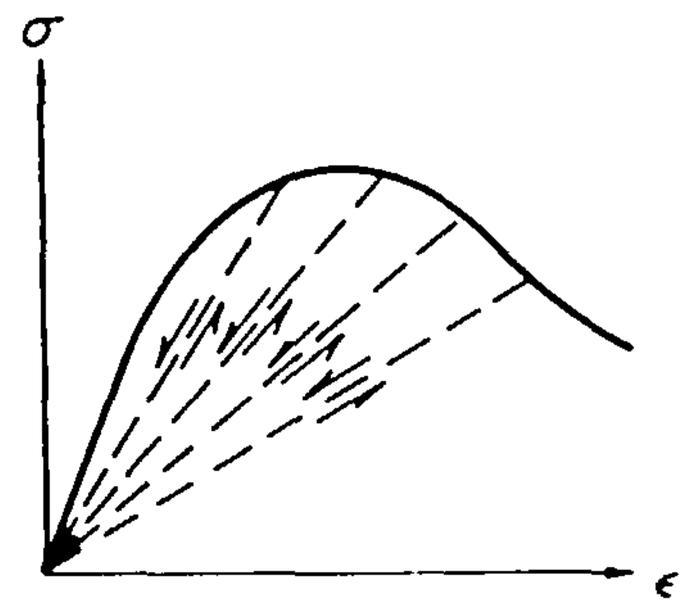

(b)

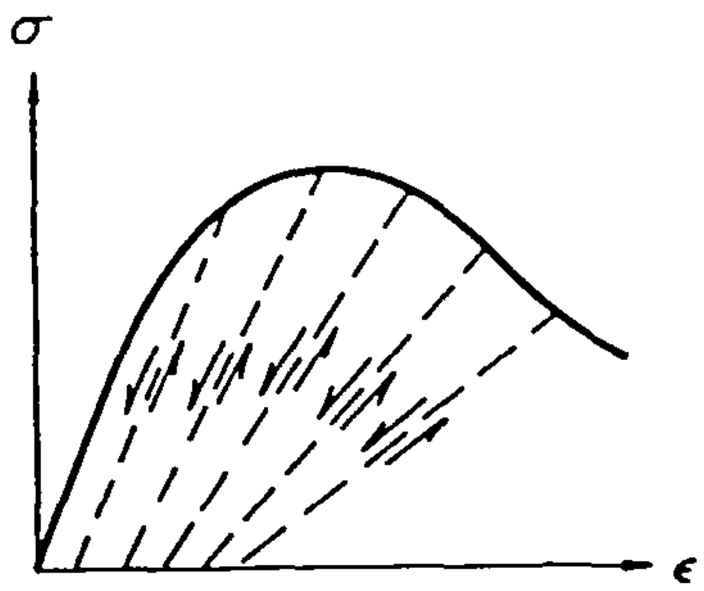

(c)

Figure 3.5: Concrete material behaviour (after Chen and Han [53])

(a) Elastic-plastic solid

(b) Progressively fracture solid

(c) Plastic-Fracture solid

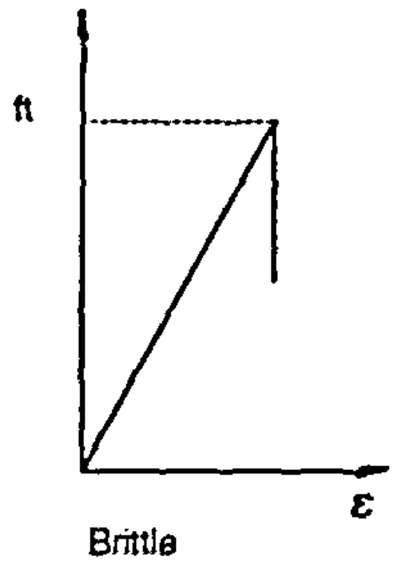

Brittle

(a)

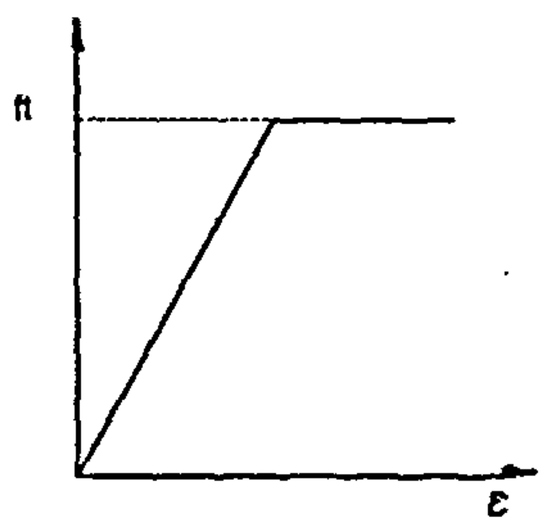

Plastic Fracture

(b)

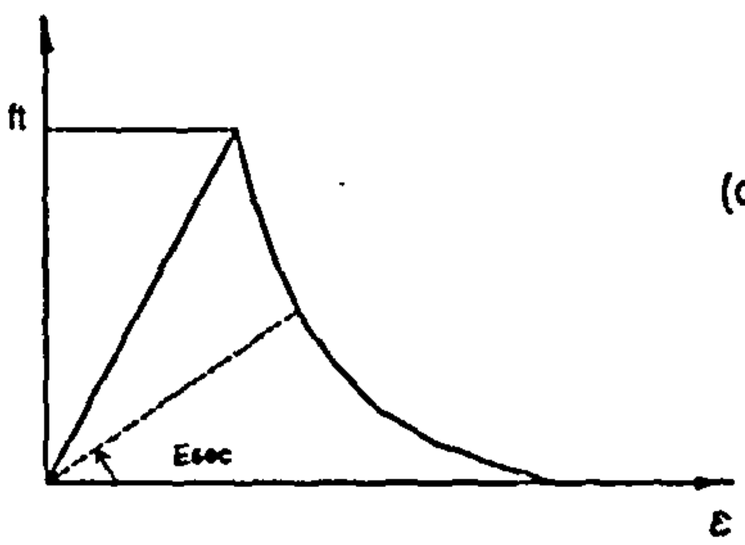

Tension stiffening

(c)

Figure 3.6: Strength criteria

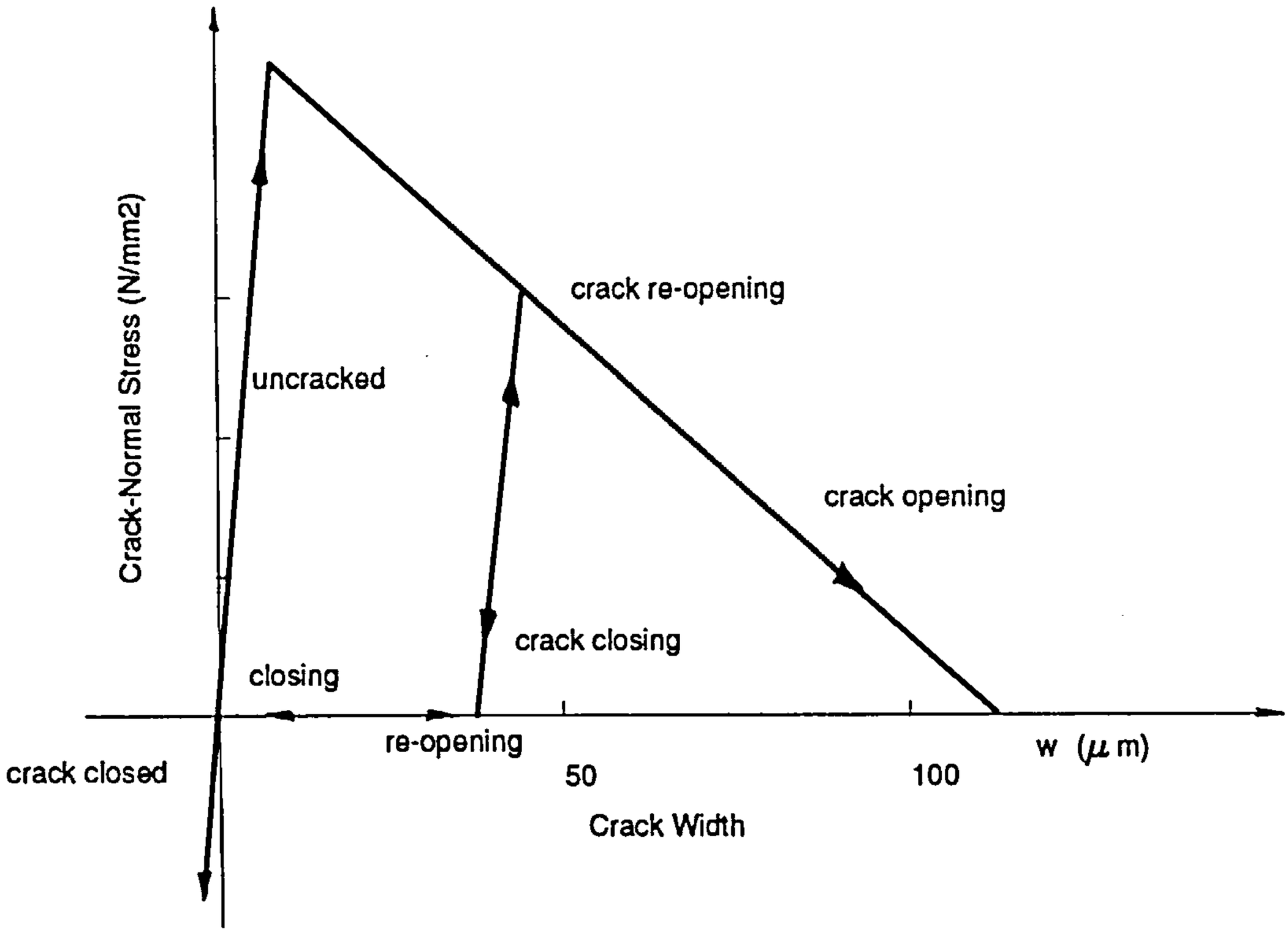

Figure 3.7: Simple approximation for tension softening of concrete (after Peterson [11] and Broadhouse [78])

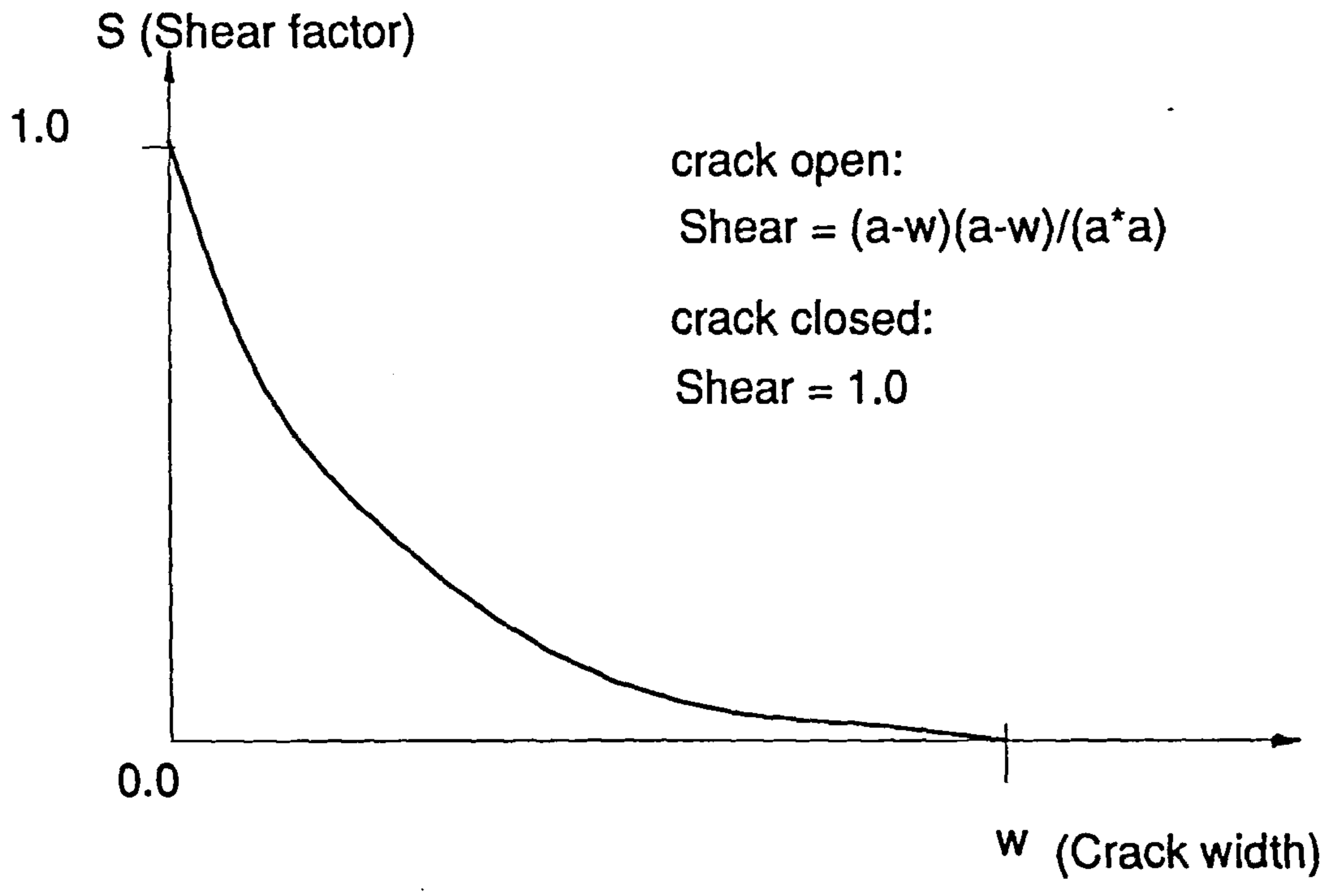

Figure 3.8: Shear retention factor for cracked element

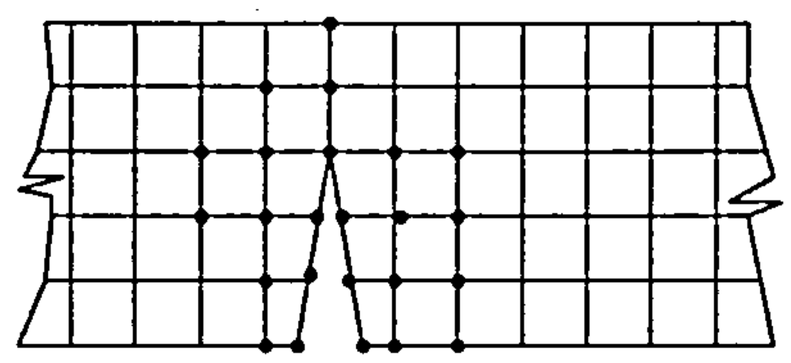

(a)

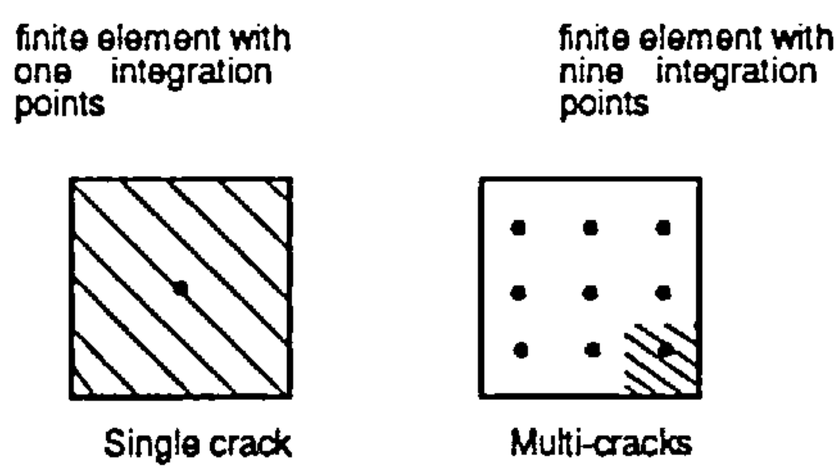

(b)

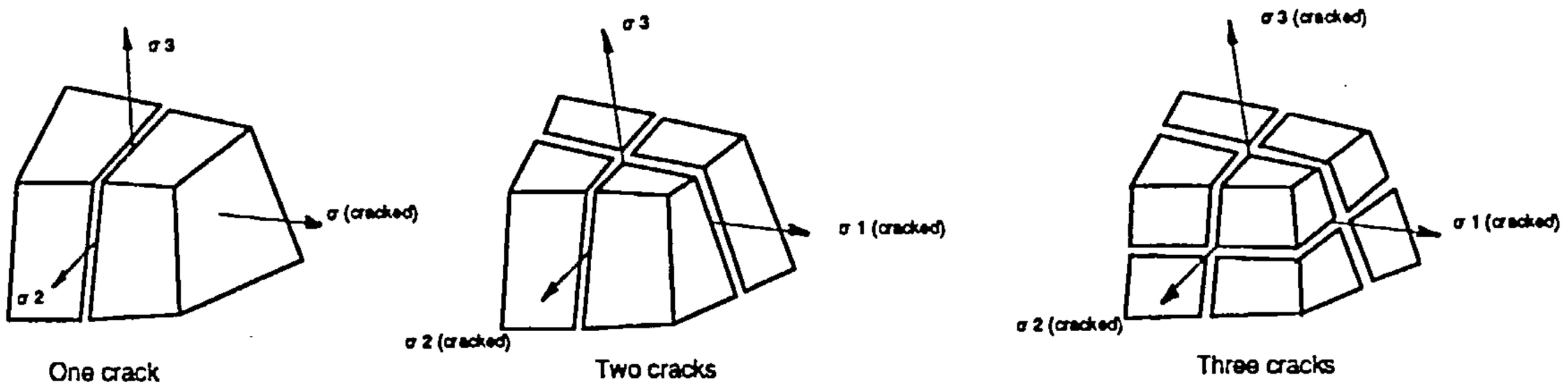

(c)

Figure 3.9: Crack representation in the finite element method

(a) Discrete cracks

(b) Smeared cracks in two dimensions

(c) Smeared cracks in three dimensions

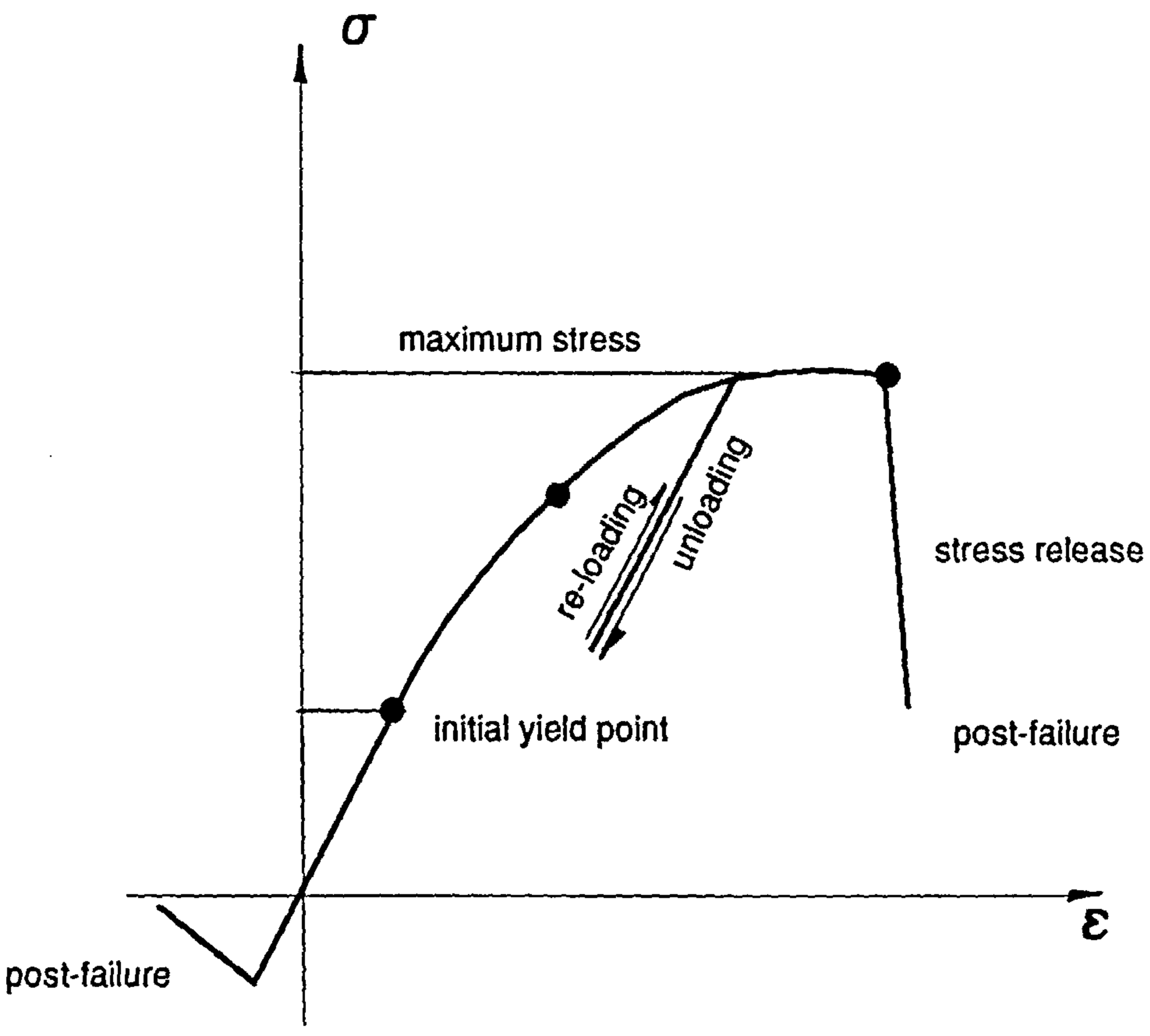

Figure 3.10: Uniaxial idealisation of the concrete model

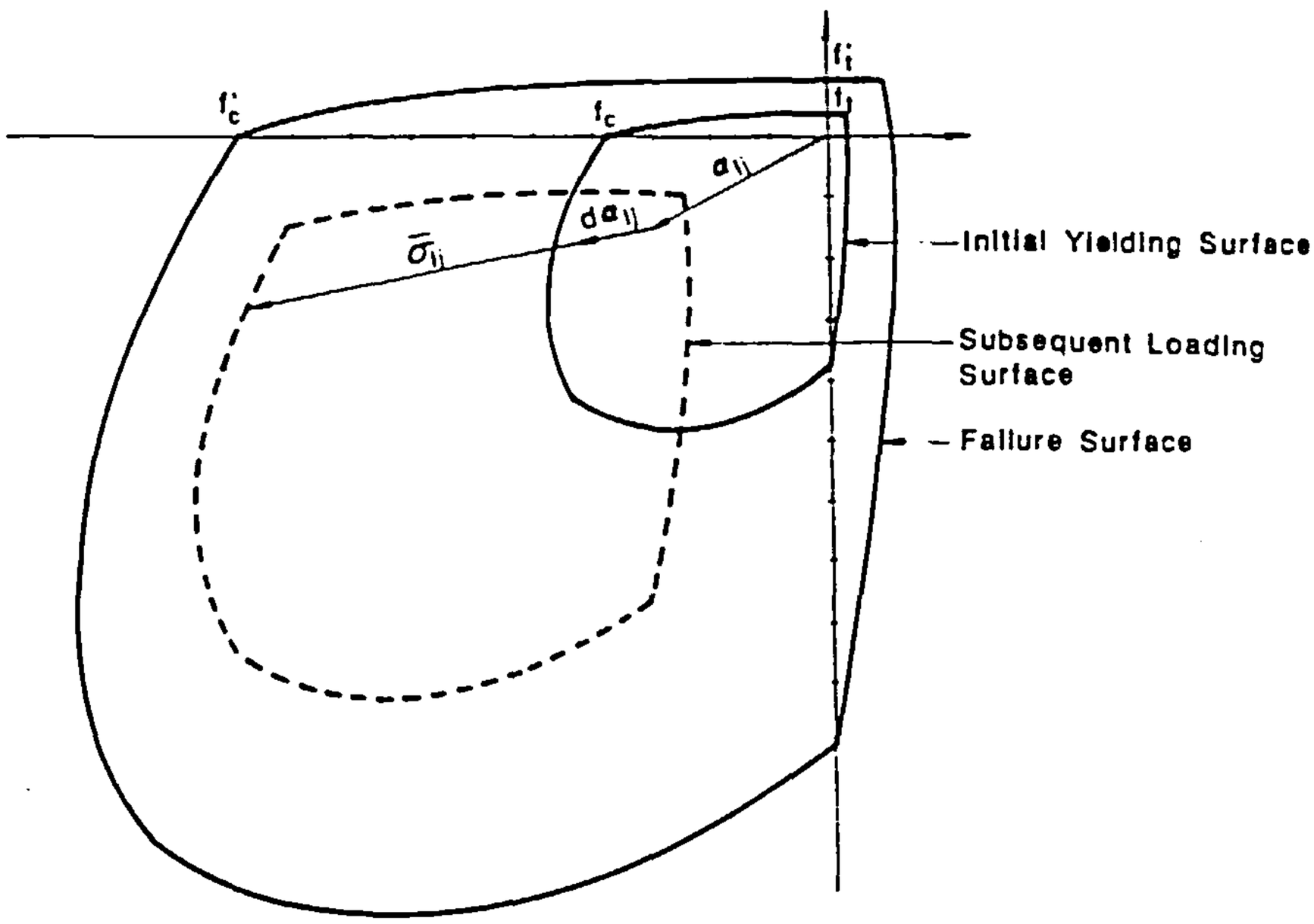

Figure 3.11: Schematic diagrams for the failure surface, the initial yielding surface and the subsequent loading surface

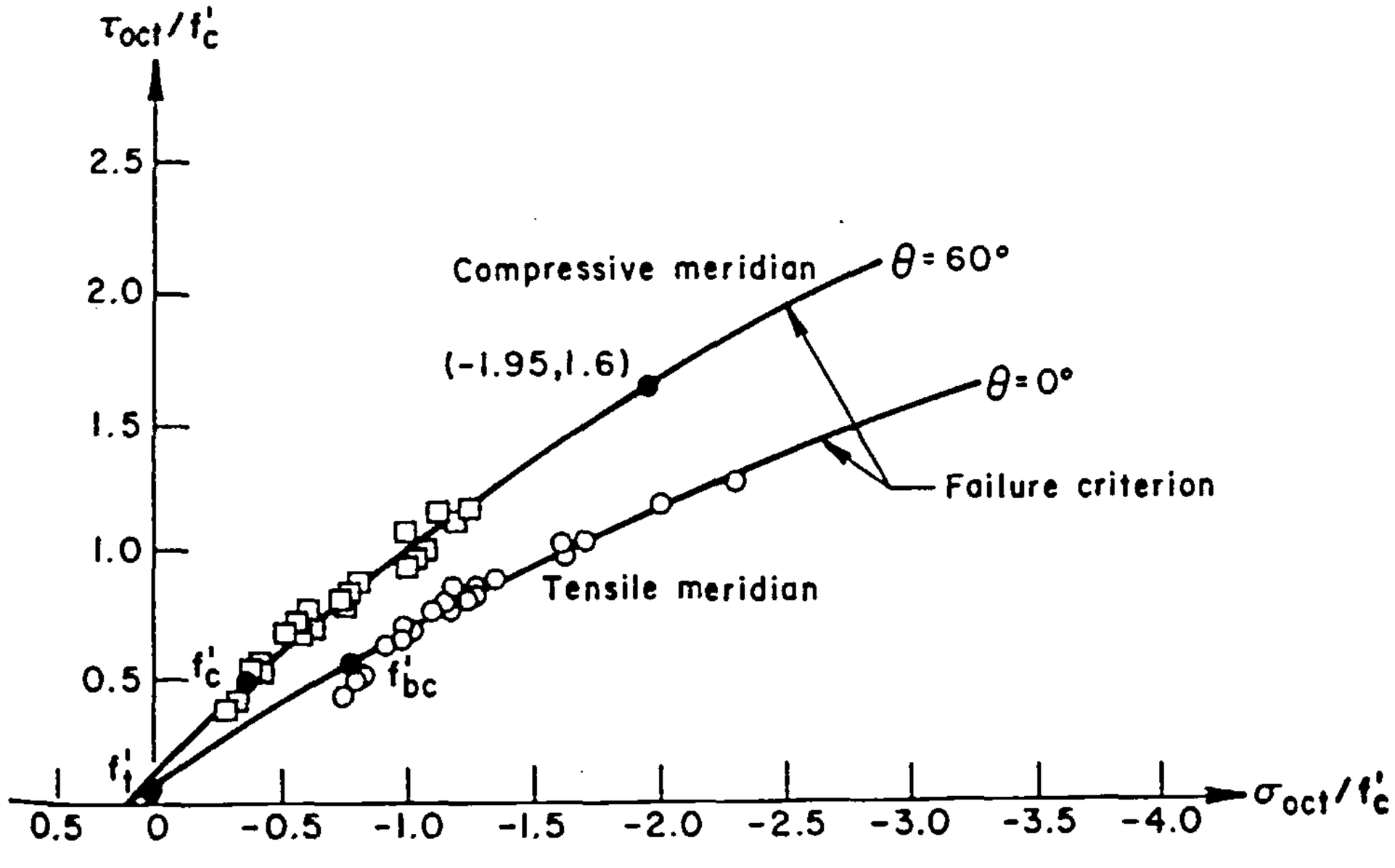

Figure 3.12: Failure criterion in octahedral shear and normal-stress plane (after Chen and Han [53])

Chapter 4

FINITE ELEMENT AND NUMERICAL PROCEDURES

4.1 INTRODUCTION

In the last three decades the finite element method has emerged as the most powerful numerical technique used in the solution of engineering problems. The origins of the method can be traced back to the lattice analogy concept put forward by McHenry [130] and the early attempt to analyse the behaviour of plane elastic solids by treating them as an assembly of discrete elements [131]. In the 1950's, Argyris and Kelsey [132] developed an efficient technique based on force matrix operations in order to analyse complicated structural systems. The technique was mainly used in the aeronautical industry. In the same period, Turner et al [133] produced the actual solution to plane stress problems using

triangular elements. Clough [134] appears to have been the first to use the term "*finite element*". Since then the numerical technique known as the finite element method has been widely used in the field of engineering.

The finite element method has been described extensively in the literature. A detailed discussion of the method and its application is given in several text books [122, 135, 136, 137].

The following aspects of the finite element method will be briefly discussed:

(1) The general background to the approach together with the formulation of the equilibrium equations governing the behaviour of a continuum using the principle of virtual displacement.

(2) The idealisation of concrete and reinforcement.

(3) The solution of the dynamic equations of equilibrium.

(4) The calculation of the externally applied forces resulting from contact-impact events.

4.2 CONCEPTS AND EQUATIONS OF EQUILIBRIUM

4.2.1 General Aspects of the Finite Element Method

The widespread use of the finite element method in the field of engineering is due mainly to the fact that any type of structure can be modelled as an assembly of finite elements. As an example a continuum of any arbitrary shape can be substituted by a finite number of subdomains, or elements of finite size but which have a simple and defined geometrical shape. A finite number of points, or nodes are identified on the element where the finite elements are to be interconnected and the conditions of equilibrium and displacement continuity between elements are to be satisfied. Interpolation functions for each element are defined so that the geometry and the displacement at each point of the finite element are dependent upon nodal values. The accuracy of the finite element solution depends on the number of elements used in the modelling of the continuum as well as on the interpolation functions.

One of the most important advantages of the finite element method is the fact that an individual element may be considered in isolation from the overall assemblage of the finite elements. Therefore, the displacement over the element can be obtained in terms of the nodal values independently of the location of the element within the model. Thus, it is possible to develop an assemblage of different types

of finite elements in which the nodal local displacement interpolation functions are left arbitrary.

4.2.2 Equations of Equilibrium

This Section deals with the derivation of the equilibrium equations governing the behaviour of a continuum subjected to an externally applied force. Vectors and matrices will be distinguished from scalar quantities by underlining. Small letters will be used for vectors and capital letters will be used for matrices.

The equilibrium of a three dimensional body defined in space by a system of cartesian coordinates and subjected to external forces is considered, the external forces acting on the body are surface traction $\underline{t}$ and body forces $\underline{b}$. These external forces include all externally applied forces and reactions and have in general three components corresponding to the three coordinate axes x, y and z. As a result of these loadings a particle of the body located initially at point $P(x, y, z)$ experiences a displacement, $\underline{d}$, having components u, v and w in the x, y and z directions respectively.

It is assumed that the externally applied forces are given and that a solution is sought for the resulting displacements, strains and stresses. To obtain a solution, the governing equations of equilibrium of the body must be established. The finite element method uses the principle of virtual displacements to establish

the governing equations of equilibrium for the body. This principle states that a deformable body is in equilibrium if the total work done by all the external loads is equal to the total work done by all the internal forces during a virtual displacement imposed on the body [135]. Therefore,

$$W_{int} = W_{ext} \tag{4.1}$$

$$\int_v \delta\underline{\varepsilon}^T \underline{\sigma} dv = \int_v \delta\underline{d}^T \underline{b} dv + \int_s \delta\underline{d}^T \underline{t} ds \tag{4.2}$$

The external work is given on the right hand side of Equation 4.2 and is equal to the actual external forces experiencing the virtual displacement $\delta\underline{d}$. The internal virtual work is given on the left hand side of Equation 4.2 and is equal to the actual stress $\underline{\sigma}$ resulting from the virtual strain $\delta\underline{\varepsilon}$ which corresponds to the imposed virtual displacement $\delta\underline{d}$. Equation 4.2 is used to establish the governing equation of static equilibrium. It is, however, possible to extend the principle of virtual work to dynamics and thereby speak in terms of dynamic equilibrium instead of static equilibrium. This can be done by a principle attributed to d' Alembert [7, 135]. On the assumption that the particle acceleration defined at the point $P(x, y, z)$ can be calculated using the principle of momentum:

$$\int_v \delta\underline{\varepsilon}^T \underline{\sigma} dv = \int_v (\delta\underline{d}^T \underline{b} - \delta d^T \rho \ddot{\underline{d}}) dv + \int_s \delta\underline{d}^T \underline{t} ds \tag{4.3}$$

$$\int_v \delta\underline{d}^T \rho \ddot{\underline{d}} dv + \int_v \delta\underline{\varepsilon}^T \underline{\sigma} dv - \int_v \delta\underline{d}^T \underline{b} dv - \int_s \delta\underline{d}^T \underline{t} ds = 0 \tag{4.4}$$

4.2.3 Discretisation of the Equilibrium Equations

In finite element analysis, the body is substituted by an assemblage of an arbitrary number of finite elements, n, with the elements being interconnected at nodal points on the element boundaries.

Consider a finite element, e, of the discrete model and let the displacement vector at any point within the element, $\underline{d}^e$, be interpolated as follows

$$\underline{d}^e = \underline{N}\,\underline{a}^e \tag{4.5}$$

where $\underline{N}$ is a matrix containing the interpolation function which relates the displacement at any point within the element, $\underline{d}^e$, to the nodal displacement $\underline{a}^e$. If the displacement is known at all points within the element the corresponding strain at any point $\underline{\varepsilon}^e$, is obtained by the differentiation of the displacement i.e.

$$\underline{\varepsilon}^e = \underline{A}\,\underline{d}^e \tag{4.6}$$

where $\underline{A}$ is a matrix which contains the differential operators. Substitution of Equation 4.5 into Equation 4.6 gives:

$$\underline{\varepsilon}^e = \underline{B}\,\underline{a}^e \tag{4.7}$$

where $\underline{B}$ is the strain-displacement matrix given by:

$$\underline{B} = \underline{A}\,\underline{N} \tag{4.8}$$

The strain-displacement matrix gives values of strain, at any point within the element, resulting from unit values of nodal displacements. In the discrete model, the equilibrium of the continuum given by Equation 4.4 may be written as the sum of the integration over the volume and surface area for all the finite elements.

$$\sum^{n}\left\{\int_v \rho \underline{N}^T \underline{N} dv \ddot{\underline{a}}^e + \int_v \underline{B}^T \underline{\sigma}^e dv - \int_v \underline{N}^T \underline{b}^e dv - \int_s \underline{N}^T \underline{t}^e ds\right\} = 0 \qquad (4.9)$$

Now the stress and strain vectors for an element are related through the constitutive matrix $\underline{D}$ i.e.

$$\underline{\sigma}^e = \underline{D}\ \underline{\varepsilon}^e \qquad (4.10)$$

$$\sum^{n}\left\{\int_v \rho \underline{N}^T \underline{N} dv \ddot{\underline{a}}^e + \int_v \underline{B}^T \underline{D}\ \underline{B} dv \underline{a}^e - \int_v \underline{N}^T \underline{b}^e dv - \int_s \underline{N}^T \underline{t}^e ds\right\} = 0 \qquad (4.11)$$

The system of expressions given by Equation 4.11 may be written as follows:

$$\underline{M}\ \ddot{\underline{a}} + \underline{K}\ \underline{a} - \underline{R} = 0 \qquad (4.12)$$

where $\underline{M}$ is the mass matrix. $\underline{K}$ is the stiffness matrix of the body and $\underline{R}$ is the vector of the externally applied forces.

4.3 FINITE ELEMENT IDEALISATIONS

In the present study, concrete is simulated by solid brick elements and the reinforcing bars are modelled using the smeared representation over the three-dimensional

concrete element. Such an idealisation has been found necessary for concrete members subjected to either impulsive or impact loadings.

4.3.1 Concrete Idealisation

Two dimensional finite element idealisation has been widely used to model concrete members and has been proved to adequately represent the state of stress in the majority of cases. This approach was considered to be straightforward to formulate and computationally more economic than a full three-dimensional idealisation. The early application of the finite element method used two dimensional constant strain triangular elements to model reinforced concrete beams [57, 60, 121]. Linear and higher order isoparametric quadrilateral elements have also been used in the case of concrete members. The advantage in using these elements over triangular elements is that the size of the concrete element can be increased within the mesh and at the same time a reduction in the number degrees of freedom is obtained.

Two dimensional finite element idealisations have been found to be adequate for many loading cases, however, a full three dimensional idealisation is required for concrete members subjected to impulsive or impact loadings. This is because under such loading concrete members experience local as well as global deformations. The local deformation which results in the development of damage under

the point of impact in all three directions and it can only adequately be considered if a three-dimensional stress-strain calculation is performed.

To idealise a member using three dimensional finite elements, tetrahedral or hexahedron elements can be used. A comparison of the numerical performance of a linear and higher order tetrahedron and a linear and higher order hexahedron has been made [138, 139] in the context of the analysis of beams. It was found that higher order elements are superior to linear elements and hexahedron elements are superior to tetrahedron elements. However, higher order elements appeared to be impractical for shock wave propagation because of the numerical noise associated with the use of a lumped mass representation of the dynamic stiffness matrix [7]. Although it was possible to calculate the frequency response, the relative cost of the analysis made it uneconomic. The development of hexahedron elements in DYNA3D concentrated on the linear eight node brick element [7, 140].

Eight Node Element

The eight node brick element shown in Figure 4.1 is used throughout the present investigation to represent concrete. The element is defined in space by eight nodes which are located at the corner points. Each nodal point has three translation degrees of freedom u, v and w corresponding to the x, y and z directions. A total of 24 degrees of freedom are therefore specified for each element. To interpolate the geometry and the displacement from the nodal values shape functions are

used with each element.

Shape Function

The shape functions are derived using a local system of coordinates ξ, η and ζ, as shown in Figure 4.1. The origin of the local coordinates is the centre of the element and each of the local coordinates varies between -1 to $+1$. Discussion of the generation and properties of the shape functions has been published previously [122, 136, 141].

The displacement at a particular point inside the element is defined uniquely using the nodal values and the following shape functions:

$$\begin{aligned} u(\xi,\eta,\zeta) &= \sum_{i=1}^{8} N_i(\xi,\eta,\zeta)u_i \\ v(\xi,\eta,\zeta) &= \sum_{i=1}^{8} N_i(\xi,\eta,\zeta)v_i \\ w(\xi,\eta,\zeta) &= \sum_{i=1}^{8} N_i(\xi,\eta,\zeta)w_i \end{aligned} \tag{4.13}$$

where $N_i(\xi,\eta,\zeta)$ is the shape function of the ith node. u_i, v_i and w_i are the nodal displacements. The eight node brick element has the following shape functions at the nodal points:

$$N_1 = 1/8(1-\xi)(1-\eta)(1-\zeta)$$

$$N_2 = 1/8(1-\xi)(1+\eta)(1-\zeta)$$

$$N_3 = 1/8(1+\xi)(1+\eta)(1-\zeta)$$

$$N_4 = 1/8(1+\xi)(1-\eta)(1-\zeta)$$

$$N_5 = 1/8(1-\xi)(1-\eta)(1+\zeta)$$

$$N_6 = 1/8(1-\xi)(1+\eta)(1+\zeta)$$

$$N_7 = 1/8(1+\xi)(1+\eta)(1+\zeta)$$

$$N_8 = 1/8(1+\xi)(1-\eta)(1+\zeta)$$

The same shape functions are used for the interpolation of the coordinates at any point inside the element. Similar expressions to those given by Equation 4.13 are used to find the coordinates at any point inside the finite element

Strain-Displacement Relationship

The strain values are calculated using Equation 4.7 which may be expanded for the eight node solid element as follows:

$$\begin{bmatrix} \varepsilon_x \\ \varepsilon_y \\ \varepsilon_z \\ \gamma xy \\ \gamma yz \\ \gamma zx \end{bmatrix} = \sum_{i=1}^{8} \begin{bmatrix} \frac{\partial N_i}{\partial x} & 0 & 0 \\ 0 & \frac{\partial N_i}{\partial y} & 0 \\ 0 & 0 & \frac{\partial N_i}{\partial z} \\ \frac{\partial N_i}{\partial x} & \frac{\partial N_i}{\partial y} & 0 \\ 0 & \frac{\partial N_i}{\partial y} & \frac{\partial N_i}{\partial z} \\ \frac{\partial N_i}{\partial x} & 0 & \frac{\partial N_i}{\partial z} \end{bmatrix} \begin{bmatrix} u_i \\ v_i \\ w_i \end{bmatrix} \tag{4.14}$$

The shape functions are defined using the local coordinates ξ, η and ζ. The strain values calculated above are derived functions in terms of the global coordinates x, y and z. Hence relationships between the local and global coordinates must be found. The expressions below are obtained using the chain rule of differentiation i.e.

$$\begin{aligned}
\frac{\partial N_i}{\partial \xi} &= \frac{\partial N_i}{\partial x}\frac{\partial x}{\partial \xi} + \frac{\partial N_i}{\partial y}\frac{\partial y}{\partial \xi} + \frac{\partial N_i}{\partial z}\frac{\partial z}{\partial \xi} \\
\frac{\partial N_i}{\partial \eta} &= \frac{\partial N_i}{\partial x}\frac{\partial x}{\partial \eta} + \frac{\partial N_i}{\partial y}\frac{\partial y}{\partial \eta} + \frac{\partial N_i}{\partial z}\frac{\partial z}{\partial \eta} \\
\frac{\partial N_i}{\partial \zeta} &= \frac{\partial N_i}{\partial x}\frac{\partial x}{\partial \zeta} + \frac{\partial N_i}{\partial y}\frac{\partial z}{\partial \zeta} + \frac{\partial N_i}{\partial z}\frac{\partial y}{\partial \zeta}
\end{aligned} \tag{4.15}$$

or in matrix form:

$$\begin{bmatrix} \frac{\partial N_i}{\partial \xi} \\ \frac{\partial N_i}{\partial \eta} \\ \frac{\partial N_i}{\partial \zeta} \end{bmatrix} = \begin{bmatrix} \frac{\partial x}{\partial \xi} & \frac{\partial y}{\partial \xi} & \frac{\partial z}{\partial \xi} \\ \frac{\partial x}{\partial \eta} & \frac{\partial y}{\partial \eta} & \frac{\partial z}{\partial \eta} \\ \frac{\partial x}{\partial \zeta} & \frac{\partial y}{\partial \zeta} & \frac{\partial z}{\partial \zeta} \end{bmatrix} \begin{bmatrix} \frac{\partial N_i}{\partial x} \\ \frac{\partial N_i}{\partial y} \\ \frac{\partial N_i}{\partial z} \end{bmatrix} = \underline{J} \begin{bmatrix} \frac{\partial N_i}{\partial x} \\ \frac{\partial N_i}{\partial y} \\ \frac{\partial N_i}{\partial z} \end{bmatrix} \tag{4.16}$$

$\underline{J}$ is the Jacobian matrix which relates the local derivatives to the global derivatives of the shape function. For an isoparametric element the matrix $\underline{J}$ is as follows:

$$\underline{J} = \begin{bmatrix} \frac{\partial \sum_{i=1}^{8} N_i}{\partial \xi} x_i & \frac{\partial \sum_{i=1}^{8} N_i}{\partial \xi} y_i & \frac{\partial \sum_{i=1}^{8} N_i}{\partial \xi} z_i \\ \frac{\partial \sum_{i=1}^{8} N_i}{\partial \eta} x_i & \frac{\partial \sum_{i=1}^{8} N_i}{\partial \eta} y_i & \frac{\partial \sum_{i=1}^{8} N_i}{\partial \eta} z_i \\ \frac{\partial \sum_{i=1}^{8} N_i}{\partial \zeta} x_i & \frac{\partial \sum_{i=1}^{8} N_i}{\partial \zeta} y_i & \frac{\partial \sum_{i=1}^{8} N_i}{\partial \zeta} z_i \end{bmatrix} \tag{4.17}$$

By inverting the matrix J the derivatives with respect to cartesian coordinates in Equation 4.14 are obtained:

$$\begin{bmatrix} \frac{\partial N_i}{\partial x} \\ \frac{\partial N_i}{\partial y} \\ \frac{\partial N_i}{\partial z} \end{bmatrix} = \underline{J}^{-1} \begin{bmatrix} \frac{\partial N_i}{\partial \xi} \\ \frac{\partial N_i}{\partial \eta} \\ \frac{\partial N_i}{\partial \zeta} \end{bmatrix} \tag{4.18}$$

where $\underline{J}^{-1}$ is the inverse of the Jacobian matrix given by:

$$\underline{J}^{-1} = \begin{bmatrix} \frac{\partial \xi}{\partial x} & \frac{\partial \eta}{\partial x} & \frac{\partial \zeta}{\partial x} \\ \frac{\partial \xi}{\partial y} & \frac{\partial \eta}{\partial y} & \frac{\partial \zeta}{\partial y} \\ \frac{\partial \xi}{\partial z} & \frac{\partial \eta}{\partial z} & \frac{\partial \zeta}{\partial z} \end{bmatrix} \tag{4.19}$$

Volume Integration

For a three dimensional element the differential volume, dv, may be written as follows:

$$dv = dx\ dy\ dz \tag{4.20}$$

Equation 4.20 can be transformed into the local coordinates of the element as follows:

$$dv = |\underline{J}| d\xi\ d\eta\ d\zeta \tag{4.21}$$

where $|\underline{J}|$ is the determinant of the Jacobian matrix. The limits of integration in the local coordinates are -1 and +1 and the volume finite element can therefore be written as follows:

$$v = \int_v dv = \int_{-1}^{1} \int_{-1}^{1} \int_{-1}^{1} |\underline{J}| d\xi\ d\eta\ d\zeta \tag{4.22}$$

which is approximated using numerical integration by

$$\sum_{i=1}^{ng}\sum_{j=1}^{ng}\sum_{k=1}^{ng}|\underline{J}|_{ijk}\,w_i\,w_j\,w_k \tag{4.23}$$

where w_i, w_j, and w_k are the weighting factors of Gaussian quadrature and ng is the number of Gaussian quadrature points. The above volume numerical approximation is used to calculate the lumped mass and the internal forces at the Gaussian quadrature points which are then summed to obtain an approximation at the element level and thereafter at the structural level.

4.3.2 Idealisation of the Reinforcement

The constitutive relations used for reinforcing bars are approximated by idealising them in one dimension. The stress-strain relationships are mainly considered to be nonlinear elastic rather than plastic. This avoids the need to define elastic and plastic strain components, flow rules and hence effective tangential elasticity matrices normally required in plastic analysis [122].

Figure 4.2 shows the trilinear stress-strain curve which forms the basis of many reinforcement models. Among these models is the type which uses the pronounced yield level where the middle segment of the trilinear stress-strain relationship is eliminated by setting $\epsilon_1^r = \epsilon_2^r$ (r represents reinforcement and 1 and 2 refer to the first and second yield points).

4.3.3 Representation of the Reinforcement

The interactive effects during the loading of a reinforced concrete member between the concrete material and the steel reinforcement make the problem of nonlinear behaviour more complex. This Section discusses the different representations used for reinforcing bars in the concrete element.

The reinforcing bars may be incorporated within the concrete finite element using one of the following representations:

(1) Discrete.

(2) Embedded.

(3) Distributed.

The discrete representation of the reinforcement is simulated using one dimensional finite elements. A typical discrete representation is shown in Figure 4.3(a). These steel bar elements are connected to the concrete (element) by linkage elements which have a spring stiffness determined by a specific bond slip relationship derived from laboratory tests.

The embedded representation, shown in Figure 4.3(b), may be used in conjunction with higher order isoparametric concrete elements. The reinforcing bar is considered to be an axial member built into the concrete element such that the displacements of the reinforcing bars are consistent with those of the concrete

element. Bond slip and dowel actions can be included in the calculation.

In the case of the distributed representation shown in Figure 4.3(c), the reinforcement is assumed to be distributed over the concrete element in the appropriate direction [57]. The contribution of the reinforcement is obtained using a ratio which is dependent on the size of the concrete element and the quantity of steel present within it. In this type of representation of the reinforcement perfect bond is assumed between the reinforcement and the surrounding concrete. This assumption gives the compatibility of displacements and thus of strain between the reinforcement and the concrete. To obtain the global response of the reinforced concrete element the resistance provided by the reinforcement is added to that of the concrete at the stress level. This representation has been adopted in this investigation, and the reinforcement is considered to act only in tension in the three global directions. No dowel action is included in the formulation.

The distributed representation with perfect bond is a reasonable idealisation of the reinforcing bars. This is because a bond slip model which simulates the interaction behaviour between the concrete material and reinforcing bars has not been developed for dynamic loading conditions such as in the case of impact loading. The research work which has been carried out by Hansen and Liepins [142] and Vos and Reinhard [143] concluded that under high rates of loading bond strength is enhanced between the concrete and reinforcement. This conclusion

can be used to justify the adoption of the distributed representation model with perfect bond.

4.4 SOLUTION OF THE DYNAMIC EQUATIONS

In the previous Section the finite element equations of equilibrium governing the dynamic response have been derived. Equation 4.12 can re-written in the following form:

$$\underline{M\ddot{a}} + \underline{F} = \underline{R} \tag{4.24}$$

where F is the resultant of all the internal forces. This is a set of a second order system of differential equations which should be satisfied at any point in time, but using numerical time integration techniques the system of equations will only be satisfied at a discrete point in time. To integrate the system of equations with respect to time either an explicit or an implicit method can be used [135]. The difference between the two methods is that the explicit method solves for the acceleration while the implicit method solves for the displacement.

The explicit method uses the equilibrium conditions at time t_0 to determine the solution of the accelerations, and then a central difference time integration procedure is employed to find the velocities and displacements at time t_1 which is equal

to $(t_0 + \Delta t)$. The explicit integration procedure can be performed at elemental level i.e. the internal nodal forces F at time t_0 can be computed and assembled element by element without assembling the full stiffness matrix. If a lumped mass matrix is adopted i.e. the mass matrix is diagonal, the dynamic governing equation, Equation 4.24, can be solved without the requirement for factorization of the dynamic matrix and a forward and backward substitution procedure. The advantage of the method is then obvious i.e. low storage is required and relatively little computing time is needed to solve the system of equations for each time step. However the method is only conditionally stable and the time step may have to be very small to ensure the convergence of the solution.

The implicit method, on the other hand, uses the equilibrium conditions at time t_1 equal to $(t_0 + \Delta t)$ to obtain the solution of the displacements at time t_1. The solution has the advantage that it is unconditionally stable but the dynamic stiffness matrix, in this case, must be fully assembled and factorized because it appears in the solution as the coefficient matrix of the unknowns.

In DYNA3D [7], the finite element code in which the concrete model has been implemented, the explicit central difference method is used. DYNA3D is a code developed to analyse three dimensional structural contact and impact problems, therefore, the saving in computing time can be significant. This is because of the number of equations involved as well as the large number of time steps i.e. the

duration of the impact event is calculated in terms of very small time increment steps. Small time step increments are required for the integration of the dynamic governing equations in order to satisfy the rapid change of the state of strain in the member.

In the next Section the explicit central difference method is discussed briefly.

4.4.1 Explicit Central Difference Method

To solve Equation 4.24, let the values of $a, \dot{a}$ and $\ddot{a}$ in the interval of time $t = 0$ up to $t = t_0$ be assumed to be known. In order to obtain these values after a further short interval in time i.e. at the point $t_1 = t_0 + \Delta t$, a linear forward movement in time is applied as follows:

Let the displacement vector $\underline{a}$ be expanded with respect to time using Taylor series at time $t = t_0$,

$$\underline{a}_1 = \underline{a}_0 + \dot{a}_0 \Delta t + \frac{1}{2}\ddot{\underline{a}}_0 \Delta t^2 + ... \tag{4.25}$$

and

$$\underline{a}_{-1} = \underline{a}_0 - \dot{\underline{a}}_0 \Delta t + \frac{1}{2}\ddot{\underline{a}}_0 \Delta t^2 - .... \tag{4.26}$$

where the subscripts 0, -1 and 1 refer to the values measured at times t_0, $t_0 - \Delta t$ and $t_0 + \Delta t$ respectively. The error in the truncated expansion is of the order of

$(\Delta t)^2$ i.e. third term truncation.

Applying the expression in Equation 4.26 at the point in time t_1 then,

$$\underline{a}_0 = \underline{a}_1 - \underline{\dot{a}}_1 \Delta t + \frac{1}{2}\underline{\ddot{a}}_1 \Delta t^2 \tag{4.27}$$

Substituting $\underline{a}_1$ from Equation 4.25 into Equation 4.27 gives the following expression:

$$\underline{\dot{a}}_1 = \underline{\dot{a}}_0 + \frac{1}{2}(\underline{\ddot{a}}_0 + \underline{\ddot{a}}_1)\Delta t \tag{4.28}$$

The displacements at time t_1 and the displacement increment are obtained from Equation 4.25.

$$\Delta \underline{a} = \underline{a}_1 - \underline{a}_0 \tag{4.29}$$

The stiffness matrix K is then updated and the internal forces are calculated using the updated Lagrangian methods for the formulation of problems involving large deformations. The accelerations $\underline{\ddot{a}}_1$ and the velocities $\underline{\dot{a}}_1$ are calculated using Equations 4.25 and 4.27 respectively.

It is then possible to proceed to the next time step i.e. $t_2 = t_1 + \Delta t$, as $\underline{a}_1, \underline{\dot{a}}_1$ and $\underline{\ddot{a}}_1$ are known.

4.5 CONTACT FORCES DURING IMPACT

In Section 4.4 a solution for the governing equation is given. The externally applied forces R are regarded as known, however, this is not true in an impact analysis where the forces acting between the impactor and the target are not known in advance and are dependent on the geometric and material properties of the impactor. They also depend on the velocity of the impactor at the time of impact. The impact forces can be calculated using discrete spring elements between the contacting bodies but then a constraint at the time of impact has to be applied on the global governing equations. DYNA3D [7, 144], however, uses the concept of master and slave segments sliding on each other. A segment is a polygon defined by the corner nodes, thus, slave and master segments give rise to slave and master nodes respectively.

The slave segments are regarded as being in contact with the master segments, if during the analysis they are found to have the same global coordinates. The slave nodes are forced to slide on the master segments until a check on the displacement shows that the either segments have separated or the normal contact forces have become tensile at which point the contacting segments are released from being in contact. The main procedure involved at the interfaces and at each explicit time integration are:

(1) Determine/update the location of each slave node by determining each of

nearest master nodes.

(2) For each master segment, determine the slave segments which are involved in the contact.

(3) Determine the tensile interface force.

The effect of contact is translated by imposing constraints on the global equations. This is done by eliminating the degrees of freedom of the slave segments which are in contact with the master segments. The respective normal nodal force components are distributed to the nearby master nodes. Tangential forces can develop between the master and slave segments in the case of an oblique impact (not a centred impact) where there is a tendency for relative motion to take place between the segments which are in contact. The tangential forces are calculated using friction laws.

4.6 CONCLUDING REMARKS

In this Chapter a description of the finite element modelling of concrete structures and the numerical procedures used in the implementation of the elastic plastic formulation.

(1) The underlying concepts of the finite element method and the derivation of the governing equations of equilibrium using the principle of virtual displacements are presented in this Chapter. The eight node isoparametric brick element which has been used to model concrete has been discussed. The smeared representation for the reinforcing bars is also described.

(2) The explicit central difference method which is used to solve the equations of equilibrium is described.

(3) The underlying concept used in the calculation of the contact force during an impact between two bodies is discussed briefly.

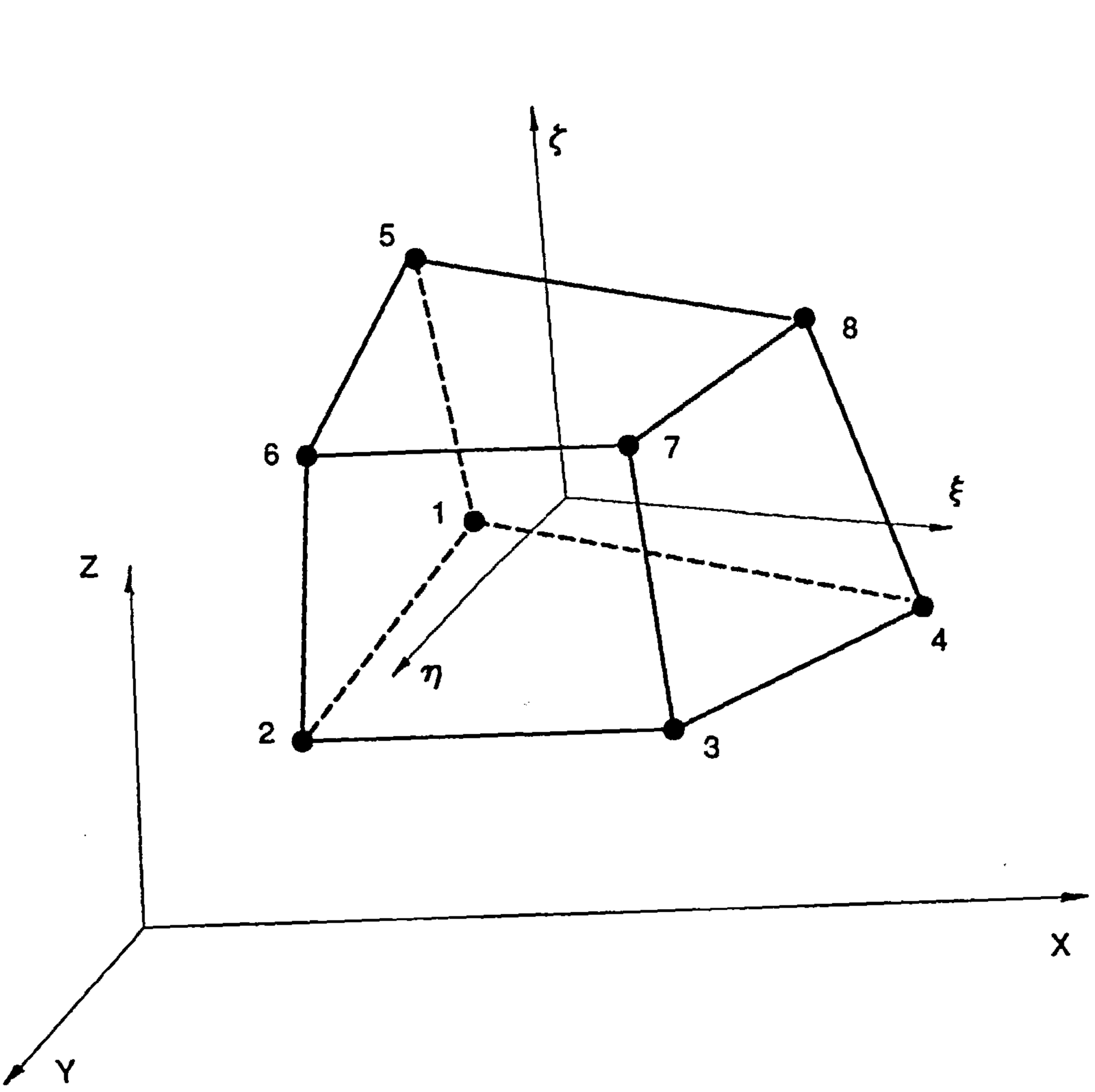

Figure 4.1: Three dimensional solid element

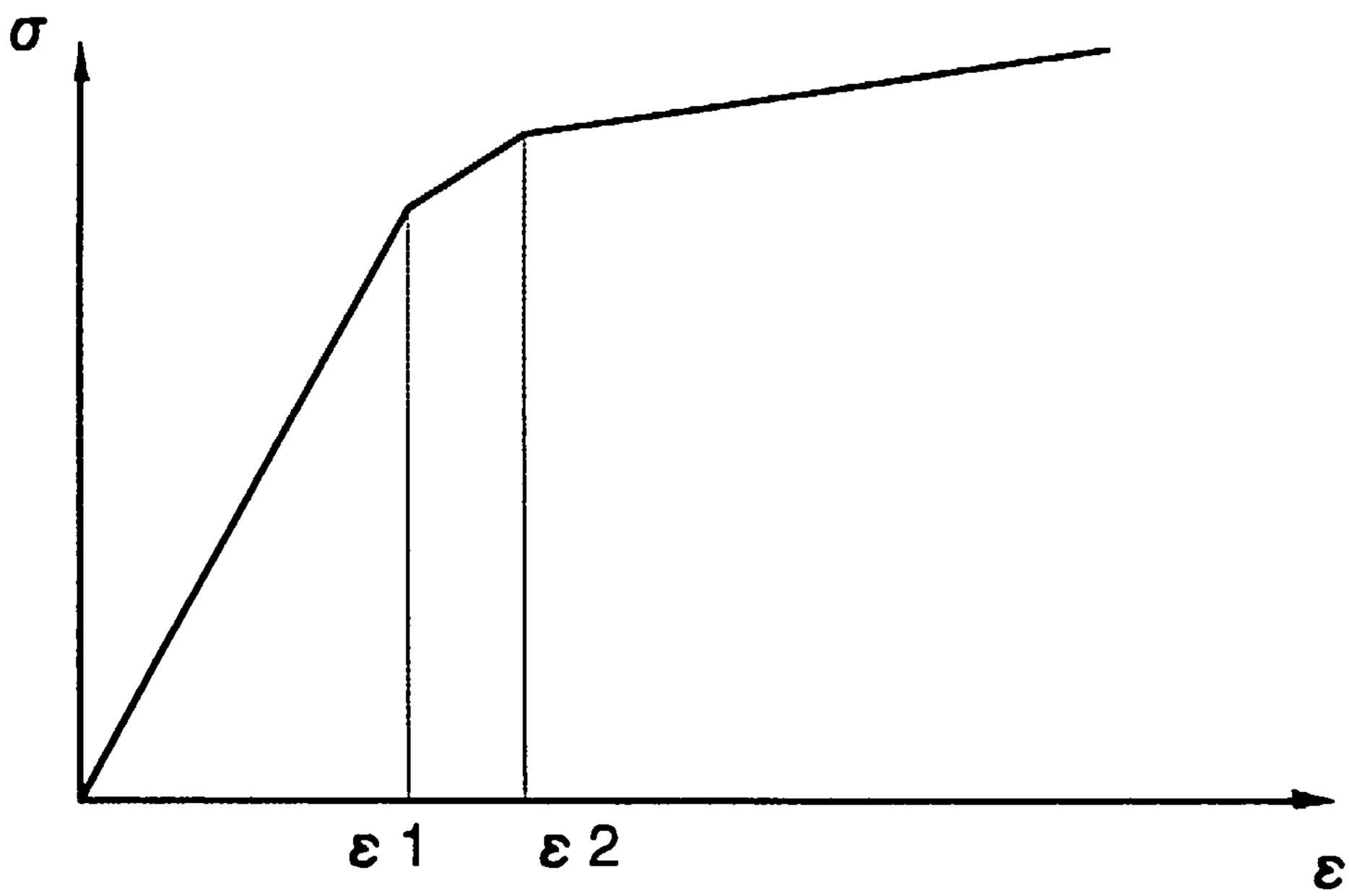

Figure 4.2: Tri-linear stress-strain relationship for reinforcement

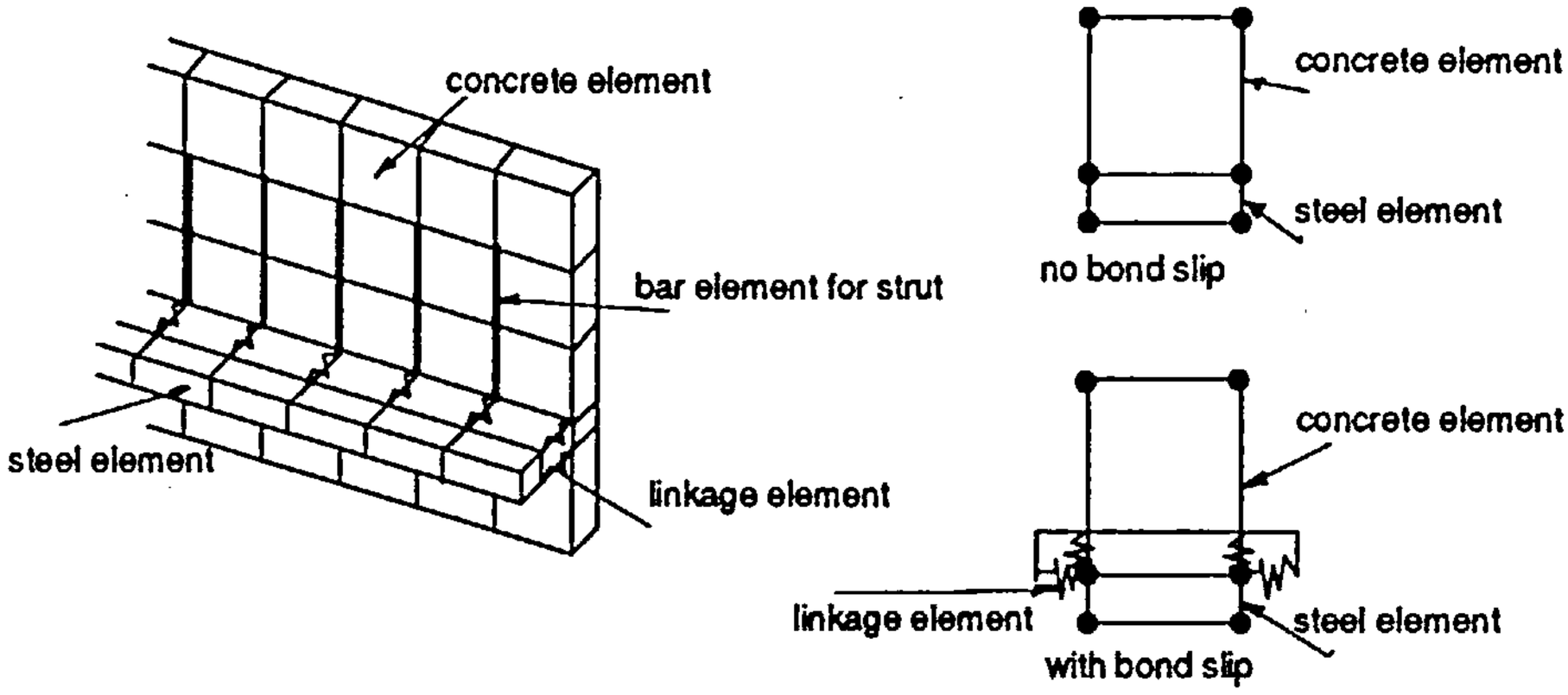

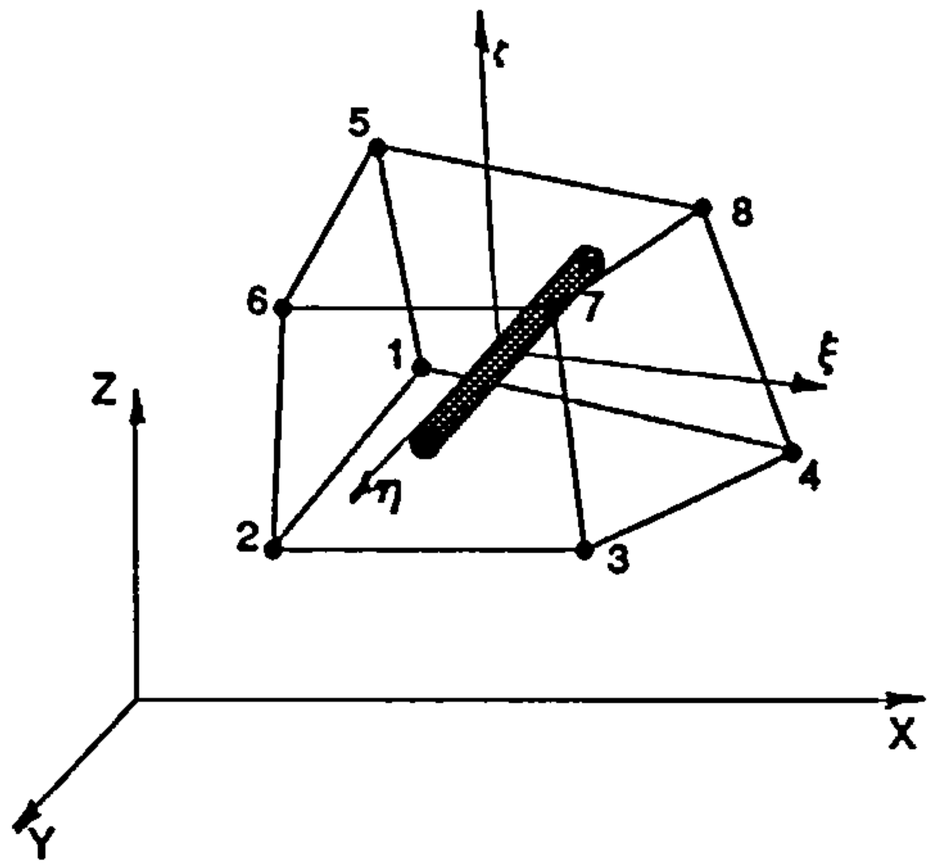

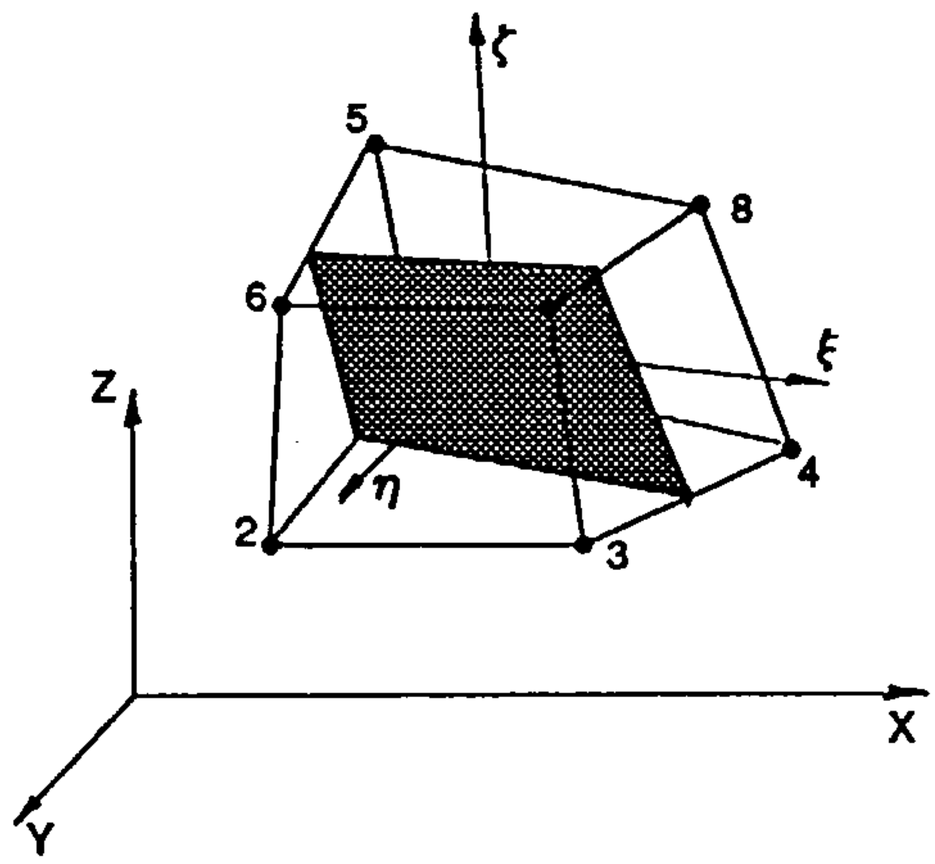

Figure 4.3: Representations of reinforcement

Chapter 5

CONCRETE MODEL: THE DEVELOPMENT OF THE CODE

5.1 INTRODUCTION

As stated in Chapter 1, the main objective of the present study was to develop a realistic tool for the non-linear analysis of reinforced concrete structures subjected to impact loadings. In order to achieve this objective a new concrete model was developed and programmed in two routines named F3DM61 and SETS61. The concrete routines were written in FORTRAN and incorporated into the finite element code DYNA3D. The two routines were programmed to perform the following tasks:

(1) F3DM61: This routine was used for the stress analysis of the concrete material and the reinforcing bars.

(2) SETS61: This routine was used for the definition and storage of the input data. This routine was also used in the evaluation of the constants for the failure function.

A description of the two routines and their incorporation into the finite element code DYNA3D is given in detail in the following Sections.

5.2 DESCRIPTION OF THE ROUTINES

5.2.1 Routine F3DM61

In finite element formulations non-linear deformation can occur either because of geometrical non-linearities i.e. non-linear strain-displacement, or because of material behaviour such as cracking and plastic deformation. Geometric non-linearity is solved in DYNA3D using the updated Lagrangian method [7, 140]. The material non-linearity, however, can be taken into consideration at the material level. Therefore the purpose of this routine is to perform the non-linear stress analysis of the newly implemented concrete model. The non-linearities considered include the material non-linear behaviour which is due to elastic-plastic deformations, cracking and crushing of concrete, yielding and plastic deformation of the reinforcing bars.

The routine was partitioned into six main segments which loop over each element. Each one of the segments had a specific task in the modelling of a phenomenon in the behaviour of a structural concrete member subjected to loading. This procedure gave greater flexibility thus allowing the model to be changed and the addition of other phenomenon associated with the behaviour of concrete and the reinforcing bars. The segments were defined as follows:

(1) Common blocks, material array and variables.

(2) Stress update and post cracking treatment.

(3) Elastic-plastic stress analysis and failure diagnostic.

(4) Calculation of the widths and directions of the cracks.

(5) Representation of the reinforcing bars.

(6) Calculation of the total stress and the crack diagnostic loading.

The overall structure of this routine is presented in the form of a flow chart which is shown in Figure 5.1 Each of the segments itemised above is highlighted in the flow chart and in the listing of the routine in Appendix D. A description of the segments in the routine and the principal variables used are discussed below.

(1) Common blocks, material array and variables

In the program F3DM61 most of the information is transferred through the argument list. However, in order to be consistent with the main code DYNA3D the required common blocks are included. These common blocks

and the principal variables are now defined.

COMMON/AUX2/

d1, d2, d3, d4, d5, d6: components of the strain rate.

wzzdt, wyydt, wxxdt: rotations in the three directions are not used.

COMMON/AUX14/

sig1, sig2, sig3, sig4, sig5, sig6: components of the total stresses i.e. concrete stress plus reinforcing bar stress contributions.

sigc1, sigc2, sigc3, sigc4, sigc5, sigc6: components of the concrete stresses.

sig7: effective plastic strain.

sigr1, sigr2, sigr3, sigr4, sigr5, sigr6: components of the stresses in the reinforcing bars.

pxr, pyr, pzr: reinforcing bars percentage in terms of the area in the x, y and z directions.

zl, zm, zn: cosine directors in the x, y and z directions.

sf1, sf2, sf3: principal stresses in the x, y and z directions.

ex1, ex2, ex3, (ef1, ef2, ef3): element extension in the three directions.

epx1, epx2, epx3: strain in the reinforcing bars in the three directions.

crak1, crak2, crak3: crack indicators for the three directions.

eps1, eps2, eps3, eps4, eps5, eps6: components of the total strain.

epv: effective plastic strain increment.

np: number of points in the strain stress curve.

COMMON/AUX33/

ix1, ix2, ix3, ix4, ix5, ix6, ix7, ix8: element nodal connectivities.

mxt: integer used to determine data addresses.

nmel: element number.

COMMON/AUX35/

rhoa: density.

cxxa: coefficients relating stress and strain.

COMMON/AUX36/

lft: integer beginning of the elements group.

llt: integer end of the element group.

COMMON/BK02/

iburn: not used.

dt1: time step.

COMMON/BK28/

summss, xke, xpe: not used.

tt: time at which a crack has occurred.

MAIN VARIABLES

at: array in which all the required data is stored for the analysis. This array includes concrete, reinforcing bars and the failure criterion constants calculated in routine SETS61 which is listed in Appendix D.

volo: current volume of the concrete element.

yms: initial tangent modulus for concrete.

pr: Poisson's ratio for concrete.

sigc: uniaxial compressive strength for concrete.

sigt: uniaxial tensile strength for concrete.

g: shear modulus for concrete.

blk: bulk modulus for concrete.

fo: characteristic crack opening length.

agg: characteristic aggregate size.

xm: characteristic hardening coefficient.

eyr: initial tangent modulus for steel.

qs: yield stress for steel.

qh: hardening modulus for steel.

epf: ultimate strain for steel.

ay, by, cy, dy (af, bf, cf, df): failure criterion constants.

cl: characteristic length of the finite element.

stiff: uniaxial stiffness after cracks have been closed.

The computational procedure for this segment i.e. segment 1, is listed in Section D.1 in Appendix D.

(2) Post cracking treatment

After the crack has been initiated but before updating the stress state in the

concrete element under consideration, the stresses of the cracked element are modified to take account of the post cracking behaviour. The crack normal stresses are decoupled from the uncracked direction and decayed to zero as a function of the crack width. The law which governs this decay in the strength of the concrete element follows a linear variation as shown in Figure 3.7. The ascending branch of the curve in Figure 3.7 models the increase in tensile strength of the concrete up to the uniaxial tensile strength. The descending branch of the curve models the decay of the tensile strength resulting from the increase in the width of the crack.

The shear of the cracked concrete element is represented by means of a shear retention factor β, indicating the percentage of elastic shear capacity that is retained after the concrete element has cracked [117, 145]. An alternative approach is to represent the shear of a cracked concrete element using an aggregate interlock model [116]. The law which governs this decay in the shear stiffness of the cracked concrete element follows a parabolic variation as a function of the crack width and the size of the aggregates as shown in Figure 3.8.

This segment, therefore, performs the post-cracking treatment of the cracked concrete element. Figure 5.2 shows the flow chart for this segment i.e. segment 2 and the computational procedure which is involved in this segment

of the routine is listed in Section D.2 in Appendix D.

(3) Elastic-plastic stress analysis and failure diagnostic

In this segment the elastic-plastic stress analysis is performed and damage to the concrete element is indicated by the use of an indicator integer ISTAT.

(1) ISTAT = 1 elastic behaviour of the concrete element.

(2) ISTAT = 2 plastic behaviour of the concrete element.

(3) ISTAT = 3 pure cracking mode of the concrete element.

(4) ISTAT = 4 mixed cracking and crushing mode of the concrete element.

(5) ISTAT = 5 pure crushing mode of the concrete element.

The flow chart for this segment is shown in Figure 5.3 and the computational procedure is listed in Section D.3 in Appendix D. The following operations are performed in this segment:

(1) A check to determine if the current set of trial stresses has violated the loading function.

(2) The determination of the number of constant strain sub-increments.

(3) The determination of the elastic-plastic stiffness and the calculation of the plastic stresses sub-increment.

(4) The determination of the failure mode of the element at the sampling point.

(5) The evaluation of the principal stresses and cosine directors.

Each of these operations are described in detail below:

At the linear stage of the numerical algorithm, a set of trial elastic stresses is computed. These trial elastic stresses are tested with respect to the loading function i.e. f. If the trial stresses do not violate the loading surface the material is undergoing elastic deformation and the governing equations of equilibrium are determined in a direct manner. If the loading surface has been violated by the stresses, the element is under plastic loading. In this case the relationship between the stress and strain is non-linear resulting in difficulties arising in the area of numerical stability and the solution convergence to an equilibrium state, particularly when the failure phenomenon is included in the analysis. Since concrete behaviour is stress history dependent, two requirements should be considered to ensure an accurate solution:

(1) The structural deformation history should not deviate from the true path.

(2) Accuracy should be maintained between the time step intervals.

These can be achieved by ensuring equilibrium between the applied forces and the corresponding internal forces at the interval stress state for each time step during the analysis. To satisfy the above requirements an incremental-iteration solution is used.

A typical calculation step consists of assuming a loading time step followed by equilibrium stress iterations. The structural stiffness need not be updated during stress iterations until the equilibrium conditions are satisfied [122]. When a new time step load increment is assumed the stiffness values are then updated. In particular this method is compatible with the organisation of the finite element code, DYNA3D, because the iterative programming is all carried out at the concrete routine level.

At each time step, the iterative procedures require the re-calculation of the material modulii and the corresponding stress and strain values. The use of either the initial stress or the initial strain can be utilised to calculate the updated state of the material [122]. The basic concept is that a solution satisfying the equilibrium conditions can be obtained by adjusting either the stress or the strain values. The difference between the initial stress and the initial strain techniques is shown in Figure 5.4. Assume that the curve AB in Figure 5.4 is the true stress-strain curve. Based on the current plastic tangent stiffness the first trial solution denoted by the point 1 in Figure 5.4 is obtained. Using the initial stress technique, the stress value at point 1 can be corrected to obtain the true value by going through iterations 2, 3 as shown in Figure 5.5. The initial stress technique, appears to be more suitable for concrete because of the effect of strain-hardening on the shape of the stress-strain curve. On the other hand iterations based on the initial

strain technique may not converge in the case of strain hardening effects as shown in Figure 5.5.

The computational procedures employed to implement the initial stress techniques make use of the strain increment obtained at the *ith* time step increment, $\underline{\varepsilon}_i$. $\underline{\varepsilon}_i$ is subdivided into a number, n, of constant strain sub-increments $\Delta\underline{\varepsilon}_i$, each strain sub-increment is equal to $\underline{\varepsilon}_i/n$, as shown in Figure 5.6. The corresponding stress sub-increment $\Delta\underline{\sigma}_i$ is calculated for each strain sub-increment $\Delta\underline{\varepsilon}_i$. The process is repeated for all sub-increments i.e. n . After each stress sub-increment the total stress is calculated and a check on the state of the material is performed using the loading functions discussed in Chapter 3.

In the iterative calculation two types of scaling are used i.e. linear and non-linear scaling procedures.

Linear scaling

At the start of the solution the response of the material is linear elastic. If the stress conditions violate the loading conditions, non-linear deformations are assumed to occur in the concrete material, which may lead to the failure of the concrete element.

In order to evaluate the stress conditions in the concrete (elastic or plastic stress states) a parameter ϖ^n is defined as the scaling factor required for the stress in a given element to satisfy the initial loading condition. It follows from the failure criterion used in the present investigation, and described in Section 3.5, that ϖ^n must satisfy the following expression:

$$\begin{aligned} f(\varpi^n \underline{\sigma}^n, f'_c) &= 0 \\ A\frac{\varpi^{(n)2}\underline{J}_2^n}{f_c'^2} + \varpi^n\lambda\frac{\sqrt{\underline{J}_2^n}}{f'_c} + B'\frac{\underline{I}_1^n}{f'_c} - 1 &= 0 \end{aligned} \tag{5.1}$$

ϖ^n can be obtained explicitly as the roots of the second degree polynomial defined by Equation 5.1.

$$\begin{aligned} \Delta &= \lambda\sqrt{\underline{J}_2^n} + B'\underline{I}_1^n \\ \varpi^n\frac{f'_c}{\underline{J}_2^n} &= (-\Delta \pm \sqrt{\Delta^2 + 4A\underline{J}_2^n})\frac{1}{2A} \end{aligned} \tag{5.2}$$

Since the initial yield surface is closed and convex, two paths are possible to reach the initial yield condition corresponding to the two roots of the second degree polynomial. Only the positive root needs to be considered. This computational procedure is performed using subroutine FAILF which is listed in Appendix D

Non-linear scaling

After the initial yield surface is reached, this can be detected by comparing ϖ^n with the current yield stress, the response of the concrete element may change either from an elastic to a plastic response and then to a fractured

element response or from an elastic response directly to a fractured element response. Since different constitutive equations and solutions are used in the elastic, plastic and fractured elements an additional scheme of scaling needs to be devised so that the appropriate value of the stress increment which is just sufficient for yielding to occur in an elastic concrete element or for fracture to occur in a plastic concrete element is used. This gives a much more accurate solution for the plastic-fracture analysis. The complete procedure, which is used in the calculation of the non-linear behaviour after the initial yielding has occurred but before the concrete has reached the fracture point, is summarised in the following five steps:

(1) The strain increment calculated and updated in the main program is then transferred to the concrete routine in order to calculate the stress and update the state of the material.

(2) A check on the previous stress state of the element is carried out to determine whether the concrete element is in the elastic or plastic regions or has failed. If the element is in the elastic region a scaling of the stress is performed as discussed below in (3). If the element is in the plastic region the procedure discussed below in (4) is followed.

(3) The elastic stress increment corresponding to the strain increment is

calculated. Again a check on the total stress is carried out to determine whether the element has yielded. If the element is in the elastic state control is returned to the main program for a new element strain increment. If there are additional elements in which the stress conditions are found to be beyond the yield limit, then a minimum factor κ^n is evaluated where $0 \leq \kappa^n \leq 1$. This represents the elastic stress conditions, $\sigma^n + \kappa_n \sigma^n$, which satisfy exactly the yield criterion i.e. $f = 0$.

Beyond this point i.e. $f > 0$, the stress-strain response of the concrete element which has yielded follows the plastic constitutive equations. Scaling of the stress conditions on the loading surfaces is necessary in order to simulate the behaviour of the material and achieve a stable solution. In this case, interpolation formulae are used to evaluate the value of κ^n.

(4) The plastic strain is calculated by subtracting the elastic strain from the total strain increment. The incremental constant strains approach is then used to simulate the plastic stress-strain curve. This computational procedure is performed using the subroutine PLAS which is listed in Appendix D.

(5) In each stress increment, the updated state of stress is examined to determine if the material has fractured. If the stress condition has

reached the fracture limits, the concrete element will either crush, crack or exhibit a mixed type of fracture depending on the fracture mode criterion discussed in Section 3.5. This computational procedure is performed using the subroutine ZAILF which is listed in Appendix D.

(6) After failure has been detected in the concrete element(s) the principal stresses and their cosine directors are calculated in order to determine the widths and directions of the cracks. This computational procedure is performed using the subroutine PRCOS which is listed in Appendix D.

(4) Calculation of crack width and direction

Having determined the failure mode in the previous segment of the concrete subroutine, the onset of cracking is checked for possible crack initiation by comparing the maximum principal stress to the tensile strength. The current crack width corresponding to the offending principal stress is then calculated as a function of the normal strain and a characteristic element length. If on checking a second crack initiates at a later stage the crack width calculation and the stress analysis are transformed to a two dimensional problem, hence taking account of the anisotropic behaviour experienced by the concrete element after the development of the first crack. A

third crack may eventually develop in the concrete element, in this case the stress analysis is further reduced to one a dimensional problem. In this concrete model, a maximum of three cracks are allowed to form in the concrete element. The cracked element are flagged for post processing and post cracking treatment in the next time step of the analysis. Figures 5.7 and 5.8 show the flow chart for this segment and the corresponding computational procedure involved in this segment is listed in Section D.4 in Appendix D

(5) Representation of the reinforcing bars

In this segment the contribution from the reinforcing bars to the strength of the reinforced concrete member is analysed. The stresses in the reinforcing bars are calculated assuming perfect bond between the concrete and steel bars. The reinforcing bars are represented as tensile stiffeners which are allowed to resist only tensile stresses. The reinforcing bars experience plastic deformation upon reaching the yield plateau and fail after the failure strain is exceeded. Figure 5.9 shows the flow chart for this segment and the corresponding computational procedure involved in this segment is listed in Section D.5 in Appendix D

(6) Calculation of the total stress and the crack diagnostic loading

In this segment the total stresses are calculated and the crack indicators are loaded. The computational procedure involved in this segment is listed in Section D.6 in Appendix D

5.2.2 Routine SETS61

This routine, when called by the main program, initialises the concrete properties and stores them in a array which is readily accessible by the concrete model routine F3DM61 i.e. passed on through argument lists.

In this routine the four constants ay, by, cy and dy used in the failure function are calculated. The procedure involved in the calculation is based on establishing a system of four equations. Each one of the equations has four unknowns which are dependent on a set of stress conditions. The stress conditions which give the default values for the four constants are described in Section 3.5.5. The computational procedure is performed using the subroutine CHENCONST which is listed in Section D.7 in Appendix D.

5.3 INCORPORATION OF ROUTINES INTO DYNA3D

The purpose of this Section is to briefly describe the steps followed during the development of the concrete model including its implementation and incorporation into the finite element code DYNA3D. This has been highlighted because the success of the material model is dependent on how well the concrete model algorithm interacts with the main code. A detailed discussion of the concrete model, including the listing, has been included in Sections 5.2. A detailed discussion of

the incorporation of concrete model into the finite element program DYNA3D is now given below.

In order to incorporate the newly developed material model into the finite element code DYNA3D the following two tasks had to be performed:

(1) Programming of the concrete model

(a) It was found necessary initially to examine the structure of the finite element program DYNA3D and to develop an understanding of the programming techniques and the utilisation of the in-core and the out-of-core storage requirements. This examination allowed, for example, the determination of the different variables which are required by the main code including i.e. the input data which define the properties of the material under investigation and which must be made available to the newly developed material model.

(b) It was also necessary to determine the variables which are dumped for the eventual post-processing operations i.e. deformations, stresses, strains, invariants, crack positions and widths, etc. It was found that the best way to overcome this problem was to study material models which were already present in the code. Among the material subroutines which were also investigated was the Winfrith model which was used to take advantage of the post-processing software TAURCON [146] which was used to plot the crack patterns resulting from this investigation.

(c) FORTRAN programming [147] of the new material subroutine had to be effective and be compatible with the vectorisation procedures present in DYNA3D [7] in order to make efficient use of the storage and the processing time.

(2) Modifications carried out in the finite element code

DYNA3D is structured in such a way that there is a main code and four overlays. Figure 5.10 shows the flow chart for the main code DYNA3D. The overlays which divide the main code perform the following functions:

Overlay 1 restart phase.

Overlay 2 input phase.

Overlay 3 initialisation phase.

Overlay 4 finite element solution.

The incorporation of the concrete routine into DYNA3D requires modifications to the main program and the overlays. For example, a storage allocation for the new concrete model is required in the main program.

In the input phase overlay, the new material properties were implemented in subroutine MATIN. A new subroutine SETS61 was programmed in which the material properties and other variables were stored. The properties of the material were also programmed in subroutine PRINTM to allow them to be printed

out for verification purposes. Additional output required i.e. relating to the steel data and the cracked elements, was added to subroutine PRINTM.

In the initialisation phase the variables were initialised in a similar manner to the existing material models.

In overlay 4, the concrete model subroutine, which was named FE3DM61 was added to subroutine FEM3D, in which the different material routines are called as shown in the flow chart in Figure 5.10.

5.4 INPUT DATA

The input data required for the newly developed concrete model is summarised below:

Concrete

(1) Initial tangent modulus.

(2) Poisson's ratio.

(3) Uniaxial compressive strength.

(4) Uniaxial tensile strength.

(5) Characteristic crack opening length

(6) Characteristic aggregate size (or shear retention factor).

(7) Characteristic hardening coefficient.

(8) Failure criterion constants.

(9) Uniaxial stress-strain curve (at least three points are required) which must be determined for the specific structural problem under investigation.

(10) Density.

Reinforcing bars

(1) Young's modulus.

(2) Yield stress.

(3) Hardening modulus.

(4) Ultimate strain.

The impact load is normally generated by an impactor which is significantly stiffer than the concrete member. It is normally either modelled in steel or as a rigid body. Thus the properties of the impactor which are required to be defined are as follows:

(1) Initial tangent modulus.

(2) Poisson's ratio.

(3) Density.

(4) Velocity of impact.

In order to undertake the analysis of a concrete member under the action of impact loadings all the concrete material input data specified above should be available. A complete set of data has not been included in any of the investigations described in the literature. In such situations, values for the material properties which have not been included have been carefully chosen so that they represent the material properties of the concrete and reinforcing bars under consideration.

The examples studied numerically in the next Chapters are aimed at demonstrating the ability of the newly developed concrete model to predict the behaviour of reinforced concrete members subjected to impact loading. A parametric study was undertaken in order to investigate the sensitivity of the new concrete model to the material parameters which were not measured in the respective investigations. It should be emphasised that ideally all the material input parameters for the new concrete model should be obtained from laboratory based investigations.

The accuracy of the new concrete model was assessed by comparing the results from the numerical analysis with those obtained from previously published laboratory tests. The output from the program can include deformations, strains, stresses, variations in the contact loads with respect to time, cracks patterns at different points in time during the impact event, local and global velocities

and acceleration histories, etc. Ideally, the validation procedure should take into consideration as many of these variables as possible, however, because of the difficulties encountered in obtaining actual recorded values for these variables at a practical level, the assessment of the accuracy of the new concrete model had to be restricted to the limited sets of results available in the literature.

5.5 CONCLUSIONS

In this Chapter the listing of the code and detailed flow charts for the algorithms used in the development of the new three-dimensional elastic-plastic fracture concrete model have been included. The new concrete model algorithm was partitioned into six independent segments. A flow chart for each segment has been included in which the operations involved in it are explained. The incorporation of the new concrete model into the general purpose finite element analysis code DYNA3D is also discussed and a flow chart detailing the algorithm of DYNA3D has been included. The list of the input material parameters required for the newly developed concrete model has been included.

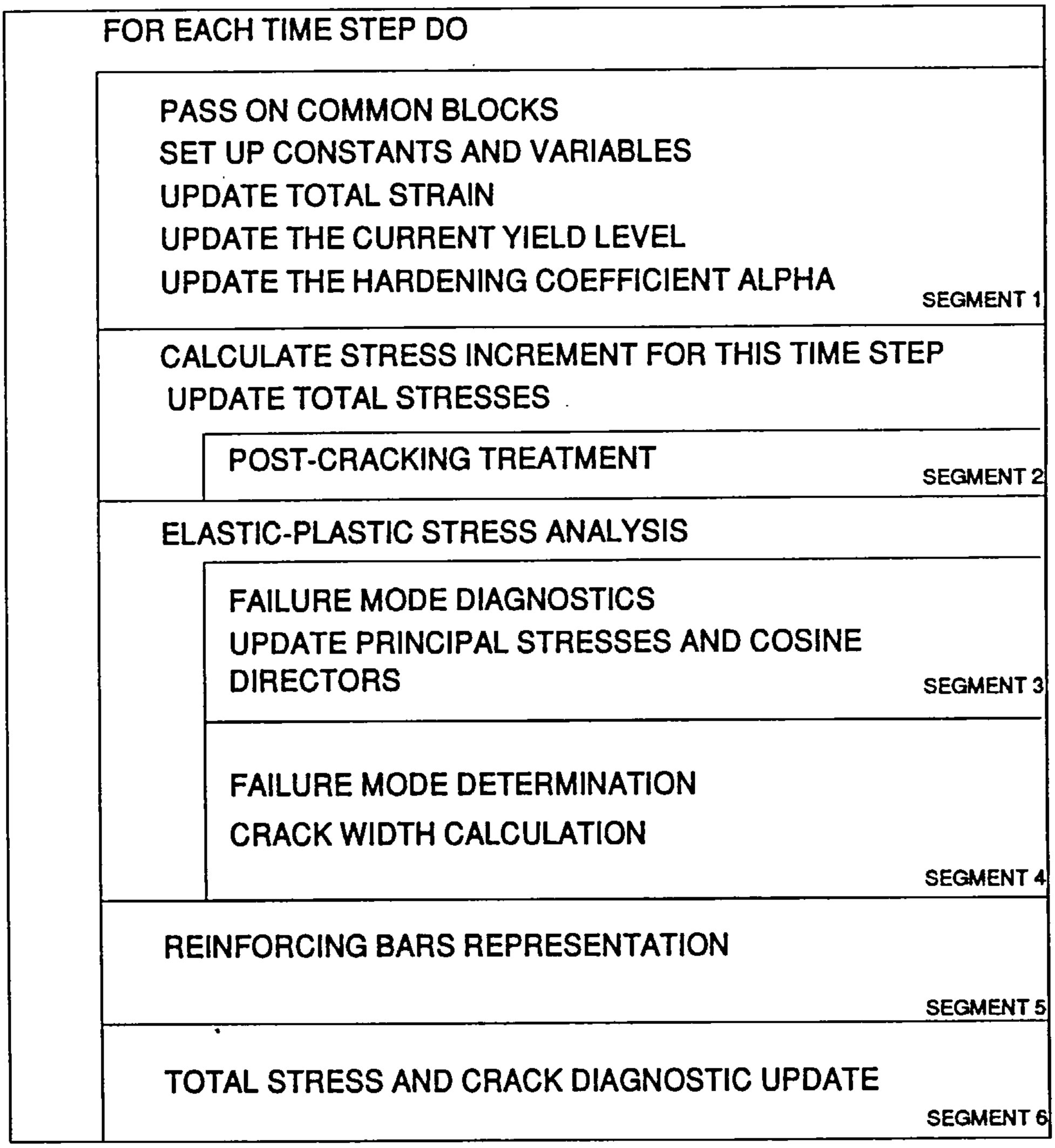

Figure 5.1: Flow chart for the main routine F3DM61

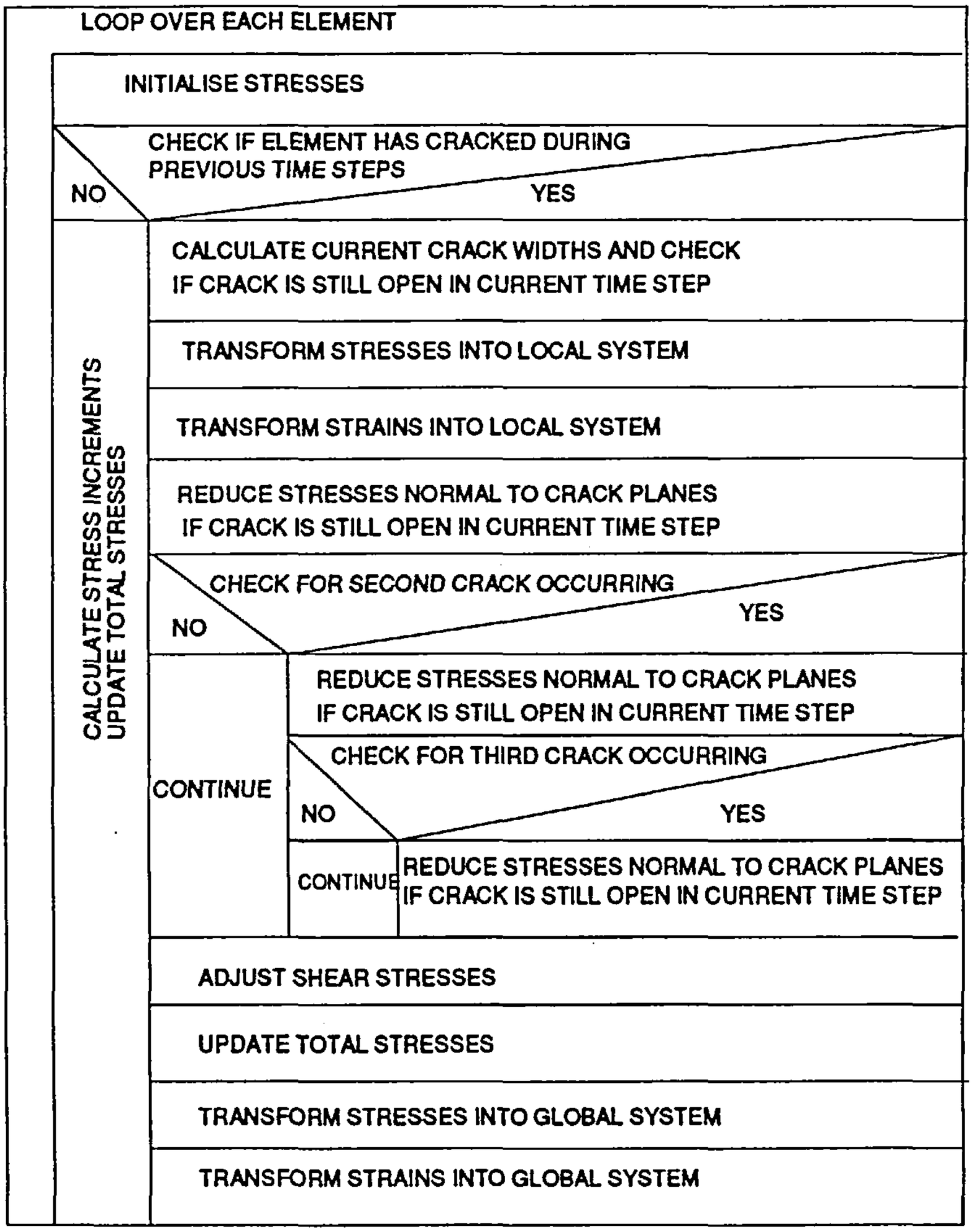

Figure 5.2: Flow chart for segment 2 of routine F3DM61

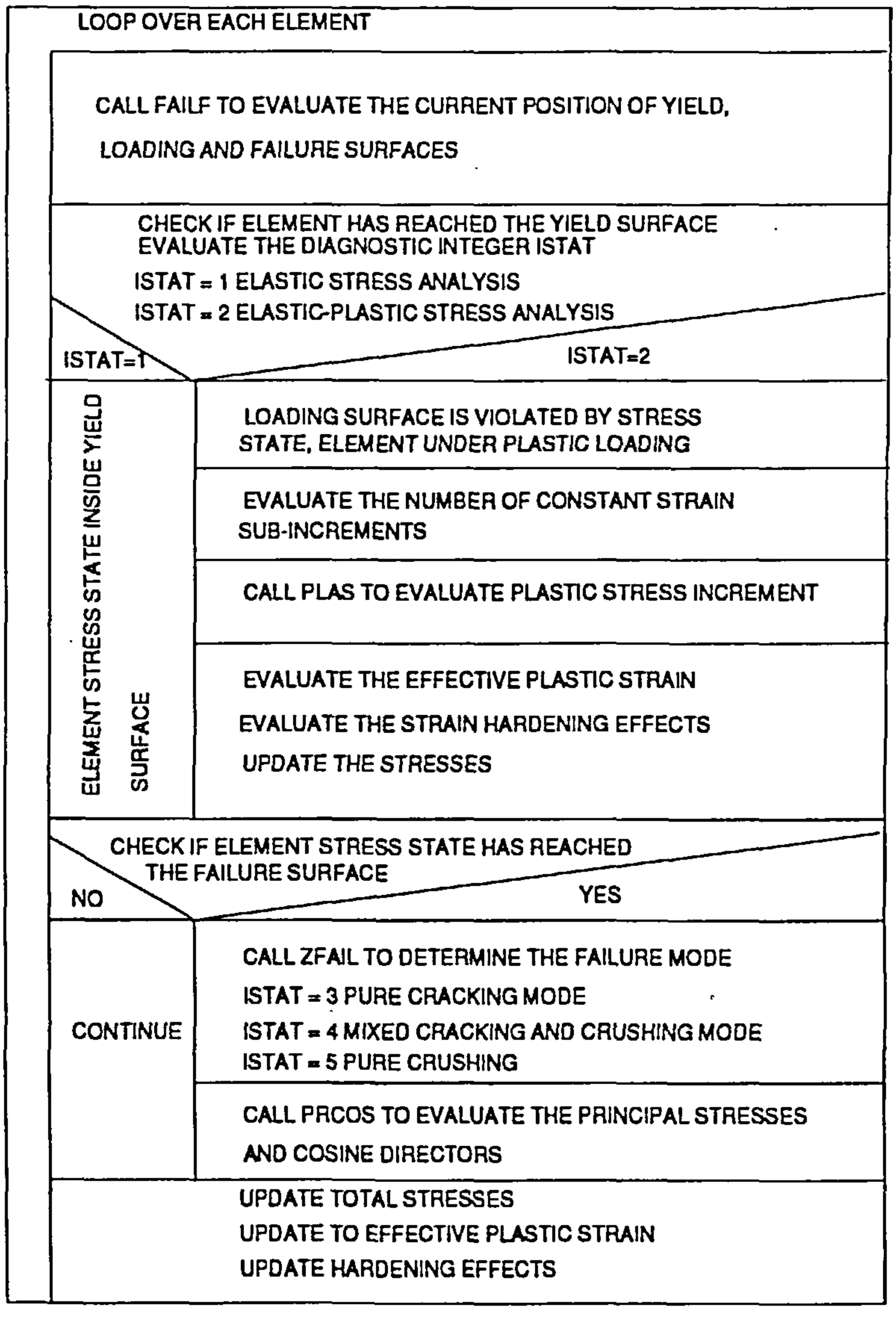

Figure 5.3: Flow chart for segment 3 of routine F3DM61

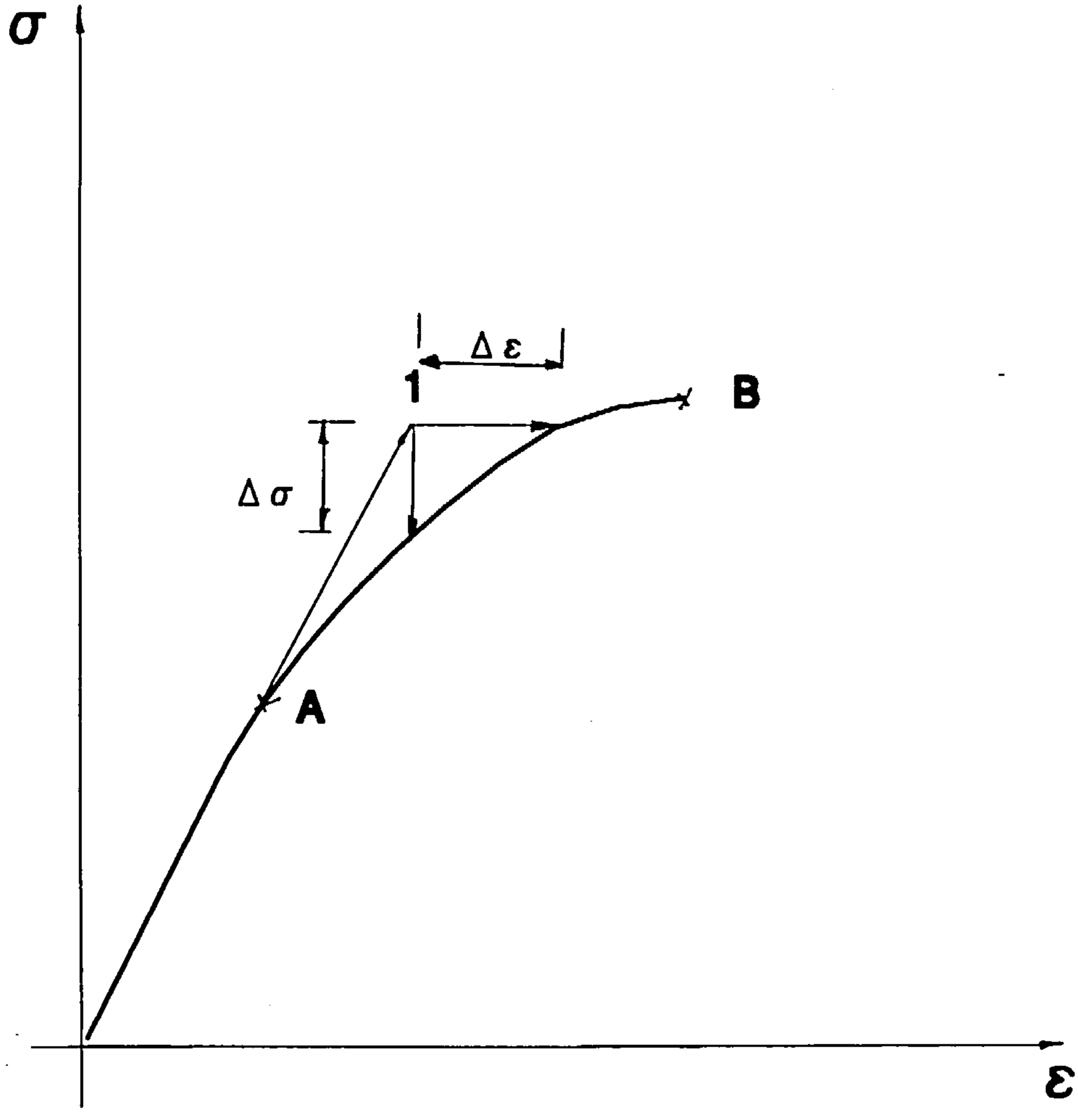

Figure 5.4: Initial stress and initial strain methods

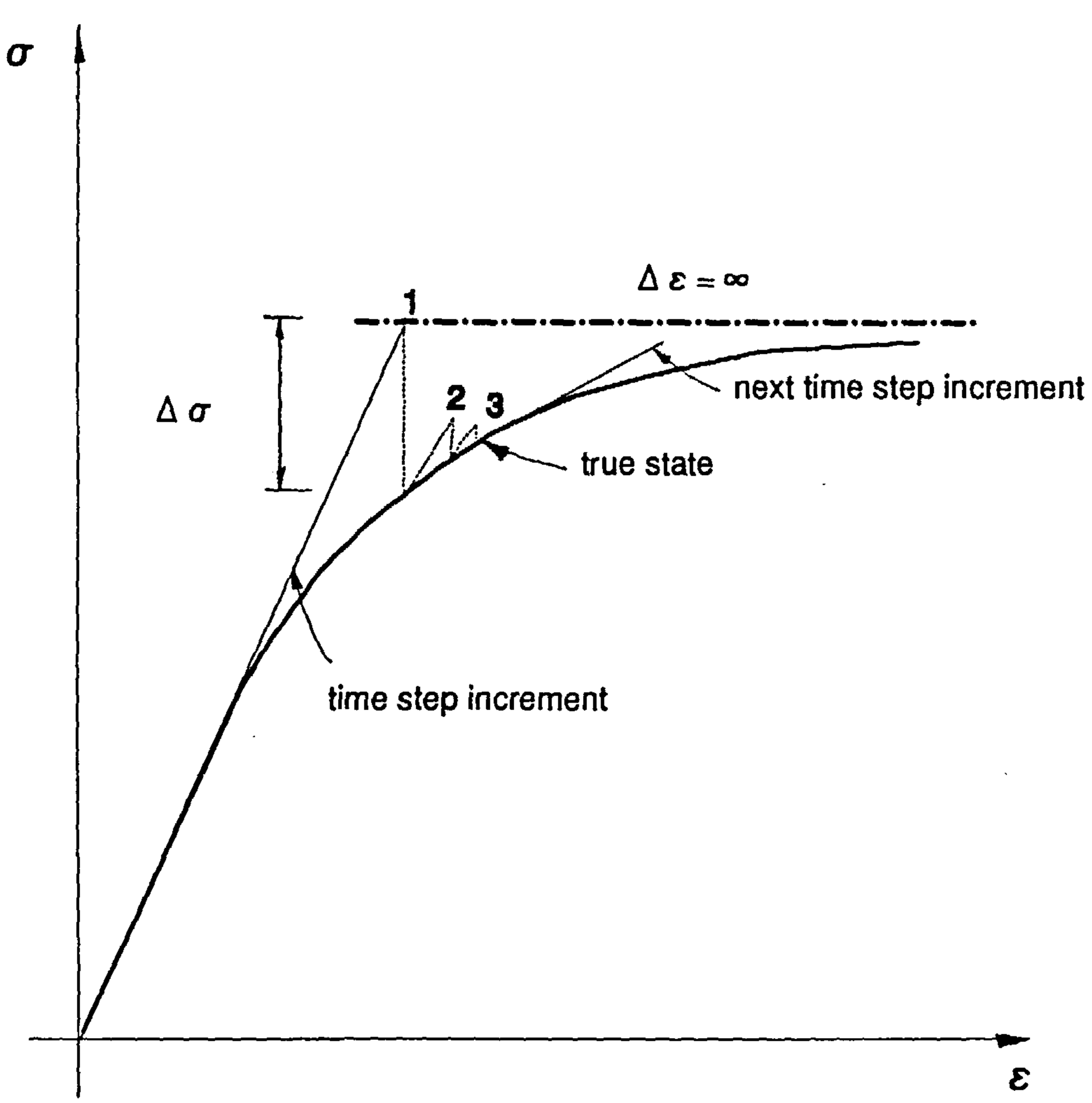

Figure 5.5: Time step increment-iteration procedure

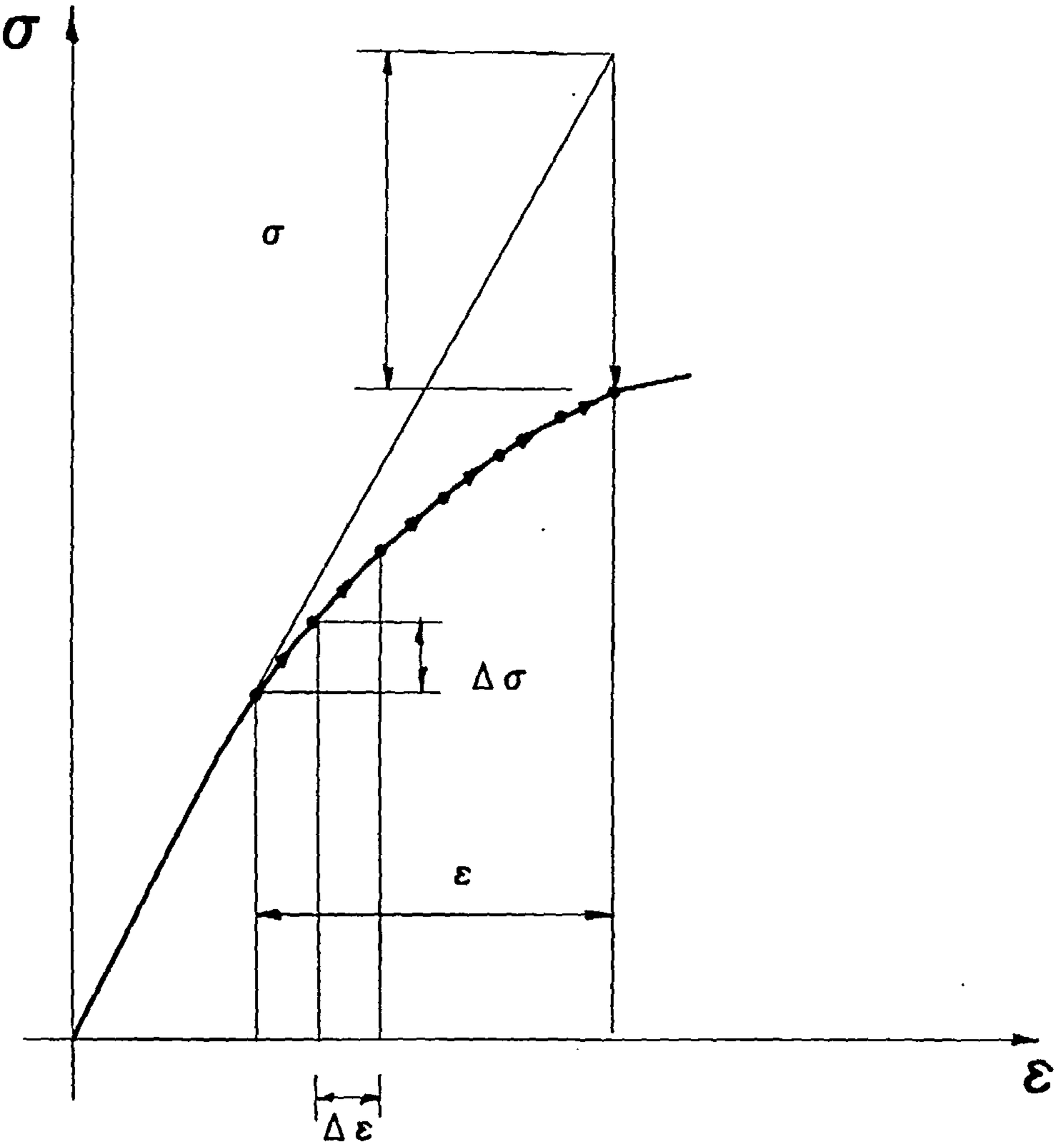

Figure 5.6: Constant strain-time step increment for the initial stress method

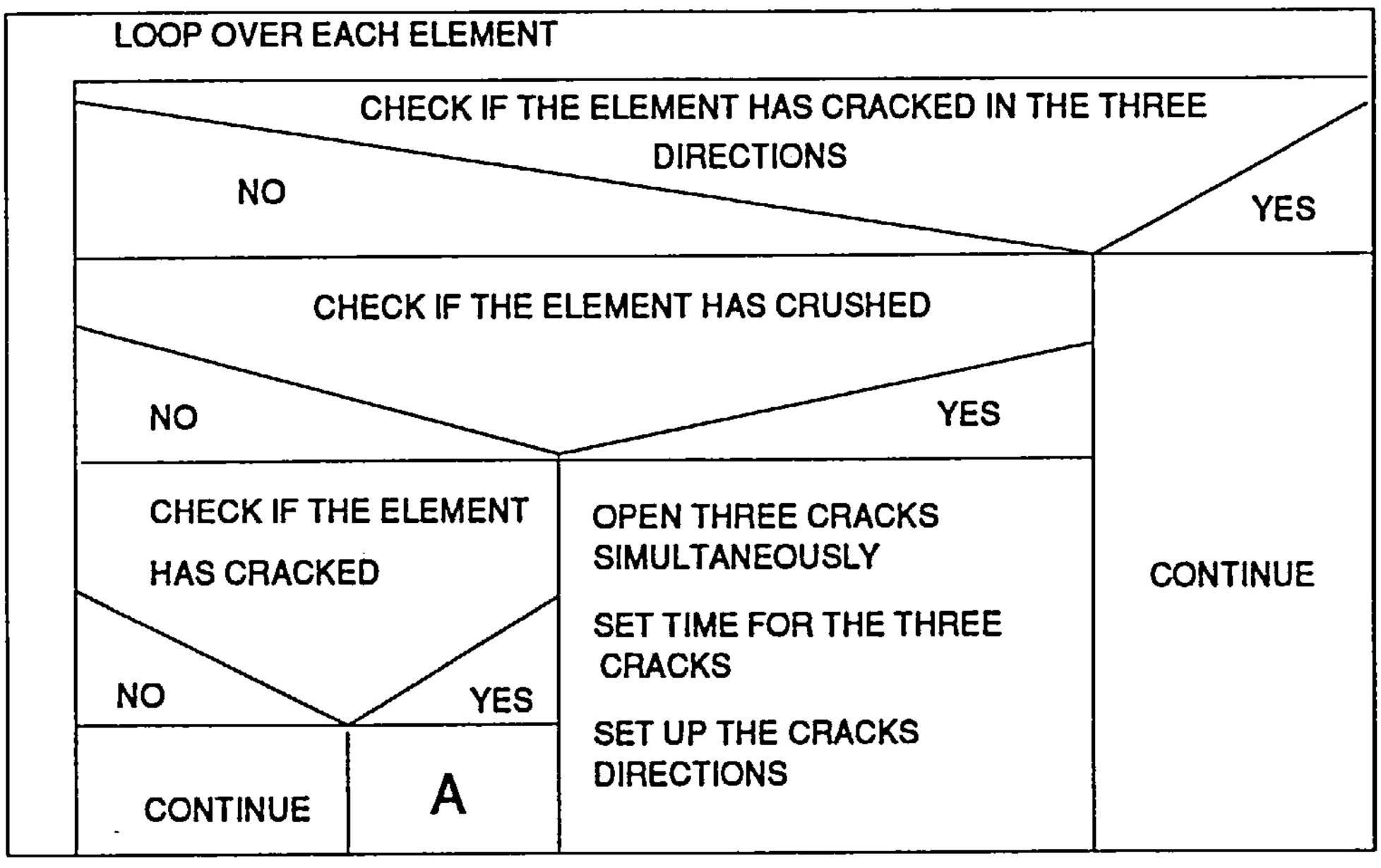

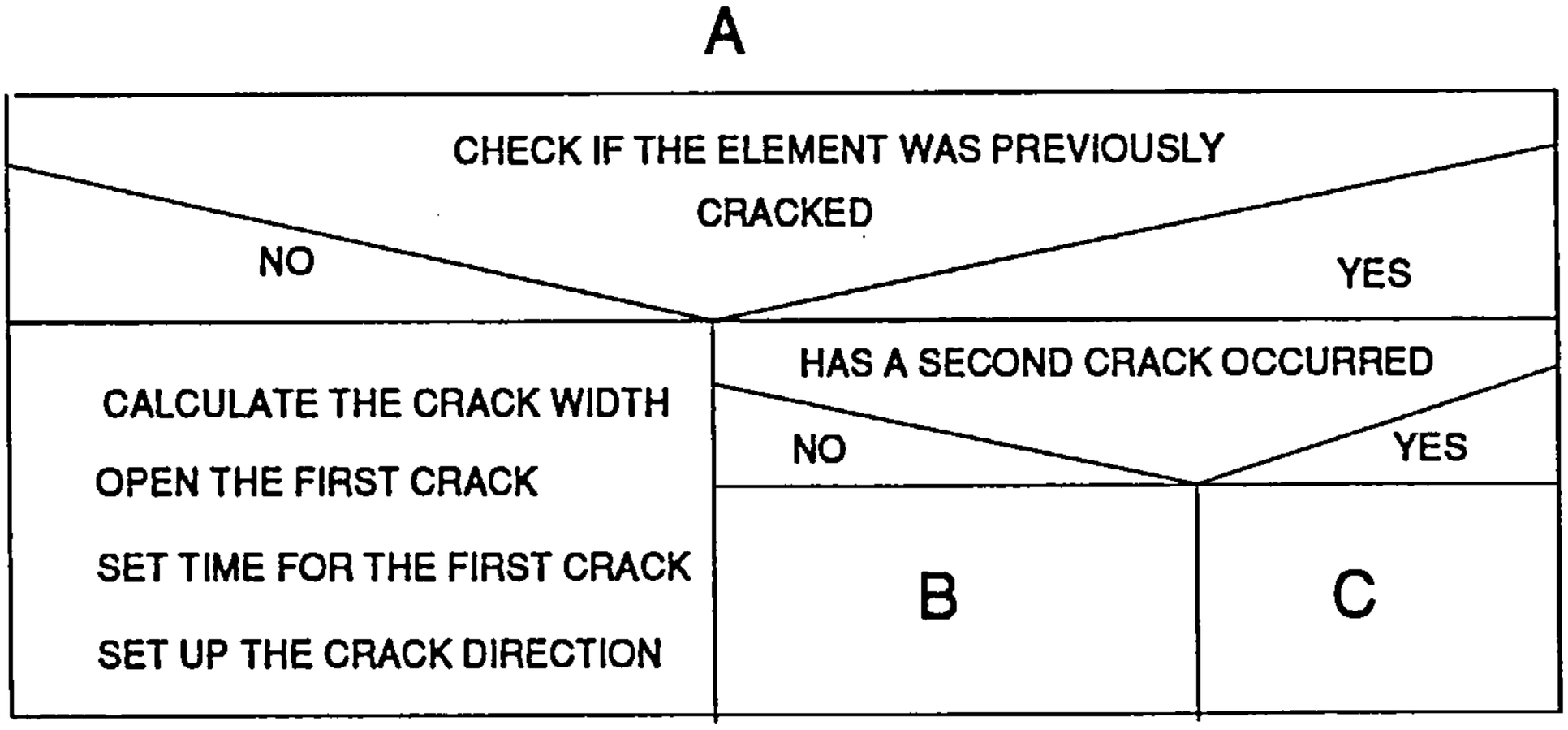

Figure 5.7: Flow chart for segment 4 of routine F3DM61: Part 1

B

TRANSFORM THE STRESSES IN THE LOCAL CRACK PLANE
CALCULATE THE MAXIMUM AND MINIMUM PRINCIPAL STRESSES
CALCULATE THE DIRECTION OF THE PRINCIPAL STRESSES
CALCULATE THE CRACK WIDTH
OPEN THE SECOND CRACK
SET TIME FOR THE SECOND CRACK

C

CHECK IF A THIRD CRACK CAN BE OPENED	
NO	YES
CONTINUE	CALCULATE THE NORMAL STRESS CALCULATE THE CRACK WIDTH OPEN THE THIRD CRACK SET TIME FOR THE THIRD CRACK

Figure 5.8: Flow chart for segment 4 of routine F3DM61: Part 2

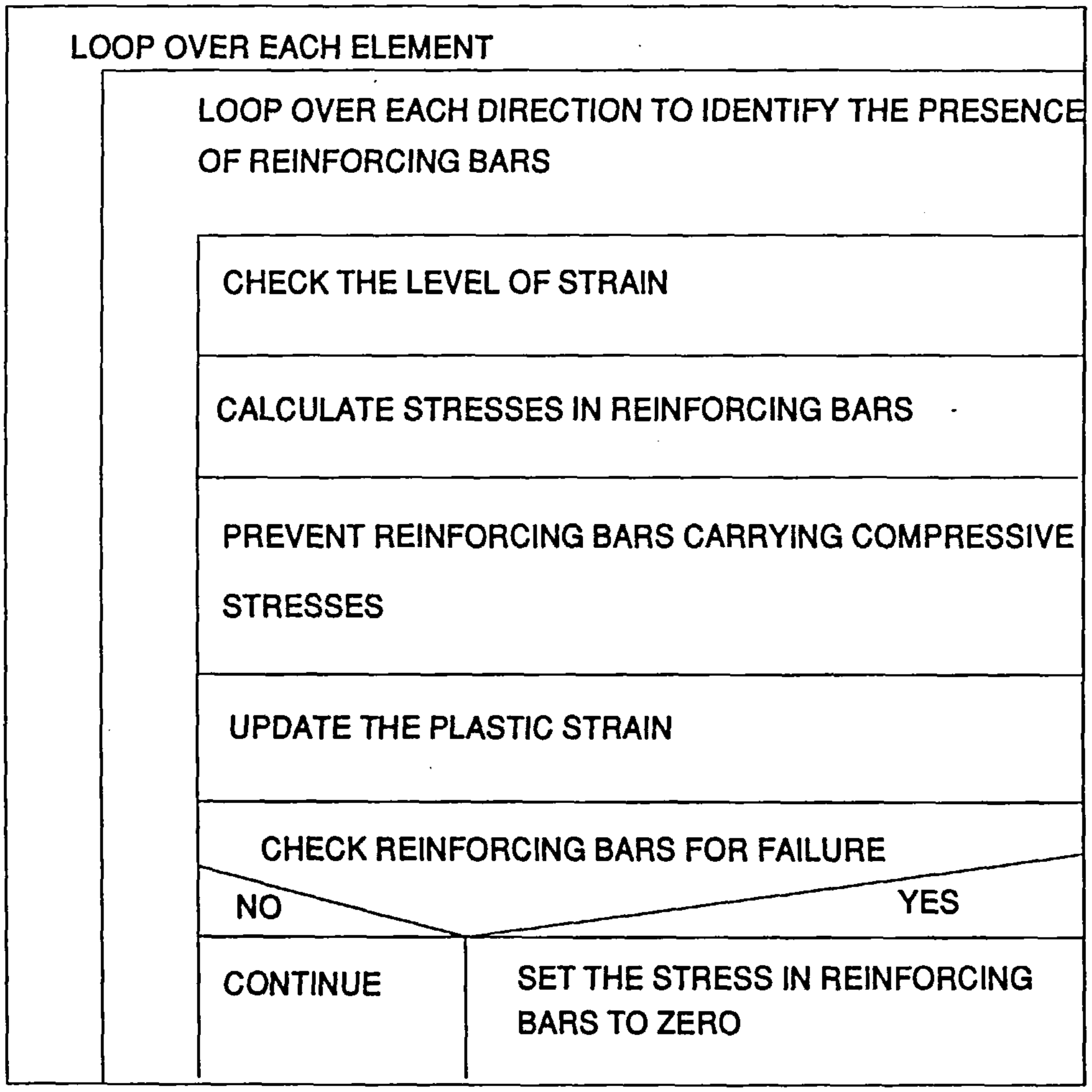

Figure 5.9: Flow chart for segment 5 of routine F3DM61

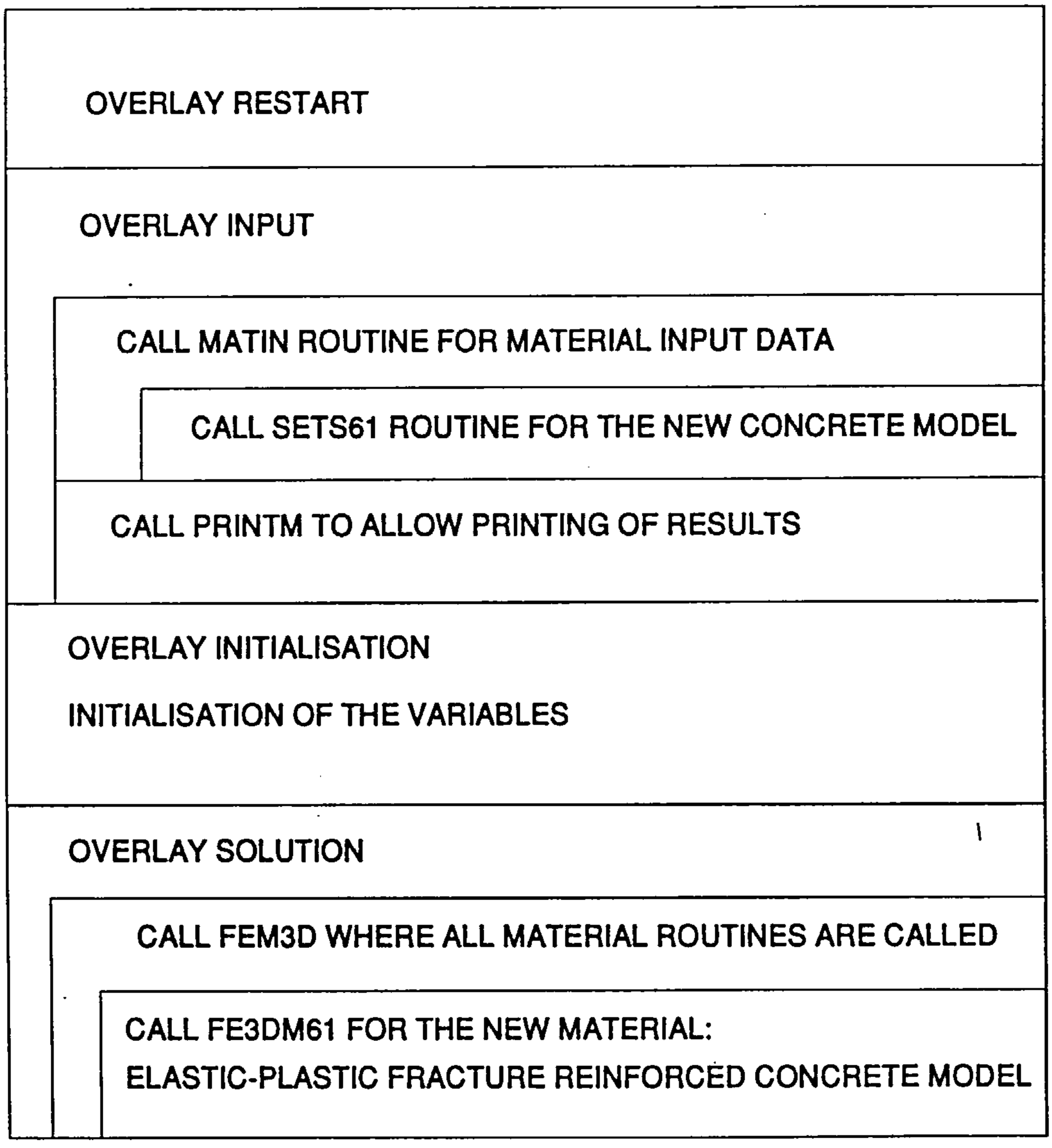

Figure 5.10: Flow chart for DYNA3D main code

Chapter 6

APPLICATION TO PLAIN CONCRETE

6.1 INTRODUCTION

In this Chapter the performance of the new concrete material model developed in this investigation is examined by analysing the behaviour of plain concrete specimens subjected to compressive impact loading.

The wide discrepancy which is evident in the published experimental results has made the selection of a benchmark test for the new concrete model very difficult. Many parameters are believed to have an influence on the results obtained from laboratory based investigations including, for example, the test conditions, measurement techniques, and the assumptions made in the processing and analysis

of the recorded output data [34].

The method of testing which is normally used requires the test specimen to be placed directly on a load measuring device in order to record the variation in the stresses during the impact event. The variation in the strains is determined normally from the output of strain gauges bonded to the lateral surface of the test specimen. The stresses are then related to the corresponding strain values in order to obtain a stress-strain curve. In the development of the stress-strain curve assumptions are made and a method of analysis is normally employed so that the effects of the different parameters which may influence the final results are eliminated. Among these parameters are, for example, inertia forces, the influence of the stress wave reflections and the differences in time which elapse between the recording of the output from the load measuring device and the strain gauges.

The factor which is believed to have the most influence on the results is the stress wave reflections which can lead to an overestimation of the magnitude of the stress values [41]. Only a limited number of the laboratory investigations [38, 41, 42] which were reviewed in Chapter 2 considered the influence of the reflection of the stress wave on the results.

Results obtained from laboratory based investigations must be used in the evaluation of the performance of the new concrete model. Two laboratory investigations

were selected i.e.

(1) The first laboratory investigation was conducted by Perry and Bischoff [45] using cylindrical test specimens.

(2) Cylindrical test specimens were also used in the second laboratory investigation which was carried out by Curbach and Eibl [42].

In each case drop hammers were used to impact the test specimens at approximately the same initial contact velocity. However, the test specimens used by Curbach and Eibl [42] were tall enough for the strain measurements to be free from any significant interference from the reflected stress waves.

The difference in time between the recording of the strain and the corresponding stress values is not a parameter which can affect the results from the numerical analysis because the stress and strain values are obtained at the same point in time. Therefore, it can be concluded that the only difference between the two laboratory investigations is that the influence of stress waves was present in the results from the laboratory tests conducted by Perry and Bischoff [45].

A detailed assessment of the ability of the new concrete model, fully implemented into DYNA3D, to predict the behaviour of the test specimens included in the two above investigations is given in the following Sections.

The numerical investigation was carried using a VAX-cluster mainframe installation at Heriot-Watt University. The finite element solutions have been compared with the results from the experimental investigations.

6.2 DESCRIPTION OF TEST SPECIMENS

A brief description of the test specimens and procedures used in each investigation is given in the following Sections.

6.2.1 Perry and Bischoff

Perry and Bischoff [45] tested plain concrete cylinders with a diameter of 101.6 *mm* and a height of 254 *mm*. The height to diameter ratio was selected to be greater than two in order to eliminate the effects of friction at the interface between the impactor and the contact face of the test specimen. However, Perry and Bischoff [45] acknowledged the presence of a disturbance in the measurement of the data due to the influence of the reflection of the stress wave which was initiated as a result of the impact load. A test specimen height of 254 *mm* did not allow sufficient time for the data to be recorded before the reflected stress waves reached the point where the measurements were recorded.

The axial and lateral strain measurement points were located at the mid-height of the test specimens. The measurement of the strains was carried out using two circumferential and two longitudinally positioned electrical resistance strain

gauges diametrically opposite each another. The axial compressive stress was measured at the base of the test specimen using a thin load measuring device.

The test specimens were impacted using a drop hammer test arrangement. The impact load was generated by a cylindrical hammer with a mass of 31.6 kilogrammes. The hammer was allowed to fall freely from a pre-determined height in order to achieve an impact velocity of 8.3 m/sec.

6.2.2 Curbach and Eibl

Plain concrete cylinders with a diameter of 100 mm and a height of 1800 mm were used in this investigation to give a height to diameter ratio equal to 18 for the following two principal reasons:

(1) To avoid the reflected stress waves initiated during impact loading from reaching the area where measurements were recorded during the tests.

(2) To minimise the influence on the results of the friction at the interface between the impactor and the contact face of the test specimens. The axial strain measurement points were located in a region 300 mm below the contact surface. The measurement of the strains was carried out using two strain gauges with a gauge length of 60 mm. The displacement was also recorded using an optical measurement system in order to calculate the stress values using the theory of wave propagation.

The load was generated by dropping a 200 kilogram hammer down a steel tube onto the test specimen. The hammer was allowed to fall freely from a pre-determined height in order to achieve an impact velocity of 8.0 m/sec

6.3 FINITE ELEMENT IDEALISATION

On the assumption that the impact pressure was uniformly distributed across the contact surfaces of the test specimens and also the impactor, only a quarter of the test arrangement was modelled in each case i.e. the two planes of symmetry of the circular cross section of each test specimen were used.

The concrete specimens used in the tests conducted by Perry and Bischoff [45] were modelled using 40 elements and 99 nodes. The concrete specimens used by Curbach and Eibl [42] were modelled using 280 brick elements and 639 nodes. In the case of both models, the nodes in the planes of symmetry were restrained in the appropriate directions in order to simulate continuity with respect to the other parts of the cylinder. All other nodes were free to move in all directions.

The finite element meshes adopted for the different components included in the numerical models are shown in Figures 6.1 and 6.2 for the investigations conducted by Perry and Bischoff [45] and Curbach and Eibl [42] respectively.

The steel hammers were modelled as cylinders with an equivalent mass of 31.6

and 200 kilograms respectively for the two investigations described above.

In the numerical analysis the hammer initially rested on the test specimen. At time t=0 the impactor was driven towards the circular cross section of the test specimen with a initial velocity for a period of time which was equal to the duration of the impact event. The material properties of the hammer and the preset velocities are detailed in Tables 6.1 and 6.2 for each investigation.

The concrete cylinder and the hammer are distinct bodies in space. Contact between the bodies is modelled by interface segments defined by the mesh connectivity. The interface segments used in this numerical analysis are the type that permit contact and separation (compression can be carried but no tension). This type of interface is referred to as sliding with voids in the INGRID users manual for the generation of the input data [148].

As explained in Section 5.4 in order to undertake an analysis using the new concrete model all the concrete material input data should ideally be available. The assumed and measured concrete material input data are detailed in Tables 6.3 and 6.4 for each investigation. A complete set of data was not included in any of the investigations described in the above Sections. Therefore, in the next Section, a parametric study was undertaken to investigate the sensitivity of the new concrete model to the material parameters which were not determined in the

two investigations.

6.4 SENSITIVITY ANALYSIS

The purpose of this section is to assess the sensitivity of the new concrete model to variations in the concrete material input parameters. The cylindrical test specimen included in the laboratory based investigation conducted by Perry and Bischoff [34] was used to examine the effect of a number of material parameters on the resulting numerical solution using the new concrete model. The input parameters which have been examined are those which are generally not defined in published descriptions of laboratory based investigations.

The study was conducted by varying one parameter at a time and keeping all the remaining parameters constant. The effect of each material parameter on the solution is discussed separately. The results obtained illustrate the behaviour of the concrete specimen in relation to the sensitivity of the new concrete model to changes in the values of specific material input parameters.

The output generated by the program during the analysis permitted the variation in the stresses and the strains with respect to time to be examined. In particular, it permitted the analysis of the values of the stresses and strains which developed in the finite elements situated on the external surface of the test specimen, at the mid height position, as shown in Figure 6.1. The resulting stress-strain curves

were terminated at the point at which material instability occurred in the solution.

6.4.1 Tensile Strength

The new concrete model requires the tensile strength of the concrete material to be input to calculate the four constants which define the failure function of the concrete material. The tensile strength of the concrete is also used to define the initiation of a crack. A crack is initiated when the maximum principal stress is found to exceed a value which is equal to the magnitude of the tensile strength of the concrete.

The actual tensile strength of the concrete in the test specimens examined in this investigation was in the majority of cases not available from the published literature. However, an estimate of the value of the tensile strength can be obtained from the compressive strength of the concrete using published relationships [17, 27, 53] i.e. $\bar{f}'_t = f'_t/f'_c = 0.1$. However, in order to investigate the sensitivity of the new concrete model to the tensile strength, three values of $\bar{f}'_t$ equal to 0.08, 0.1 and 0.12 have been examined.

The results have shown that the new concrete model is sensitive to the value of $\bar{f}'_t$ and hence to the magnitude of the tensile strength of the concrete. The four constants which define the failure function for a specific concrete are determined using its tensile and compressive strengths. Table 6.5 shows the dependence of

the constants in the failure function on the value of $\bar{f}_t'$. The resulting axial and lateral stress-strain curves obtained from the three test runs are shown in Figure 6.3. The stress-strain curves show that the strength and ductility of the concrete specimen increase with increasing values of $\bar{f}_t'$. The predicted maximum compressive strengths were 36.3, 41.5, 55.3 N/mm^2 for values of $\bar{f}_t'$ equal to 0.08, 0.1 and 0.12 respectively. It can be concluded from the stress-strain curves in Figure 6.3 that the concrete specimens with low tensile strengths are generally weaker than those with the higher tensile strengths.

The results from these test runs also show that the value of $\bar{f}_t'$ equal to 0.1 provides a reasonable simulation of the stress-strain curve obtained from the laboratory tests as shown in Figure 6.7. This value has consequently been adopted for the new concrete model.

6.4.2 Poisson's Ratio

Three test runs have been undertaken using values of Poisson's ratio equal to 0.17, 0.2 and 0.22. The results obtained from the test runs are shown in Figure 6.4. The three stress-strain curves, shown in Figure 6.4, for the three values of Poisson's ratio are almost identical. Therefore, it can be concluded that when the value of Poisson's ratio varies from 0.17 to 0.22 it has negligible effect on the predicted behaviour of the concrete specimen when the new concrete model is used. The value of Poisson's ratio adopted for the new concrete model is therefore 0.2.

6.4.3 Hardening Coefficient

The hardening coefficient defines the amount of isotropic and kinematic hardening strain experienced in the concrete element. The amount of isotropic and kinematic hardening produced during plastic deformation in concrete is not known. Typical values between 0.15 and 0.20 have been recommended for metals [93] but no guidance on corresponding values for concrete could be found. A sensitivity study was therefore undertaken in order to determine an acceptable value for use with the newly developed concrete model.

To investigate the effect of the hardening coefficient on the new concrete model six test runs were undertaken using values of the hardening coefficient of 0.85, 0.875, 0.90, 0.925 and 0.95. The resulting axial and lateral stress-strain curves are shown in Figure 6.5. The variation in the stress-strain curves obtained from the six test runs shows that the new concrete model is sensitive to the hardening coefficient. The maximum stress values were found to increase as the hardening coefficient approached a value of 1. The hardening value which was found to give an acceptable simulation of the behaviour of concrete during plastic deformation in the laboratory based investigation was 0.9 as shown in Figure 6.7. This value has consequently been adopted for the new concrete model.

6.4.4 Effect of Shear Retention Factor

The shear stresses in a cracked concrete element are represented by a shear retention factor β, which indicates the percentage of the elastic shear capacity which is retained after the concrete element has cracked [117, 119] An alternative approach is to represent the shear in a cracked concrete element using an aggregate interlock model. The law which governs this decay in the shear stiffness of the cracked concrete element takes the form of a parabolic function expressed in terms of the crack width and the size of the aggregates [116] as shown in Figure 3.8.

A characteristic value of the aggregate size and the crack width are normally required as input data, however, if these values are not available the shear retention factor is used to model the retained strength in the cracked concrete element. To investigate the effect of the shear retention factor three test runs have been undertaken. In one of the test runs a very low value of β i.e 0.01 (the shear stiffness of the cracked concrete element is reduced by a factor equal to 0.01 i.e. $G_c = 0.01G$) was used to simulate a smooth and almost frictionless crack surface. In the second case a very high value of β was used i.e. 0.9 (the shear stiffness of the cracked concrete element is reduced by 0.9 i.e. $G_c = 0.9G$) representing a fully interlocked crack surface. In the third numerical test an intermediate value of β was used i.e 0.4 which has been recommended by several researchers [117, 119].

The influence of the shear retention factor has been studied by comparing the

resulting stress strain curves. The stress-strain curves obtained from the three test runs were found to be identical. This is because the crack which developed in the concrete specimen ran parallel to the axis of the applied load therefore it can be deduced that the shear stresses developed in the numerical solution were low.

6.4.5 Summary

Ideally all the input parameters for the concrete material in a particular structural concrete member should be determined experimentally. However, if any of the input parameters for the numerical analysis are not available, values which are used to represent the concrete material under consideration must be estimated carefully. The sensitivity study described above has examined the influence on the new concrete model of a number of input parameters which are normally not available in the published description of investigations. In the absence of more definite laboratory derived data the values identified in the sensitivity study could be used as default values.

The recommended default values for these input parameters are detailed below:

(1) The ratio between the uniaxial tensile and compressive strengths $\bar{f}'_t = 0.1$

(2) Poisson's ratio $\mu = 0.2$

(3) Shear retention factor $\beta = 0.4$

(4) Characteristic hardening coefficient equal to 0.9.

6.5 RESULTS AND ANALYSIS

6.5.1 Perry and Bischoff

The variations in the axial compressive stress and in the lateral and axial strains with respect to time were obtained from the numerical analysis, as shown in Table 6.6. The variations in the stresses and strains were obtained using the concrete material input data detailed in Table 6.1.

Figure 6.6 shows the lateral and axial stress-strain curves predicted by the new concrete model. Figure 6.7 shows the predicted and the measured stress-strain curves (averaged from a number of published curves [45]).

The following observations can be made with respect to these results:

(a) Description of the stress-strain curve obtained from laboratory tests:

- A linear stress-strain relationship can be noted to exist between 0 to 75 percent of the maximum strength.
- Between 75 percent and 100 percent of the maximum strength the stress-strain curve had a pronounced curvature which is representative of non-linear behaviour. It also included several fluctuations.

- When the maximum strength was reached the test specimen continued to deform under a constant stress until failure occurred i.e. a plateau was present in the stress-strain curve.

(b) Description of the stress-strain curve obtained from the numerical analysis:

- The predicted stress-strain curve was also linear up to 75 percent of the maximum strength.
- Between 75 percent and 100 percent of the maximum strength the curvature of the predicted stress-strain curve, representing non-linear behaviour, was not so pronounced as in the case of the curve obtained from laboratory tests.
- After the maximum strength was reached the strength dropped which indicates that the element had failed in a brittle manner.

It can be concluded from the above descriptions that:

(1) The two curves constructed using the results from the numerical analysis and the laboratory tests were in agreement over the region up to 80 percent of the maximum strength. After this point there is a significant difference between the two curves particularly with respect to the variation in the magnitudes of the stresses.

(2) The maximum strength obtained from laboratory tests was predicted accurately by the new concrete model i.e. the difference between the two values

was only 6 percent.

(3) Figures 6.8(a)-(c) show the predicted deformed shapes and the development of the cracks on the lateral surface of the cylindrical test specimen at several stages during the numerical analysis. Figures 6.9(a)-(c) show the predicted deformed shapes and the development of cracks on a section through the cylindrical test specimen at several stages during the numerical analysis. The deformed shapes of the cylindrical test specimen are plotted at full scale. The crack patterns present in the test specimens during the laboratory tests were not reported so it was not possible to make comparisons with the results from the numerical analysis. It was, however, reported that the type of failure was brittle resulting in the disintegration of the middle portion of the test specimens in addition to the formation of longitudinal cracks. It is generally recognised [31, 36, 38] that in a uniaxial compressive test, the cracks develop parallel to the longitudinal axis of the test specimen i.e. parallel to the direction of the applied loading, which is clearly shown in the results obtained from the numerical analysis which was undertaken in the present investigation.

6.5.2 Curbach and Eibl

A quasi-static and impact analyses have been performed and the results examined in detail. The stress and strain histories were obtained from elements located on the lateral surface of the concrete specimen, at distance of approximately 300

mm from the contact face. The position of the finite elements corresponded to the region where the measurements in the laboratory tests were taken.

The stress and strain histories are given in Tables 6.8 and 6.7 which were obtained using the concrete material input data detailed in Table 6.2. They were combined to obtain the stress-strain curves shown in Figure 6.10 for the results obtained from the quasi-static and impact analyses. Figure 2.16 shows the corresponding measured stress-strain curves reported by Curbach and Eibl [42]. The predicted stress-strain curves for the impact and quasi-static loadings have also been compared to the stress-strain curves obtained from the laboratory tests. The resulting curves are shown in Figures 6.11 and 6.12 respectively.

The position of the element from which the stress and strain values were calculated is shown in Figure 6.2.

The following observations have been made from these results:

(a) Description of the impact stress-strain curve obtained from laboratory tests:

- A linear stress-strain relationship was evident between 0 to 40 percent of the maximum strength.
- Between 40 and 95 percent of the maximum strength the stress-strain curve showed a pronounced curvature which is characteristic of non-linear behaviour.

- It is interesting to note that 30 percent of the maximum strain value occurred between 95 and 100 percent of the maximum strength.

(b) Description of the impact stress-strain curve obtained from the numerical analysis:

- The stress-strain curve varied with a curvature which was less pronounced from the origin up to the maximum stress.
- After the maximum strength had been reached the strength dropped sharply due to the occurrence of a brittle failure. The shape of the stress-strain curve showed that the material had experienced little plasticity before failure occurred in compression as a result of the development of secondary tensile stresses.
- The overall shape of the stress-strain curve predicted by the new concrete model, particularly the descending branch of the stress-strain curve, is consistent with the results obtained from previously published laboratory tests [43].

The following conclusions can be made from the results obtained from the numerical analysis which has been described above.

(1) Figure 6.10 shows that the predicted concrete strength increased as the rate of loading increased. The differences between the predicted and measured maximum strength were not significant but the paths which the predicted

and measured stress-strain curves followed to reach their respective maximum strengths did not coincide, as shown in Figure 6.11.

(2) The predicted maximum strength compares reasonably well with the value obtained from laboratory tests i.e. the difference was 6 percent.

(3) The predicted and measured strain values at maximum strength were in agreement. It is interesting to note that in the laboratory test 30 percent of the relative deformation of the concrete (strain) was obtained under approximately constant stress i.e. 95 percent to 100 percent of the maximum strength whereas the predicted strength drops at this particular strain value, as shown in Figure 6.11.

(4) It can be noted in Figure 6.10 that the initial secant modulus of elasticity had not been affected by the rate of loading but the secant modulus varied up to the maximum strength. This stress-strain behaviour is consistent with the results obtained from laboratory tests conducted by Ahmed and Shah [43]. The stress-strain curves obtained from the laboratory tests exhibited a substantial variation in the initial modulus of elasticity as shown in Figure 2.16.

(5) The stress-strain behaviour predicted by the new concrete model is similar to

the stress-strain curve which is characteristic of the elastic-plastic-fracture concrete model, as shown in Figure 3.10.

The new concrete model has accurately simulated the stress-stress curve obtained from laboratory tests under quasi-static loading, as shown in Figure 6.12. Essentially, a difference of 12 percent has been obtained between the predicted and measured strains at maximum strength whereas a difference of 6 percent was obtained between the predicted and measured maximum strengths.

The static stress-strain curve reported by Curbach and Eibl [42] appears to have been terminated when the maximum strain was reached. The strength did not drop which resulted in a ductile failure in the test specimen. Whereas, the predicted static stress-strain curve was terminated after the maximum strength had been reached because at this point instability occurred in the solution process and was accompanied by a drop in the load carrying capacity of the test specimen.

6.6 CONCLUSIONS

The following conclusions can be drawn from the results obtained from the numerical modelling, using the newly developed concrete model, of the behaviour of plain concrete test specimens subjected to static and impact loadings described in the previous Sections.

(1) The new concrete model can, within acceptable levels of accuracy, predict the behaviour observed, in the laboratory tests, of plain concrete test specimens subjected to static and impact compressive loadings.

(2) The predicted stress-strain curve under static loading was found to be in good agreement with the stress-strain curve obtained from laboratory tests.

(3) The predicted impact stress-strain curves were found to be in good agreement with those obtained from laboratory tests up to 80 percent of the measured maximum strength for the two test specimens examined. The disagreement between the predicted and measured stress-strain curves was found when the stresses reached their maximum values. The experimental results have shown that after the maximum strength is reached the concrete experienced deformation under a constant stress up to failure, whereas in the results from the numerical analysis the magnitude of the stress drops off rapidly after reaching its maximum value. This can be explained in terms of the post-cracking behaviour implemented in the new concrete model.

(4) The deformed shapes and crack patterns observed in the laboratory tests are simulated well in the results obtained from the numerical analysis.

(5) A sensitivity study was carried out in order to examined the influence on the new concrete model of some of the input parameters which are normally not available in the published literature. Recommended values for these parameters obtained from the sensitivity study should be used in the absence of definitive data from laboratory based investigations.

Modulus of elasticity of steel	200000 N/mm^2
Poisson's ratio for steel	0.3
Density	7800 kg/m^3
Mass	31.6 kg
Contact velocity V	8.3 m/sec

Table 6.1: Assumed loading and impact hammer properties for tests conducted by Perry and Bischoff [45]

Modulus of elasticity of steel	200000 N/mm^2
Poisson's ratio for steel	0.3
Density	7800 kg/m^3
Mass	200 kg
Contact velocity	8.0 m/sec

Table 6.2: Assumed loading and impact hammer properties for tests conducted by Curbach and Eibl [42]

Compressive strength	26.7 N/mm^2
Tensile strength	2.67 N/mm^2
Crack opening length	$45\mu m$.
Aggregate size or (β shear reduction factor)	(0.4)
Modulus of elasticity	32590 N/mm^2
Poisson's ratio	0.2
Hardening coefficient	0.9
Density	2227 kg/m^3

Table 6.3: Assumed and measured material properties for tests conducted by Perry and Bischoff [45]

Compressive strength	42.0 N/mm^2
Tensile strength	4.20 N/mm^2
Crack opening length	$45\mu m$
Aggregate size or (β shear reduction factor)	(0.4)
Modulus of elasticity	31800 N/mm^2
Poisson's ratio	0.2
Hardening coefficient	0.9
Density	2330 kg/m^3

Table 6.4: Assumed and measured material properties for tests conducted by Curbach and Eibl tests [42]

$\bar{f}_t' = f_t'/f_c'$	A	B	C	D
0.08	2.8358	0.5663	11.8250	0.2722
0.1	2.0108	0.9714	9.1412	0.2312
0.12	1.4603	1.2413	7.3548	0.2035

Table 6.5: Failure function constants and their dependence on $\bar{f}_t'$

Time(milliseconds)	Stress (N/mm^2)	Axial Strain (mm/m)	Lateral Strain (mm/m)
0.000E+00	0.000E+00	-0.477E-03	0.596E-04
0.328E+00	0.472E-01	0.715E-03	-0.119E-03
0.375E+00	0.179E+00	0.477E-02	-0.715E-03
0.422E+00	0.502E+00	0.153E-01	-0.215E-02
0.469E+00	0.117E+01	0.348E-01	-0.501E-02
0.516E+00	0.251E+01	0.772E-01	-0.107E-01
0.563E+00	0.471E+01	0.146E+00	-0.212E-01
0.610E+00	0.797E+01	0.249E+00	-0.386E-01
0.657E+00	0.124E+02	0.391E+00	-0.654E-01
0.703E+00	0.180E+02	0.575E+00	-0.104E+00
0.750E+00	0.277E+02	0.796E+00	-0.158E+00
0.797E+00	0.340E+02	0.104E+01	-0.229E+00
0.844E+00	0.382E+02	0.127E+01	-0.320E+00
0.891E+00	0.404E+02	0.149E+01	-0.429E+00
0.938E+00	0.415E+02	0.186E+01	-0.553E+00
0.985E+00	0.311E+02	0.188E+01	-0.691E+00
0.103E+01	0.258E+02	0.209E+01	-0.836E+00
0.108E+01	0.226E+02	0.231E+01	-0.992E+00
0.113E+01	0.206E+02	0.255E+01	-0.116E+01
0.117E+01	0.194E+02	0.281E+01	-0.133E+01
0.122E+01	0.187E+02	0.309E+01	-0.151E+01
0.127E+01	0.244E+02	0.337E+01	-0.170E+01

Table 6.6: Predicted variation in the stress and strain values with respect to time for the dynamic test conducted by Perry and Bischoff [45]

Time(milliseconds)	Stress (N/mm^2)	Strain (mm/m)
0.000E+00	0.000E+00	0.763E-02
0.785E+00	0.827E-01	0.763E-02
0.831E+00	0.179E+00	0.954E-02
0.877E+00	0.369E+00	0.191E-01
0.923E+00	0.715E+00	0.286E-01
0.969E+00	0.131E+01	0.477E-01
0.102E+01	0.231E+01	0.725E-01
0.106E+01	0.389E+01	0.120E+00
0.111E+01	0.650E+01	0.202E+00
0.115E+01	0.102E+02	0.315E+00
0.120E+01	0.154E+02	0.479E+00
0.125E+01	0.219E+02	0.681E+00
0.129E+01	0.313E+02	0.934E+00
0.134E+01	0.401E+02	0.121E+01
0.138E+01	0.492E+02	0.152E+01
0.143E+01	0.580E+02	0.181E+01
0.148E+01	0.649E+02	0.208E+01
0.152E+01	0.687E+02	0.231E+01
0.157E+01	0.676E+02	0.246E+01
0.162E+01	0.486E+02	0.254E+01
0.166E+01	0.360E+02	0.259E+01
0.171E+01	0.326E+02	0.260E+01
0.175E+01	0.294E+02	0.260E+01
0.180E+01	0.234E+02	0.260E+01
0.185E+01	0.184E+02	0.262E+01
0.189E+01	0.158E+02	0.264E+01
0.194E+01	0.179E+02	0.268E+01

Table 6.7: Predicted variation in the stress and strain values with respect to time for the dynamic loading test conducted by Eibl and Curbach [42]

Time (milliseconds)	Stress (N/mm^2)	Strain (mm/m)
0.000E+00	0.000E+00	0.763E-02
0.462E+00	-0.994E-09	0.763E-02
0.969E+00	0.282E-02	0.763E-02
0.148E+01	0.856E+00	0.324E-01
0.198E+01	0.120E+02	0.380E+00
0.249E+01	0.319E+02	0.103E+01
0.295E+01	0.361E+02	0.126E+01
0.346E+01	0.352E+02	0.127E+01
0.397E+01	0.361E+02	0.139E+01
0.448E+01	0.399E+02	0.156E+01
0.498E+01	0.402E+02	0.152E+01
0.549E+01	0.404E+02	0.172E+01
0.595E+01	0.406E+02	0.176E+01
0.646E+01	0.407E+02	0.170E+01
0.697E+01	0.408E+02	0.186E+01
0.748E+01	0.409E+02	0.187E+01
0.799E+01	0.317E+02	0.188E+01
0.849E+01	0.263E+02	0.189E+01
0.895E+01	0.250E+02	0.190E+01
0.946E+01	0.278E+02	0.191E+01
0.997E+01	0.327E+02	0.202E+01

Table 6.8: Predicted variation in the stress and strain values with respect to time for the static loading test conducted by Eibl and Curbach [42]

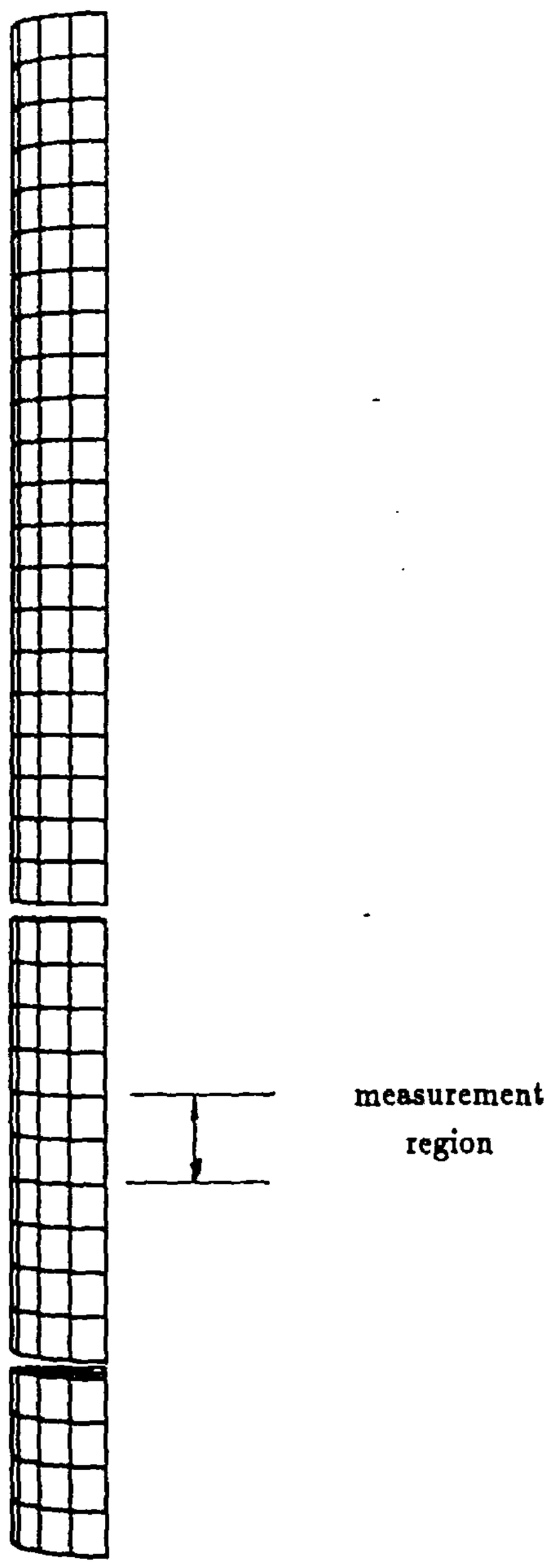

Figure 6.1: Layout of the mesh for the specimens tested by Perry and Bischoff [45]

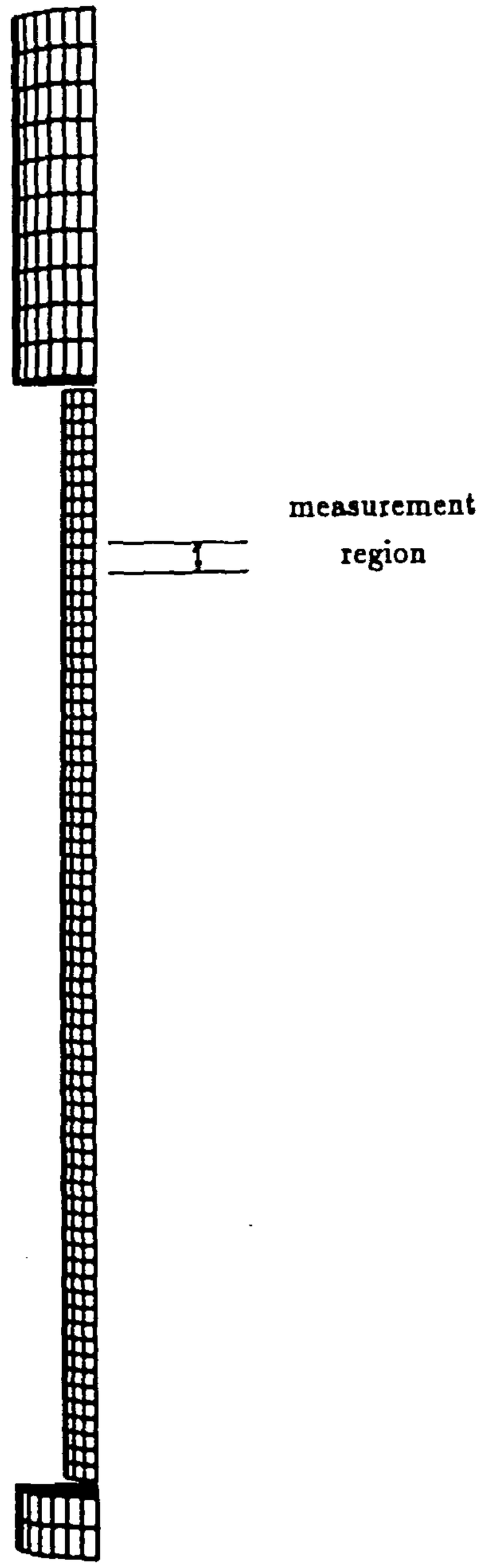

Figure 6.2: Layout of the mesh for the specimen tested by Curbach and Eibl [42]

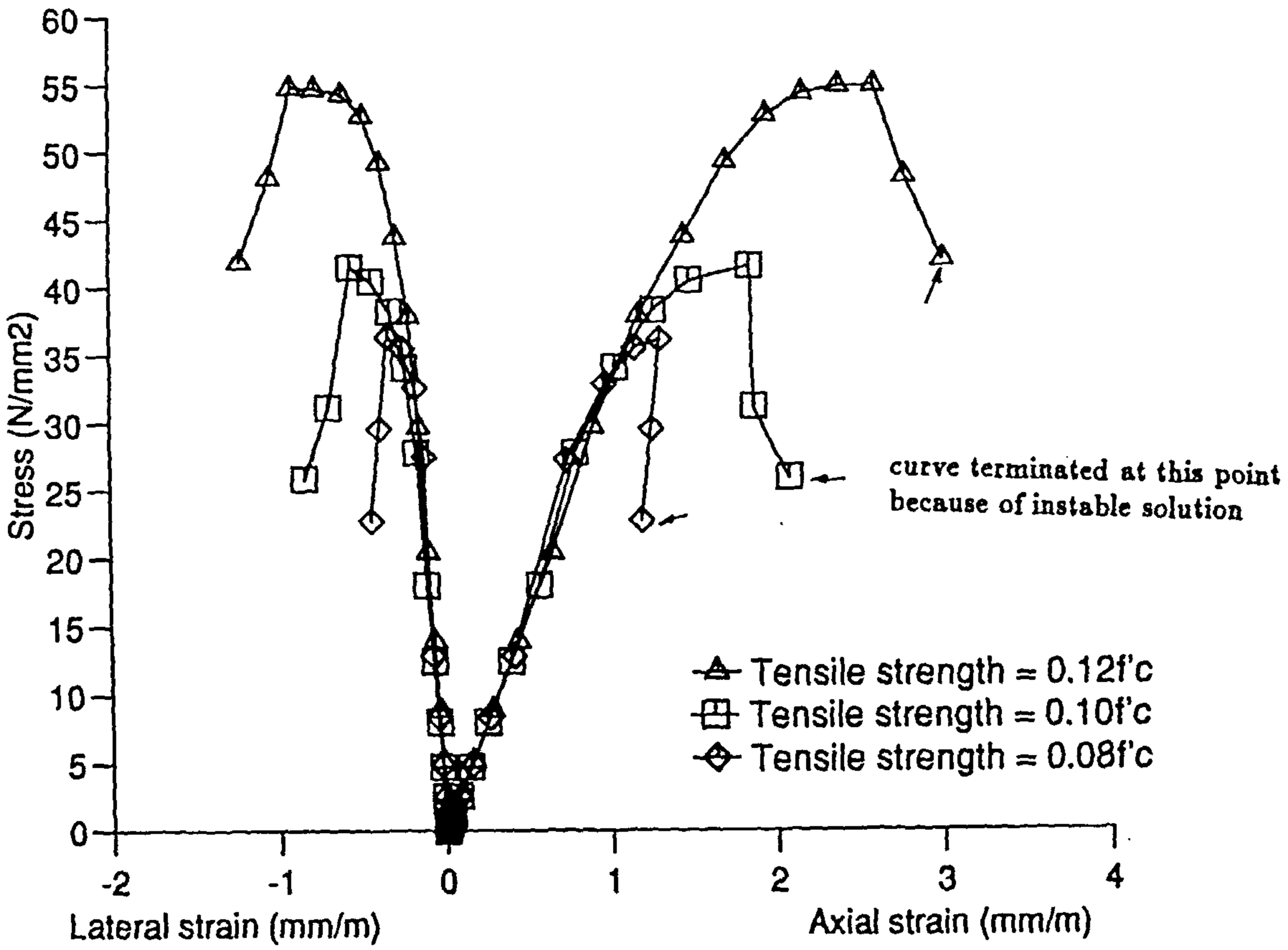

Figure 6.3: Tensile strength sensitivity

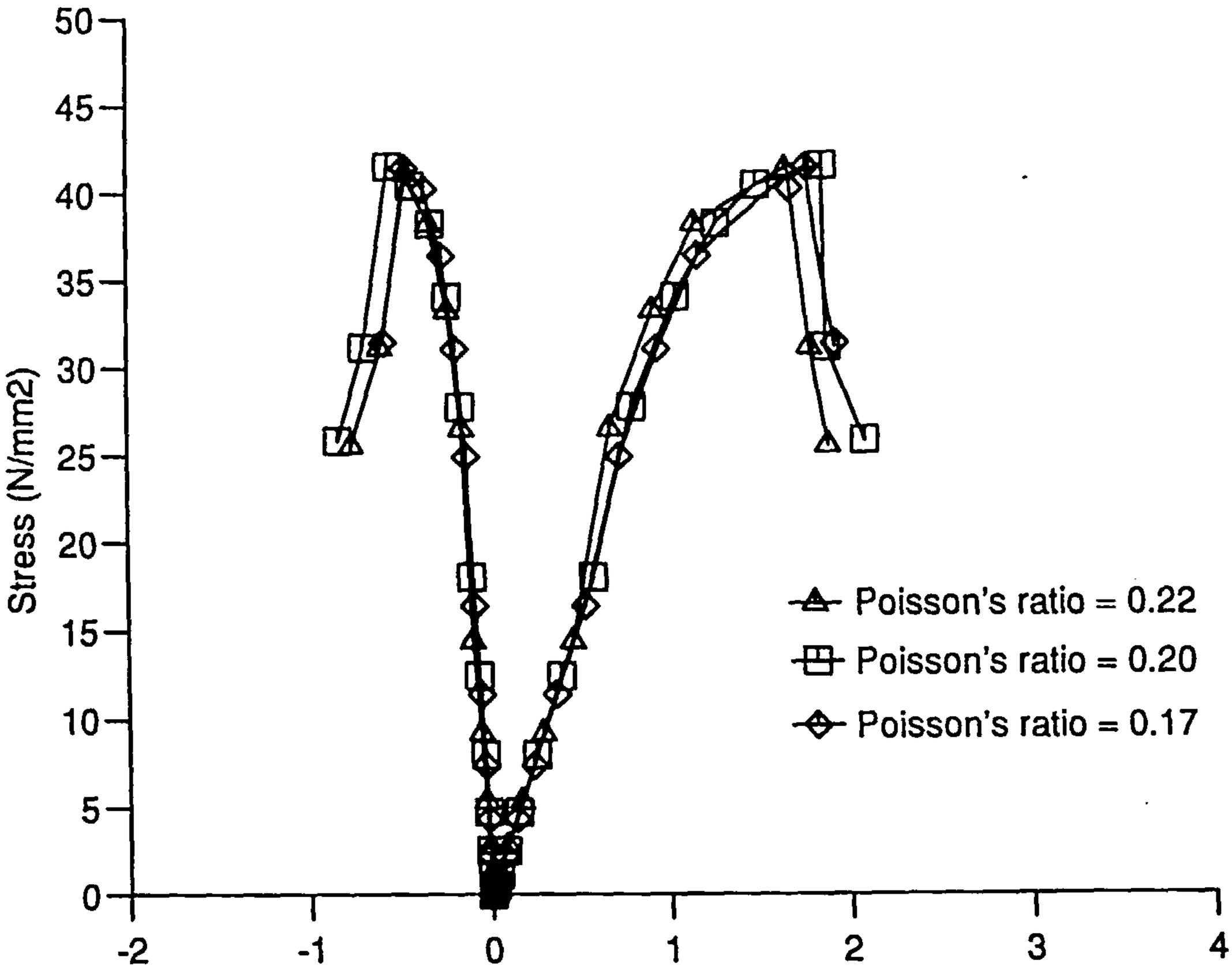

Figure 6.4: Poisson's ratio sensitivity

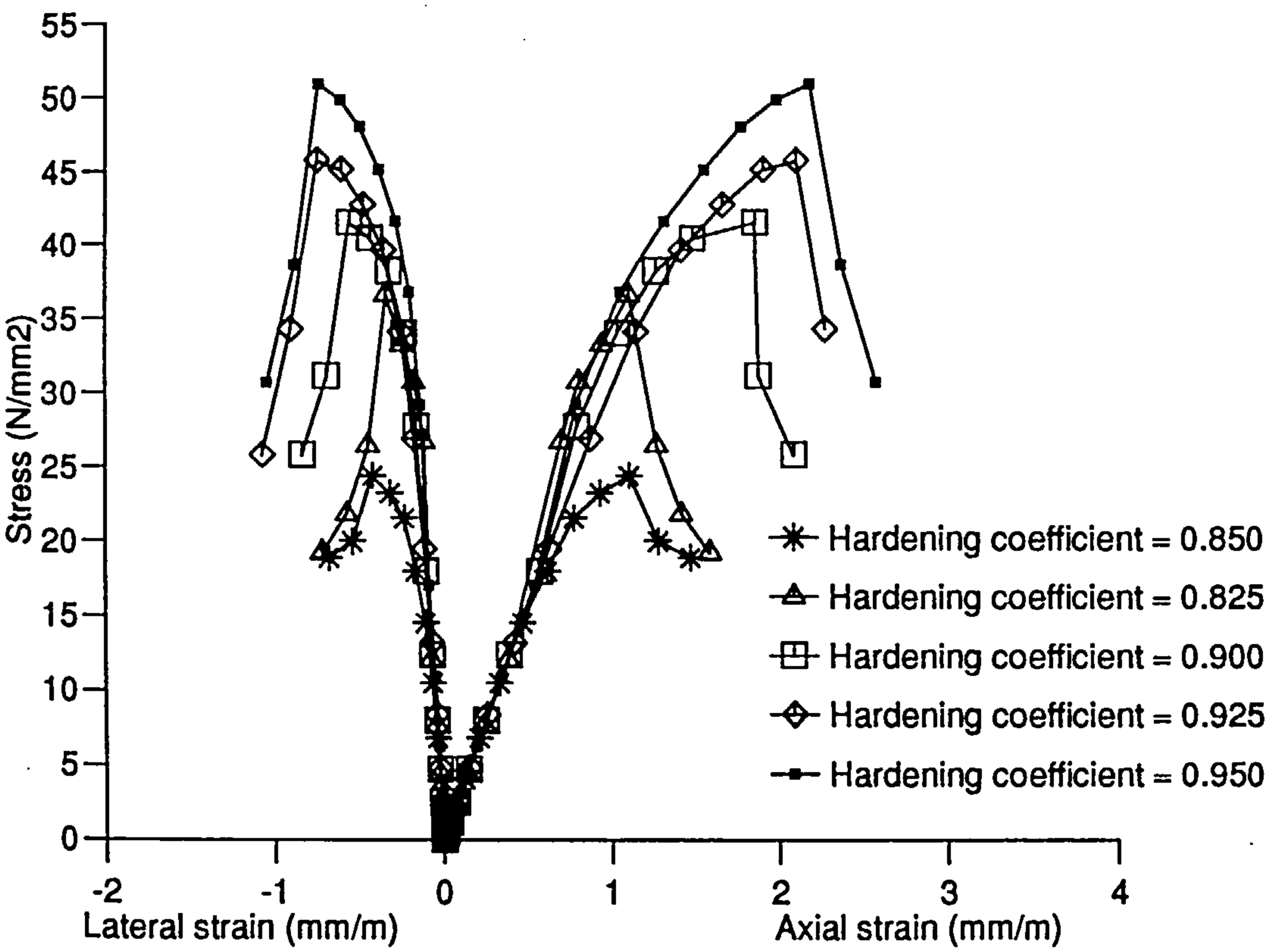

Figure 6.5: Hardening coefficient sensitivity

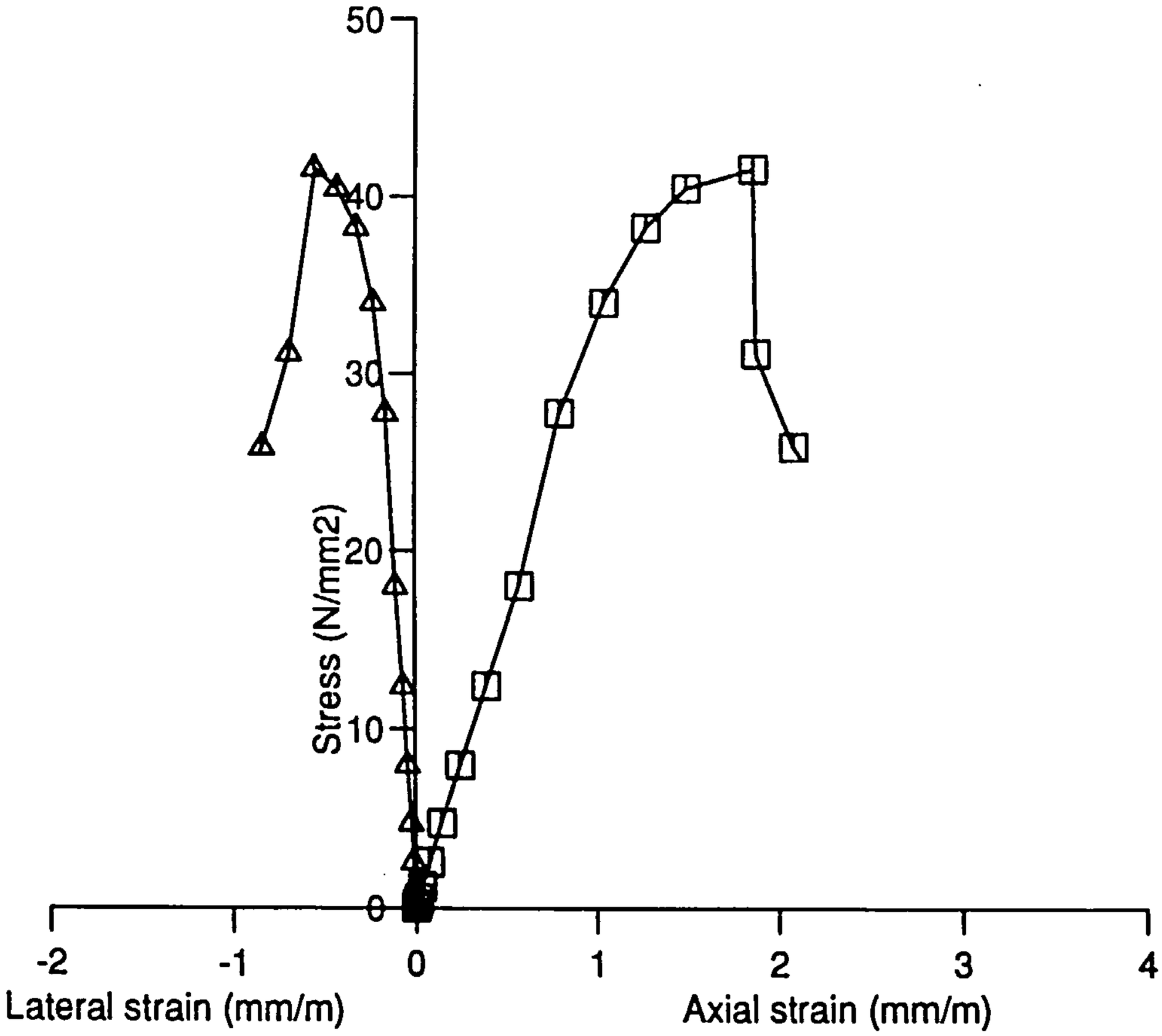

Figure 6.6: Predicted impact compressive stress-strain curves for the specimen tested by Perry and Bischoff [45]

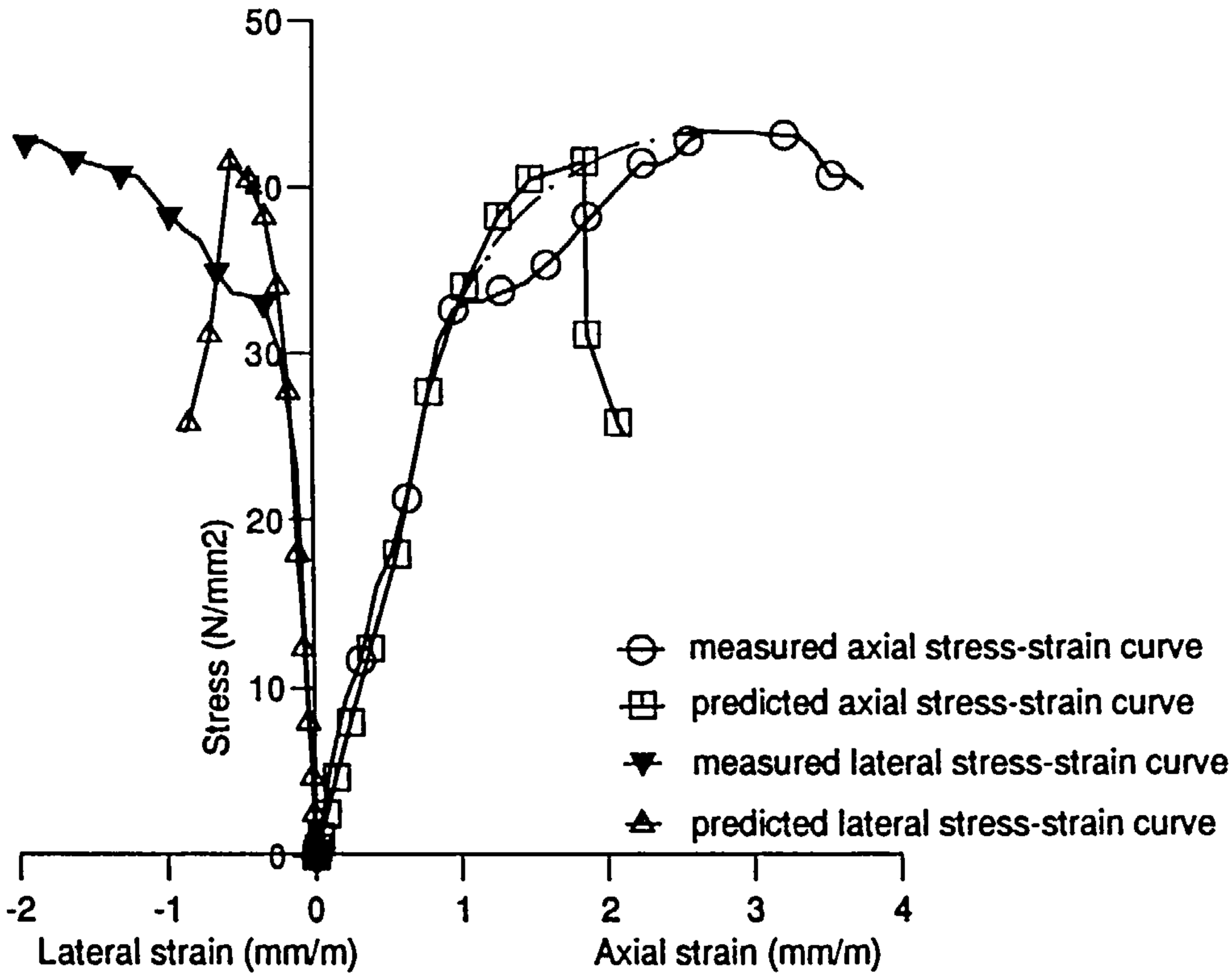

Figure 6.7: Predicted and measured impact stress-strain curves for the specimen tested by Perry and Bischoff [45]

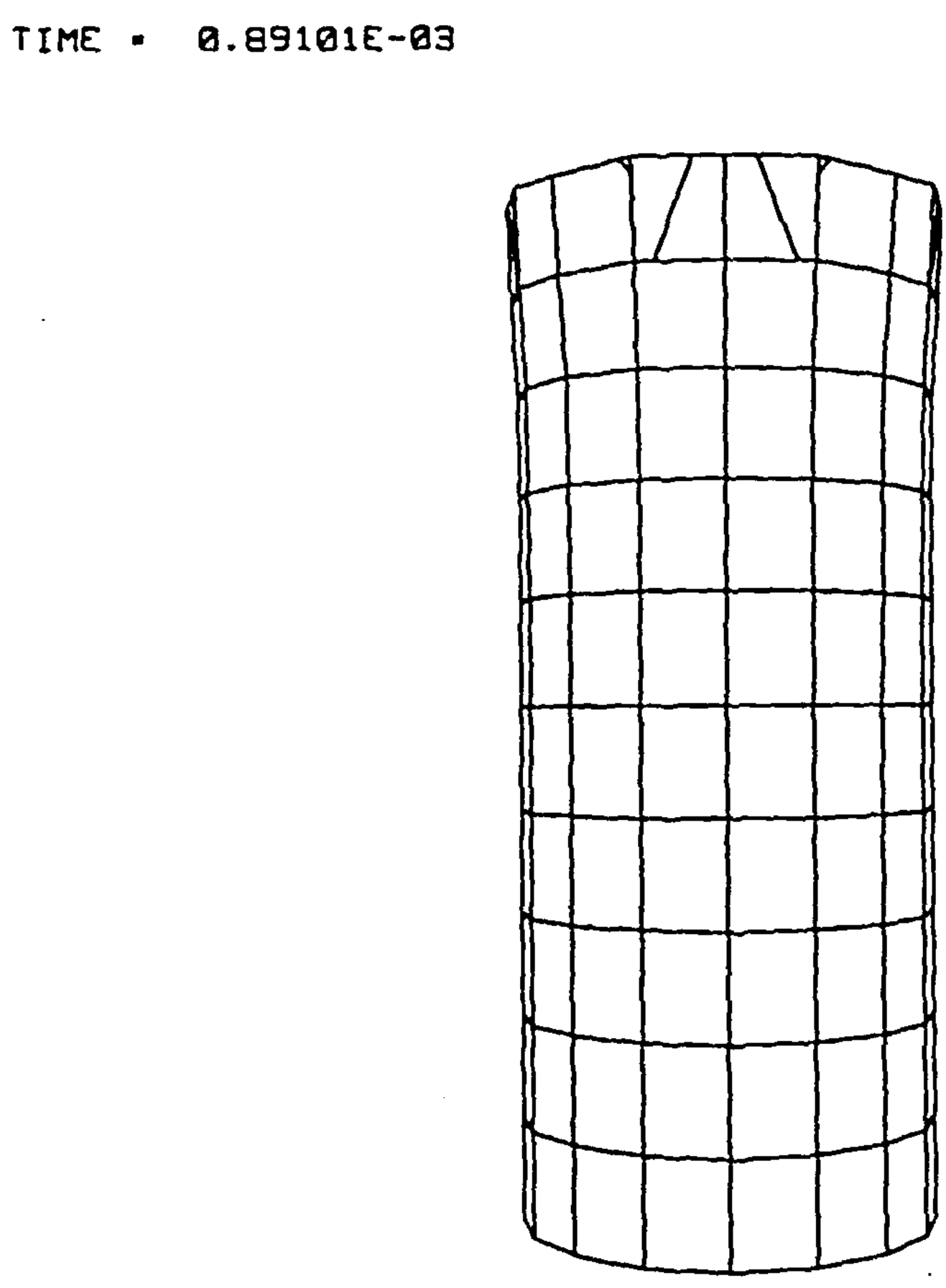

Figure 6.8: (a) Predicted deformed shape and crack pattern for the cylinder tested by Perry and Bischoff [45] at time 0.89101E-03 seconds

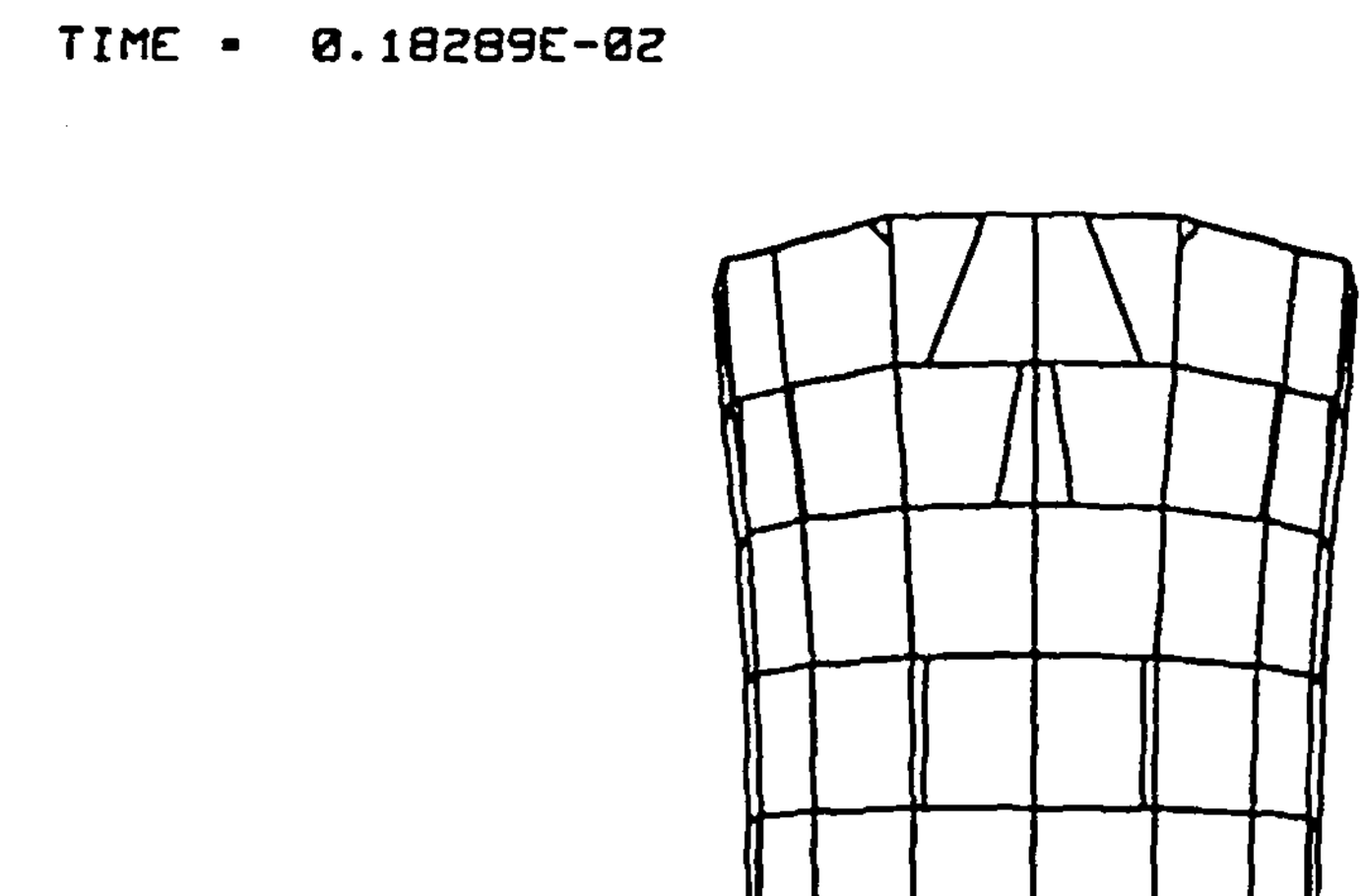

Figure 6.8(b) Predicted deformed shape and crack pattern for the cylinder tested by Perry and Bischoff [45] at time 0.18289E-02 seconds

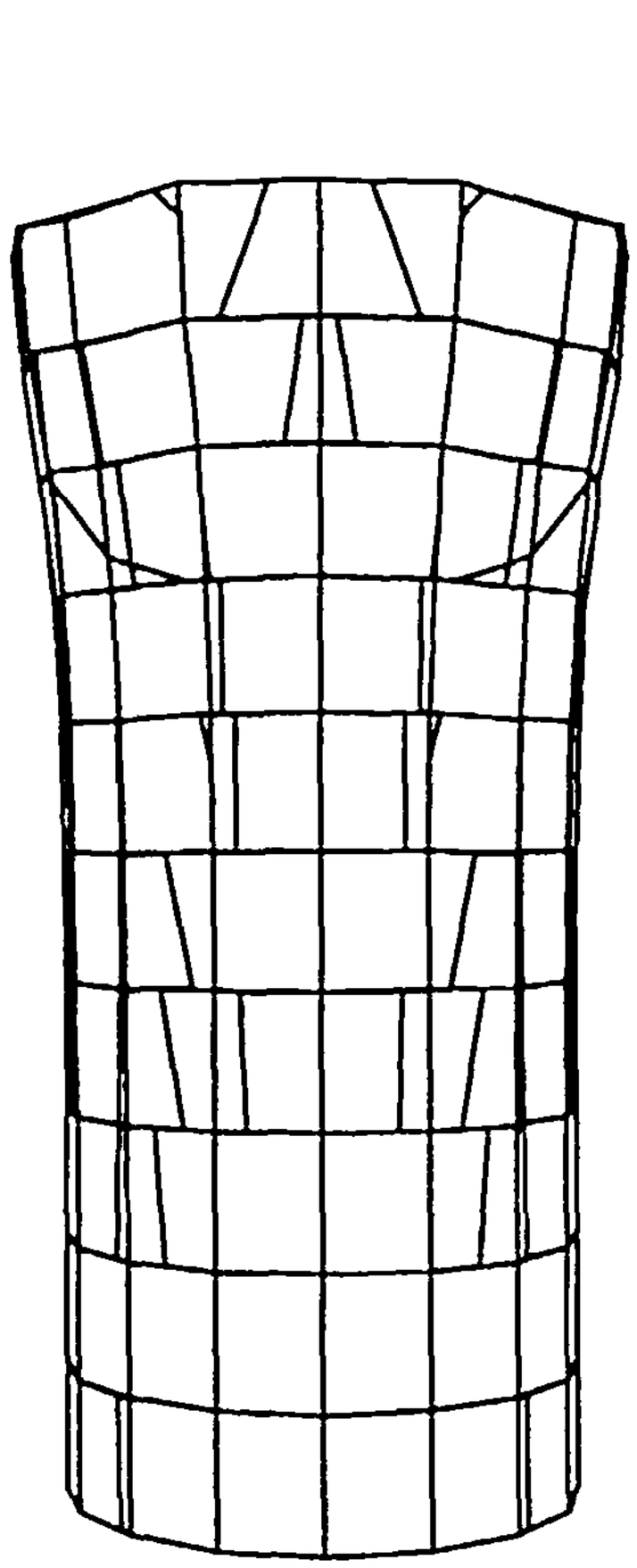

Figure 6.8(c)Predicted deformed shape and crack pattern for the cylinder tested by Perry and Bischoff [45] at time 0.29544E-02 seconds

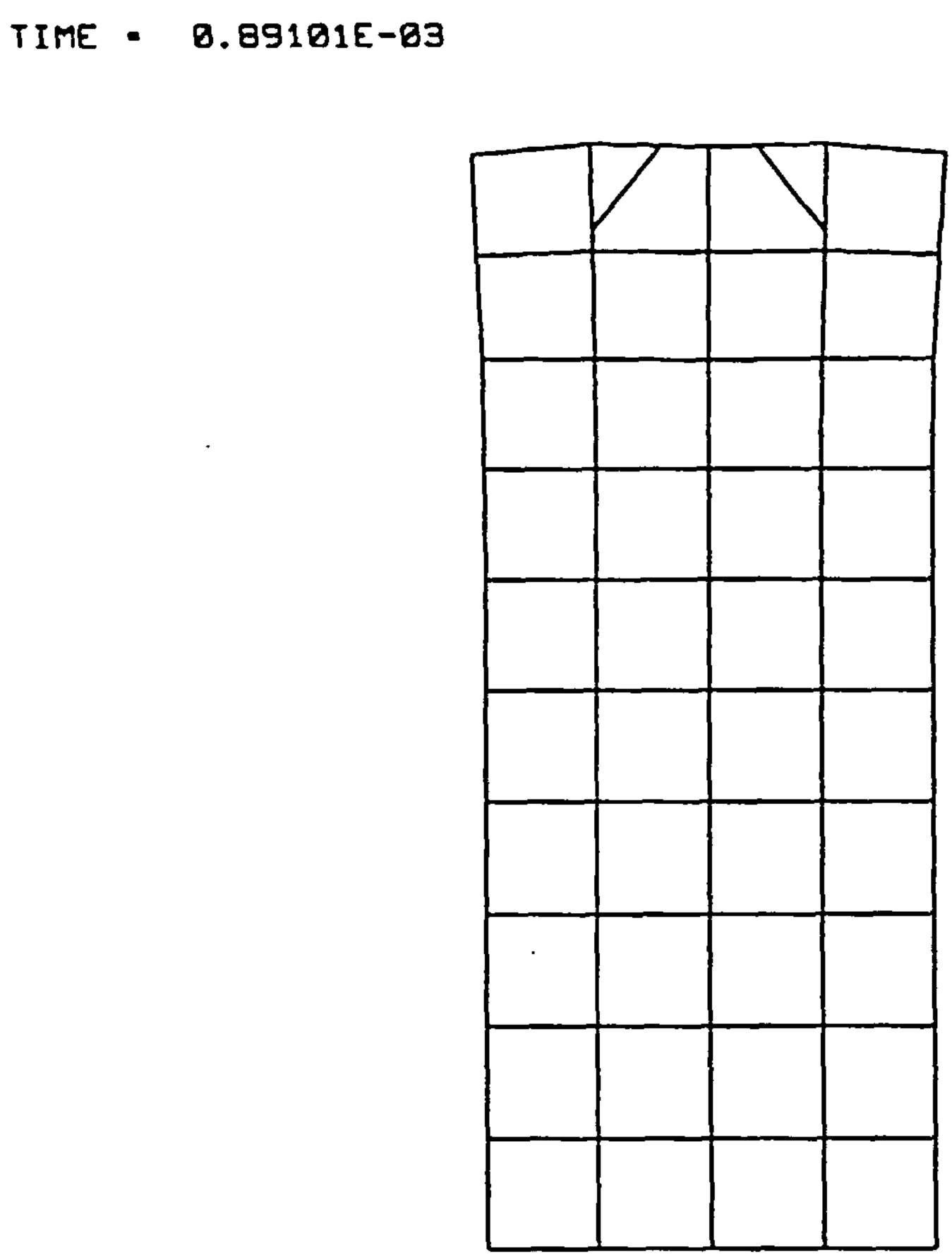

Figure 6.9: (a) Predicted deformed shape and crack pattern for a section through the cylinder tested by Perry and Bischoff [45] at time 0.89101E-03 seconds

TIME = 0.18289E-02

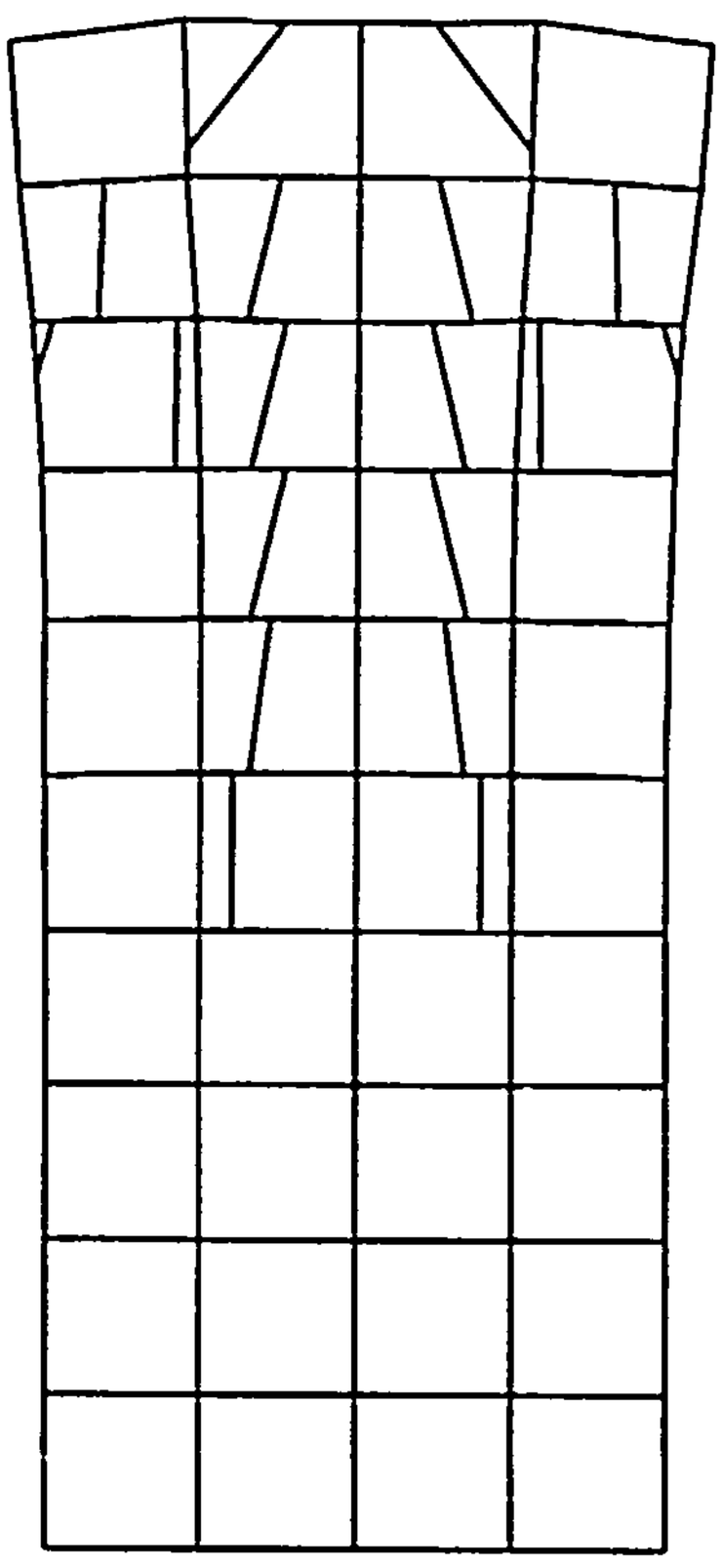

Figure 6.9(b) Predicted deformed shape and crack pattern for a section through the cylinder tested by Perry and Bischoff [45] at time 0.18289E-02 seconds

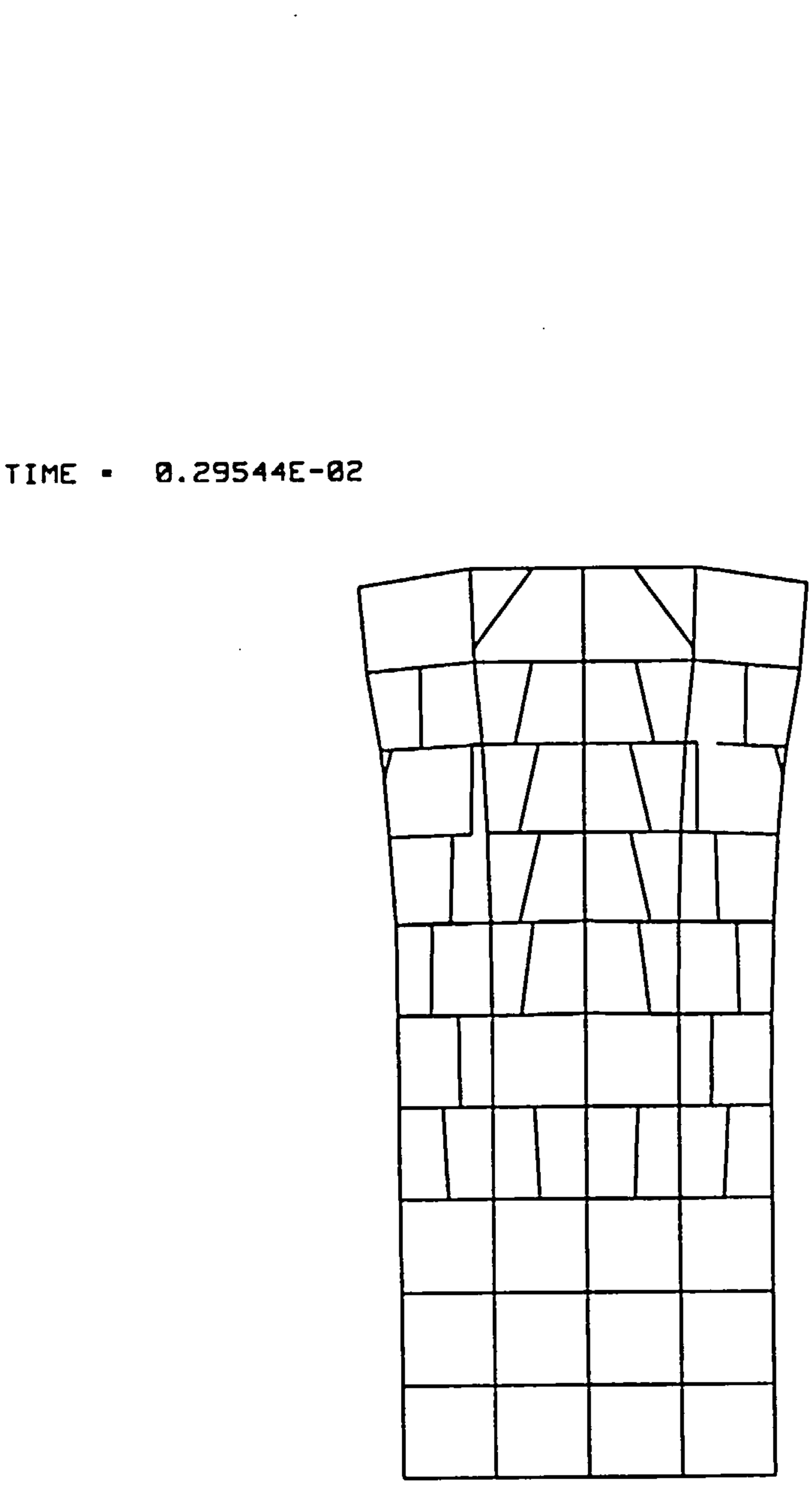

Figure 6.9(c) Predicted deformed shape and crack pattern for a section through the cylinder tested by Perry and Bischoff [45] at time 0.29544E-02 seconds

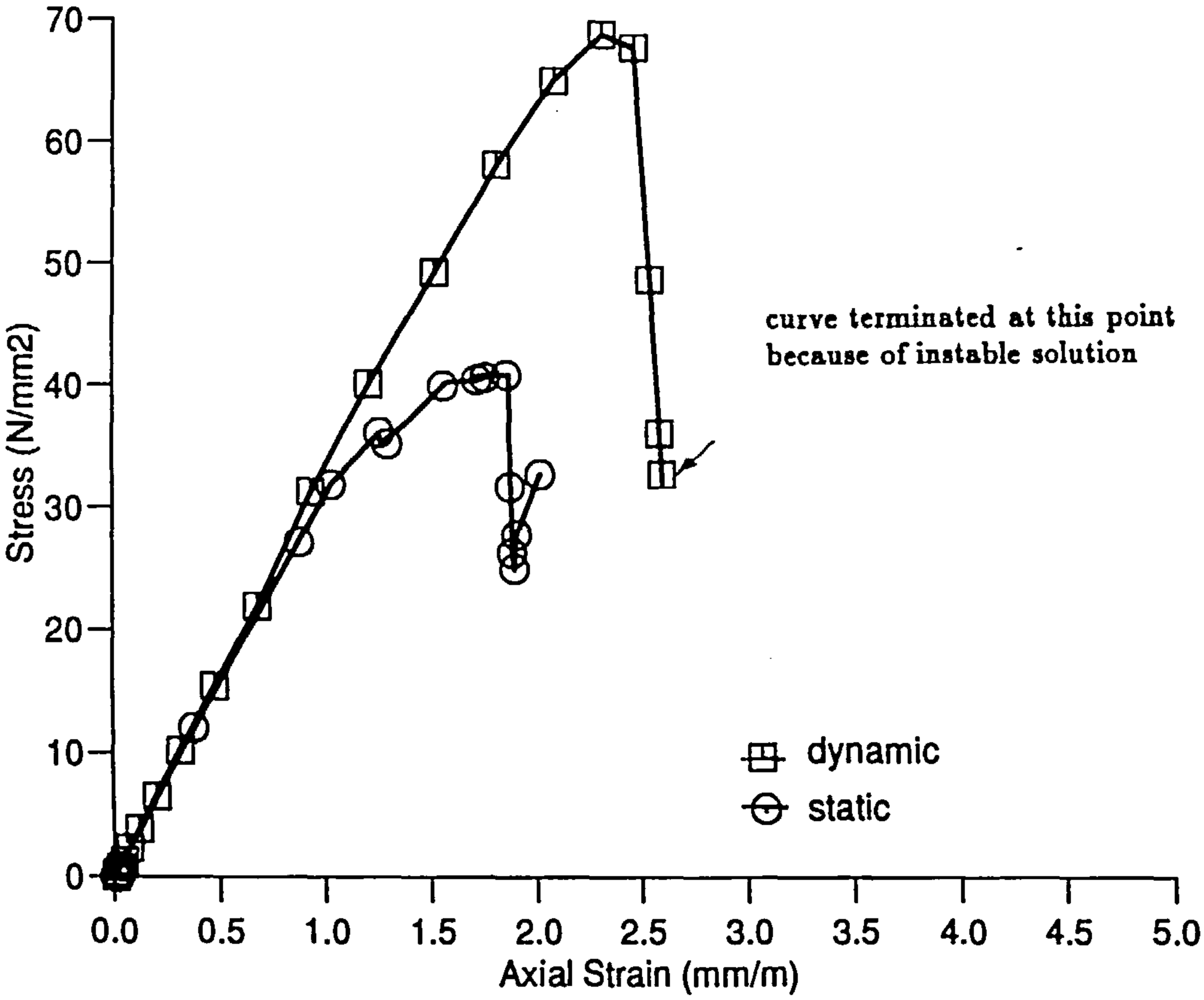

Figure 6.10: Predicted static and impact compressive stress-strain curves for the specimen tested by Curbach and Eibl [42]

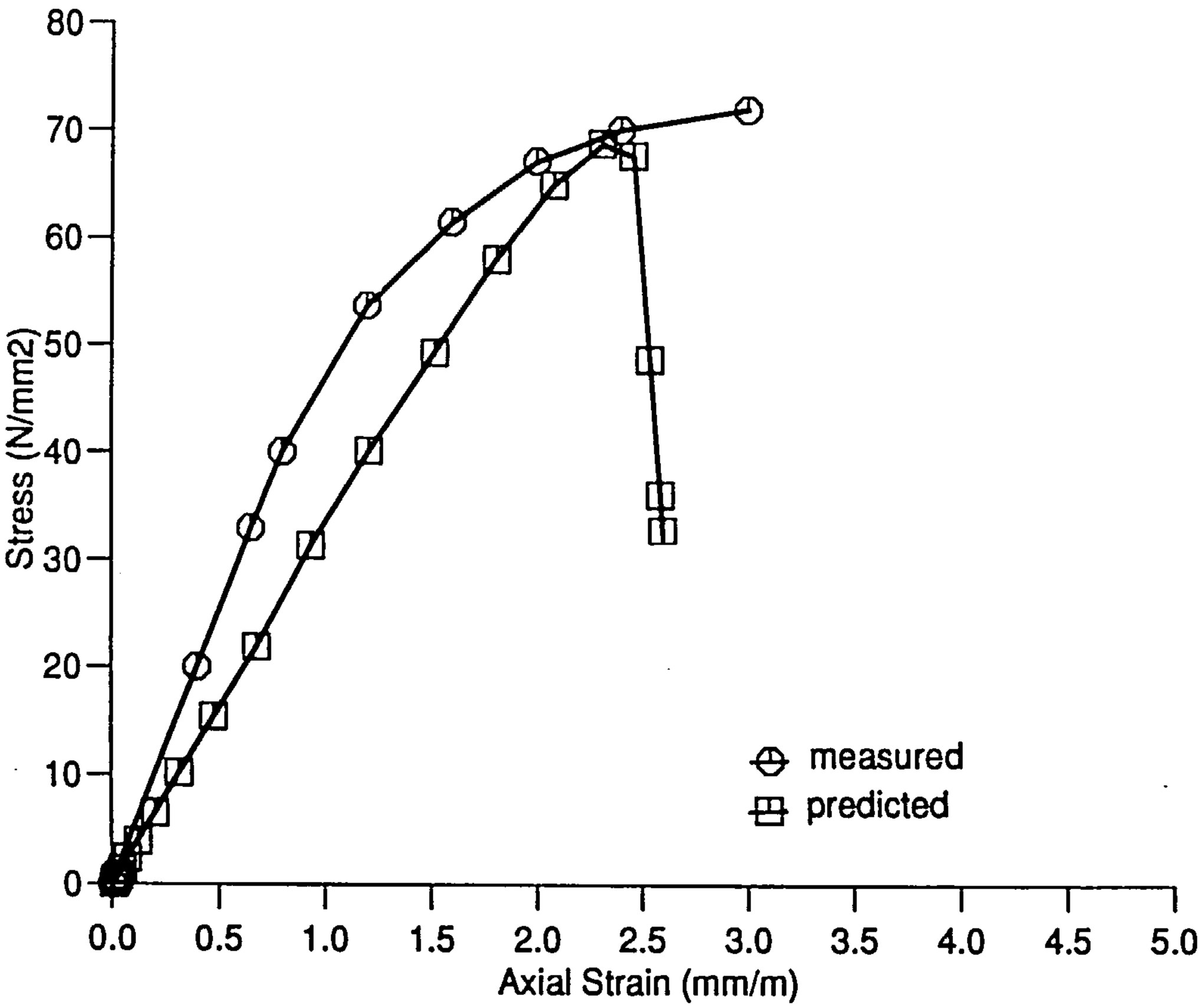

Figure 6.11: Predicted and measured impact stress-strain curves for the specimen tested by Curbach and Eibl [42]

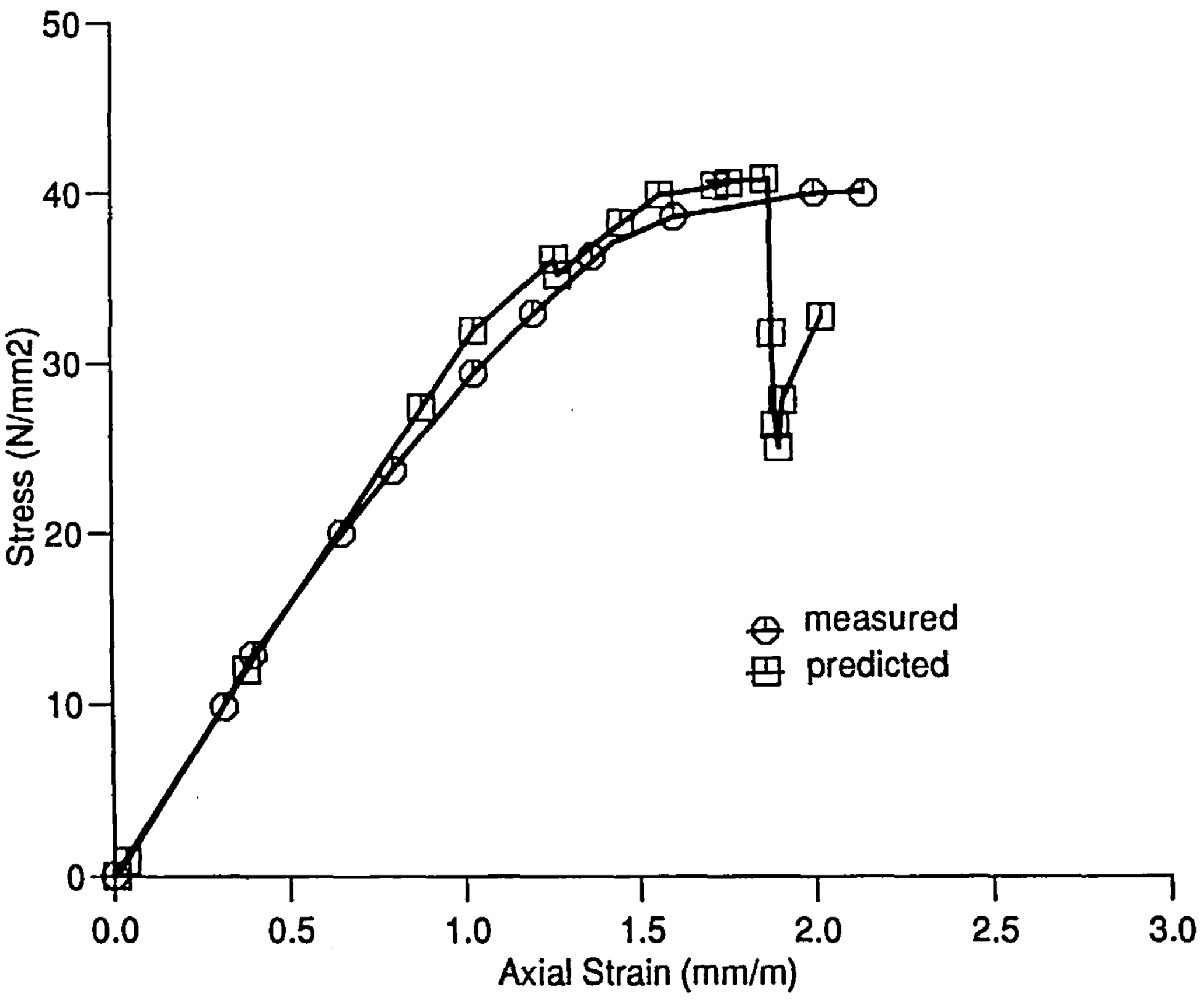

Figure 6.12: Predicted and measured static stress-strain curves for the specimen tested by Curbach and Eibl [42]

Chapter 7

APPLICATION TO REINFORCED CONCRETE MEMBERS

7.1 INTRODUCTION

This Chapter demonstrates the ability of the new fully implemented reinforced concrete model to analyse real impact problems. To this end a number of reinforced concrete members from previously published laboratory based investigations which have been subjected to impact loadings have been analysed. The results obtained using DYNA3D, incorporating the newly developed concrete model, are examined and compared with the results obtained from the laboratory tests.

The problems analysed included an eighth scale reinforced micro-concrete beam and portal frame, and a full size reinforced concrete beam. These members were chosen for the following reasons:

(1) Reasonably detailed information was available in each case.

(2) The impact loadings were assumed to be applied directly to the concrete member. In several test arrangements pads are present between the impactor and the contact surface of the concrete member. A comprehensive study of the influence of a number of pad materials (layers of plywood, rubber and steel) has been carried out [4] and it has been concluded that the type of pad does have an influence on the magnitude of the impact load transmitted to the concrete member and thus on the resulting behaviour of the concrete member. Numerical modelling of layers of rubber, plywood or steel is very a complex task to undertake. Therefore, the cases in which the impact loadings can be assumed to be directly applied to the concrete members are considered to be more suitable for inclusion in this investigation.

7.2 BEHAVIOUR OF REINFORCED CONCRETE MEMBERS UNDER IMPACT LOADINGS

Structural concrete members such as beams and plates subjected to impact loading undergo a number of behavioural mechanisms which progressively leads to their complete collapse. These mechanisms develop at different points in time during the impact event, but they are interrelated such that the extent of the damage inflicted on the concrete member because of any one mechanism is dependent on the presence and influence of the previous mechanisms. The failure mechanisms are also very much dependent on the support conditions of the member. For example, a pinned member will respond differently to impact loading compared to a member in which the boundary conditions are simply supported. A pinned member is prevented from lifting at the supports and therefore the modes which develop differ from those of a simply supported structure which tends to experience uplift at the supports. A brief description of the most dominant mechanisms is given below. A more detailed interpretation has been published previously [149].

(1) Surface crushing :

During the first few microseconds of an impact, large stress waves are transmitted into the contact area of the concrete member. This causes complete

pulverization of the concrete in this area which results in the development of a crater at the surface of the member. The size and shape of the crater is a function of the shape of the contact surface of the impact, the velocity at which the impactor is travelling at the time of contact and the cross section of the structural concrete member.

(2) Concrete plug :

The stress waves encounter on their passage through to the opposite face of the concrete member a large number of internal wave reflectors, such as aggregate particles. As a result momentum is progressively accumulated and deposited into the concrete as the stress waves are dissipated. If a large momentum is deposited under the impact load before the concrete member has responded to any flexural modes then a local punching shear failure, which is commonly referred to as a concrete plug, will develop. The boundaries of the concrete plug are defined by a region possessing large velocity gradients. This would eventually be expected to lead to the development of cracks.

(3) Scabbing :

This is initiated during the response of the concrete to impact loading and it is associated with an internal expansion of the concrete due to the reflection of the incident compressive stress waves i.e. compressive deformations always generate dilation at right angles to the incident stresses which results

in a failure of the concrete in tension in a direction parallel to the incident compressive stresses, usually along the flexural reinforcing bars. Scabbing is apparent by the detachment of concrete in an area at right angles to the impact load and situated at the opposite face of the member from the one which had been impacted.

(4) Global flexural response :

The flexural response of the concrete member under impact loading develops progressively as momentum is transmitted away from the region where the load is first applied towards the support regions. The flexural response is very slow compared to the formation of the concrete plug. The flexural response of a structural member subjected to impact loading is influenced by the support conditions for the member.

In the following Sections descriptions of the concrete members which have been analysed are given together with details of the finite element idealisation. The predicted behaviour of the concrete members over the duration of the impact is discussed. The various mechanisms which are involved in the failure including; the local deformation under the impact load, the concrete plug formation and the global flexural deformation are also discussed.

7.3 MICRO-CONCRETE MEMBERS

Watson and Ang [150] investigated experimentally the resistance and behaviour of micro-reinforced concrete beams and a portal frame subjected to impact loadings. They tested a large number of approximately eighth scale reinforced micro-concrete beams subjected to impact loading at mid span. Two types of beam have been investigated, a simply supported beam and a beam which was continuous with two columns (portal frame). Each type of beam investigated was analysed using the newly developed concrete model and the results were compared to those obtained from the laboratory tests. The beam and the portal frame which were selected were designated as DB1-3 in test series A and DF1-7 in test series F respectively in the original investigation.

7.3.1 Description of Tests

Figures 7.1 and 7.2 show details of the geometry of the beam and the portal frame, the reinforcement layout, the boundary conditions and the impacting device. The total length of the beam was 542 mm. The supports were positioned at distance of 50 mm in from each end of the beam. The effective span of the beam was therefore reduced to 442 mm. The beam cross section was 44 mm $\times$ 65 mm.

The reinforcement cage consisted of six longitudinal bars, three in the tension region and the other three were located in the compression region of the beam.

The stirrups were spaced uniformly along the length of the beam. All the reinforcement was made from black annealed wires with diameters of 4.0 and 3.15 mm for the longitudinal reinforcement and diameters of 2.0 and 1.61 mm for the transverse reinforcement (stirrups).

The portal frame consisted of a 486 mm long beam and two 600 mm high columns. The beam intersected the columns at mid height which reduced its effective length to 398 mm. The columns were simply supported at their upper ends and pinned at their bases. The effective height of the column was estimated to be 502 mm.

The reinforcement in the beam in the portal frame was identical to the simply supported beam described above. Details of the layout of the column reinforcement are shown in Figure 7.2.

The beam and the portal frame were tested in a specially designed test arrangement. The impact load was initiated at the mid span of the two beams. A steel rod with a diameter of 28.0 mm, and a mass of 1.78 kg was driven to achieve a velocity of 15.75 m/sec at the point of contact with a stationary pressure bar. The steel pressure bar was 28mm in diameter, 1000mm in length. It was mounted in a linear bearing which was in contact with the surface of the concrete member at mid span.

An additional vertical load of 5 kN was applied to the cross section of the upper end of the two columns of the portal frame in order to prevent them from lifting up when the impact load was applied.

7.3.2 Finite Element Idealisation

On the assumption that the impact load was to be uniformly applied to the beams, only a quarter of each test arrangement was idealised into finite elements. The two planes of symmetry of the square, rectangular and circular cross sections of the column, beams and impacting device respectively were used.

The concrete members were modelled using 312 solid elements and 618 nodes for the beam and 724 solid elements and 1380 nodes for the portal frame. In the case of both models, the nodes in the planes of symmetry were restrained in the appropriate directions in order to simulate continuity with respect to the other parts of the overall system. All other nodes were free to move in any direction.

The finite element meshes used in the numerical model for the different parts of the beam and the portal frame are shown in Figures 7.3 and 7.4 respectively.

The reinforcing bars were included in the model as discrete entities i.e. smeared over the solid elements. The quantity of reinforcement in any element was calculated in terms of the local fraction of the element cross section that is occupied

by the reinforcing bars.

The properties of the concrete and reinforcement used in the analysis are shown in Table 7.1. It should be noted that not all the data required for the analysis was reported and as a consequence, several values had to be assumed.

In the numerical analysis the impacting rod initially rested on the pressure bar which was itself resting on the surface of the beams. At time t=0 the rod was driven towards the pressure bar with a contact velocity of 15.75 m/sec. The pressure bar reacted with the rod and impacted the concrete beams at mid span. The static loads at the upper surfaces of the two columns were applied before the initiation of the impact load and remained constant over the duration of the impact event. This was achieved using the dynamic relaxation solution procedure available in the finite element program.

The concrete members and the impacting device are distinct bodies in space. The interaction between them is achieved by using contact interface segments of the type that permit contact and separation. This type of interface is referred to as sliding with voids in the users manual for INGRID which was used for the generation of the input data [148].

The impacting device was assumed to be made of steel and Table 7.2 shows the

material properties used in the numerical analysis.

7.3.3 Results from the Analysis

The plots of the predicted deformed shapes together with the predicted crack patterns for the beam and the portal frame from the numerical analysis are shown in Figures 7.5 and 7.6 respectively. The deformed shapes of the beam and the portal frame are plotted at full scale. They provide a clear insight into the behaviour of the concrete members at different time intervals during the impact event. Figures 7.7 and 7.8 show the distribution of the cracks obtained from the laboratory tests in the beam and the portal frame respectively [150].

The predicted deformations and crack distribution were found to be similar to those obtained in the laboratory tests as discussed below:

(1) The concrete elements under the pressure bar were found to be severely deformed and the reinforcing bars had yielded in the three directions. It can be concluded that this type of deformation can be considered to be the mechanism which led to the formation of the crater.

(2) At mid span the beams experienced local shear deformations which produced diagonal cracks under the pressure bar and within an area inclined at 45 degrees to the impacted area. Therefore, the crack patterns formed a cone

shape similar to the concrete plug shown in Figures 7.7 and 7.8.

The calculated widths of the concrete plug agree with the corresponding measurements found in the laboratory tests conducted by Watson and Ang [150]. A detailed comparison of the plug widths is included in Table 7.3. The cracks which form the concrete plug appeared during the first mode of deformation of the beam. They have mainly resulted from a combination of stress conditions dominated by shear stresses.

(3) Away from the concrete plug the numerical analysis reproduced a number of the cracks which were observed in the laboratory tests on the beams. The beam in the portal frame was stiffer than the simply supported beam because of the differences in the support conditions. The maximum measured and predicted deflections for the beam and the beam in the portal frame are shown in Table 7.4. The two beams were otherwise very similar in all aspects except in the support conditions.

(4) Figures 7.5(a)-(e) and 7.6(a)-(e), confirmed that the surface crushing and the concrete plug develop during the early stages of the impact event. The concrete plug is fully established after approximately 5 milliseconds from the initiation of the impact. The formation of the concrete plug is due to the concentration of the momentum deposited around the localised area of the impact surface. This is caused by the localised large velocity gradient

in the region under the impact load as shown in Figure 7.9.

Greater damage is inflicted on the concrete in the region of the concrete plug after its formation. This is due to the increase in the velocity gradient which is related to an increase in the shear force applied to the elements under the impact region.

The predicted flexural response is due to the first and third modes of excitement (the even modes i.e. 2, 4, etc are ignored because of the symmetrical property of structural members in terms of the geometry and the loadings i.e. the structural members were impacted at mid span). The third mode of excitement causes reverse bending of the beams and hence the formation of flexural cracks at their upper surface. Higher modes of excitement may have occurred during the analysis but their presence has not been detected in the resulting crack pattern. Alternatively they may have had little effect on the behaviour of the concrete member.

Furthermore the global response of the concrete members i.e. vibration (modal responses) has appeared during the elastic response of the member. Once plastic deformations have occurred the dynamic vibrations are reduced very rapidly and the predominant deformations inflicted on the members are permanent.

(5) Figures 7.10 and 7.11 show the predicted impact force histories for the beam and the portal frame respectively. The maximum predicted impact force for the beam and portal frame show good correlation with those obtained in the laboratory tests. Differences of the order of 11 and 5 percent were found between the computed and the averaged measured impact loads for the beam and the portal frame respectively. The maximum pulse recorded during the laboratory tests occurred at 0.350 milliseconds after the rod contacted the pressure bar whereas the predicted maximum value occurred for both tests 0.660 milliseconds after the impact had been initiated as shown in Figure 7.12.

7.3.4 Summary

When the new concrete model was used to analyse the behaviour of two micro-concrete members the results obtained were found to be in agreement with those obtained in the laboratory tests. In particular, good agreement was found with the magnitude of the impact load, the deflections at mid span and the crack pattern under the impact load. However, the prediction of the global deformations which are due to higher modes of vibration was not as good as those obtained for the first mode, although higher modes of vibration were evident by the presence of cracks in the upper surface of the beams.

Concrete	values
Compressive strength	39.5 N/mm^2
Tensile strength	3.97 N/mm^2
Crack opening length	$45\mu m$
Aggregate size or (β shear reduction factor)	(0.4)
Modulus of elasticity	30500 N/mm^2
Poisson's ratio	0.2
Density	2400 kg/m^3
Hardening coefficient	0.9

Reinforcement (wire)	values
σ_y yield stress	250 N/mm^2
E modulus of elasticity of steel	$200000 N/mm^2$
E_T hardening modulus	0 N/mm^2
ϵ_u ultimate elongation	2%

Table 7.1: Assumed and measured reinforced concrete properties for tests conducted by Watson and Ang [150]

Steel Rod	Values
Modulus of elasticity of steel	200000 N/mm^2
Poisson's ratio for steel	0.3
Contact velocity V	15.56 m/sec

Pressure bar	Values
Modulus of elasticity of steel	200000 N/mm^2
Poisson's ratio for steel	0.3
Contact velocity V	0.0 m/sec

Table 7.2: Assumed and measured properties of the impacting device for the tests conducted by Watson and Ang [150]

	Computed (mm)	Measured (mm)
Beam	155	144.5
Portal	166	159

Table 7.3: Predicted and measured plug widths for the impact loading tests on beams conducted by Watson and Ang [150]

	Computed (mm)	Measured (mm)
Beam	7.92	10.3
Portal	5.12	4.2

Table 7.4: Predicted and measured deflections at mid-span for the impact loading tests on beams conducted by Watson and Ang [150]

7.4 FULL SIZE CONCRETE MEMBER

Eibl et al [151] conducted a series of tests on reinforced concrete beams subjected to impact loading. One of these beams was included in the present investigation because of the extent of the information which was available. The selected beam was designated as B80/2 in the original investigation.

7.4.1 Description of the Test Specimen

Figure 7.13 show details of the beam geometry, the reinforcement layout, the boundary conditions and the impactor which was used to generate the impact loads.

The total length of the beam was 4600 *mm*. The supports were positioned at a distance of 300 *mm* in from each end of the beam. The effective span of the beam was therefore reduced to 4000 *mm*. The breadth and depth of the beam were 250 *mm* and 350 *mm* respectively. The reinforcement cage consisted of six 28 *mm* diameter bars, three on the tensile side and three on the compressive side of the beam and 12 *mm* diameter rectangular shaped stirrups. The spacing of the stirrups was varied along the length of the beam. At the impact region the number of stirrups was doubled over a length of 1320 *mm* to avoid a premature local failure due to the concentration of shear stresses under the impact loading.

The beam was tested in a specially designed test arrangement. A solid steel

cylinder was dropped from a pre-determined height and guided onto the beam at mid span. The solid steel cylinder had a diameter of 200 mm, a length of approximately 420.0 mm and a mass of 100 kg. It was dropped from a pre-set height to reach a contact velocity of $8.9m/sec$. In addition, a 300 kN concentrated load was applied to the upper surface of the beam above each of the supports in order to prevent the beam from lifting up at the supports during the impact event.

7.4.2 Finite element Idealisation

On the assumption that the impact load is going to be uniformly applied to the beams, only a quarter of the test arrangement was idealised into finite elements. The two planes of symmetry of the cross section of the beam were also used.

The concrete beam was modelled using 384 solid elements and 721 nodes. The nodes in the planes of symmetry were restrained in the appropriate directions in order to simulate continuity with respect to the other parts of the system. All other nodes were free to move in any direction.

The finite element meshes for the different components included in the numerical model are shown Figure 7.14.

The reinforcing bars were included in the model as discrete entities i.e. smeared

over the solid elements. The quantity of reinforcement in any element was calculated as a local fraction of cross section of the element which is occupied by the reinforcing bars. The properties of the concrete and reinforcement used in the analysis are given in Table 7.5.

In the numerical analysis the solid steel cylindrical impacting device initially rested on the test specimen. At time t=0 it was driven towards the concrete member with a contact velocity of 8.9 m/sec for a period of time.

The static load at each support was applied before the initiation of the impact load and remained constant for the duration of the impact event. This was achieved using the dynamic relaxation solution procedure available in the finite element program.

The concrete member and the impacting device are distinct bodies in space. The interaction between them is achieved by using contact interface segments of the type that permit contact and separation. This type of interface is referred to as sliding with voids in the users manual for INGRID which was used for the generation of the input data [148].

The impacting device was assumed to be made of steel with the properties detailed in Table 7.6.

7.4.3 Results from the Analysis

The predicted deformed shape of the beam together with the predicted crack patterns shown in Figure 7.15 provide a clear insight into the behaviour of the beam at different time steps during the impact event. The deformed shapes of the beam are plotted at full scale. A description of the predicted behaviour of the beam during the impact event is given below:

(1) The concrete plug formed in the early stages of the impact event after approximately 9 milliseconds had elapsed.

(2) Approximately 20 milliseconds after the formation of the concrete plug the beam was experiencing the first mode of deformation therefore flexural cracks continued to form along the tensile region. The mode of deformation then reverted to a higher mode resulting in the formation of flexural cracks at the upper surface of the beam. Further cracks formed near the supports because the beam was prevented from lifting up by the presence of the 300 kN loads which had been applied above the support prior to the application of the impact loading. Simultaneously a number of flexural cracks in the upper surface of the beam closed which confirmed that the beams had undergone several modes of deformation.

(3) At the contact surface the finite elements were severely deformed and the reinforcing bars had yielded in the three directions. Spurious deformations

also occurred in the finite elements immediately under the impact load. This is believed to have been the result of the absence of bond slip between the concrete and reinforcement (a smeared model with perfect bond was adopted in the simulation of the reinforcing bars). However, the maximum permanent deflection at the tensile surface of the beam cross section was found to be in reasonable agreement with the deflection of the beam obtained in the laboratory test i.e. the difference was 17 percent.

(4) Figure 7.16 shows that good agreement was obtained between the computed and measured impact force values.

7.4.4 Summary

In the analysis of a full size reinforced concrete member all the mechanisms including the crater, the concrete plug, and global deformations which are usually observed in laboratory tests were predicted. In addition the maximum residual deformation and impact forces agreed with those obtained in the laboratory test.

The predicted crack patterns agreed closely with the crack patterns observed in the laboratory tests, particularly the formation of the concrete plug and the flexural cracks in the upper surface of the beam. The closing and re-opening of the flexural cracks on the upper surface of the beam indicates that the beam experienced several modes of global deformation.

7.5 CONCLUSIONS

Two types of reinforced concrete member i.e eighth scale and full size reinforced concrete members, were analysed using the new reinforced concrete model developed in this investigation. The main conclusions which can be drawn from the results obtained are as follows:

(1) The new reinforced concrete model which has been developed was found to be able to predict the behaviour, including the different failure mechanisms observed in laboratory tests, of reinforced concrete members subjected to impact loadings. This was particularly the case in the context of the following:

- Local behaviour i.e. crater formation at the contact surface, the development of concentrated flexural cracks under the impact load which result in the formation of a concrete plug.
- Global behaviour including several modes of deformation and the formation of flexural cracks at the upper surface of the beam, the closing and reopening of these cracks.

(2) In the analysis of the eighth scale reinforced micro-concrete members the model was found to produce results which were in reasonable agreement with those obtained in laboratory tests. In particular the impact load-time

histories, the maximum deflections at mid span and the crack patterns under the impact load were found to be in reasonable agreement with those obtained in laboratory tests. However, the prediction of the global deformations which are due to higher modes of deformation was not as good as the prediction of the first mode of deformation. Nevertheless the existence of these higher modes of deformation was confirmed in the numerical analysis by the presence of the flexural cracks at the upper surface of the beams.

(3) The solution obtained for the full size reinforced concrete beam was more accurate than the solutions obtained for the eighth scale reinforced concrete members. All the mechanisms which are normally found in laboratory tests were predicted, including the crater, the concrete plug, and global deformations. In addition the maximum residual deformation and impact forces were in reasonable agreement with those obtained in laboratory tests.

(4) The predicted crack patterns agreed closely with those normally obtained in the laboratory tests, particularly in the context of the formation of the concrete plug and the presence of flexural cracks at the upper surface of the beams.

Concrete	values
Compressive strength	42 N/mm^2
Tensile strength	3.3 N/mm^2
Crack opening length	45μm
Aggregate size or (β shear reduction factor)	(0.4)
Modulus of elasticity	33000 N/mm^2
Poisson's ratio	0.2
Density	2400 kg/m^3
Hardening coefficient	0.9

Reinforcement (wire)	values
σ_y yield stress	450 N/mm^2
E modulus of elasticity of steel	196000N/mm^2
E_T hardening modulus	0 N/mm^2
ϵ_u ultimate elongation	2%

Table 7.5: Assumed and measured reinforced concrete properties for tests conducted by Eibl et al [151]

Solid Steel Cylinder	Values
Modulus of elasticity of steel	200000 N/mm^2
Poisson's ratio for steel	0.3
Contact velocity V	8.9 m/sec
Pre-load	300 kN

Table 7.6: Assumed and measured properties of the solid steel cylinder for tests conducted by Eibl et al [151]

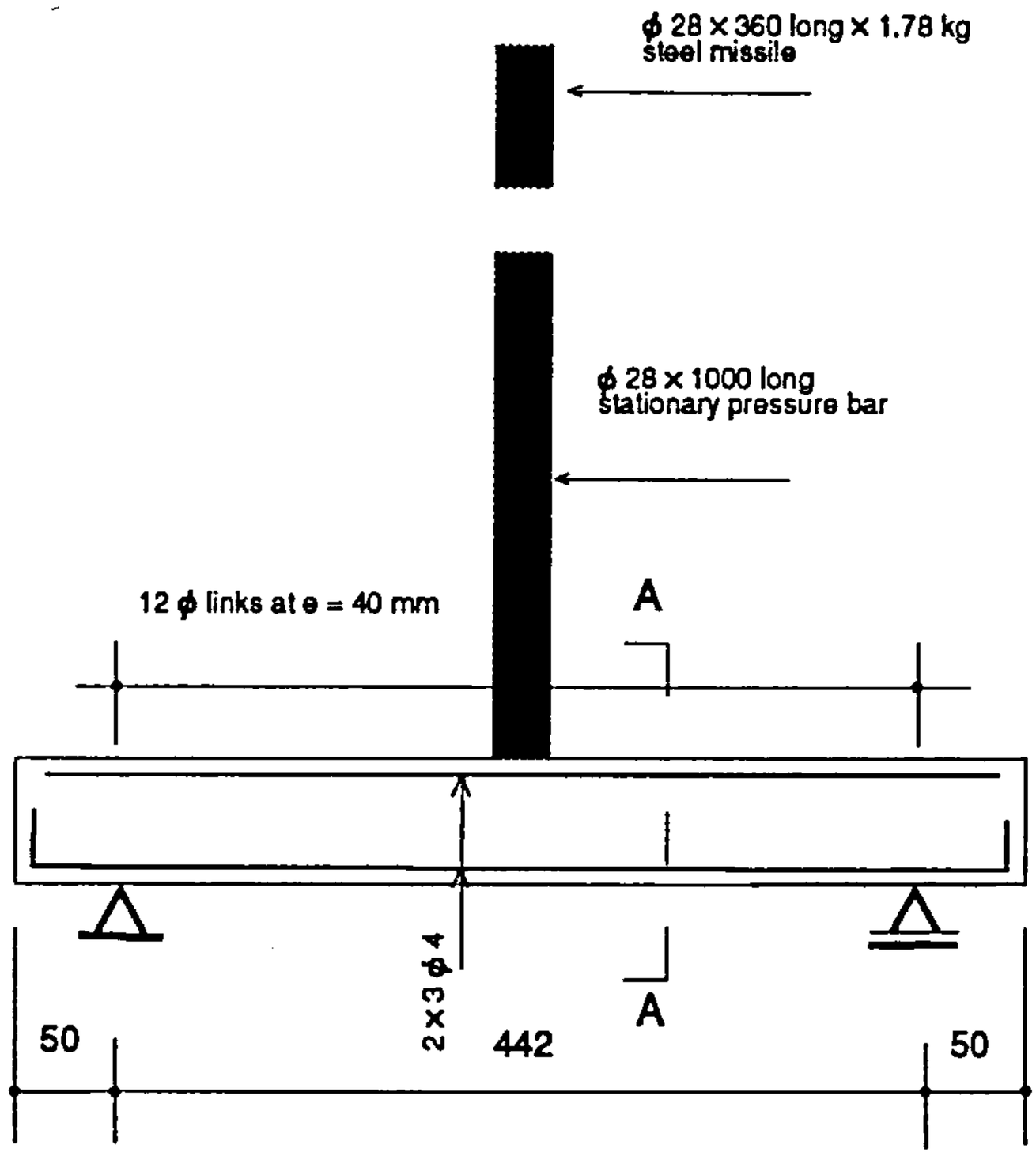

concrete cover to the
side of the stirrups is 4 mm

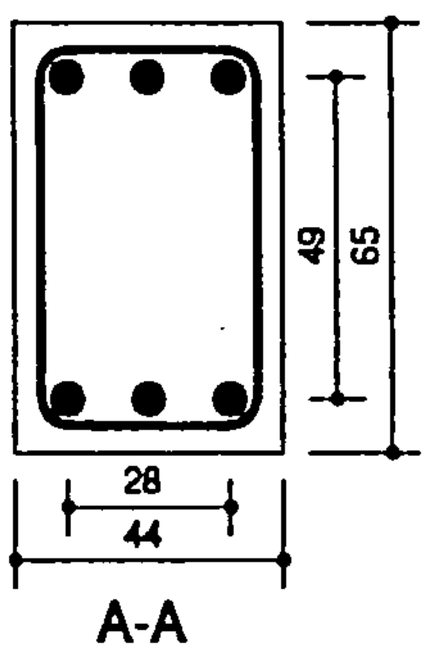

Figure 7.1: Dimensions, reinforcement and loading arrangement for the beam tested by Watson and Ang [150]

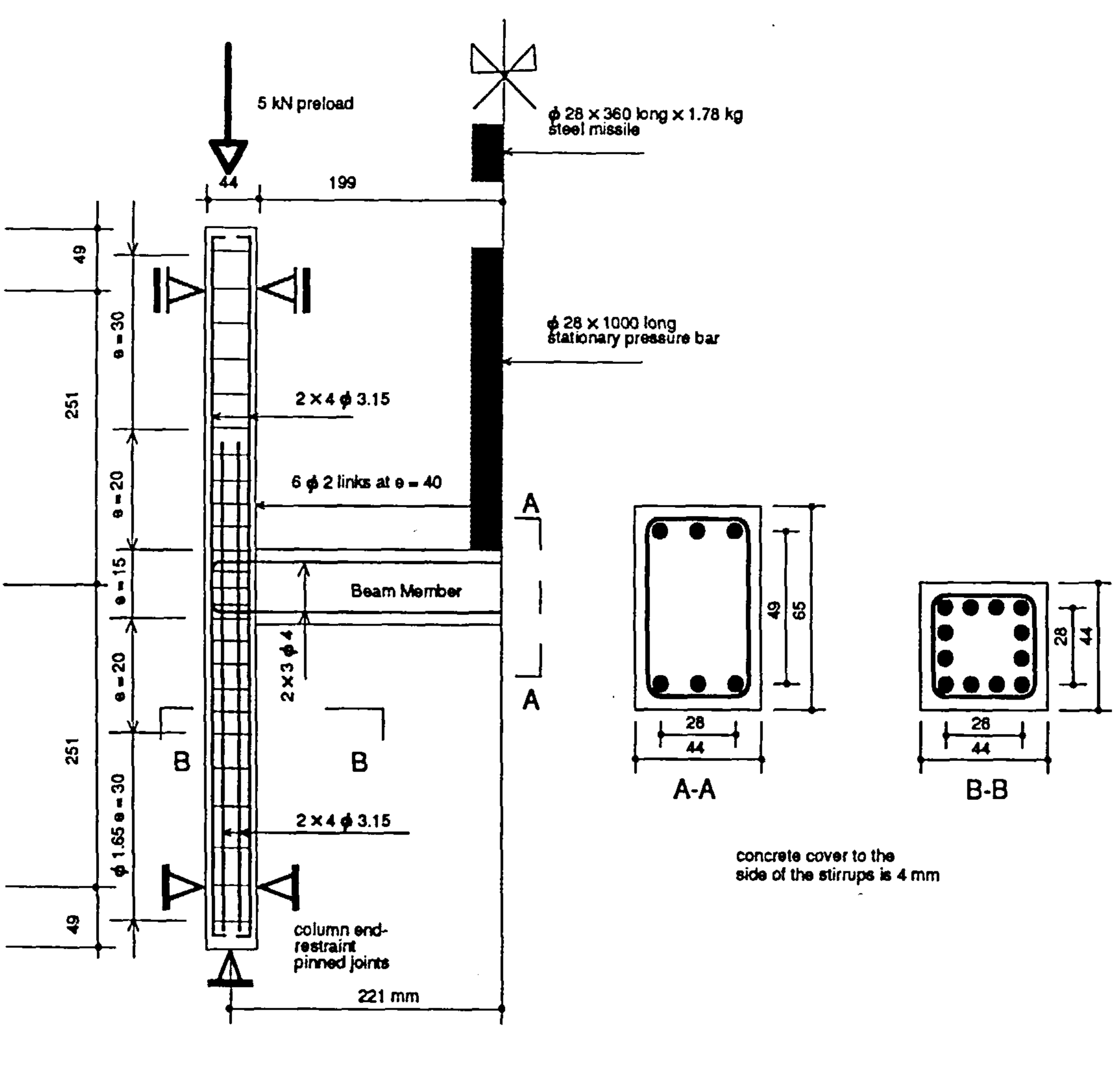

Figure 7.2: Dimensions, reinforcement and loading arrangement for the portal frame tested by Watson and Ang [150]

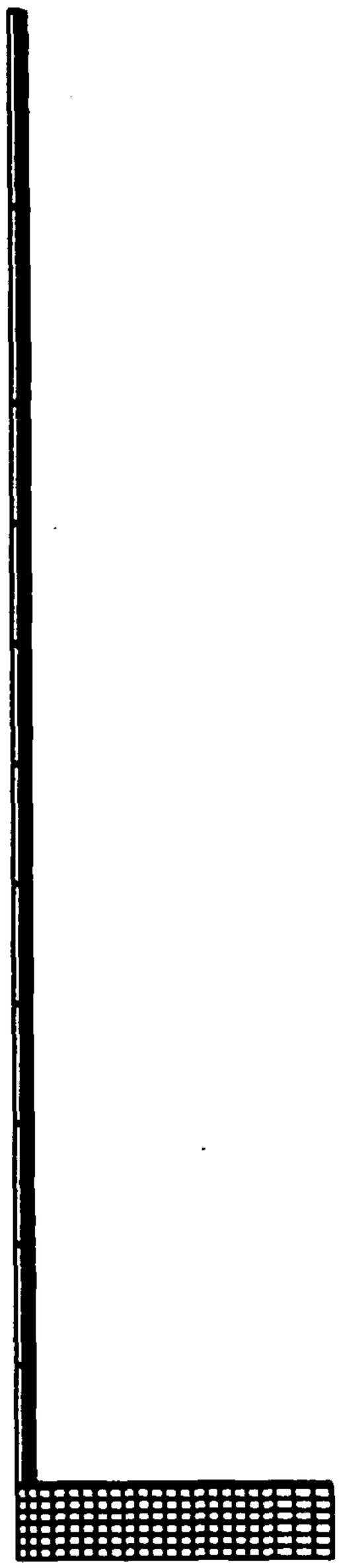

Figure 7.3: Layout of the mesh for the beam tested by Watson and Ang [150]

Figure 7.4: Layout of the mesh for the portal frame tested by Watson and Ang [150]

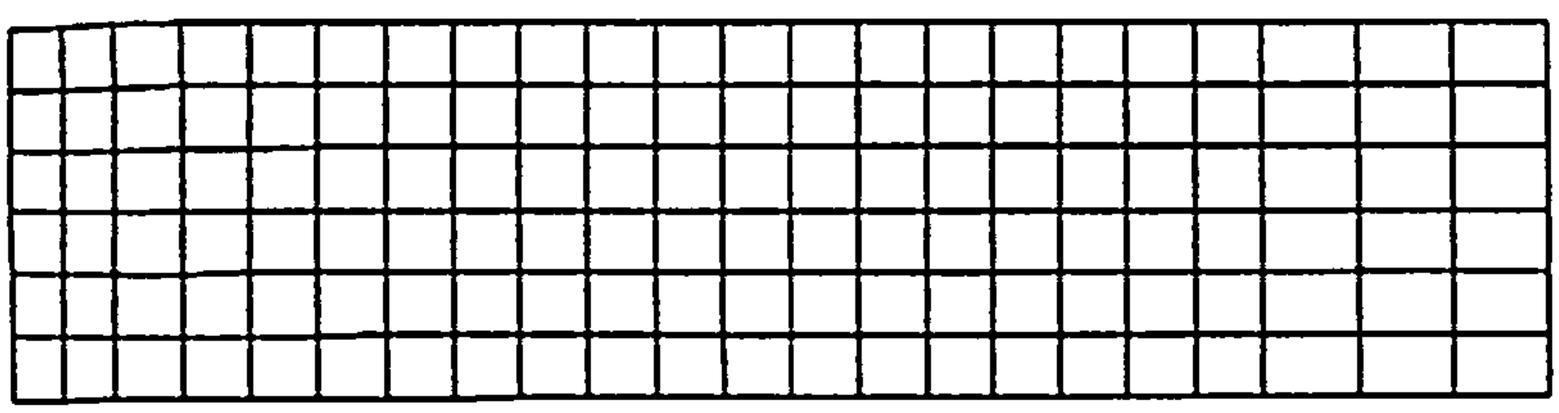

Figure 7.5: (a) Predicted deformed shape and crack pattern for the beam tested by Watson and Ang [150] at time 0.18114E-02 seconds

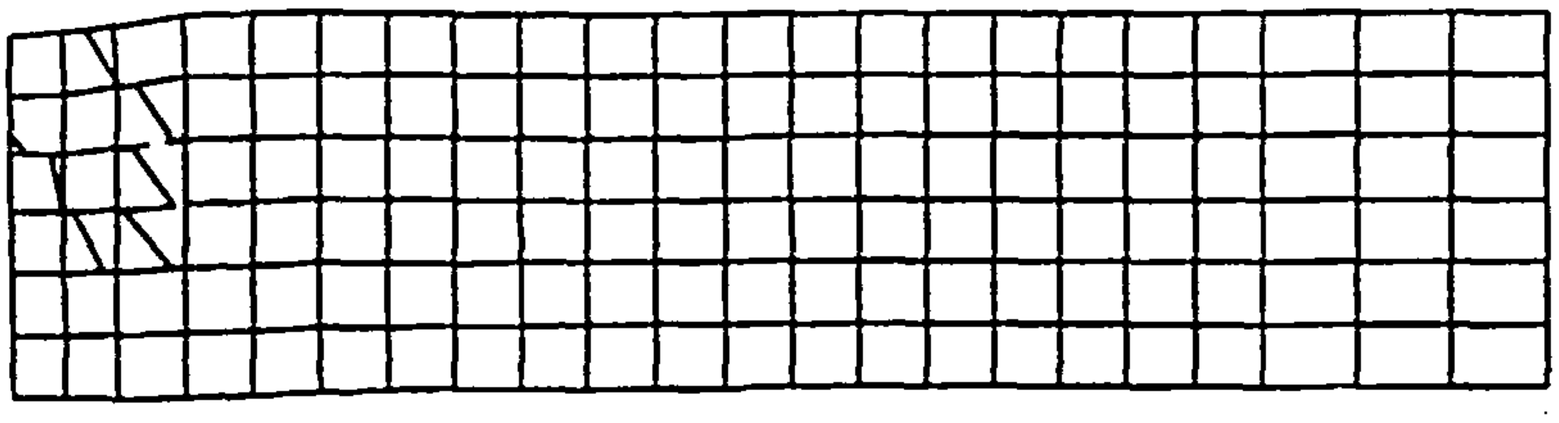

Figure 7.5(b) Predicted deformed shape and crack pattern for the beam tested by Watson and Ang [150] at time 0.36605E-02 seconds

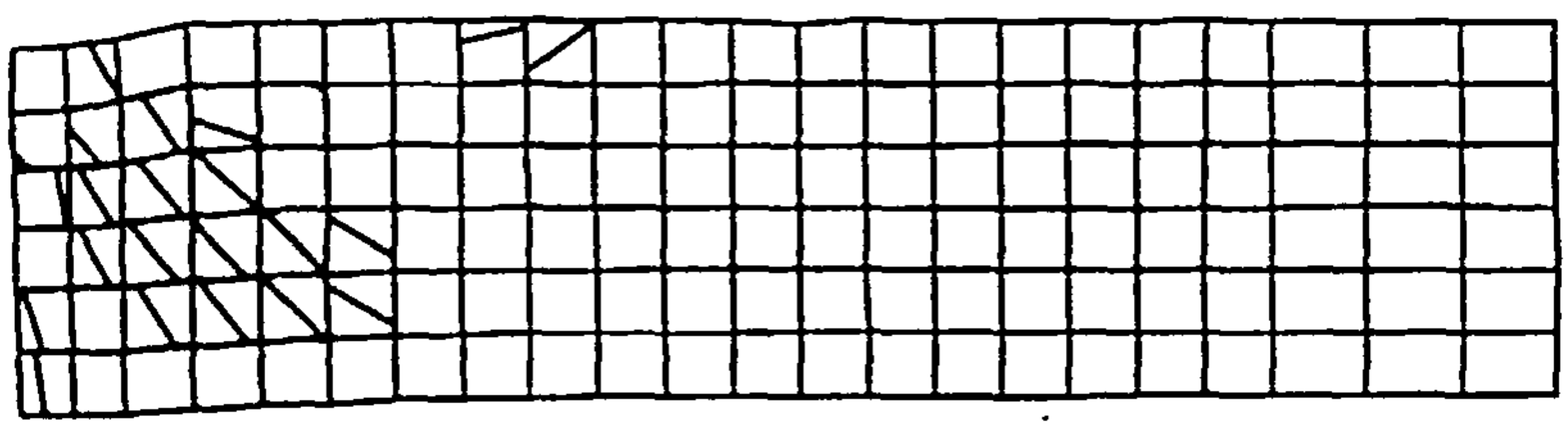

Figure 7.5(c) Predicted deformed shape and crack pattern for the beam tested by Watson and Ang [150] at time 0.49151E-02 seconds

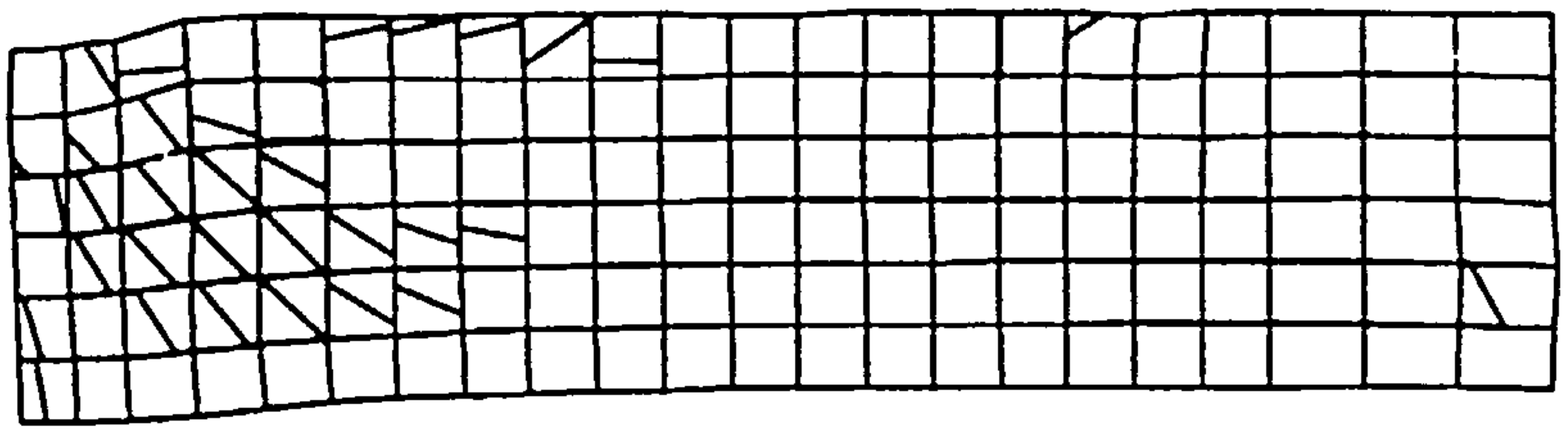

Figure 7.5(d) Predicted deformed shape and crack pattern for the beam tested by Watson and Ang [150] at time 0.61599E-02 seconds

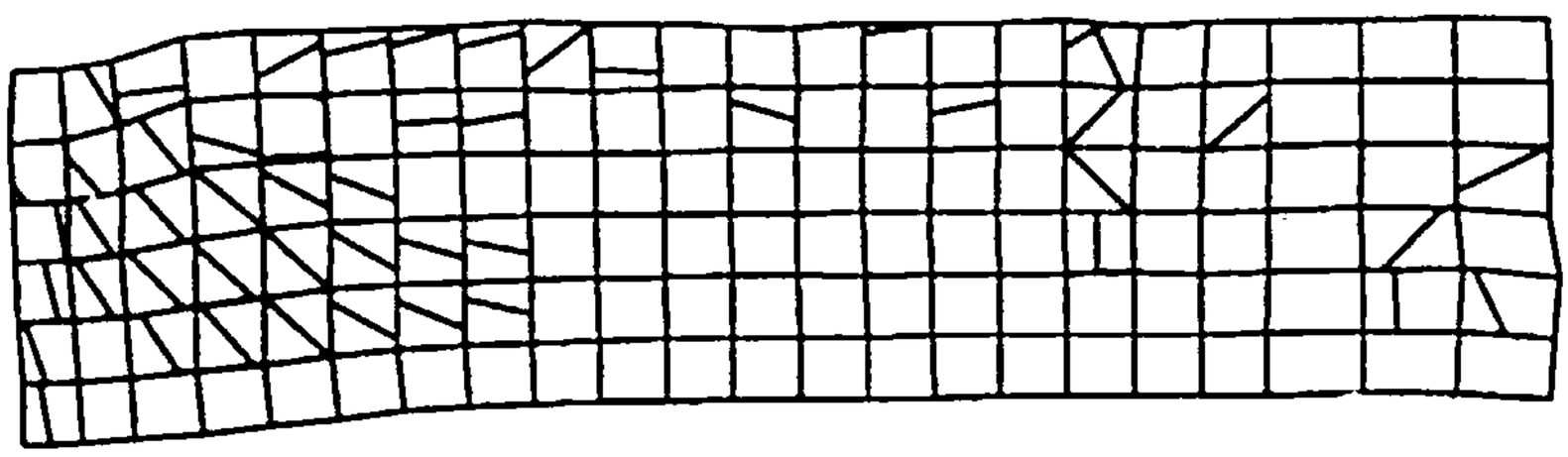

Figure 7.5(e) Predicted deformed shape and crack pattern for the beam tested by Watson and Ang [150] at time 0.74848E-02 seconds

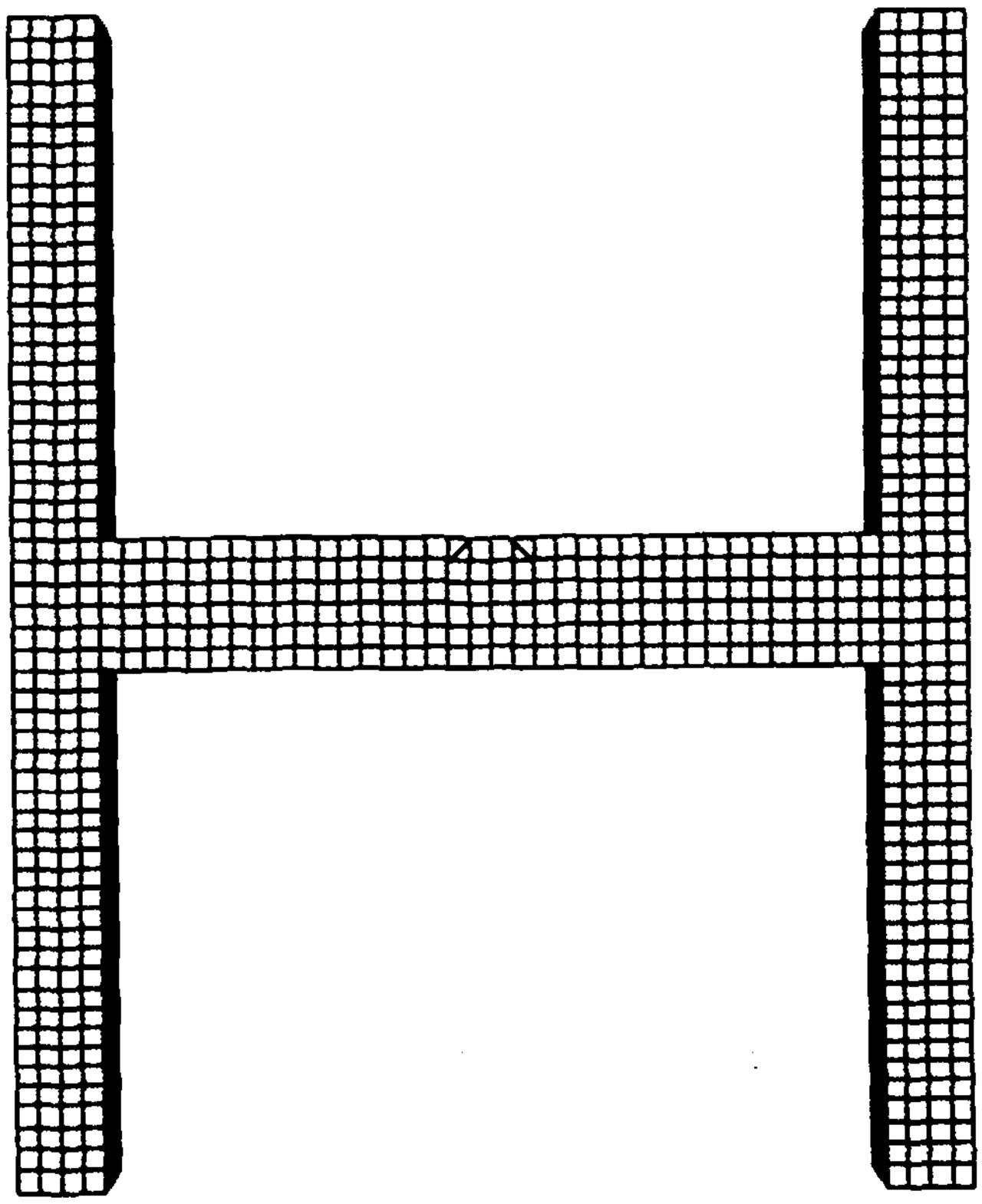

Figure 7.6: (a) Predicted deformed shape and crack pattern for the portal frame tested by Watson and Ang [150] at time 0.18584E-02 seconds

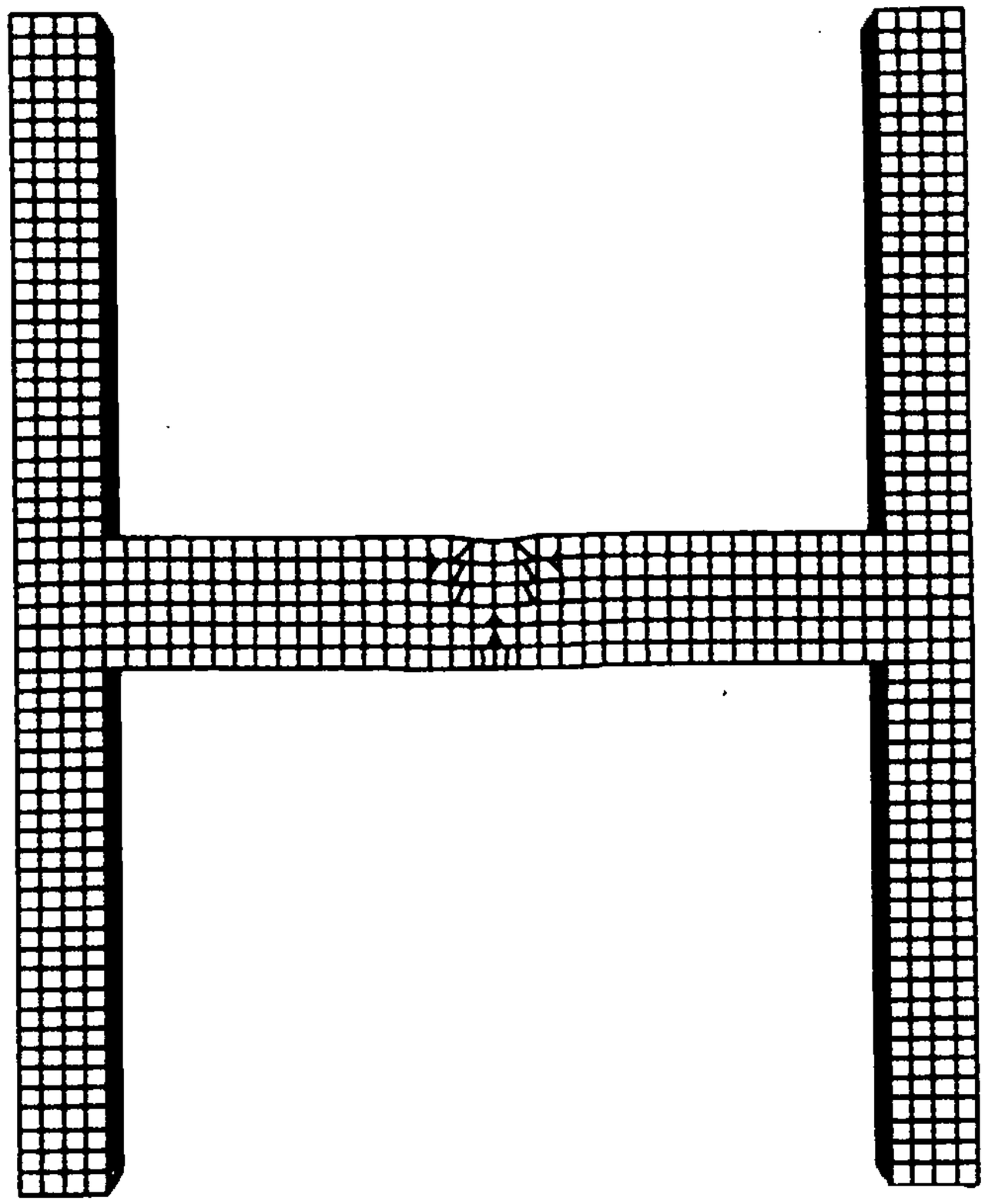

Figure 7.6(b) Predicted deformed shape and crack pattern for the portal frame tested by Watson and Ang [150] at time 0.30970E-02 seconds

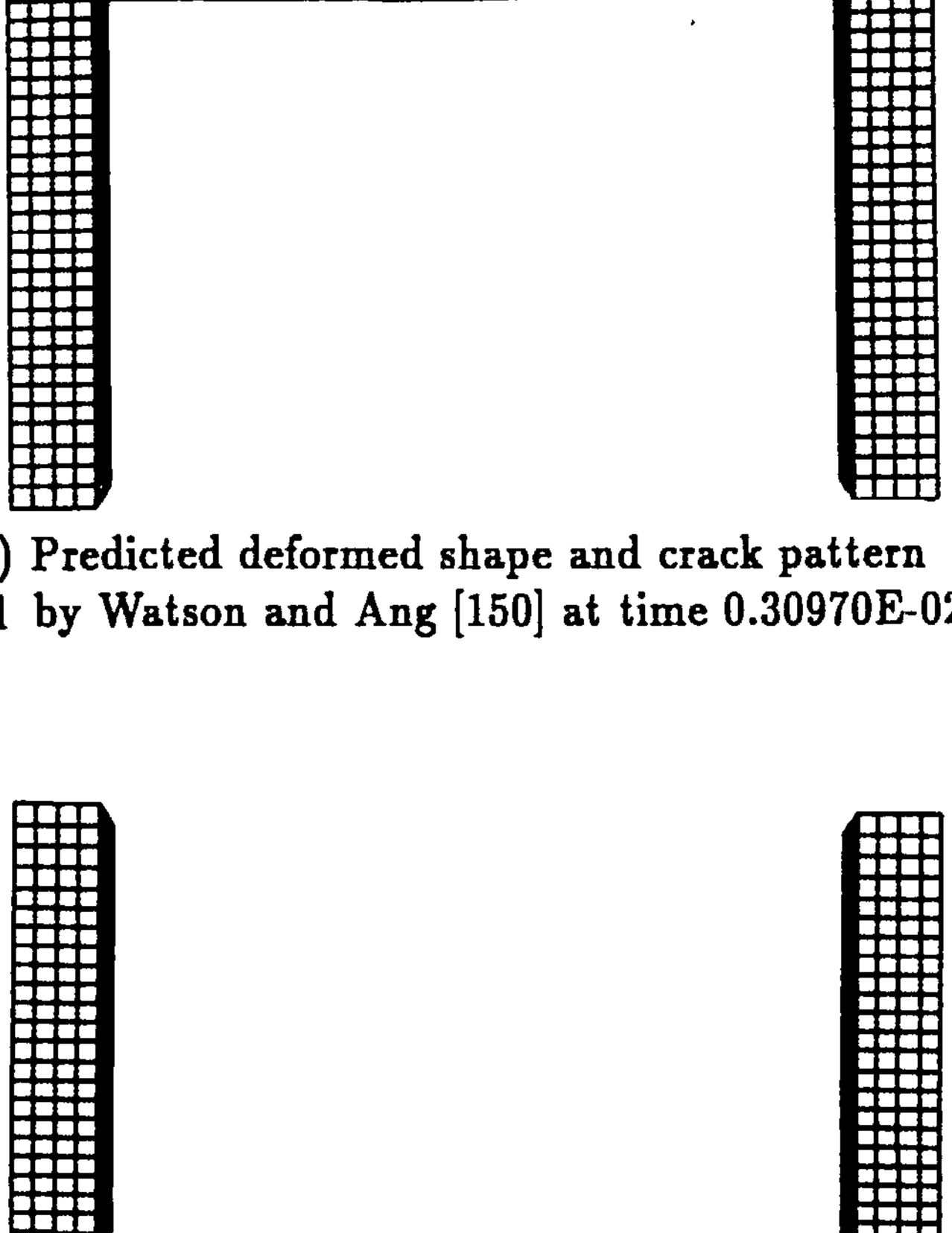

Figure 7.6(c) Predicted deformed shape and crack pattern for the portal frame tested by Watson and Ang [150] at time 0.43341E-02 seconds

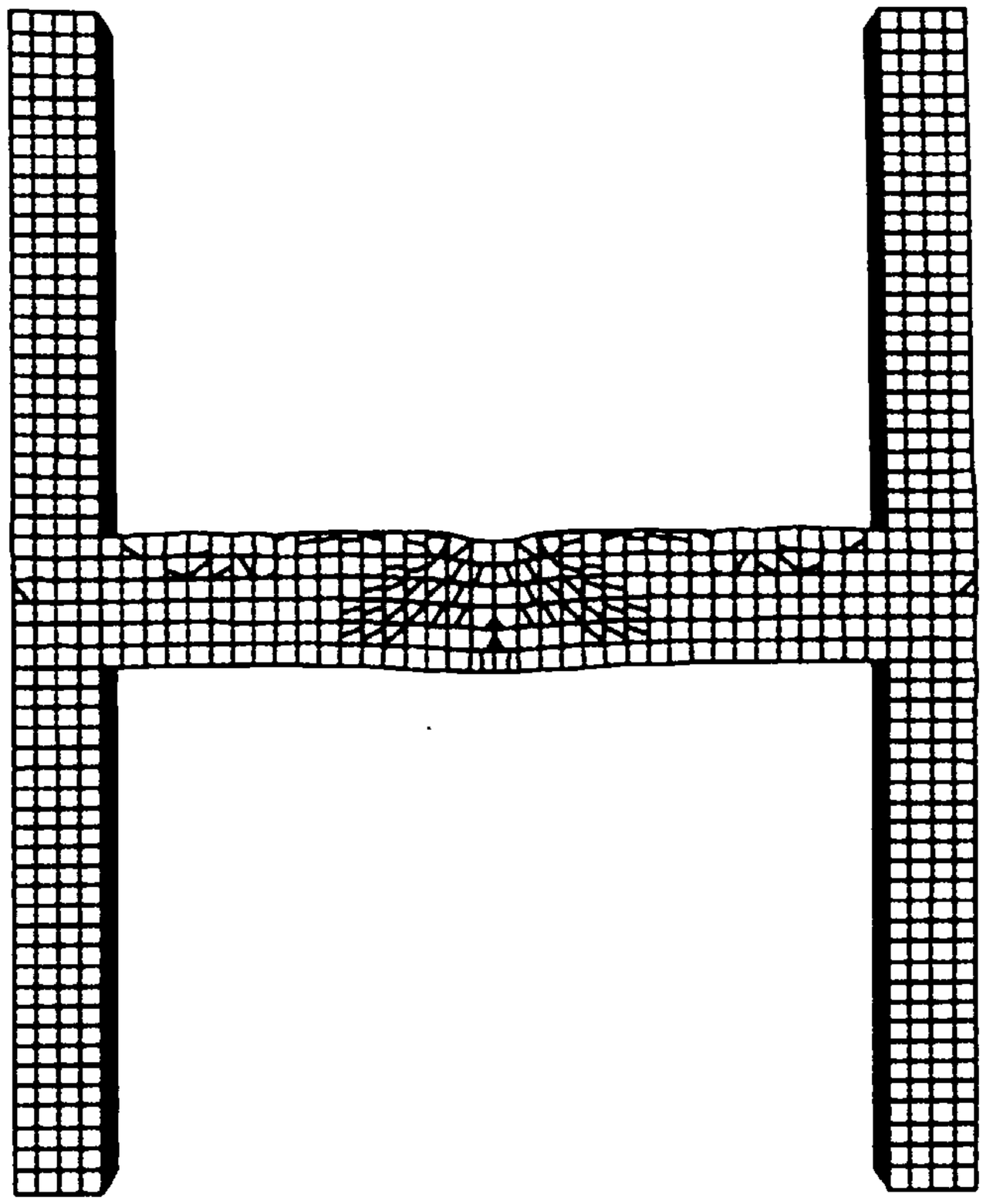

Figure 7.6(d) Predicted deformed shape and crack pattern for the portal frame tested by Watson and Ang [150] at time 0.56168E-02 seconds

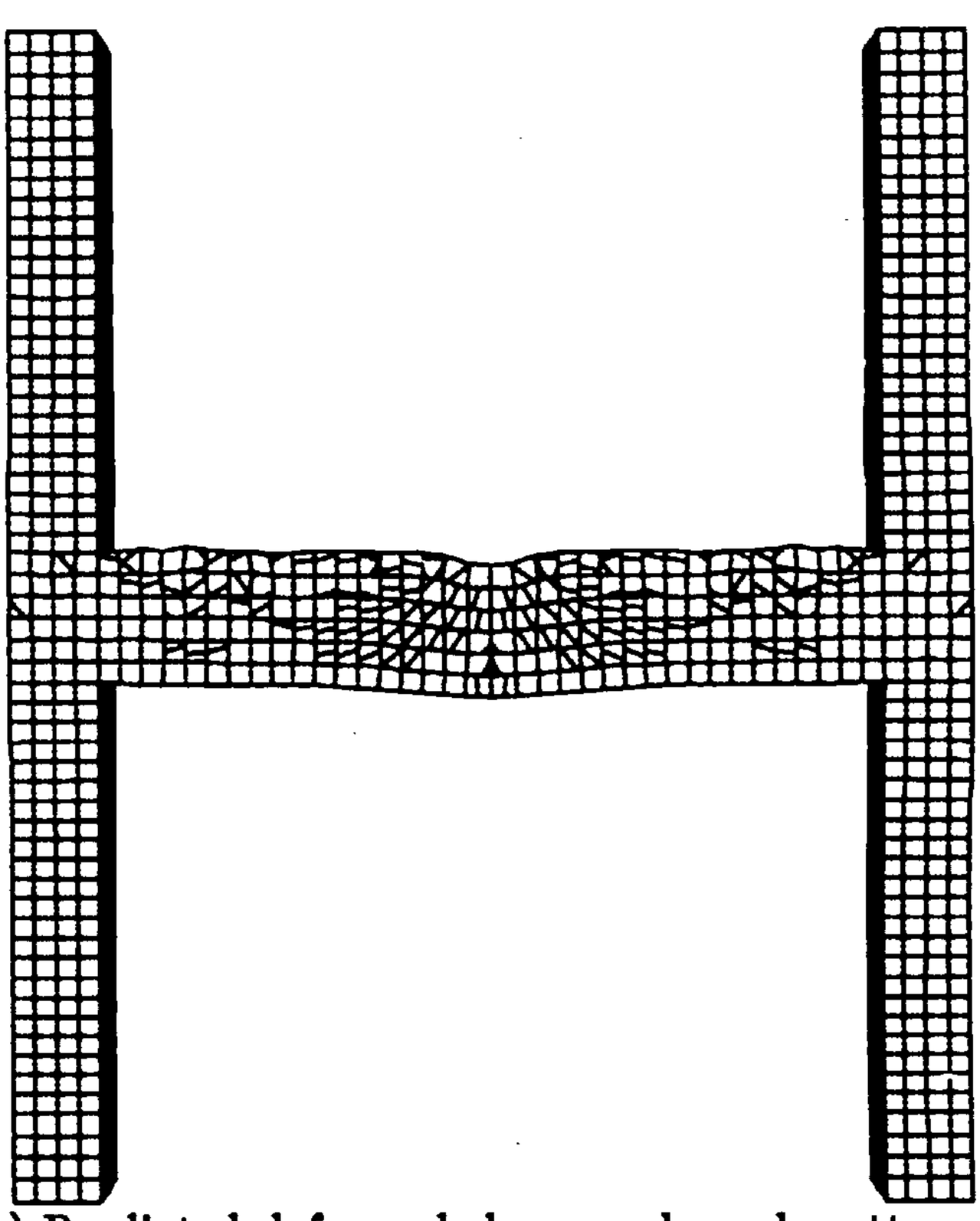

Figure 7.6(e) Predicted deformed shape and crack pattern for the portal frame tested by Watson and Ang [150] at time 0.74765E-02 seconds

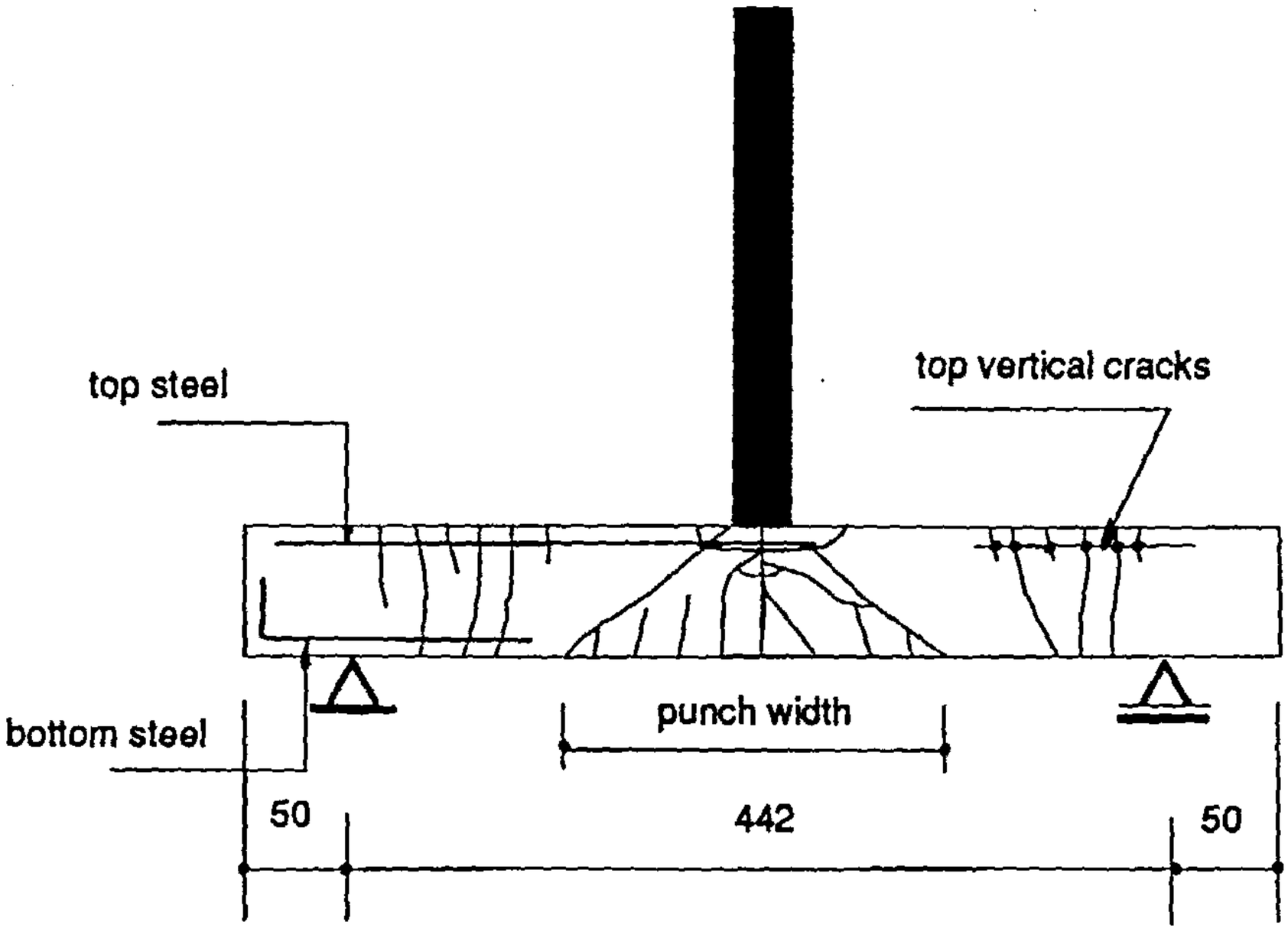

Figure 7.7: Actual crack pattern in the beam tested by Watson and Ang [150]

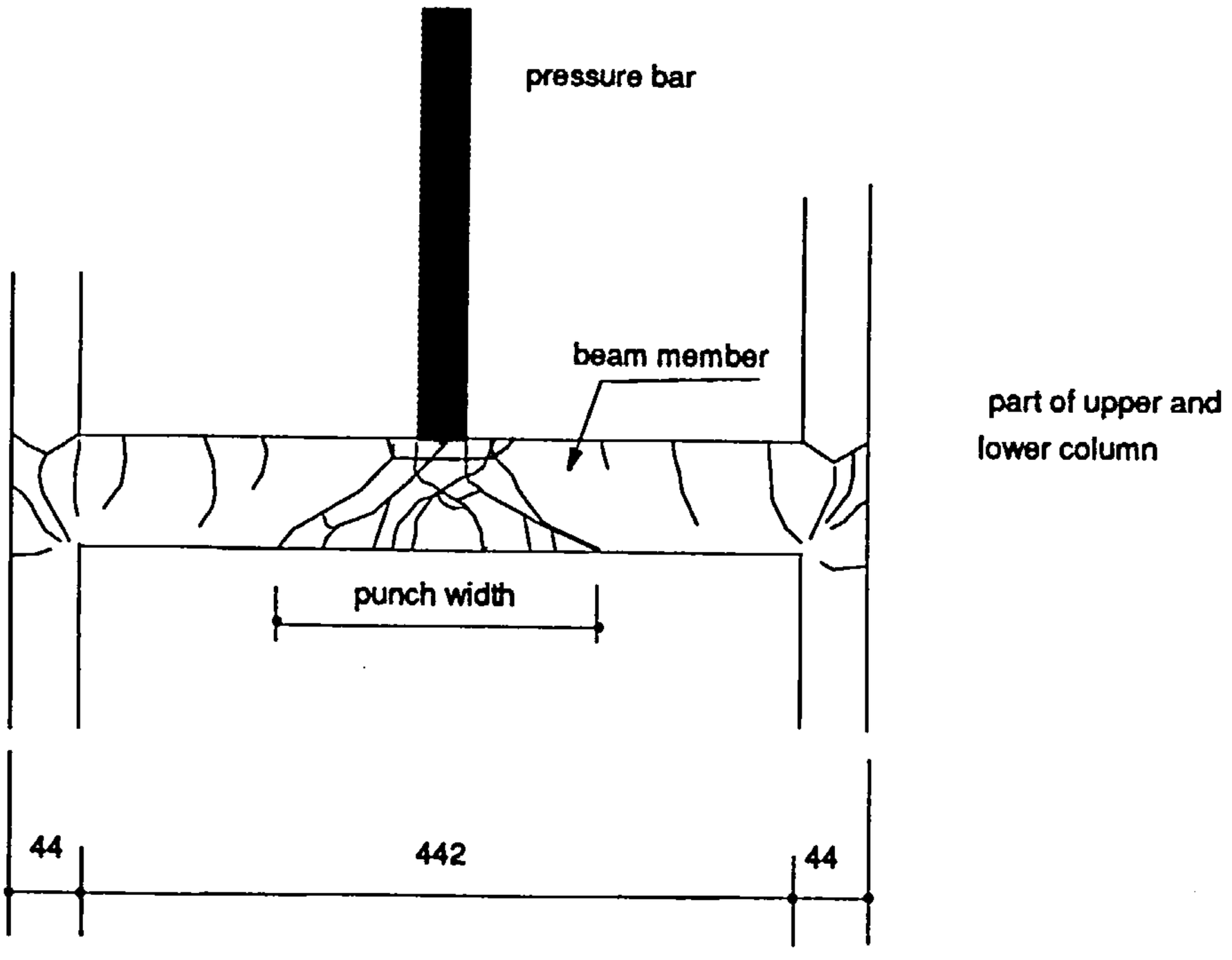

Figure 7.8: Actual crack pattern in the portal frame tested by Watson and Ang [150]

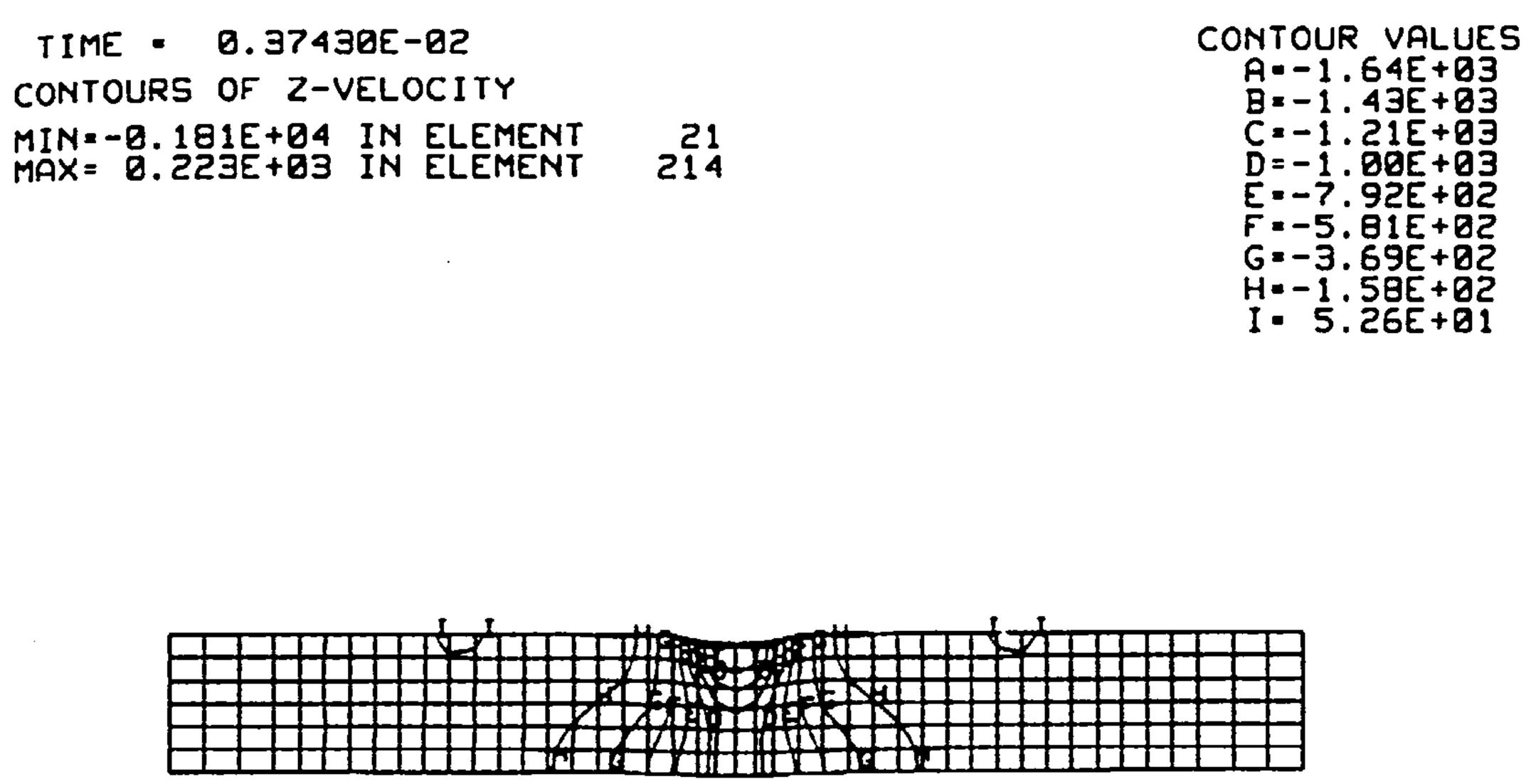

Figure 7.9: Lateral variation in the velocity for the beam tested by Watson and Ang Watson and Ang [150]

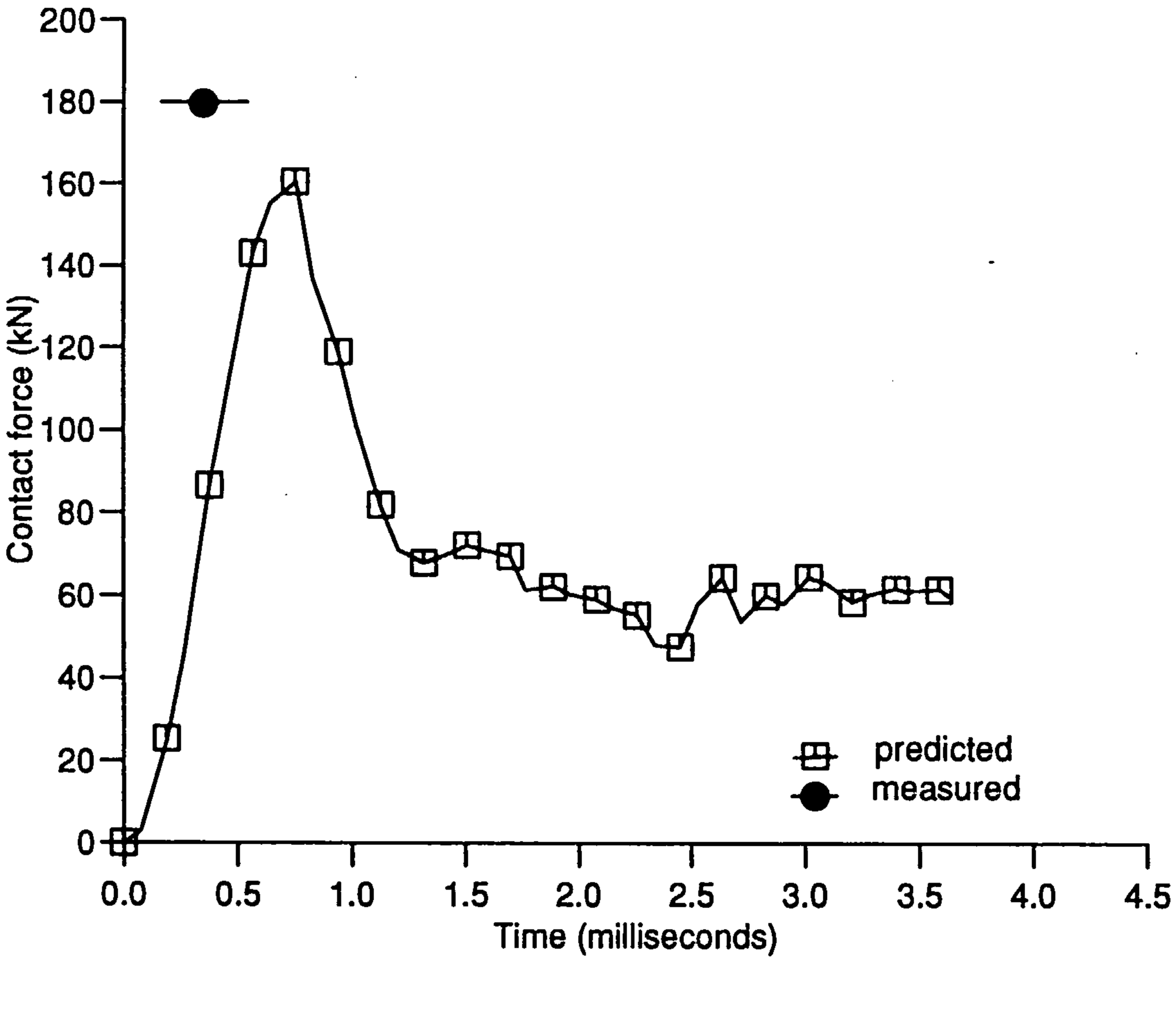

Figure 7.10: Predicted and measured impact force results for the beam tested by Watson and Ang [150]

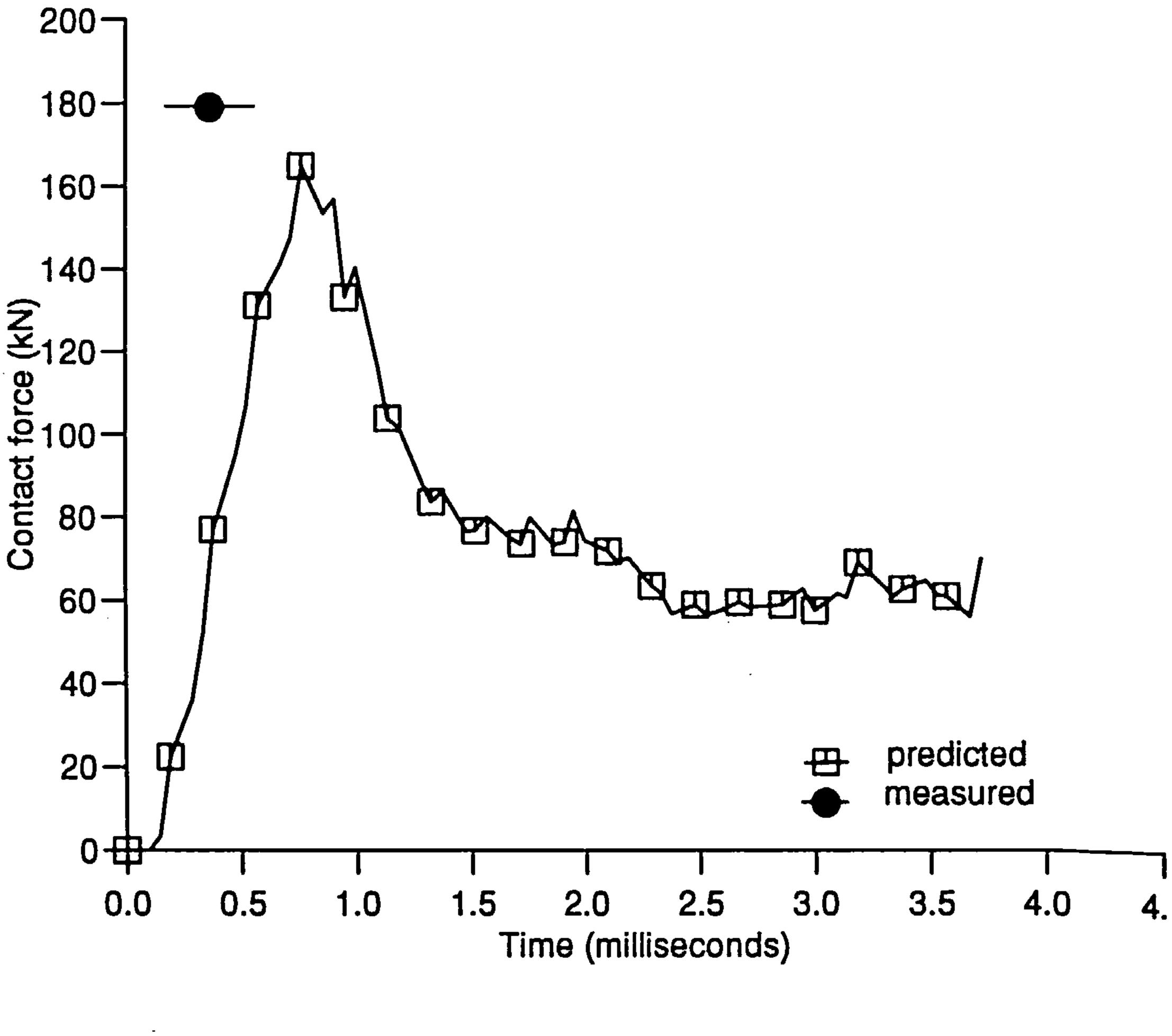

Figure 7.11: Predicted and measured impact force results for the portal frame tested by Watson and Ang [150]

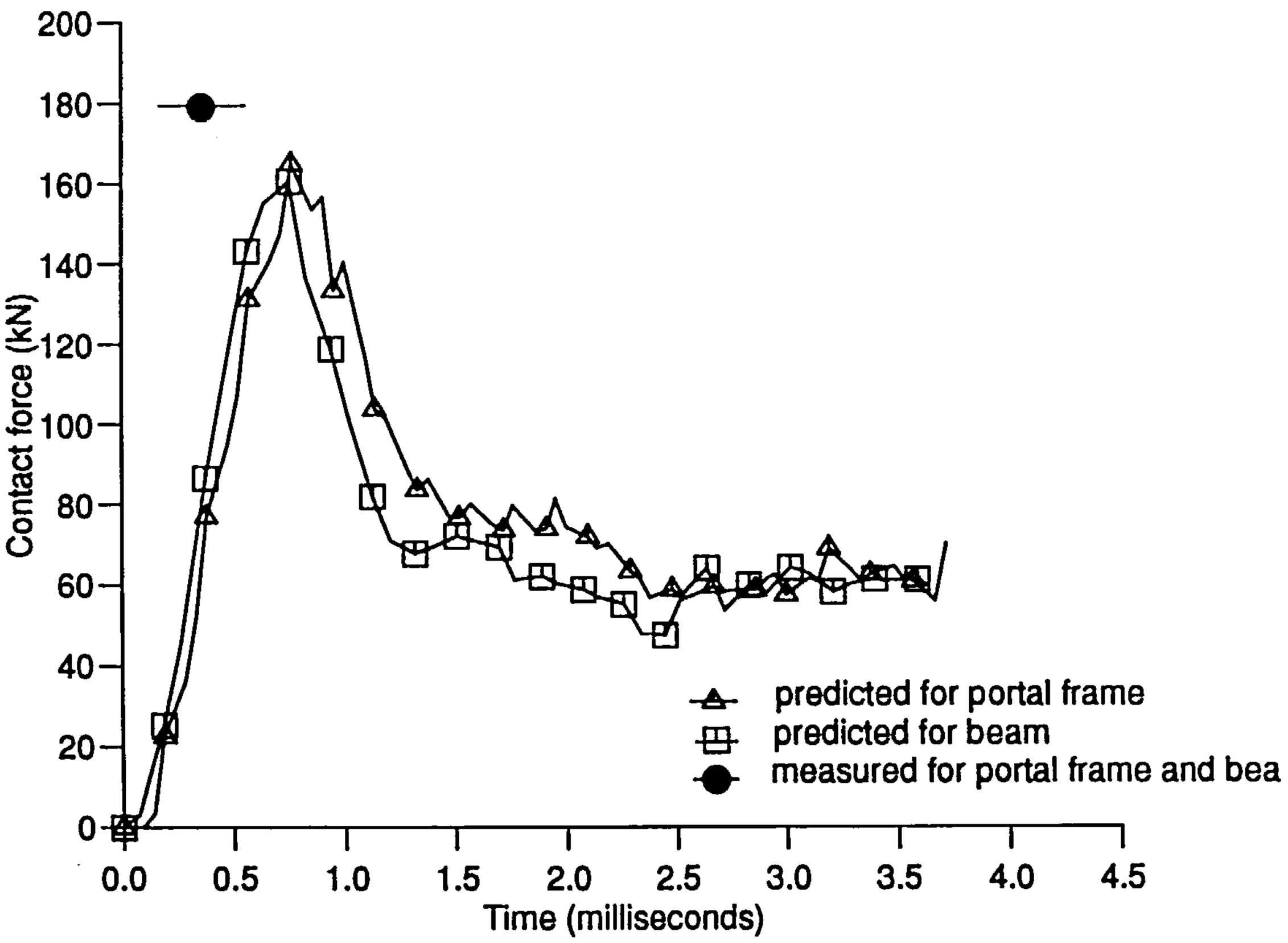

Figure 7.12: Predicted impact force results for the beam and the portal frame tested by Watson and Ang [150]

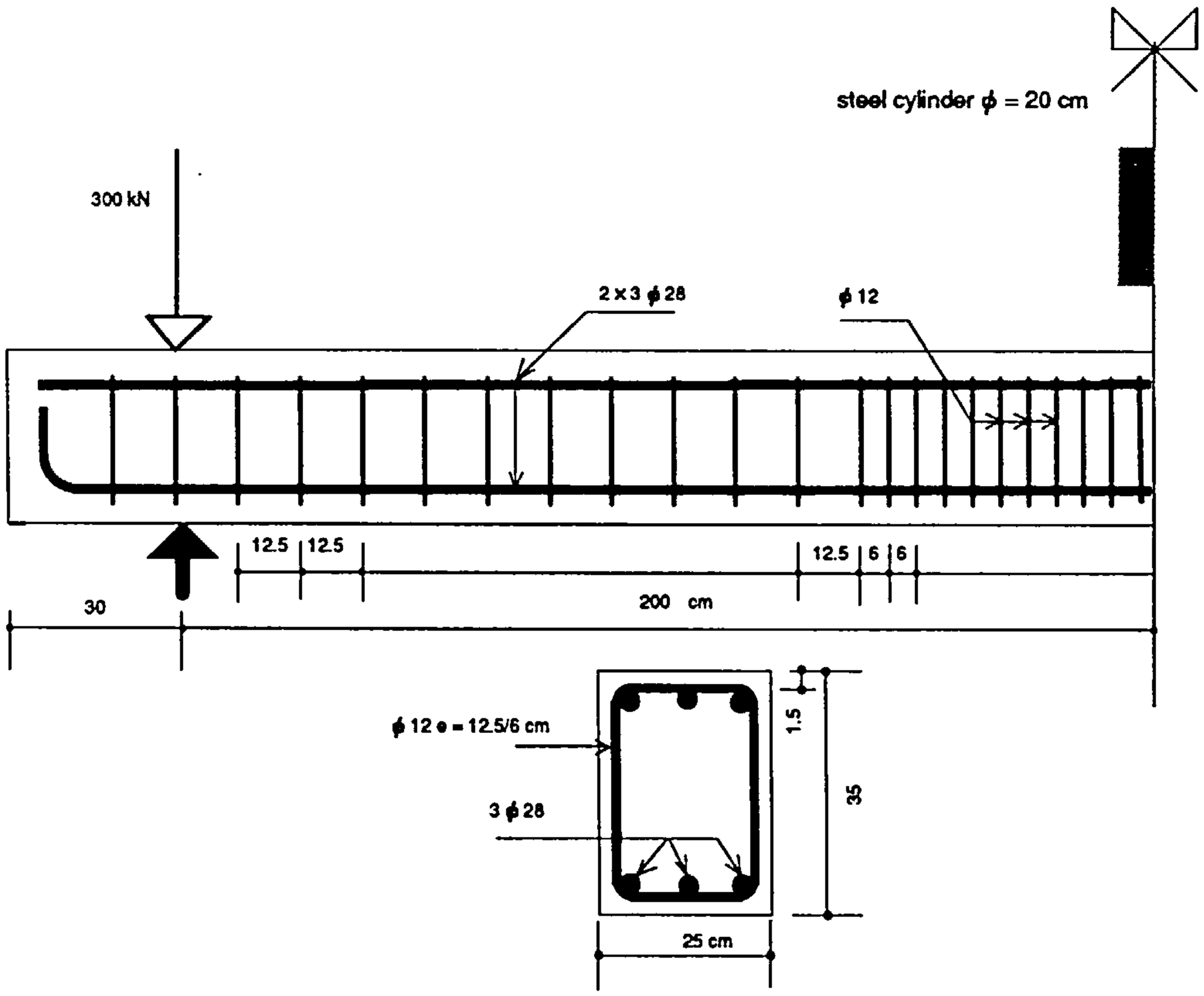

Figure 7.13: Dimensions, reinforcement and loading arrangement for the beam tested by Eibl et al [151]

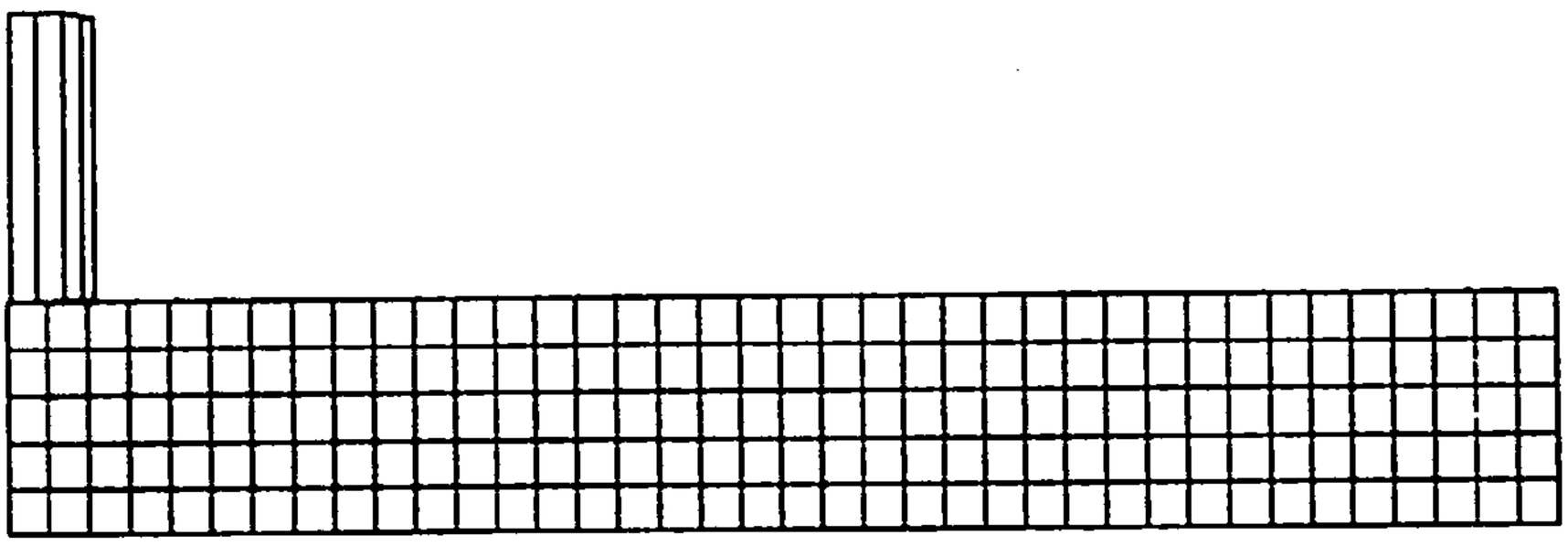

Figure 7.14: Layout of the mesh for the beam tested by Eibl et al [151]

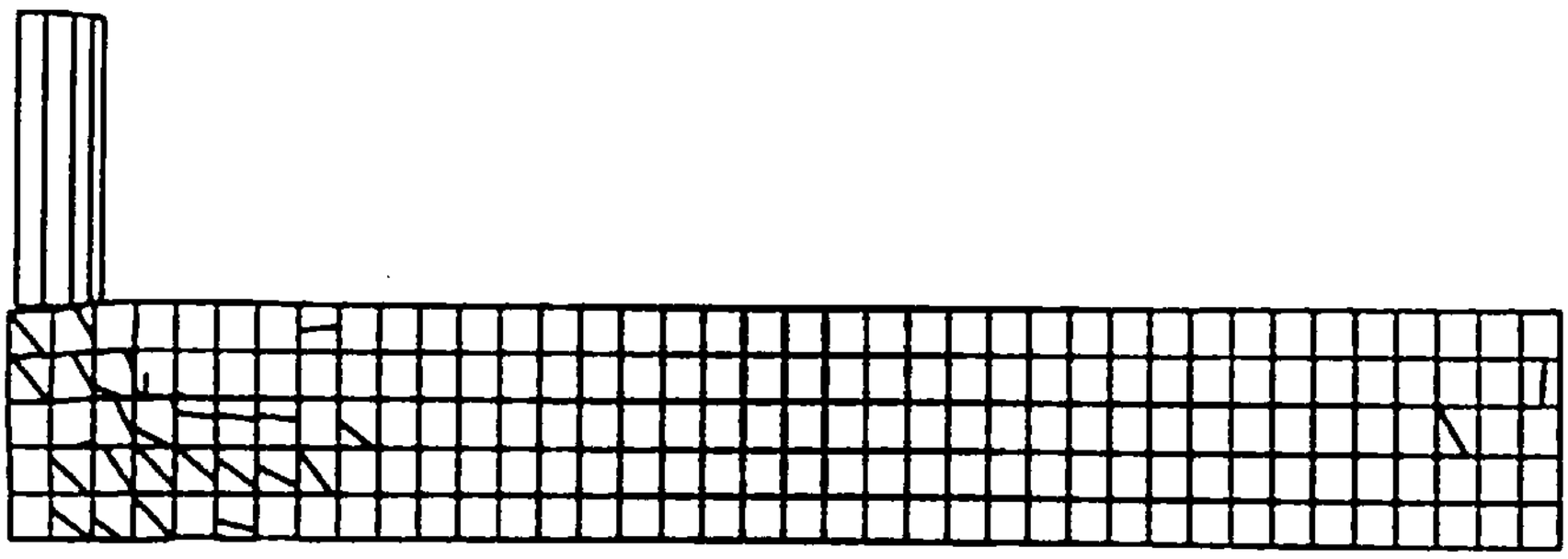

Figure 7.15: (a) Predicted deformed shape and crack pattern for the beam tested by Eibl et al [151] at time 0.93873E-02 seconds

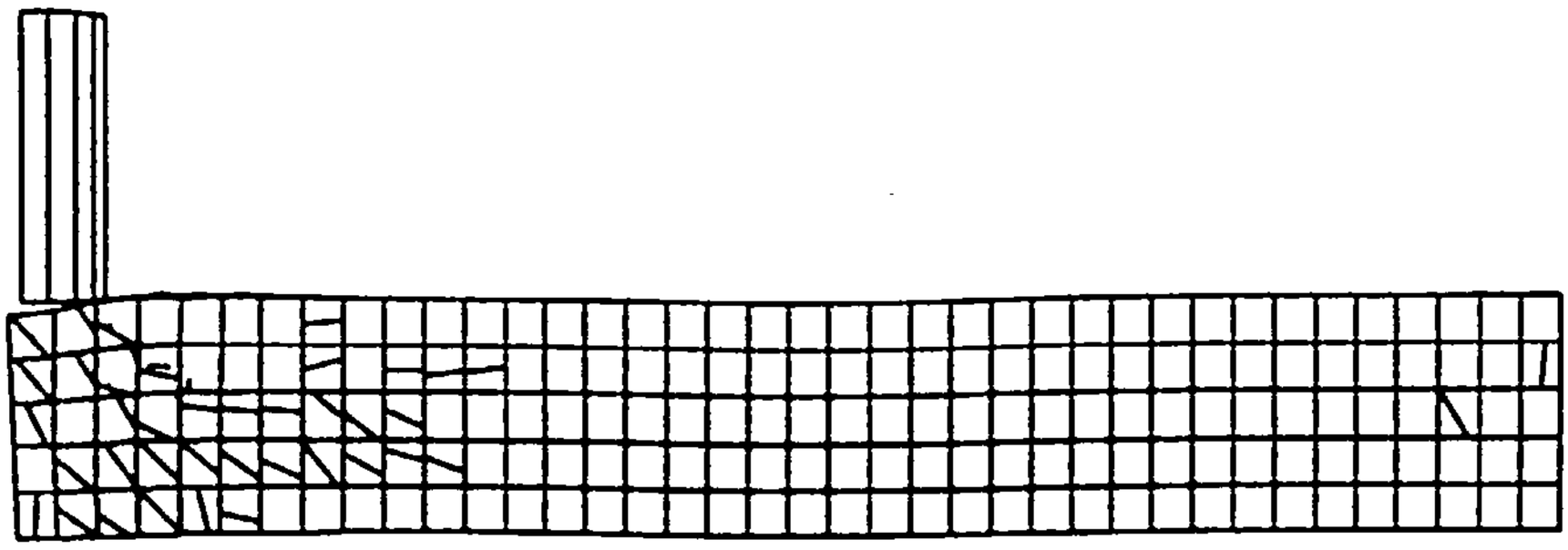

Figure 7.15(b)Predicted deformed shape and crack pattern for the beam tested by Eibl et al [151] at time 0.19325E-01 seconds

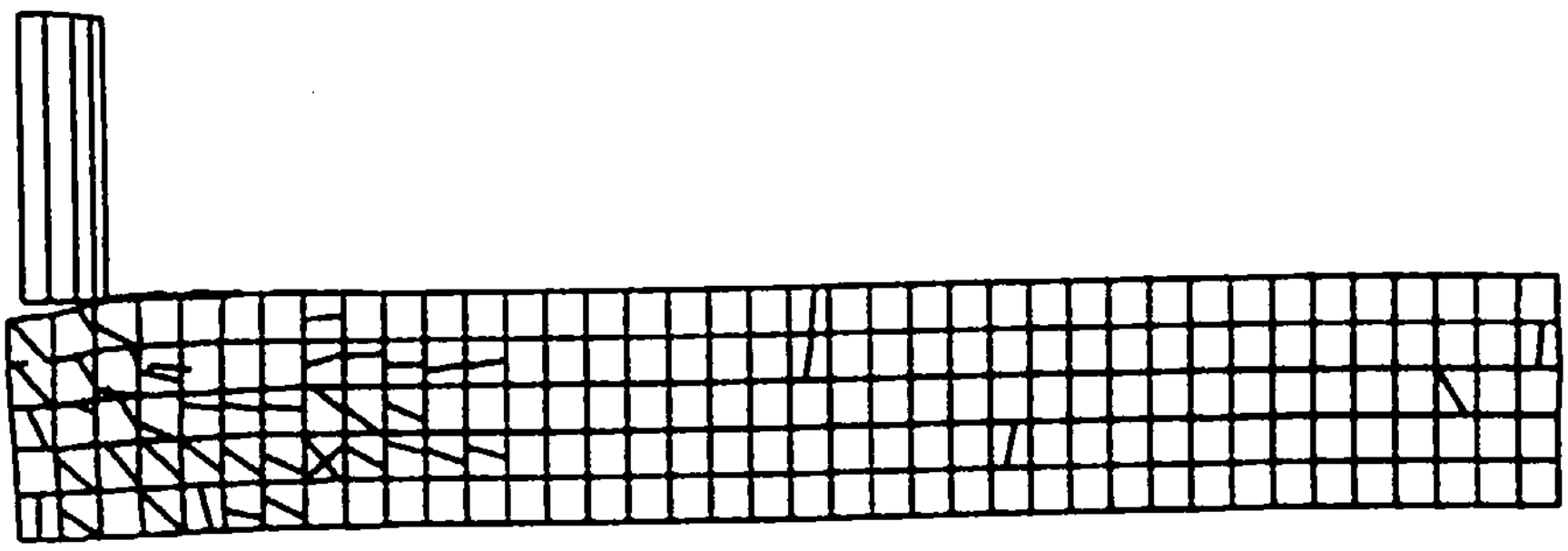

Figure 7.15(c)Predicted deformed shape and crack pattern for the beam tested by Eibl et al [151] at time 0.29314E-01 seconds

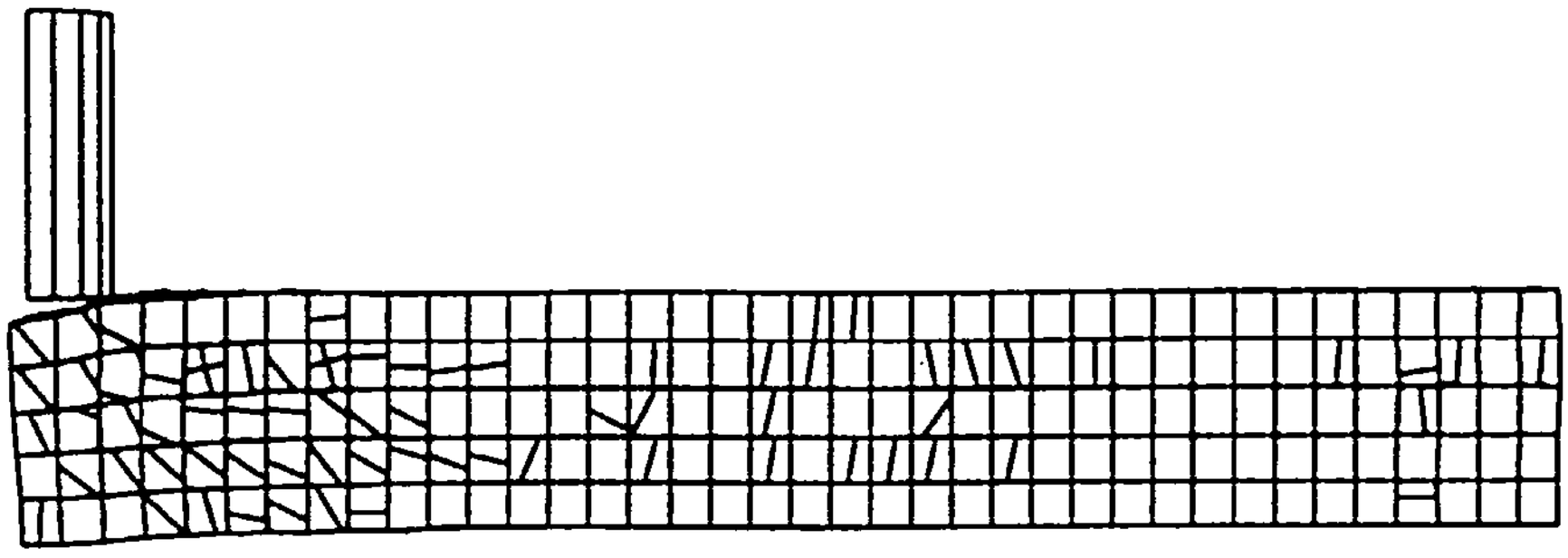

Figure 7.15(d)Predicted deformed shape and crack pattern for the beam tested by Eibl et al [151] at time 0.39158E-01 seconds

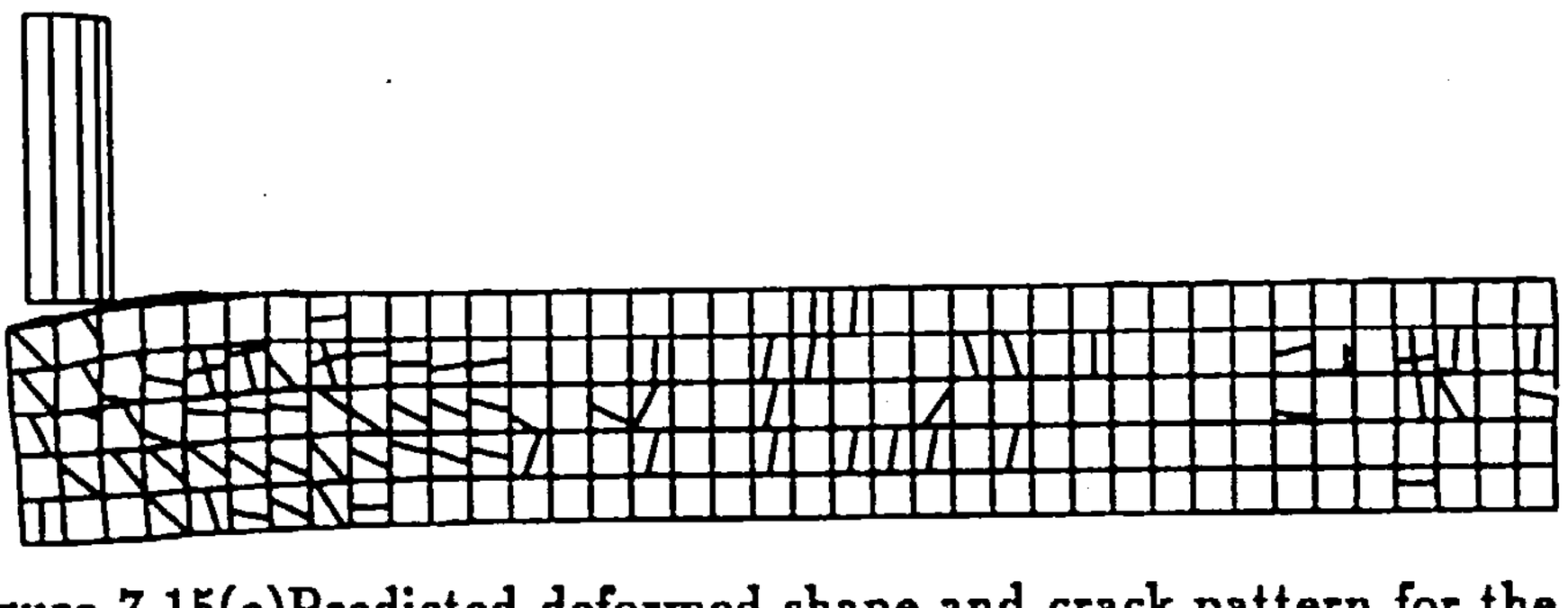

Figure 7.15(e)Predicted deformed shape and crack pattern for the beam tested by Eibl et al [151] at time 0.49297E-01 seconds

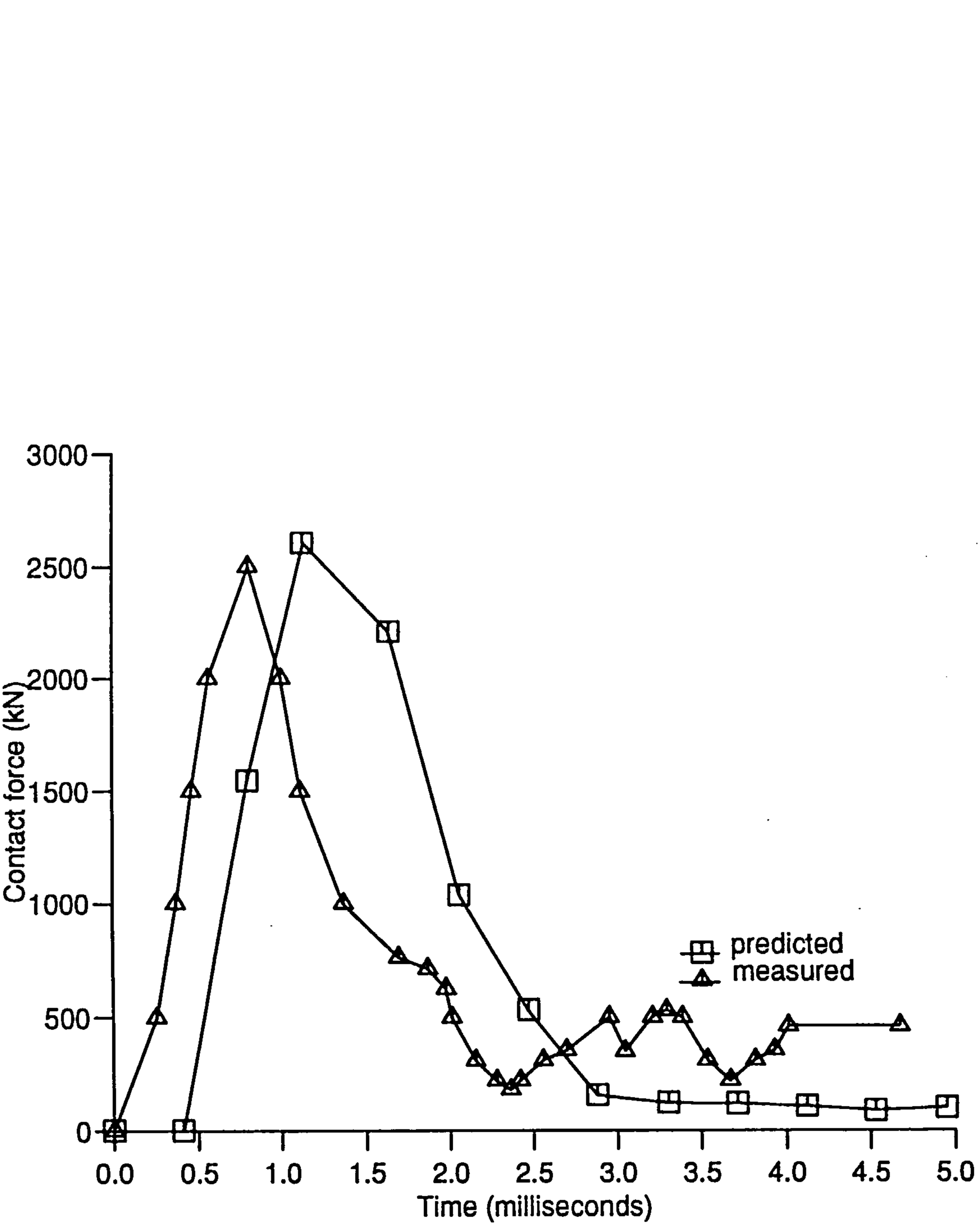

Figure 7.16: Predicted and measured impact force curves for the beam tested by Eibl et al [151]

Chapter 8

CONCLUSIONS AND RECOMMENDATIONS FOR FUTURE WORK

8.1 SUMMARY

A new non-linear concrete model suitable for the three dimensional analysis of structural concrete members subjected to impact loading has been developed. The model has used a triaxial stress formulation which was based on a four parameter failure criterion combined with the incremental theory of plasticity.

In view of the uncertainties associated with the specification of the material properties, a relatively simple constitutive model which is dependent on readily available uniaxial properties has been adopted for concrete.

The stress-strain relationship for concrete in compression has been modelled using an elastic-plastic strain hardening model accompanied by fracture of the material at maximum strength. The direction and magnitude of the plastic straining

is governed by the normality condition of an associated flow rule together with isotropic and kinematic hardening rules. The influence of the rate of loading on the concrete was introduced by modifying the yield and loading surfaces.

In tension, the concrete is assumed to be elastic until cracking takes place. Cracking of the concrete is controlled by the maximum stress criterion. A smeared crack model has been used which has included a tension softening model based on a bilinear approximation of the relationship between the crack normal stress and its width. A model for the reduction in the shear stress of the cracked concrete element has also been included which was based on either a direct reduction in the shear stress or a reduction based on a parabolic relationship between the crack width and the size of the aggregate particles. A maximum of three orthogonal cracks are allowed to form at the sampling points. Closing and reopening of the cracks are permitted in this formulation in order to simulate the occurrence of modal deformations resulting from the vibration of the structural concrete members.

Failure of the concrete is determined using a crushing coefficient which is based on a dual criterion. Three different modes of failure can be identified by the crushing coefficient i.e. cracking, crushing and mixed cracking and crushing modes.

The reinforcing bars are represented as tensile stiffeners which are smeared over

the entire cross section of the element in the appropriate directions. Perfect bonding is assumed between the concrete and the reinforcing bars.

The reinforced concrete formulation described above was written in FORTRAN and incorporated into the finite element source code DYNA3D.

In order to examine and demonstrate the capability of the program in the analysis of structural concrete members a number of plain and reinforced concrete members, from previously published laboratory test programmes, which had been subjected to static and impact loadings have been analysed. The concrete members which have been analysed included:

(1) Two plain concrete test specimens (cylinders) which had been subjected to static and impact compressive loadings.

(2) Two eighth scale reinforced micro-concrete members i.e. a simply supported beam and a portal frame which had been subjected to impact loadings.

(3) A full size clamped reinforced concrete beam subjected to impact loading.

The results obtained using the newly developed concrete model were compared with the published results obtained from the laboratory based test programmes.

8.2 CONCLUSIONS

The following conclusions can be drawn from the results obtained from the numerical analysis described in the previous Chapters:

PLAIN CONCRETE

(1) The new concrete model developed in this investigation has been used successfully to predict the behaviour observed in the laboratory tests on plain concrete test specimens subjected to static and impact compressive loadings.

(2) The predicted stress-strain curve for static loading was found to be in good agreement with the stress-strain curve obtained from the laboratory tests. The predicted impact stress-strain curves for plain concrete were found to be in good agreement with those obtained from the laboratory tests up to a specific stress level i.e. on average 80 percent of the maximum strength for the two test specimens examined.

(3) The agreement between the computed and laboratory test results in terms of the stress values was not as good as it was for the values of strain after the maximum strength had been reached. The laboratory test results have

shown that after the maximum stress had been reached the concrete continues to deform under a constant stress up to failure, whereas in the computed results the stress drops off as soon as the maximum stress is reached. This form of behaviour can be explained in terms of the post-cracking behaviour implemented in the new concrete model.

REINFORCED CONCRETE MEMBERS

(1) The new reinforced concrete model which has been developed was found to be able to predict the overall behaviour and the principal failure mechanisms observed in the laboratory tests on reinforced concrete members subjected to impact loadings. The localised behaviour of the structural concrete members was successfully simulated i.e. the formation of the crater at the contact surface and the development of a number of flexural cracks concentrated under the impact load which result in the formation of the concrete plug. The global behaviour of the member was also successfully simulated including the different modes of deformation i.e. the formation of flexural cracks at the upper surface of the beams and the closing and reopening of cracks in general.

(2) In the analysis of eighth scale reinforced concrete members, the results obtained from the finite element solutions were found to agree, to a reasonable degree of accuracy, with the results from laboratory tests. In particular, reasonable agreement was found with respect to the impact load-time histories, the maximum deflection at mid span and the distribution of cracks

under the impact load. However, the prediction of the global deformations associated with the higher modes of deformation was not as good as the corresponding values for the first mode of deformation.

(3) The finite element solutions obtained for the full size reinforced concrete member were found to be more accurate than the solutions obtained from the eighth scale reinforced micro-concrete members. All the mechanisms which are normally found in tests on beams were predicted, including the formation of the crater and the concrete plug, and the resulting global deformations. In addition the maximum residual deformation and impact forces were in reasonable agreement with the values obtained in the laboratory test on the beam.

The predicted distribution of the cracks largely agreed with the majority of the cracks normally found in laboratory tests on beams, particularly the formation of the concrete plug cracks and the flexural cracks at the upper surface of the beam. The closing and re-opening of these flexural cracks indicates that the beam had experienced several modes of global deformation.

8.3 RECOMMENDATIONS FOR FUTURE WORK

This investigation has highlighted the following areas which are in need of further study:

(1) The enhancement of the new concrete model to account for rate effects in the form of strain rate dependent potential functions. This can be achieved as follows:

- The development of plastic behaviour using non-associated potential functions so that tensile and compressive stress conditions are separated.
- The potential functions should relate the strain rate to the corresponding stress. They can be derived from a survey of the available published work or by simply using those reported by the CEB Task Group [1].

(2) Improvements in the modelling of the behaviour of the reinforcing bars can be achieved by including strain rate effects and the effect of bond slip between the reinforcing bars and the concrete.

(3) Improvements in the cracking model can be achieved by using non-orthogonal crack representations.

(4) Additional laboratory tests are required, particularly investigations into the influence of rate effects on concrete subjected to uniaxial and multiaxial

stress conditions in order that the failure criteria which have been developed can be modified to account for strain rate effects on concrete.

(5) A laboratory based investigation is required to examine the influence of loading rate on bond forces between concrete and reinforcing bars.

Appendix A

GEOMETRICAL CONSIDERATIONS

A failure criterion for an initially isotropic and homogeneous material can be expressed in terms of the principal stresses σ_1, σ_2, and σ_3 as follows:

$$f(\sigma_1, \sigma_2, \sigma_3) = 0 \tag{A.1}$$

If Equation A.1 is to be used as a general criterion, it needs to be associated with three symmetric invariants of the stress tensor i.e. Equation A.1 may take the following form:

$$f(I_1, I_2, I_3) = 0 \tag{A.2}$$

where

$I_1 = \sigma_1 + \sigma_2 + \sigma_3$ is the first stress invariant.

$I_2 = 0.5(\sigma_1^2 + \sigma_2^2 + \sigma_3^2)$ is the second stress invariant.

$I_3 = \frac{1}{3}(\sigma_1^3 + \sigma_2^3 + \sigma_3^3)$ is the third stress invariant.

It is possible to decompose these three stress invariants relationships into combined invariant relationships in the stress space which have the following geometrical interpretations:

The principal stress deviators are:

$$s_i = \sigma_i - \frac{1}{3}I_1 \qquad \text{where } (i = 1, 2, 3).$$

The three symmetric invariant relationships of the deviatoric stress tensor are:

$$\begin{aligned} J_1 &= s_1 + s_2 + s_3 = 0 \\ J_2 &= \frac{1}{2}(s_1^2 + s_2^2 + s_3^2) \\ &= \frac{1}{6}((\sigma_1 - \sigma_2)^2 + (\sigma_2 - \sigma_3)^2 + (\sigma_1 - \sigma_3)^2) \\ J_3 &= \frac{1}{3}(s_1^3 + s_2^3 + s_3^3) \end{aligned} \tag{A.3}$$

A failure criterion can be interpreted as a surface in the cartesian coordinate system shown in Figure A.1, where the axes are σ_1, σ_2, and σ_3.

The diagonal d which is equidistant from the three axes, is determined by a unit vector $\vec{e} = \frac{1}{\sqrt{3}}(1, 1, 1)$. Every point on the diagonal d is characterized by $\sigma_1 = \sigma_2 = \sigma_3$, which corresponds to a hydrostatic stress state with the deviatoric stresses being equal to zero. The diagonal d is called the hydrostatic axis.

Consider an arbitrary point $P(\sigma_1, \sigma_2, \sigma_3)$ in Figure A.1. The point P is determined by the vector $\vec{OP}$. This vector may be decomposed into two components. The first component $\vec{ON}$ is along the hydrostatic axis and the second component

$\vec{NP}$ is in the plane perpendicular to the hydrostatic axes.

The length of $\vec{ON}$ is given by:

$$|\vec{ON}| = \xi = \vec{OP}\vec{e} = (\sigma_1, \sigma_2, \sigma_3)[1,1,1]^T = \frac{1}{\sqrt{3}} I_1$$

The components of $\vec{ON}$ i.e. the projection of the vector $\vec{ON}$ on the three axes are given by:

$$\vec{ON} = \frac{I_1}{3}(1,1,1)$$

The components of $\vec{NP}$ are determined by:

$$\vec{NP} = \vec{OP} - \vec{ON} = (\sigma_1, \sigma_2, \sigma_3) - \frac{I_1}{3}(1,1,1) = (s_1, s_2, s_3)$$

The squared length of $\vec{NP}$ is:

$$|\vec{NP}|^2 = \rho^2 = s_1^2 + s_2^2 + s_3^2 = 2J_2$$

and thus:

$$\rho = \sqrt{2J_2} \qquad (\rho \geq 0)$$

It can be noted that $\vec{ON}$ defines the hydrostatic part of the stresses present at the point P. $\vec{NP}$ defines the deviatoric part of the stresses at that point. The plane perpendicular to the hydrostatic axis is called the deviatoric plane.

Since the hydrostatic stress invariant (I_1) and the second deviatoric stress invariant (J_2) have been given a geometrical interpretation, it is convenient to use them in defining the general failure criterion. Thus, Equation A.2 becomes

$$f(I_1, J_2, J_3) = 0 \qquad \text{(A.4)}$$

To obtain a geometrical interpretation of the invariant J_3, the deviatoric plane is considered as shown in Figure A.2. The projections of the cartesian coordinates σ_1, σ_2 and σ_3 intersect the deviatoric plane and make equal angles i.e. 120^0. The angle θ shown in Figure A.2 is measured from the positive σ_1-axis and situated in the deviatoric plane. The unit vector $\vec{i}$, along the projection of σ_1 on the deviatoric plane, is determined by:

$$\vec{i} = \frac{1}{\sqrt{6}}(2, -1, -1)$$

Thus:

$$\vec{NP} \cdot \vec{i} = \rho cos(\theta),$$

i.e. $$\cos(\theta) = \frac{1}{\sqrt{2J_2}}(s_1, s_2, s_3)\frac{1}{\sqrt{6}}[2 - 1 - 1]^T = \frac{1}{2\sqrt{3}\sqrt{J_2}}(2s_1 - s_2 - s_3)$$

By using the equations given by the deviatoric invariant such as $s_2 + s_3 = -s_1$, it follows that:

$$cos(\theta) = \frac{\sqrt{3}s_1}{2\sqrt{J_2}} = \frac{2\sigma_1 - \sigma_2 - \sigma_3}{2\sqrt{3}\sqrt{J_2}}$$

If $\sigma_1 \geq \sigma_2 \geq \sigma_3$, then $$0 \leq \theta \leq 60^0$$

Using the trigonometric identity $cos(3\theta) = 4cos^3(\theta) - 3cos(\theta)$, the following relationship is obtained i.e.

$$cos(3\theta) = \frac{3\sqrt{3}}{2}\frac{J_3}{J_2^{3/2}}$$

where $cos(3\theta)$ is also an invariant. The failure surface given by Equation A.4 is identical to:

$$f(I_1, J_2, cos(3\theta)) = 0 \qquad \text{(A.5)}$$

where the invariant variables have been given a geometrical meaning.

A physical meaning also exists for I_1 and J_2. The octahedral normal stress (σ_{oct}) is related to I_1, while the squared value of the octahedral shear stress (τ_{oct}) is a function of J_2.

$$\sigma_{oct} = \frac{1}{\sqrt{3}} I_1$$

$$\tau_{oct} = \sqrt{2/3} J_2$$

σ_{oct} and τ_{oct} are the stresses which act in planes which make equal angles with the principal stress directions.

The invariants of the strain tensor can also be calculated as follows:

$I'_1 = \epsilon_1 + \epsilon_2 + \epsilon_3$ is the first strain invariant.

$I'_2 = 0.5(\epsilon_1^2 + \epsilon_2^2 + \epsilon\_3^2)$ is the second strain invariant.

$I_{3'} = \frac{1}{3}(\epsilon_1^3 + \epsilon_2^3 + \epsilon_3^3)$ is the third strain invariant.

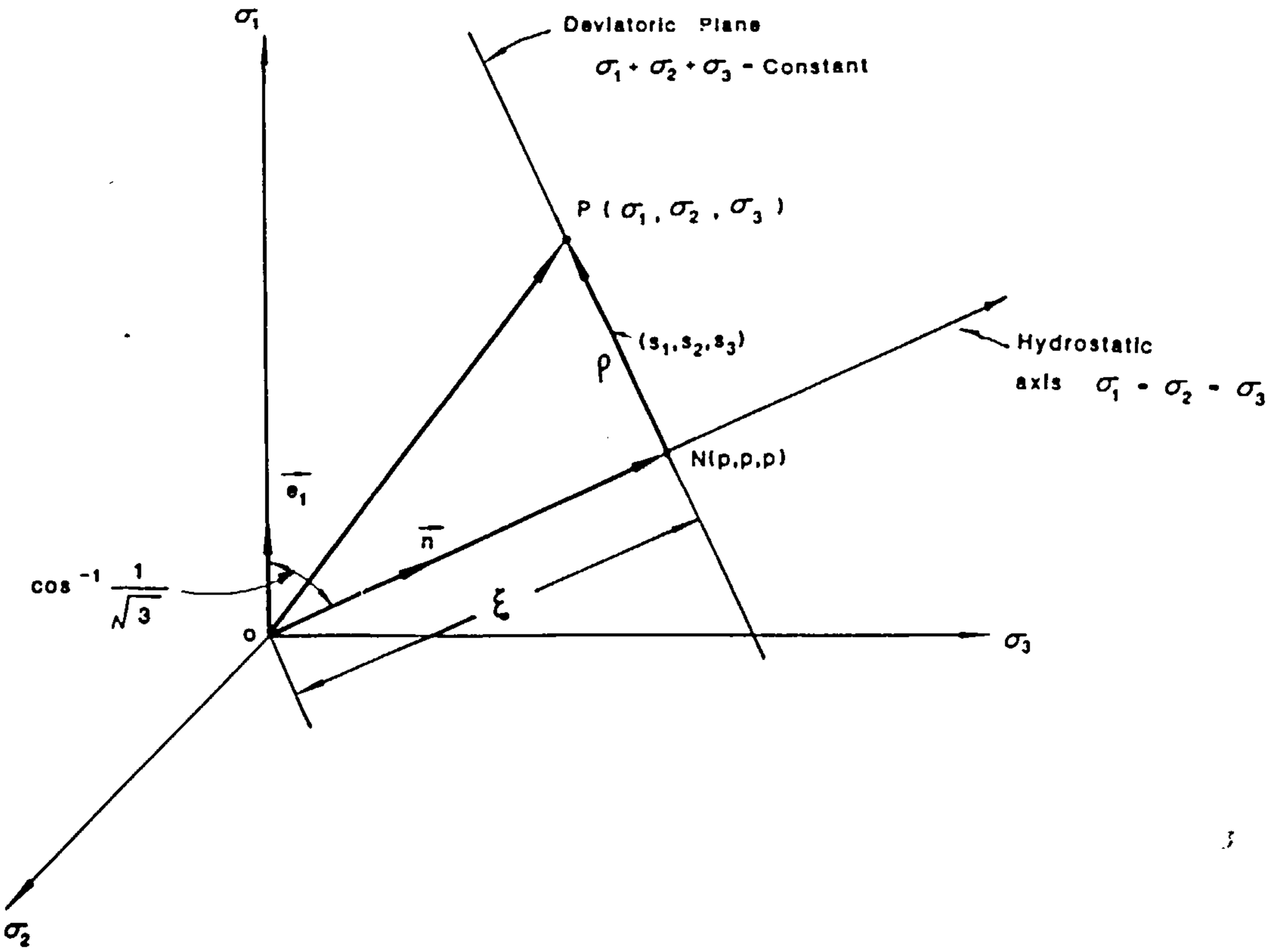

Figure A.1: Haigh-Westergarrd coordinate system

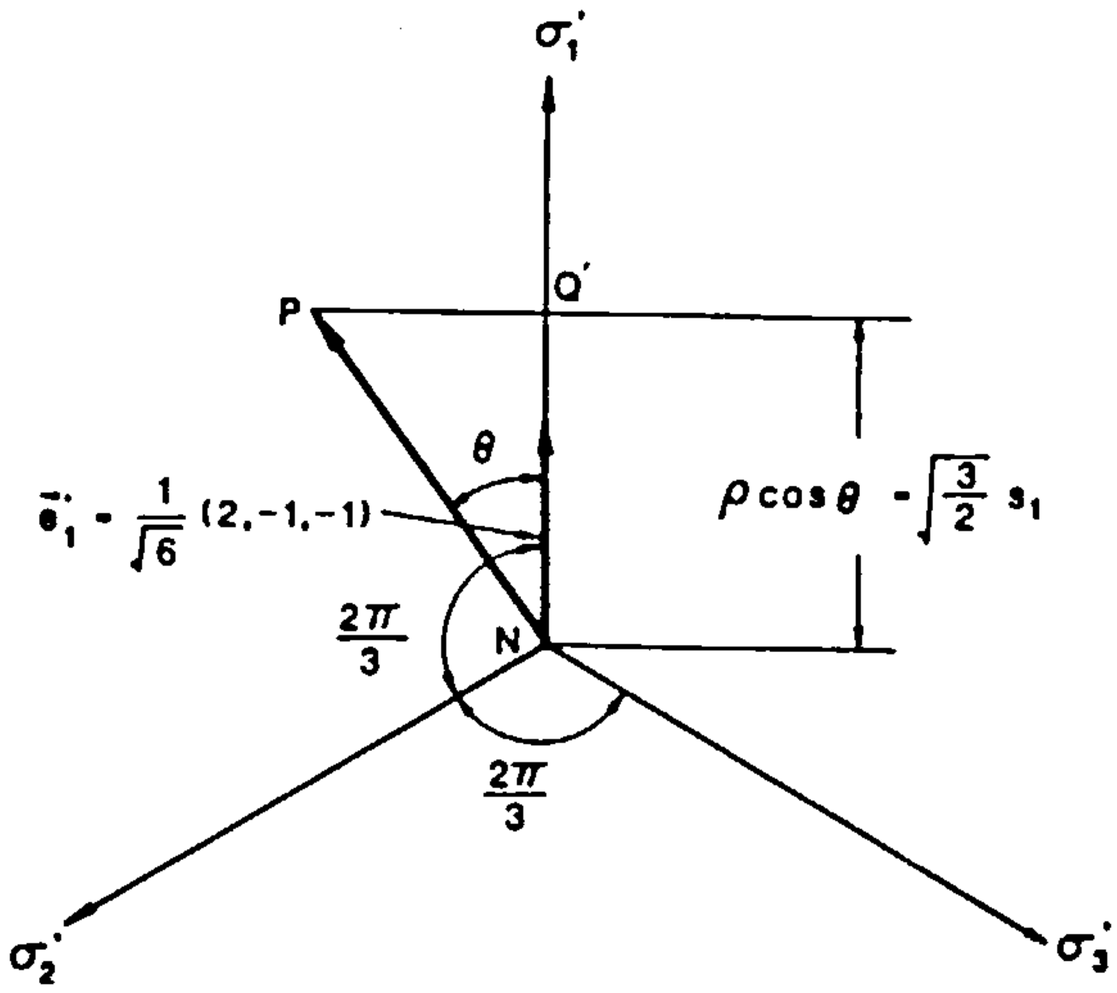

Figure A.2: Deviatoric plane

Appendix B

DERIVATION OF THE PLASTIC STIFFNESS MATRIX

The elastic-plastic stress increment relationships are given by:

$$\sigma = (D^E + D^P)d\varepsilon \tag{B.1}$$

where σ and $d\varepsilon$ are the stress and strain vectors respectively and are given by:

$$\sigma = \{\sigma_x, \sigma_y, \sigma_z, \sigma_{xy}, \sigma_{yz}, \sigma_{zx}\}^T \tag{B.2}$$

$$d\varepsilon = \{d\varepsilon_x, d\varepsilon_y, d\varepsilon_z, d\varepsilon_{xy}, d\varepsilon_{yz}, d\varepsilon_{zx}\}^T \tag{B.3}$$

D^E and D^P in Equation B.1 are the elastic and plastic elemental stiffness matrices. They are defined explicitly in the following Sections.

B.1 Elemental Elastic Stiffness Matrix

In the case of initially isotropic material, before yielding or cracking the stress and strain are related linearly by the expression below:

$$D^E = \begin{bmatrix} K+\frac{4}{3}G & K-\frac{2}{3}G & K-\frac{2}{3}G & 0 & 0 & 0 \\ K-\frac{2}{3}G & K+\frac{4}{3}G & K-\frac{2}{3}G & 0 & 0 & 0 \\ K-\frac{2}{3}G & K-\frac{2}{3}G & K+\frac{4}{3}G & 0 & 0 & 0 \\ 0 & 0 & 0 & G & 0 & 0 \\ 0 & 0 & 0 & 0 & G & 0 \\ 0 & 0 & 0 & 0 & 0 & G \end{bmatrix}$$

where

$$K = \frac{E}{3(1-2\nu)}$$
$$G = \frac{E}{2(1+\nu)}$$

E is Young's modulus and ν Poisson's ratio.

B.2 Elemental Plastic Stiffness Matrix

The components of the plastic stiffness matrix D^P are functions of the type of failure criterion and hardening laws. This investigation uses the associated flow rule to determine the plastic strain increment, where the potential function, g, is assumed to be the same as the yield or the loading functions, f. In the case of the above conditions the plastic stiffness matrix is given by:

$$D^P = -\frac{D^E\{\frac{\partial f}{\partial \sigma}\}\{\frac{\partial f}{\partial \sigma}\}^T(D^E)^T}{\{\frac{\partial f}{\partial \sigma}\}^T D^E\{\frac{\partial f}{\partial \sigma}\} + Rc(1-M)\{\frac{\partial f}{\partial \sigma}\}^T\sigma - R\overline{H}M\frac{\partial f}{\partial \tau}} \qquad \text{(B.4)}$$

where M is the hardening coefficient ($0 < M \leq 1$). $\overline{H}$ and c are two material constants which are obtained from the actual stress-strain curve for the concrete

under investigation. Only three values of stress and strain can be used in the input data, but the minimum and maximum values must correspond to the beginning of the initial yielding and failure under compression respectively. The detailed calculation for $\overline{H}$ and c is given in Appendix C. The following expressions are derived later in the Appendix:

$$R = \sqrt{\{\frac{\partial f}{\partial \sigma}\}^T \{\frac{\partial f}{\partial \sigma}\}}$$

$$\frac{\partial f}{\partial \tau}$$

To develop the components of the plastic stiffness matrix D^P, differentiation of the failure function with respect to the components of the stress tensor is necessary. $\{\partial f/\partial \sigma\}$ the gradient of the generalised loading surface is therefore calculated by applying the chain rule of differential equations as follows:

$$\frac{\partial f}{\partial \sigma} = \frac{\partial f}{\partial I_1}\frac{\partial I_1}{\partial \sigma} + \frac{\partial f}{\partial J_2}\frac{\partial J_2}{\partial \sigma} + \frac{\partial f}{\partial cos(3\theta)}\frac{\partial cos(3\theta)}{\partial \sigma} \quad \text{(B.5)}$$

In the present investigation, the function f in Equation B.4 is the four parameter failure criterion developed by Hsieh et al [91].

$$f = A\frac{J_2}{f_c^2} + B\frac{\sqrt{J_2}}{f_c} + C\frac{\sigma_1}{f_c} + D\frac{I_1}{f_c} - 1$$

where σ_1 is the maximum principal stress, which can be obtained explicitly using the following expression:

$$\sigma_1 = \frac{1}{3}I_1 + \frac{2}{\sqrt{3}}\sqrt{J_2}cos\theta$$

A new expression for f is derived after substituting the expression for σ_1 in the

expression for f as follows:

$$f = A\frac{J_2}{f_c^2} + \lambda\frac{\sqrt{J_2}}{f_c} + B'\frac{I_1}{f_c} - 1$$

This new expression for f has exactly the same structural components as the four parameter failure criterion reported by Ottosen [74]. The difference between the two failure criteria is in the formulation of the function λ. λ in this case has the following form:

$$\lambda = B' + C'cos\theta$$

where B' and C' are two new constants given by the following expressions:

$$B' = \frac{C}{3} + D$$

$$C' = \frac{2C}{\sqrt{3}}$$

Derivation of Equation B.5

In this Section the partial differential of the failure criterion is set equal to:

$$\frac{\partial f}{\partial \sigma} = \beta_1\phi_1 + \beta_2\phi_2 + \beta_3\phi_3$$

where

$$\beta_1 = \frac{\partial f}{\partial I_1}$$

$$\beta_2 = \frac{\partial f}{\partial J_2}$$

$$\beta_3 = \frac{\partial f}{\partial cos(3\theta)}$$

and

$$\phi_1 = \frac{\partial I_1}{\partial \sigma}$$

$$\phi_1 = \frac{\partial J_2}{\partial \sigma}$$

$$\phi_1 = \frac{\partial cos(3\theta)}{\partial \sigma}$$

After differentiation for all the variables and algebraic manipulation the following expression is obtained:

$$\beta_1 = B'/f_c$$

$$\beta_2 = \frac{\partial f}{\partial J_2} = \frac{\partial}{\partial J_2}(\frac{AJ_2}{f_c^2} + \frac{\lambda\sqrt{J_2}}{f_c})$$

$$2f_c^2\sqrt{J_2}\beta_2 = A + Bf_c + C'f_c(cos\theta - cos(3\theta)\frac{sin\theta}{sin(3\theta)})$$

$$\beta_3 = \frac{\partial f}{\partial cos(3\theta)} = \frac{\partial}{\partial cos(3\theta)}(\lambda\frac{\sqrt{J_2}}{f_c})$$

$$\beta_3 = \frac{C'}{3}\frac{\sqrt{J_2}}{f_c}\frac{sin\theta}{sin(3\theta)}$$

$$\phi_1 = \frac{\partial I_1}{\partial \sigma} = \{\ 1\ \ 1\ \ 1\ \ 0\ \ 0\ \ 0\ \}^T$$

$$J_2 = 0.5(s_x^2 + s_y^2 + s_z^2) + \sigma_{xy}^2\sigma_{yz}^2\sigma_{zx}^2$$

$$\phi_2 = \frac{\partial J_2}{\partial \sigma} = \frac{\partial J_2}{\partial s_x}\frac{\partial s_x}{\partial \sigma} + \frac{\partial J_2}{\partial s_y}\frac{\partial s_y}{\partial \sigma} + \frac{\partial J_2}{\partial s_z}\frac{\partial s_z}{\partial \sigma}$$
$$+ \frac{\partial J_2}{\partial \sigma_{xy}}\frac{\partial \sigma_{xy}}{\partial \sigma} + \frac{\partial J_2}{\partial \sigma_{yz}}\frac{\partial \sigma_{yz}}{\partial \sigma} + \frac{\partial J_2}{\partial \sigma_{zx}}\frac{\partial \sigma_{zx}}{\partial \sigma}$$

$$\phi_2 = \{\ s_x\ \ s_y\ \ s_z\ \ 2\sigma_{xy}\ \ 2\sigma_{xy}\ \ 2\sigma_{zx}\ \}^T$$

$$\phi_3 = \frac{\partial cos(3\theta)}{\sigma} = \frac{\partial cos(3\theta)}{\partial J_3}\frac{\partial J_3}{\partial \sigma} + \frac{\partial cos(3\theta)}{\partial J_2}\frac{\partial J_2}{\partial \sigma}$$

$$
\begin{aligned}
\phi_3 &= 1.5(\sqrt{\frac{3}{J_2}}(\frac{\partial J_3}{\partial \sigma} - \frac{J_3}{J_2}\frac{\partial J_2}{\partial \sigma})) \\
J_3 &= s_x s_y s_z + 2\sigma_{xy}\sigma_{yz}\sigma_{zx} - s_x\sigma_{yz}^2 - s_y\sigma_{zx}^2 - s_z\sigma_{xy}^2 \\
\frac{\partial J_3}{\partial \sigma} &= \frac{\partial J_3}{\partial s_x}\frac{\partial s_x}{\partial \sigma} + \frac{\partial J_3}{\partial s_y}\frac{\partial s_y}{\partial \sigma} + \frac{\partial J_3}{\partial s_z}\frac{\partial s_z}{\partial \sigma} \\
&+ \frac{\partial J_3}{\partial \sigma_{xy}}\frac{\partial \sigma_{xy}}{\partial \sigma} + \frac{\partial J_3}{\partial \sigma_{yz}}\frac{\partial \sigma_{yz}}{\partial \sigma} + \frac{\partial J_3}{\partial \sigma_{zx}}\frac{\partial \sigma_{zx}}{\partial \sigma} \\
s_x &= \frac{1}{3}(2\sigma_x - \sigma_y - \sigma_z) \\
s_y &= \frac{1}{3}(2\sigma_y - \sigma_x - \sigma_z) \\
s_z &= \frac{1}{3}(2\sigma_z - \sigma_x - \sigma_y) \\
\frac{\partial s_x}{\partial \sigma} &= \frac{1}{3}\{2 \quad -1 \quad -1 \quad 0 \quad 0 \quad 0\}^T \\
\frac{\partial s_y}{\partial \sigma} &= \frac{1}{3}\{-1 \quad 2 \quad -1 \quad 0 \quad 0 \quad 0\}^T \\
\frac{\partial s_z}{\partial \sigma} &= \frac{1}{3}\{-1 \quad -1 \quad 2 \quad 0 \quad 0 \quad 0\}^T \\
\frac{\partial J_3}{\partial s_x} &= s_y s_z - \sigma_{yz}^2 \\
\frac{\partial J_3}{\partial s_y} &= s_x s_z - \sigma_{zx}^2 \\
\frac{\partial J_3}{\partial s_z} &= s_x s_y - \sigma_{xy}^2 \\
\frac{\partial J_3}{\partial \sigma_{xy}} &= 2(\sigma_{yz}\sigma_{zx} - s_z\sigma_{xy}) \\
\frac{\partial J_3}{\partial \sigma_{yz}} &= 2(\sigma_{xy}\sigma_{zx} - s_x\sigma_{yz}) \\
\frac{\partial J_3}{\partial \sigma_{zx}} &= 2(\sigma_{xy}\sigma_{yz} - s_y\sigma_{zx}) \\
\frac{\partial \sigma_{xy}}{\partial \sigma} &= \{0 \quad 0 \quad 0 \quad 1 \quad 0 \quad 0\}^T \\
\frac{\partial \sigma_{yz}}{\partial \sigma} &= \{0 \quad 0 \quad 0 \quad 0 \quad 1 \quad 0\}^T \\
\frac{\partial \sigma_{zx}}{\partial \sigma} &= \{0 \quad 0 \quad 0 \quad 1 \quad 0 \quad 1\}^T
\end{aligned}
$$

After differentiation and algebraic manipulation the following expression is obtained for $\frac{\partial J_3}{\partial \sigma}$:

$$\frac{\partial J_3}{\partial \sigma} = \begin{Bmatrix} \frac{1}{3}(2s_y s_z - s_x s_z - s_x s_y - 2\sigma_{yz}^2 + \sigma_{zx}^2 + \sigma_{xy}^2) \\ \frac{1}{3}(2s_x s_z - s_y s_z - s_x s_y - 2\sigma_{zx}^2 + \sigma_{yz}^2 + \sigma_{xy}^2) \\ \frac{1}{3}(2s_x s_y - s_y s_z - s_z s_x - 2\sigma_{xy}^2 + \sigma_{yz}^2 + \sigma_{zx}^2) \\ 2(\sigma_{yz}\sigma_{zx} - s_z\sigma_{xy}) \\ 2(\sigma_{xy}\sigma_{zx} - s_x\sigma_{yz}) \\ 2(\sigma_{xy}\sigma_{yz} - s_y\sigma_{zx}) \end{Bmatrix}$$

The model allows the loading surface to have an isotropic expansion and at the same time to translate. In this case the specific form of the loading surface f is taken to be:

$$f = A\frac{\bar{J}_2}{\tau^2} + B\frac{\sqrt{\bar{J}_2}}{\tau} + C\frac{\bar{\sigma}_1}{\tau} + D\frac{\bar{I}_1}{\tau} - 1 = 0$$

where the stress invariants are as follows:

$$\bar{I}_1 = \bar{\sigma}_x + \bar{\sigma}_y + \bar{\sigma}_z$$

$$\bar{J}_2 = 0.5(\bar{s}_x^2 + \bar{s}_y^2 + \bar{s}_z^2) + \bar{\sigma}_{xy}^2 + \bar{\sigma}_{yz}^2 + \bar{\sigma}_{zx}^2$$

and

$$\bar{\sigma}_x = \sigma_x - \alpha_x$$

$$\bar{s}_x = s_x - \alpha_x + \frac{1}{3}(\alpha_x + \alpha_y + \alpha_z)$$

$$\bar{\sigma}_{xy} = \sigma_{xy} - \alpha_{xy}$$

$$\bar{\sigma}_y = \sigma_y - \alpha_y$$

$$\bar{s}_y = s_y - \alpha_y + \frac{1}{3}(\alpha_x + \alpha_y + \alpha_z)$$

$$\bar{\sigma}_{yz} = \sigma_{yz} - \alpha_{yz}$$

$$\bar{\sigma}_z = \sigma_z - \alpha_z$$

$$\bar{s}_z = s_z - \alpha_z + \frac{1}{3}(\alpha_x + \alpha_y + \alpha_z)$$

$$\bar{\sigma}_{zx} = \sigma_{zx} - \alpha_{zx}$$

In this case the tensor α characterizes the translation of the centre of the loading surface. τ is the isotropic strain hardening rate function. ε_P is the effective plastic strain.

The differentiation of the loading surface $\partial f/\partial \tau$ is now possible after all the variables involved in the loading function have been defined:

$$\frac{\partial f}{\partial \tau} = -(A\frac{\bar{J}_2}{\tau^2} + 1)$$

Equation B.4 is a symmetric (6×6) matrix. It is composed of 21 individual elements.

Appendix C

TANGENT MODULUS CALCULATION

Equation 3.34 in Section 3.5 contains two material constants $\overline{H}$ and c. These material constants are obtained from the stress-strain curve for the concrete under investigation. In the case of uniaxial compressive conditions, the only component which does not vanish is σ_3. Accordingly, the only remaining component of Ziegler's hardening parameter is $\alpha_3 = \alpha$ [152, 95, 93].

For a given concrete stress-strain curve the tangent modulus can be evaluated from the following relationship:

$$d\sigma = H d\varepsilon^P \tag{C.1}$$

In the case of uniaxial conditions the general loading function takes the following form:

$$\sigma - \alpha = \tau \tag{C.2}$$

Using Equations 3.26 and 3.29 the loading function given by Equation C.2 becomes an incremental form of the variable:

$$d\sigma = M\overline{H}d\varepsilon^P + c(1-M)\tau d\varepsilon^P \tag{C.3}$$

Now comparing Equations C.1 and C.3 the expression for the tangent modulus H is obtained as follows:

$$H = M\overline{H} + c(1-M)\tau \tag{C.4}$$

Since M can have an arbitrary value (M can take any value between 0.0 and 1) this implies that

$$\overline{H} = H \tag{C.5}$$

and

$$c = \frac{H}{\tau} \tag{C.6}$$

where $\overline{H}$ is the tangent modulus due to strain hardening associated with isotropic expansion and H is the tangent modulus due to strain hardening.

In order to calculate the tangent modulus H a stress-strain curve for the concrete under investigation is necessary. At least three points are required on the stress-strain curve. The points must cover the entire plastic portion of the stress-strain curve i.e. the first point must start at the yield point and the last point must be at maximum strength. Figure C.1 shows a typical stress-strain curve on which four points have been marked.

The stress increment between two points is calculated as follows:

$$\Delta\sigma = E\Delta\epsilon$$

$$\Delta\epsilon = \Delta\epsilon_e + \Delta\epsilon_p$$

$$\Delta\epsilon_e = \Delta\sigma/E_i$$

$$\Delta\sigma = E\Delta\sigma/E_i + E\Delta\epsilon_p$$

$$\Delta\sigma(1 - E/E_i) = E\Delta\epsilon_p$$

Hence

$$H = \frac{E}{1 - E/E_i} \tag{C.7}$$

The values of the stress and strain increments are adjusted by interpolation between the actual points in order to obtain the best fit for the stress-strain curve. The interpolation method used to achieve the best fit is detailed in Section 5.2.1

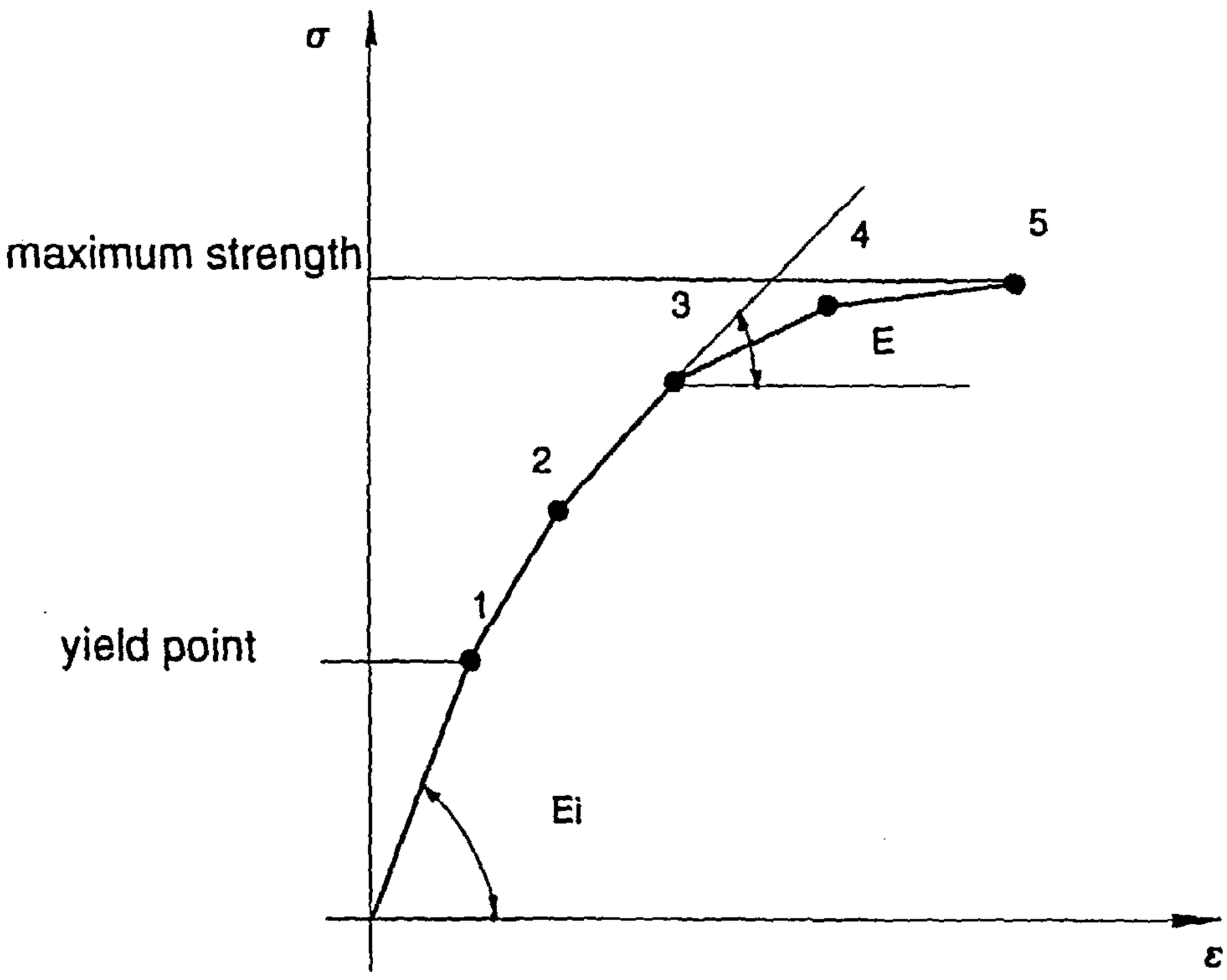

Figure C.1: Typical input for an uniaxial compressive stress-strain curve

Appendix D

CONCRETE MODEL LISTING

```
      subroutine f3dm61(at,volo)
c
c  ELASTIC-PLASTIC FRACTURE REINFORCED CONCRETE MODEL
c
      dimension dsigc1(128),dsigc2(128),dsigc3(128),dsigc4(128),
     1 dsigc5(128),dsigc6(128),alf(128,6),dafa(128,6),ud(128,6),
     2 st1(128),st2(128),st3(128),st4(128),st5(128),st6(128),
     3 stt1(128),stt2(128),stt3(128),stt4(128),stt5(128),stt6(128),
     4 ep1(128),ep2(128),ep3(128),ep4(128),ep5(128),ep6(128),
     5 dp(3),ot(128,6),volo(1),psigc(128,6),t(128,6),deps(128,6),
     7 de(128,6),press(128),cphi(128),acphi(128),ps1(128),ps2(128),
     8 ps3(128),at(1),stss(128,10),dpres(128)
c
      dimension ft(128),ra(128),fto(128),ftn(128),yld(128),
     1 fti(128),rm(128),efp(128),dmu(128),xm(128),ai1(128),
     2 sigc(128),sigt(128),pr(128),yms(128),blk(128),g(128),
     3 ay(128),by(128),cy(128),dy(128),af(128),bf(128),cf(128),
     4 dff(128),epf(128),qh(128),rg(128),qs(128),eyr(128),
     5 fo(128),agg(128),cl(128),stiff(128),yield(128),xh(128),
     6 cp(6,6),afa(128,6),ym(128),ex(128,3),davg(128),pnew(128),
     8 str(128),pold(128),save(128),psave(128),as2(128),
     9 as3(128),istat(128)
c
```

D.1 SEGMENT 1

```
c      COMMON BLOCKS, MATERIAL ARRAY AND PRINCIPAL VARIABLES
c
```

```
      common/bk02/iburn,dt1,dt2,isdo
      common/bk28/summss,xke,xpe,tt
      common/aux2/d1(128),d2(128),d3(128),d4(128),d5(128),
     1            d6(128),wzzdt(128),wyydt(128),wxxdt(128)
      common/aux14/
     1 sig1(128),sig2(128),sig3(128),sig4(128),sig5(128),sig6(128),
     1 sig7(128),
     2 sigc1(128),sigc2(128),sigc3(128),sigc4(128),sigc5(128),
     3 sigc6(128),sigr1(128),sigr2(128),sigr3(128),pxr(128),
     4 pyr(128),pzr(128),zl(128,3),zm(128,3),zn(128,3),
     5 sf1(128),sf2(128),sf3(128),ef1(128),ef2(128),ef3(128),
     6 epx1(128),epx2(128),epx3(128),crak1(128),crak2(128),crak3(128),
     7 eps1(128),eps2(128),eps3(128),eps4(128),eps5(128),eps6(128),
     8 ex1(128),ex2(128),ex3(128),tc1(128),tc2(128),tc3(128),epv(128),
     9 np(128)
c
      common/aux18/dd(128),df(128)
      common/aux33/ix1(128),ix2(128),ix3(128),ix4(128),ix5(128),
     1            ix6(128),ix7(128),ix8(128),mxt(128),nmel
      common/aux35/rhoa(128),cxxa(128)
      common/aux36/lft,llt
c
      dimension zzl(128,3),zzm(128,3),zzn(128,3),beta(128),
     1          icrak1(128),icrak2(128),icrak3(128)
c
      integer mm,mit
c
      equivalence (ex(1,1),ex1(1)),(ex(1,2),ex2(1)),(ex(1,3),ex3(1)),
     1            (yld(1),yield(1))
c
      data done/1.e0/,dtwo/2.e0/,dthree/3.e0/,dsmall/1.0E-5/,
     1     fur3d/1.333333333/,third/0.333333333333333/,
     2     d99/0.99999999999999E0/,
     3     pi/3.14159265358979323846264338327950288419716939937510E0/,
     4     tjon/-1.0/
      dthird=done/dthree
      dr23r3=dthree*sqrt(dthree)/dtwo
      dr23=dtwo/dthree
c      pi=atan(1.)*4.
      rfur3d=sqrt(done/fur3d)
c
      if(tt-tjon.gt.1.0e-7) kount=0
      tjon=tt
      kount=kount+1
```

```
c
c       SET MATERIAL ARRAY
c
        do 10 i=lft,llt
c
c       IF YOU NEED IT FOR DIAGNOSTIC PURPOSES, YOU CAN FIND
c       THE ELEMENT NUMBER IN LOOPS OVER I=LFT,LLT BY INSERTING
c       inel=(kount-1)*128+i-lft+1 INSIDE THE LOOP
c
        inel=(kount-1)*128+i-lft+1
        mx=48*(mxt(I)-1)
        yms(i)=at(mx+1)
        ym(i)=yms(i)*dt1
        pr(i)=at(mx+2)
        sigc(i)=at(mx+3)
        sigt(i)=at(mx+4)
        g(i)=at(mx+40)*dt1
        blk(I)=ym(I)/(done-dtwo*pr(i))
        fo(I)=at(mx+5)
        agg(I)=at(mx+6)
        xm(I)=0.90
        eyr(I)=at(mx+7)
        qs(I)=at(mx+8)
        qh(I)=at(mx+9)
        epf(I)=at(mx+10)
        ay(i)=at(mx+36)
        by(i)=at(mx+37)
        cy(i)=at(mx+38)/0.866025404
        dy(i)=at(mx+39)+dthird*at(mx+38)
        af(i)=at(mx+36)
        bf(i)=at(mx+37)
        cf(i)=at(mx+38)/0.866025404
        dff(i)=at(mx+39)+dthird*at(mx+38)
        np=at(mx+31)
        cl(i)=volo(i)**third
        stiff(i)=at(mx+1)/cl(i)
        yield(i)=abs(at(mx+21))
        davg(i)=third*(d1(i)+d2(i)+d3(i))
        cxxa(i)=(fur3d*at(mx+40)+at(mx+41))
        alpha=(done+at(mx+2))/(done-dtwo*at(mx+2))
c
        icrak1(i)=int(crak1(i)+0.2)
        icrak2(i)=int(crak2(i)+0.2)
        icrak3(i)=int(crak3(i)+0.2)
```

```
   10 continue
c
      do 20 i=lft,llt
c
c     UPDATE THE TOTAL STRAIN TENSOR
c     UPDATE THE YIELD LEVEL
c     UPDATE THE HARDENING
c
      eps1(i)=eps1(i)+d1(i)*dt1
      eps2(i)=eps2(i)+d2(i)*dt1
      eps3(i)=eps3(i)+d3(i)*dt1
      eps4(i)=eps4(i)+d4(i)*dt1
      eps5(i)=eps5(i)+d5(i)*dt1
      eps6(i)=eps6(i)+d6(i)*dt1
c
      yld(i)=yield(i)
      do 21 J=1,6
      ud(i,j)=0.0
   21 afa(i,j)=alf(i,j)
   20 continue
c
```

D.2 SEGMENT 2

```
      do 600 i=lft,llt
c
c     STRESS UPDATE AND POST FAILURE TREATMENT
c
c     UPDATE CONCRETE STRESS
c     CRACKED ELEMENT WITH ALL CRACKS CLOSED ARE TREATED
c     AS ISOTROPIC IN COMPRESSION
c
      mx=48*(mxt(i)-1)
      inel=(kount-1)*128+i-lft+1
      dsigc1(i)=0.0
      dsigc2(i)=0.0
      dsigc3(i)=0.0
      dsigc4(i)=0.0
      dsigc5(i)=0.0
      dsigc6(i)=0.0
      if(icrak1(i).ne.0) goto 603
c
c     UNCRACKED ELEMENT (OR ALL CRACKS CLOSED)
```

```
c
  602 press(i)=blk(i)*davg(i)
      dsigc1(i)=press(i)+2.*g(i)*(d1(i)-davg(i))
      dsigc2(i)=press(i)+2.*g(i)*(d2(i)-davg(i))
      dsigc3(i)=press(i)+2.*g(i)*(d3(i)-davg(i))
      dsigc4(i)=g(i)*d4(i)
      dsigc5(i)=g(i)*d5(i)
      dsigc6(i)=g(i)*d6(i)
c
      st1(i)=sigc1(i)
      st2(i)=sigc2(i)
      st3(i)=sigc3(i)
      st4(i)=sigc4(i)
      st5(i)=sigc5(i)
      st6(i)=sigc6(i)
c
c     TOTAL CONCRETE STRESS
c
      sigc1(i)=sigc1(i)+dsigc1(i)
      sigc2(i)=sigc2(i)+dsigc2(i)
      sigc3(i)=sigc3(i)+dsigc3(i)
      sigc4(i)=sigc4(i)+dsigc4(i)
      sigc5(i)=sigc5(i)+dsigc5(i)
      sigc6(i)=sigc6(i)+dsigc6(i)
c
      goto 600
c
c     CRACKED ELEMENT
c     ROTATE TO CRACK-NORMAL COORDINATES:-
c
c     1) TOTAL STRAIN TENSOR
c
  603 do 610 J=1,3
      ex(i,j)=(eps1(i)*zl(i,j)*zl(i,j)+eps2(i)*zm(i,j)*zm(i,j)+
     1  eps3(i)*zn(i,j)*zn(i,j)+eps4(i)*zl(i,j)*zm(i,j)+
     2  eps5(i)*zm(i,j)*zn(i,j)+eps6(i)*zn(i,j)*zl(i,j))*cl(i)
  610 continue
c
c     IF ALL CRACKS ARE CLOSED, GO BACK TO ISOTROPIC
c     TREATMENT
c

      if(ex(i,1).gt.0.)goto 601
      if(icrak2(I).eq.0)goto 602
```

```
      if(ex(i,2).gt.0.)goto 601
      if(icrak3(i).eq.0)goto 602
      if(ex(i,3).le.0.) goto 602
c
c     2) USE THE PREVIOUS STRESS FOR CRACKED CONCRETE
c
 601  do 611 j=1,3
      t(i,j)=sigc1(i)*zl(i,j)*zl(i,j)+sigc2(i)*zm(i,j)*zm(i,j)
     1 +sigc3(i)*zn(i,j)*zn(i,j)+2.*sigc4(i)*zl(i,j)*zm(i,j)
     2 +2.*sigc5(i)*zm(i,j)*zn(i,j)+2.*sigc6(i)*zn(i,j)*zl(i,j)
  611 continue
c
      t(i,4)=sigc1(i)*zl(i,1)*zl(i,2)+sigc2(i)*zm(i,1)*zm(i,2)
     1 +sigc3(i)*zn(i,1)*zn(i,2)
     2 +sigc4(i)*(zl(i,1)*zm(i,2)+zl(i,2)*zm(i,1))
     3 +sigc5(i)*(zm(i,1)*zn(i,2)+zm(i,2)*zn(i,1))
     4 +sigc6(i)*(zn(i,1)*zl(i,2)+zn(i,2)*zl(i,1))
c
      t(i,5)=sigc1(i)*zl(i,2)*zl(i,3)+sigc2(i)*zm(i,2)*zm(i,3)
     1 +sigc3(i)*zn(i,2)*zn(i,3)
     2 +sigc4(i)*(zl(i,2)*zm(i,3)+zl(i,3)*zm(i,2))
     3 +sigc5(i)*(zm(i,2)*zn(i,3)+zm(i,3)*zn(i,2))
     4 +sigc6(i)*(zn(i,2)*zl(i,3)+zn(i,3)*zl(i,2))
c
      t(i,6)=sigc1(i)*zl(i,1)*zl(i,3)+sigc2(i)*zm(i,1)*zm(i,3)
     1 +sigc3(i)*zn(i,1)*zn(i,3)
     2 +sigc4(i)*(zl(i,1)*zm(i,3)+zl(i,3)*zm(i,1))
     3 +sigc5(i)*(zm(i,1)*zn(i,3)+zm(i,3)*zn(i,1))
     4 +sigc6(i)*(zn(i,1)*zl(i,3)+zn(i,3)*zl(i,1))
c
c     3) STRAIN RATE TENSOR
c
      do 613 j=1,3
      de(i,j)=d1(i)*zl(i,j)*zl(i,j)+d2(i)*zm(i,j)*zm(i,j)
     1 +d3(i)*zn(i,j)*zn(i,j)+d4(i)*zl(i,j)*zm(i,j)
     2 +d5(i)*zm(i,j)*zn(i,j)+d6(i)*zn(i,j)*zl(i,j)
  613 continue
c
      de(i,4)=2.*d1(i)*zl(i,1)*zl(i,2)+2.*d2(i)*zm(i,1)*zm(i,2)
     1 +2.*d3(i)*zn(i,1)*zn(i,2)
     2 +d4(i)*(zl(i,1)*zm(i,2)+zl(i,2)*zm(i,1))
     3 +d5(i)*(zm(i,1)*zn(i,2)+zm(i,2)*zn(i,1))
     4 +d6(i)*(zn(i,1)*zl(i,2)+zn(i,2)*zl(i,1))
c
```

```
      de(i,5)=2.*d1(i)*zl(i,2)*zl(i,3)+2.*d2(i)*zm(i,2)*zm(i,3)
     1 +2.*d3(i)*zn(i,2)*zn(i,3)
     2 +d4(i)*(zl(i,2)*zm(i,3)+zl(i,3)*zm(i,2))
     3 +d5(i)*(zm(i,2)*zn(i,3)+zm(i,3)*zn(i,2))
     4 +d6(i)*(zn(i,2)*zl(i,3)+zn(i,3)*zl(i,2))
c
      de(i,6)=2.*d1(i)*zl(i,3)*zl(i,1)+2.*d2(i)*zm(i,3)*zm(i,1)
     1 +2.*d3(i)*zn(i,3)*zn(i,1)
     2 +d4(i)*(zl(i,3)*zm(i,1)+zl(i,1)*zm(i,3))
     3 +d5(i)*(zm(i,3)*zn(i,1)+zm(i,1)*zn(i,3))
     4 +d6(i)*(zn(i,3)*zl(i,1)+zn(i,1)*zl(i,3))
c
      s1=t(i,1)
      s2=t(i,2)
      sfa=1.
      sfb=1.
      sfc=1.
      if(ex(i,1).gt.0.0)go to 620
c
c     FIRST CRACK IS CLOSED
c
      t(i,1)=t(i,1)+de(i,1)*ym(i)
      if(t(i,1).gt.0.0) t(i,1)=0.0
      sfa=1.
      goto 627
c
c     FIRST CRACK IS OPEN
c
  620 goto (621,622,624),icrak1(i)
c
c     PATH1 - DESCENDING BRANCH
c
  621 if(ex(i,1).ge.fo(i)) goto 624
      if(ex(i,1).lt.ef1(i)) goto 622
      t(i,1)=sf1(i)*(fo(i)-ex(i,1))/(fo(i)-ef1(i))
      sf1(i)=t(i,1)
      ef1(i)=ex(i,1)
      goto 625
c
c     PATH2 - LOADING/UNLOADING TO/FROM DESCENDING BRANCH
c
  622 icrak1(i)=2
      if(ex(i,1).lt.ef1(i))go to 623
      icrak1(i)=1
```

```
      goto 621
  623 t(i,1)=sf1(i)+stiff(i)*(ex(i,1)-ef1(i))
      if(t(i,1).lt.0.0) t(i,1)=0.0
      goto 625
c
c     PATH 3 - FULLY OPEN
c
  624 icrak1(i)=3
      t(i,1)=0.0
c
  625 if(agg(i).le.0.0) goto 626
      sfa=1.-ex(i,1)/agg(i)
      sfa=sfa*sfa
      if(ex(i,1).ge.agg(i)) sfa=0.
      goto 627
  626 sfa=abs(agg(i))
c
  627 if(icrak2(i).eq.0) goto 644
c
c     A SECOND CRACK EXISTS
c
      if(ex(i,2).gt.0.0)go to 628
c
c     SECOND CRACK IS CLOSED
c
      t(i,2)=t(i,2)+de(i,2)*ym(i)
      if(t(i,2).gt.0.0) t(i,2)=0.0
      sfb=1.0
      goto 635
c
c     SECOND CRACK IS OPEN
c
  628 goto (629,630,632),icrak2(i)
c
c     PATH 1
c
  629 if(ex(i,2).ge.fo(i)) goto 632
      if(ex(i,2).lt.ef2(i)) goto 630
      t(i,2)=sf2(i)*(fo(i)-ex(i,2))/(fo(i)-ef2(i))
      sf2(i)=t(i,2)
      ef2(i)=ex(i,2)
      goto 633
c
c     PATH 2
```

```
c
  630 icrak2(i)=2
      if(ex(i,2).lt.ef2(i)) goto 631
      icrak2(i)=1
      go to 629
  631 t(i,2)=sf2(i)+stiff(i)*(ex(i,2)-ef2(i))
      if(t(i,2).lt.0.0) t(i,2)=0.0
      goto 633
c
c     PATH 3
c
  632 icrak2(i)=3
      t(i,2)=0.0
c
  633 if(agg(i).le.0.0) goto 634
      sfb=1.-ex(i,2)/agg(i)
      sfb=sfb*sfb
      if(ex(i,2).ge.agg(i)) sfb=0.0
      goto 635
  634 sfb=abs(agg(i))
c
  635 if(icrak3(i).eq.0) goto 643
c
c     A THIRD CRACK EXISTS
c
      if(ex(i,3).gt.0.0) goto 636
c
c     THIRD CRACK IS CLOSED
c
      t(i,3)=t(i,3)+de(i,3)*ym(i)
      if(t(i,3).gt.0.0) t(i,3)=0.0
      sfc=1.
      goto 645
c
c     THIRD CRACK IS OPEN
c
  636 goto (637,638,640),icrak3(i)
c
c     PATH 1
c
  637 if(ex(i,3).gt.fo(i)) goto 640
      if(ex(i,3).lt.ef3(i)) goto 638
      t(i,3)=sf3(i)*(fo(i)-ex(i,3))/(fo(i)-ef3(i))
      sf3(i)=t(i,3)
```

```
      ef3(i)=ex(i,3)
      goto 641
c
c     PATH 2
c
  638 icrak3(i)=2
      if(ex(i,3).lt.ef3(i)) goto 639
      icrak3(i)=1
      goto 637
  639 t(i,3)=sf3(i)+stiff(i)*(ex(i,3)-ef3(i))
      if(t(i,3).lt.0.0) t(i,3)=0.0
      goto 641
c
c     PATH 3
c
  640 icrak3(i)=3
      t(i,3)=0.0
c
  641 if(agg(i).le.0.0) goto 642
      sfc=1.-ex(i,3)/agg(i)
      sfc=sfc*sfc
      if(ex(i,3).ge.agg(i)) sfc=0.0
      goto 645
  642 sfc=abs(agg(i))
      goto 645
c
c     COUPLING OF REMAINING STRESSES TO CRACK-NORMAL STRAINS
c
  643 t(i,3)=t(i,3)+ym(i)*de(i,3)+pr(i)*(t(i,1)+t(i,2)-s1-s2)
      goto 645
c
  644 temp1=ym(i)/(1.-pr(i)*pr(i))
      temp2=pr(i)/(1.-pr(i))
      t(i,2)=t(i,2)+temp1*(de(i,2)+pr(i)*de(i,3))+temp2*(t(i,1)-s1)
      t(i,3)=t(i,3)+temp1*(pr(i)*de(i,2)+de(i,3))+temp2*(t(i,1)-s1)
c
c  UPDATE AND MODIFY ROTATED SHEAR STRESSES BY THE SHEAR FACTORS
c
  645 t(i,4)=(t(i,4)+g(i)*de(i,4))*sfa*sfb
      t(i,5)=(t(i,5)+g(i)*de(i,5))*sfb*sfc
      t(i,6)=(t(i,6)+g(i)*de(i,6))*sfc*sfa
c
c       ROTATE BACK TO GLOBAL COORDINATES
c
```

```
c       1) STRESSES
c
       sigc1(i)=t(i,1)*zl(i,1)*zl(i,1)+t(i,2)*zl(i,2)*zl(i,2)
      1 +t(i,3)*zl(i,3)*zl(i,3)+2.*t(i,4)*zl(i,1)*zl(i,2)
      2 +2.*t(i,5)*zl(i,2)*zl(i,3)+2.*t(i,6)*zl(i,3)*zl(i,1)
c
       sigc2(i)=t(i,1)*zm(i,1)*zm(i,1)+t(i,2)*zm(i,2)*zm(i,2)
      1 +t(i,3)*zm(i,3)*zm(i,3)+2.*t(i,4)*zm(i,1)*zm(i,2)
      2 +2.*t(i,5)*zm(i,2)*zm(i,3)+2.*t(i,6)*zm(i,3)*zm(i,1)
c
       sigc3(i)=t(i,1)*zn(i,1)*zn(i,1)+t(i,2)*zn(i,2)*zn(i,2)
      1 +t(i,3)*zn(i,3)*zn(i,3)+2.*t(i,4)*zn(i,1)*zn(i,2)
      2 +2.*t(i,5)*zn(i,2)*zn(i,3)+2.*t(i,6)*zn(i,3)*zn(i,1)
c
       sigc4(i)=t(i,1)*zl(i,1)*zm(i,1)+t(i,2)*zl(i,2)*zm(i,2)
      1 +t(i,3)*zl(i,3)*zm(i,3)
      2 +t(i,4)*(zl(i,1)*zm(i,2)+zl(i,2)*zm(i,1))
      3 +t(i,5)*(zl(i,2)*zm(i,3)+zl(i,3)*zm(i,2))
      4 +t(i,6)*(zl(i,3)*zm(i,1)+zl(i,1)*zm(i,3))
c
       sigc5(i)=t(i,1)*zm(i,1)*zn(i,1)+t(i,2)*zm(i,2)*zn(i,2)
      1 +t(i,3)*zm(i,3)*zn(i,3)
      2 +t(i,4)*(zm(i,1)*zn(i,2)+zm(i,2)*zn(i,1))
      3 +t(i,5)*(zm(i,2)*zn(i,3)+zm(i,3)*zn(i,2))
      4 +t(i,6)*(zm(i,3)*zn(i,1)+zm(i,1)*zn(i,3))
c
       sigc6(i)=t(i,1)*zn(i,1)*zl(i,1)+t(i,2)*zn(i,2)*zl(i,2)
      1 +t(i,3)*zn(i,3)*zl(i,3)
      2 +t(i,4)*(zn(i,1)*zl(i,2)+zn(i,2)*zl(i,1))
      3 +t(i,5)*(zn(i,2)*zl(i,3)+zn(i,3)*zl(i,2))
      4 +t(i,6)*(zn(i,3)*zl(i,1)+zn(i,1)*zl(i,3))
c
       st1(i)=sigc1(i)
       st2(i)=sigc2(i)
       st3(i)=sigc3(i)
       st4(i)=sigc4(i)
       st5(i)=sigc5(i)
       st6(i)=sigc6(i)
c
  600 continue
c
```

D.3 SEGMENT 3

```
      do 300 i=1ft,11t
c
c     ELASTIC-PLASTIC STRESS ANALYSIS AND FAILURE DIAGNOSTIC
c
c     THIS LOOP DETERMINES THE STATE OF THE CONCRETE
c     ELEMENT AS FOLLOWS:-
c
c      1) ISTAT = 1 ---------> ELEMENT IN ELASTIC STATE
c      2) ISTAT = 2 ---------> ELEMENT IN PLASTIC STATE
c      3) ISTAT = 3 ---------> PURE CRACKING OF THE ELEMENT
c      4) ISTAT = 4 ---------> CRACKING AND CRUSHING OF THE ELEMENT
c      5) ISTAT = 5 ---------> PURE CRUSHING OF THE ELEMENT
c
       mx=48*(mxt(i)-1)
       inel=(kount-1)*128+i-1ft+1
c
       call failf(sigc1,sigc2,sigc3,sigc4,sigc5,sigc6,
      1           ay,by,cy,dy,ai1,as2,as3,sita,afa,ft,1,i)
c
       psave(i)=ft(i)/yld(i)
       if(save(i).lt.psave(i)) goto 68
          save(i)=psave(i)
          goto 69
      68 if(icrak3(i).ge.3) goto 69
          if(ft(i)-yld(i)) 72,72,74
c
      72 istat(i)=1
c
      69 continue
          goto 300
c
      74 istat(i)=2
c
c     RESTORE THE OLD STRESS
c
       ra(i)=0.0
       call failf(st1,st2,st3,st4,st5,st6,
      1           ay,by,cy,dy,ai1,as2,as3,sita,afa,fto,1,I)
c
       if((1-fto(i)/yld(i)).lt.0.001) goto 160
       ra(i)=(yld(i)-fto(i))/(ft(i)-fto(i))
       ftn(i)=ft(i)
```

```
c
      do 150 j=1,np
      st1(i)=st1(i)+ra(i)*dsigc1(i)
      st2(i)=st2(i)+ra(i)*dsigc2(i)
      st3(i)=st3(i)+ra(i)*dsigc3(i)
      st4(i)=st4(i)+ra(i)*dsigc4(i)
      st5(i)=st5(i)+ra(i)*dsigc5(i)
      st6(i)=st6(i)+ra(i)*dsigc6(i)
c
      call failf(st1,st2,st3,st4,st5,st6,
     1           ay,by,cy,dy,ai1,as2,as3,sita,afa,fti,1,i)
c
      if(abs(1.-fti(i)/yld(i)).le.0.001) goto 160
      if(fti(i)-yld(i)) 120,160,130
 120  fto(i)=fti(i)
      ra(i)=ra(i)+(1-ra(i))*(yld(i)-fto(i))/(ftn(i)-fto(i))
      go to 150
 130  ftn(i)=fti(i)
      ra(i)=ra(i)*(yld(i)-fto(i))/(ftn(i)-fto(i))
 150  continue
c
c     CALCULATE THE NUMBER OF CONSTANT STRAIN SUB-INCREMENTS
c
 160  mit=(ft(i)-yld(i))/yld(i)
c
c     FORCE AT LEAST ONE SUB-INCREMENT
c
      mm=mit+1
      rm(i)=(1-ra(i))/mm
      deps(i,1)=rm(i)*d1(i)
      deps(i,2)=rm(i)*d2(i)
      deps(i,3)=rm(i)*d3(i)
      deps(i,4)=rm(i)*d4(i)
      deps(i,5)=rm(i)*d5(i)
      deps(i,6)=rm(i)*d6(i)
c
      do 310 im=1,mm
      call plas(st1,st2,st3,st4,st5,st6,at,pr,xh,ay,by,cy,
     1          dy,yld,xm,ym,yms,cp,I)
c
c  SET THE PLASTIC SUB-INCREMENT STRESSES TO ZERO
c
      dsigc1(i)=0.0
```

```
      dsigc2(i)=0.0
      dsigc3(i)=0.0
      dsigc4(i)=0.0
      dsigc5(i)=0.0
      dsigc6(i)=0.0
c
      do 311 j=1,6
c
c     CALCULATE THE PLASTIC STRESSES
c
      xx=0.0
      do 312 k=1,6
 312  xx=xx +cp(j,k)*deps(i,k)*dt1
      psigc(i,j)=xx
 311  continue
c
      dsigc1(i)=psigc(i,1)
      dsigc2(i)=psigc(i,2)
      dsigc3(i)=psigc(i,3)
      dsigc4(i)=psigc(i,4)
      dsigc5(i)=psigc(i,5)
      dsigc6(i)=psigc(i,6)
c
      stt1(i)=st1(i)+dsigc1(i)
      stt2(i)=st2(i)+dsigc2(i)
      stt3(i)=st3(i)+dsigc3(i)
      stt4(i)=st4(i)+dsigc4(i)
      stt5(i)=st5(i)+dsigc5(i)
      stt6(i)=st6(i)+dsigc6(i)
c
      ep1(i)=1./yms(i)*dsigc1(i)-pr(i)/yms(i)*(dsigc2(i)+dsigc3(i))
      ep2(i)=1./yms(i)*dsigc2(i)-pr(i)/yms(i)*(dsigc1(i)+dsigc3(i))
      ep3(i)=1./yms(i)*dsigc3(i)-pr(i)/yms(i)*(dsigc1(i)+dsigc2(i))
      ep4(i)=2.*(1.+pr(i))/yms(i)*dsigc4(i)
      ep5(i)=2.*(1.+pr(i))/yms(i)*dsigc5(i)
      ep6(i)=2.*(1.+pr(i))/yms(i)*dsigc6(i)
c
c     CALCULATE THE INCREMENTAL EFFECTIVE STRAIN
c
      efp(i)=( (deps(i,1)-ep1(i))**2+(deps(i,2)-ep2(i))**2+
     1          (deps(i,3)-ep3(i))**2+0.5*( (deps(i,4)-ep4(i))**2+
     2          (deps(i,5)-ep5(i))**2+(deps(i,6)-ep6(i))**2) )*2/3
      efp(i)=sqrt(efp(i))*dt1
c
```

```
c       ..
c
        dmu(i)=xh(i)/yld(i)*(1.-xm(i))*efp(i)
        dafa(i,1)=dmu(i)*(st1(i)-afa(i,1))
        dafa(i,2)=dmu(i)*(st2(i)-afa(i,2))
        dafa(i,3)=dmu(i)*(st3(i)-afa(i,3))
        dafa(i,4)=dmu(i)*(st4(i)-afa(i,4))
        dafa(i,5)=dmu(i)*(st5(i)-afa(i,5))
        dafa(i,6)=dmu(i)*(st6(i)-afa(i,6))
c
        do 309 j=1,6
c
c    INCREMENT THE HARDENING EFFECTS
c
        afa(i,j)=afa(i,j)+dafa(i,j)
        ud(i,j)=ud(i,j)+deps(i,J)
  309 continue
c
        call failf(stt1,stt2,stt3,stt4,stt5,stt6,
     1             ay,by,cy,dy,ai1,as2,as3,sita,afa,yld,1,i)
c
        call failf(stt1,stt2,stt3,stt4,stt5,stt6,
     1             af,bf,cf,dff,ai1,as2,as3,sita,afa,ft,2,i)
c
        ra(i)=1.
        if(ft(i).lt.sigc(i)) goto 320
        if(abs(ft(i)-sigc(i))/sigc(i).le.0.01) goto 330
c
        call failf(st1,st2,st3,st4,st5,st6,
     1             af,bf,cf,dff,ai1,as2,as3,sita,afa,fto,2,i)
c
        ra(i)=0.
        if(fto(i).ge.sigc(i)) goto 330
        ra(i)=(sigc(i)-fto(i))/(ft(i)-fto(i))
c
 330    stt1(i)=st1(i)+ra(i)*dsigc1(i)
        stt2(i)=st2(i)+ra(i)*dsigc2(i)
        stt3(i)=st3(i)+ra(i)*dsigc3(i)
        stt4(i)=st4(i)+ra(i)*dsigc4(i)
        stt5(i)=st5(i)+ra(i)*dsigc5(i)
        stt6(i)=st6(i)+ra(i)*dsigc6(i)
c
        call zfail(stt1,stt2,stt3,stt4,stt5,stt6,alpha,beta,istat,sigc,ay,
     1             by,cy,dy,ps1,ps2,ps3,zzl,zzm,zzn,i,inel)
```

```
c
      st1(i)=stt1(i)
      st2(i)=stt2(i)
      st3(i)=stt3(i)
      st4(i)=stt4(i)
      st5(i)=stt5(i)
      st6(i)=stt6(i)
      goto 315
 320  st1(i)=stt1(i)
      st2(i)=stt2(i)
      st3(i)=stt3(i)
      st4(i)=stt4(i)
      st5(i)=stt5(i)
      st6(i)=stt6(i)
 310  continue
c
 315  sigc1(i)=st1(i)
      sigc2(i)=st2(i)
      sigc3(i)=st3(i)
      sigc4(i)=st4(i)
      sigc5(i)=st5(i)
      sigc6(i)=st6(i)
c
      do 299 j=1,6
  299 alf(i,j)=afa(i,j)
      yield(I)=yld(i)
      d1(i)=ud(i,1)
      d2(i)=ud(i,2)
      d3(i)=ud(i,3)
      d4(i)=ud(i,4)
      d5(i)=ud(i,5)
      d6(i)=ud(i,6)
c
      epv(i)=efp(i)
      sig7(i)=sig7(i)+epv(i)
  300 continue
c
```

D.4 SEGMENT 4

```
      do 500 i=lft,llt
c
c     CALCULATION OF CRACK WIDTH AND DIRECTIONS
```

```
c
c     DIRECTIONS OF FURTHER FAILURES ARE FORCED TO ALIGN WITH
c     THOSE OF PREVIOUS FAILURE
c     A SINGLE TENSILE CRACK OCCURS FOR STRESS STATES WITH A
c     LARGEST TENSILE COMPONENT. FOR PURELY COMPRESSIVE STRESS
c     STATE, THREE SIMULTANEOUS ORTHOGONAL CRACKS ARE INITIATED,
c     WHICH WILL COME INTO EFFECT WHEN THE ELEMENT EXPANDS IN ANY
c     DIRECTION.
c
      inel=(kount-1)*128+i-lft+1
  381 if(icrak3(i).gt.0) goto 500
c
c     DO NOT LOOK FOR NEW CRACKS IF ELEMENT IS CRUSHED,
c     IF ELEMENT IS FULLY CRACKED
c     OR IF ELEMENT HAS NOT FAILED THIS TIME IN COMPRESSION;
c     IF THERE IS TENSILE STRESS, ELEMENT CANNOT CRUSH
c
      if(istat(i).eq.5) then
      if(ps1(i).gt.0) goto 341
c
c     ELEMENT HAS CRUSHED IN PURE COMPRESSION;
c     FLAG THREE SIMULTANEOUS ORTHOGONAL CRACKS.
c
      icrak1(i)=3
      icrak2(i)=3
      icrak3(i)=3
      tc1(i)=tt
      tc2(i)=tt
      tc3(i)=tt
      do 481 j=1,3
      zl(i,j)=zzl(i,j)
      zm(i,j)=zzm(i,j)
      zn(i,j)=zzn(i,j)
  481 continue
c
      goto 500
c
      end if
c
  331 if(istat(i).eq.3.) then
  341 if(icrak1(i).gt.0) goto 1361
      if(ps1(i).lt.(sigt(i))/dtwo) goto 500
c
c     CALCULATE CRACK NORMAL EXTENSION
```

```
c
      ef1(i)=(eps1(i)*zzl(i,1)*zzl(i,1)+eps2(i)*zzm(i,1)*zzm(i,1)+
     1      . eps3(i)*zzn(i,1)*zzn(i,1)+eps4(i)*zzl(i,1)*zzm(i,1)+
     2        eps5(i)*zzm(i,1)*zzn(i,1)+eps6(i)*zzn(i,1)*zzl(i,1))*cl(i)
c
c    CANNOT FORM A CRACK IF ELEMENT IS COMPRESSED IN THIS DIRECTION
c

      if(ef1(i).lt.1.e-9) goto 500
c
c     FLAG FIRST CRACK
c
      ex1(i)=ef1(i)
      sf1(i)=ps1(i)
      icrak1(I)=1
      tc1(I)=tt
      DO 482 j=1,3
      zl(i,j)=zzl(i,j)
      zm(i,j)=zzm(i,j)
      zn(i,j)=zzn(i,j)
  482 continue
c
      goto 500
 1361 do 1362 j=1,3
      cphi(j)=zl(i,j)*zzl(I,1)+zm(i,j)*zzm(i,1)+zn(i,j)*zzn(i,1)
      acphi(j)=abs(cphi(j))
 1362 continue
      jmin=1
      do 1363 jb=2,3
      if(acphi(jb).gt.acphi(jmin))jmin=jb
 1363 continue
      if(jmin.eq.1) goto 500
      if(icrak2(i).gt.0) goto 1364
c
c     DETERMINE STRESSES IN ORIGINAL CRACK PLANE
c
      do 423 j=1,3
      ot(i,j)=sigc1(i)*zl(i,j)*zl(i,j)+sigc2(i)*zm(i,j)*zm(i,j)+
     1 sigc3(i)*zn(i,j)*zn(i,j)+
     2 2.*sigc4(i)*zl(i,j)*zm(i,j)+2.*sigc5(i)*zm(i,j)*zn(i,j)+
     3        2.*sigc6(i)*zl(i,j)*zn(i,j)
  423 continue
c
      ot(i,5)=sigc1(i)*zl(i,2)*zl(i,3)+sigc2(i)*zm(i,2)*zm(i,3)+
```

```
     1          sigc3(i)*zn(i,2)*zn(i,3)+
     2          (zl(i,2)*zm(i,3)+zl(i,3)*zm(i,2))*sigc4(i)+
     3          (zm(i,2)*zn(i,3)+zm(i,3)*zn(i,2))*sigc5(i)+
     4          (zl(i,3)*zn(i,2)+zl(i,2)*zn(i,3))*sigc6(i)
c
c      NOW FIND MAX AND MIN STRESS IN THIS PLANE
c
      if(abs(ot(i,5)).gt.1.) goto 1365
c
c     STRESSES ARE ALREADY PRINCIPAL
c
      if(ot(i,3).gt.ot(i,2)) goto 1366
      sf2(i)=ot(i,2)
      if(sf2(i).lt.(0.5*sigt(i)))goto 500
      goto 1367
1366  sf2(i)=ot(i,3)
      if(sf2(i).lt.(0.5*sigt(i)))goto 500
      zl2=zl(i,2)
      zl3=zl(i,3)
      zm2=zm(i,2)
      zm3=zm(i,3)
      zn2=zn(i,2)
      zn3=zn(i,3)
      zl(i,2)=zl3
      zl(i,3)=zl2
      zm(i,2)=zm3
      zm(i,3)=zm2
      zn(i,2)=zn3
      zn(i,3)=zn2
      goto 1367
1365 aa=sqrt(ot(i,5)**2+.25*(ot(i,2)-ot(i,3))*(ot(i,2)-ot(i,3)))
      bb=.5*(ot(i,2)+ot(i,3))
      sf2(i)=bb+aa
      if(sf2(i).lt.(sigt(i))/dtwo) goto 500
      smin=bb-aa
      para=(sf2(i)-ot(i,2))/ot(i,5)
      zzm(i,1)=sqrt(1./(1.+para*para))*sign(1.,ot(i,5))
      zzn(i,1)=zzm(i,1)*para
      para=(smin-ot(i,2))/ot(i,5)
      zzm(i,2)=sqrt(1./(1.+para*para))*sign(1.,ot(i,5))
      zzn(i,2)=zzm(i,2)*para
c
c     RELATE THESE DIRECTIONS TO GLOBAL COORDINATES
c
```

```
      zm1=zl(i,2)
      zn1=zl(i,3)
      zm2=zm(i,2)
      zn2=zm(i,3)
      zm3=zn(i,2)
      zn3=zn(i,3)
      zl(i,2)=zzm(i,1)*zm1+zzn(i,1)*zn1
      zl(i,3)=zzm(i,2)*zm1+zzn(i,2)*zn1
      zm(i,2)=zzm(i,1)*zm2+zzn(i,1)*zn2
      zm(i,3)=zzm(i,2)*zm2+zzn(i,2)*zn2
      zn(i,2)=zzm(i,1)*zm3+zzn(i,1)*zn3
      zn(i,3)=zzm(i,2)*zm3+zzn(i,2)*zn3
c
c    CALCULATE CRACK NORMAL EXTENSION
c
 1367 ef2(i)=(eps1(i)*zl(i,2)*zl(i,2)+eps2(i)*zm(i,2)*zm(i,2)+
     1        eps3(i)*zn(i,2)*zn(i,2)+eps4(i)*zl(i,2)*zm(i,2)+
     2        eps5(i)*zm(i,2)*zn(i,2)+eps6(i)*zn(i,2)*zl(i,2))*cl(i)
c
c    CANNOT FORM A CRACK IF ELEMENT IS COMPRESSED IN THIS DIRECTION
c
      if(ef2(i).lt.1.e-9) goto 500
      ex2(i)=ef2(i)
      icrak2(i)=1
      tc2(I)=tt
c
      goto 500
c
c    SECOND CRACK ALREADY EXISTS, SEE IF WE CAN FLAG A THIRD.
c
 1364 if(jmin.eq.2) goto 500
c
c  DIRECTION OF MAXIMUM STRESS IS OK
c  HOW ABOUT ITS MAGNITUDE?
c
      sf3(i)=sigc1(i)*zl(i,3)*zl(i,3)+sigc2(i)*zm(i,3)*zm(i,3)+
     1        sigc3(i)*zn(i,3)*zn(i,3)+2.*zl(i,3)*zm(i,3)*sigc4(i)
     2       +2.*zm(i,3)*zn(i,3)*sigc5(i)+2.*zl(i,3)*zn(i,3)*sigc6(i)
      if(sf3(i).lt.(.5*sigt(i))) goto 500
c
      ef3(i)=(eps1(i)*zl(i,3)*zl(i,3)+eps2(i)*zm(i,3)*zm(i,3)+
     1        eps3(i)*zn(i,3)*zn(i,3)+eps4(i)*zl(i,3)*zm(i,3)+
     2        eps5(i)*zm(i,3)*zn(i,3)+eps6(i)*zn(i,3)*zl(i,3))*cl(i)
c
```

```
c    CANNOT FORM A CRACK IF ELEMENT IS COMPRESSED IN THIS DIRECTION
c
      if(ef3(i).lt.1.e-9) goto 500
      ex3(i)=ef3(i)
      icrak3(i)=1
      tc3(i)=tt
      goto 500
      endif
c
       if(istat(i).eq.4) then
       if(beta(i).lt.1.5)sigt(i)=sigt(i)*(1+ps3(i)/sigc(i))
       if(beta(i).ge.1.5)sigt(i)=sigt(i)*(1+ps2(i)/sigc(i))*
      1                          (1+ps3(i)/sigc(i))
       goto 341
       endif
c
  500 continue
c
```

D.5 SEGMENT 5

```
c      REPRESENTATION OF REINFORCING BARS
c
       do 701 i=lft,llt
c
c    TREAT X-REINFORCEMENT
c
       if(pxr(i).gt.0.)then
       if(epx1(i).le.epf(i)) then
c
c     CALCULATE CURRENT YIELD STRESS
c
       ak=qh(i)*epx1(i)+qs(i)
       sigr1(i)=sigr1(i)+dt1*d1(i)*eyr(i)
c
c     PREVENT REBARS CARRYING COMPRESSIVE STRESS
c
        sigr1(i)=amax1(sigr1(i),0.0)
c
c     CORRECT FOR MATERIAL YIELD
c
       ax2=abs(sigr1(i))-ak
       if(aX2.gt.0.0)then
```

```
      scale=ak/abs(sigr1(i))
c
c     UPDATE PLASTIC STRAIN
c
      rg(i)=.3937007874*eyr(i)
      epx1(i)=epx1(i)+(1.-scale)*sigr1(i)*dthird/rg(i)
c
c     ADJUST STRESS TO CONFORM TO FLOW STRESS
c
      sigr1(i)=scale*sigr1(i)
c
c     TEST FOR REBAR FAILURE
c
      if(epx1(i).gt.epf(i)) then
      sigr1(i)=0.0
      epx1(i)=epf(i)+0.0001
      endif
      endif
      endif
      endif
  701 continue
c
      do 702 i=lft,llt
c
c     TREAT Y-REINFORCEMENT
c
      if(pyr(i).gt.0.0)then
      if(epx2(i).le.epf(i))then
      ak=qh(i)*epx2(i)+qs(i)
      sigr2(i)=sigr2(i)+dt1*d2(i)*eyr(i)
      sigr2(i)=amax1(sigr2(i),0.0)
      ay2=abs(sigr2(i))-ak
      if(ay2.gt.0.0)then
      scale=ak/abs(sigr2(i))
      rg(i)=.3937007874*eyr(i)
      epx2(i)=epx2(i)+(1.-scale)*sigr2(i)*dthird/rg(i)
      sigr2(i)=scale*sigr2(i)
      if(epx2(i).gt.epf(i))then
      epx2(i)=epf(i)+0.0001
      sigr2(i)=0.0
      endif
      endif
      endif
      endif
```

```
  702 continue
c
      do 703  i=lft,llt
c
c   TREAT Z-REINFORCEMENT
c
      if(pzr(i).gt.0.0)then
      if(epx3(i).le.epf(i))then
      ak=qh(i)*epx3(i)+qs(i)
      sigr3(i)=sigr3(i)+dt1*d3(i)*eyr(i)
      sigr3(i)=amax1(sigr3(i),0.0)
      az2=abs(sigr3(i))-ak
      if(az2.gt.0.0)then
      scale=ak/abs(sigr3(i))
      rg(i)=.3937007874*eyr(i)
      epx3(i)=epx3(i)+(1.-scale)*sigr3(i)*dthird/rg(i)
      sigr3(i)=scale*sigr3(i)
      if(epx3(i).gt.epf(i))then
      epx3(i)=epf(i)+0.0001
      sigr3(i)=0.0
      endif
      endif
      endif
      endif
  703 continue
c
```

D.6 SEGMENT 6

```
      do 800 i=lft,llt
c
c       CALCULATION OF TOTAL STRESSES AND LOAD CRACK
c       INDICATOR ARRAY
c
      sig1(i)=(1-pxr(i))*sigc1(i)+pxr(i)*sigr1(i)
      sig2(i)=(1-pyr(i))*sigc2(i)+pyr(i)*sigr2(i)
      sig3(i)=(1-pzr(i))*sigc3(i)+pzr(i)*sigr3(i)
      sig4(i)=sigc4(i)
      sig5(i)=sigc5(i)
      sig6(i)=sigc6(i)
c
      crak1(i)=float(icrak1(i))
      crak2(i)=float(icrak2(i))
```

```
      crak3(i)=float(icrak3(i))
  700 continue
c
      return
      end
c
      subroutine failf(s1,s2,s3,s4,s5,s6,
     1                 a,b,c,d,ai1,as2,as3,sita,afa,fff,k,i)
c
      dimension s1(128),s2(128),s3(128),s4(128),s5(128),s6(128),
     1  sta1(128),sta2(128),sta3(128),sta4(128),sta5(128),sta6(128),
     2  sita(128),ai1(128),aj2(128),aj3(128),as2(128),as3(128),
     3  argi(128),bbb(128),dpres(128),a(128),b(128),c(128),d(128),
     4  fff(128),ss1(128),ss2(128),ss3(128),ss4(128),ss5(128),ss6(128),
     5  afa(128,6),ffn(128)
      data done/1.e0/,dtwo/2.e0/,dthree/3.e0/,dsmall/1.0e-5/,
     1     d99/0.99999999999999E0/
      dthird=done/dthree
      dr23r3=dthree*sqrt(dthree)/dtwo
      dr23=dthree/dtwo
c
      sta1(i)=s1(i)
      sta2(i)=s2(i)
      sta3(i)=s3(i)
      sta4(i)=s4(i)
      sta5(i)=s5(i)
      sta6(i)=s6(i)
c
      if(k.ge.2) goto 1
c
      sta1(i)=s1(i)-afa(i,1)
      sta2(i)=s2(i)-afa(i,2)
      sta3(i)=s3(i)-afa(i,3)
      sta4(i)=s4(i)-afa(i,4)
      sta5(i)=s5(i)-afa(i,5)
      sta6(i)=s6(i)-afa(i,6)
    1 continue
      ai1(i)=sta1(i)+sta2(i)+sta3(i)
      ss1(I)=sta1(i)-ai1(i)*dthird
      ss2(I)=sta2(i)-ai1(i)*dthird
      ss3(I)=sta3(i)-ai1(i)*dthird
      ss4(I)=sta4(i)
      ss5(I)=sta5(i)
      ss6(I)=sta6(i)
```

```
c
c      DEVIATORIC STRESS INVARIANTS
c
       as2(i)=0.5*(ss1(i)**2+ss2(i)**2+ss3(i)**2)+ss4(i)**2+ss5(i)**2+
     1        ss6(i)**2
       as3(i)=ss1(i)*(ss2(i)*ss3(i)-ss5(i)*ss5(i))-
     1        ss4(i)*(ss4(i)*ss3(i)-ss5(i)*ss6(i))+
     2        ss6(i)*(ss4(i)*ss5(i)-ss2(i)*ss6(i))
       if(abs(as2(i)).ge.dsmall)then
       argi(i)=dr23r3*as3(i)/(as2(i)**dr23)
       if(abs(argi(i)).gt.1.e0)argi(i)=sign(1.e0,argi(i))
       sita(i)=dthird*acos(argi(i))
       else
       sita(i)=0.
       endif
c
c .............c'=2c/3**(.5),  d=b'=c/3+d
c
       dlamda=b(i)+c(i)*cos(sita(i))
       bbb(i)=dlamda*sqrt(as2(i)) + d(i)*ai1(i)
       fff(i)=(-bbb(i)+sqrt(bbb(i)*bbb(i)+4.*a(i)*as2(i)))/(2*a(i))
c
       return
       end
c
       subroutine plas(s1,s2,s3,s4,s5,s6,at,pr,xh,ay,by,cy,
     1              dy,yld,xm,ym,yms,cp,i)
       dimension s1(128),s2(128),s3(128),s4(128),s5(128),s6(128),
     2  pr(128),xh(128),cp(6,6),afa(128,6),yms(128),
     3  ay(128),by(128),cy(128),dy(128),di1(128),ds2(128),ds3(128),
     4  dsita(128),sta(128,6),yld(128),at(1),xm(128),
     5 sig(128),str(128),stss(128,3),strn(128,3),sss(128),ym(128)
c
       data done/1.e0/,dtwo/2.e0/,dthree/3.e0/,dsmall/1.0e-5/
       dthird=done/dthree
       dr23r3=dthree*sqrt(dthree)/dtwo
       dr23=dthree/dtwo
       dsr3=sqrt(dthree)
       call failf(s1,s2,s3,s4,s5,s6,
     1            ay,by,cy,dy,di1,ds2,ds3,dsita,afa,str,1,i)
c
       call har(str,at,ym,xh,i)
c
c    PLASTIC STRESSES
```

```
c
      sta(i,1)=s1(i)-di1(i)*dthird-afa(i,1)
      sta(i,2)=s2(i)-di1(i)*dthird-afa(i,2)
      sta(i,3)=s3(i)-di1(i)*dthird-afa(I,3)
      sta(i,4)=s4(i)-afa(i,4)
      sta(i,5)=s5(i)-afa(i,5)
      sta(i,6)=s6(i)-afa(i,6)
c
      x2=dy(i)/(done-dtwo*pr(i))
      x3=done+pr(I)
      x4=yms(i)*(done-pr(i))/((done+pr(i))*(done-dtwo*pr(i)))
      x5=yms(i)*pr(i)/((done+pr(i))*(done-dtwo*pr(i)))
      x6=done-dtwo*pr(i)
c
      if(abs(ds2(I)).lt.dsmall) ds2(i)=dsmall
      bb1=dy(i)
      if(abs(sin(dthree*dsita(i))).ge.0.001) goto 1000
      bb2=dtwo*ay(i)*sqrt(ds2(i))/yld(i)+by(i)+cy(i)/dsr3
      bb3=0.0
      go to 2000
 1000 b1=dtwo*ay(i)*sqrt(ds2(i))/yld(i)+ by(i)
      b2=dtwo/dsr3*cy(i)
      b3=cos(dsita(i))
      b4=-cos(dthree*dsita(i))
      b5=sin(dsita(i))/sin(dthree*dsita(i))
      bb2=b1+b2*(b3+b4*b5)
      bb3=cy(i)/ds2(i)*sin(dsita(i))/sin(dthree*dsita(i))
c
 2000 ph1=bb2*sta(i,1)/(dtwo*sqrt(ds2(i)))+bb3*
     1       (sta(i,2)*sta(i,3)-sta(i,4)**2+dthird*ds2(i))
c
      ph2=bb2*sta(i,2)/(dtwo*sqrt(ds2(i)))+bb3*
     1       (sta(i,1)*sta(i,3)-sta(i,5)**2+dthird*ds2(i))
c
      ph3=bb2*sta(i,3)/(dtwo*sqrt(ds2(i)))+bb3*
     1       (sta(i,1)*sta(i,2)-sta(i,6)**2+dthird*ds2(i))
c
      ph4=bb2*sta(i,4)/(dtwo*sqrt(ds2(i)))+bb3*
     1       (sta(i,5)*sta(i,6)-sta(i,3)*sta(i,4))
c
      ph5=bb2*sta(i,5)/(dtwo*sqrt(ds2(i)))+bb3*
     1       (sta(i,6)*sta(i,4)-sta(i,1)*sta(i,5))
c
      ph6=bb2*sta(i,6)/(dtwo*sqrt(ds2(i)))+bb3*
```

```
     1       (sta(i,4)*sta(i,5)-sta(i,2)*sta(i,6))
c
      bb4=ph1**2+ph2**2+ph3**2+dtwo*(ph4**2+ph5**2+ph6**2)
c
      w1=xh(i)*xm(i)*(ay(i)*ds2(i)/(yld(i)*yld(i))+done)
      w2=sqrt(dtwo*bb1*bb1 + dtwo*dthird*bb4)
      w3=yms(i)*(dthree*bb1*bb1/x6 + bb4/x3)
      w4=xh(i)/yld(i)*(1-xm(i))
      w5=(s1(i)-afa(i,1))*(bb1+ph1)+(s2(i)-afa(i,2))*(bb1+ ph2)+
     1    (s3(i)-afa(i,3))*(bb1+ph3)
      w6=(s4(i)-afa(i,4))*ph4+(s5(i)-afa(i,5))*ph5+
     1    (s6(i)-afa(i,6))*ph6
c
      w= w1*w2 + w3 + w4*(w5+w6)*w2
c
      x1=yms(i)*yms(i)/w
c
      cp(1,1)=x4-x1*(bb1/x6+ph1/x3)**2
      cp(2,2)=x4-x1*(bb1/x6+ph2/x3)**2
      cp(3,3)=x4-x1*(bb1/x6+ph3/x3)**2
c
      cp(4,4)=yms(i)/(dtwo*x3)-x1*(ph4/x3)**2
      cp(5,5)=yms(i)/(dtwo*x3)-x1*(ph5/x3)**2
      cp(6,6)=yms(i)/(dtwo*x3)-x1*(ph6/x3)**2
c
      cp(1,2)=x5-x1*(bb1/x6+ph1/x3)*(bb1/x6+ph2/x3)
      cp(2,1)=cp(1,2)
      cp(1,3)=x5-x1*(bb1/x6+ph1/x3)*(bb1/x6+ph3/x3)
      cp(3,1)=cp(1,3)
      cp(2,3)=x5-x1*(bb1/x6+ph2/x3)*(bb1/x6+ph3/x3)
      cp(3,2)=cp(2,3)
c
      cp(1,4)=-x1*(bb1/x6+ph1/x3)*ph4/x3
      cp(4,1)=cp(1,4)
      cp(2,4)=-x1*(bb1/x6+ph2/x3)*ph4/x3
      cp(4,2)=cp(2,4)
      cp(3,4)=-x1*(bb1/x6+ph3/x3)*ph4/x3
      cp(4,3)=cp(3,4)
      cp(1,5)=-x1*(bb1/x6+ph1/x3)*ph5/x3
      cp(5,1)=cp(1,5)
      cp(2,5)=-x1*(bb1/x6+ph2/x3)*ph5/x3
      cp(5,2)=cp(2,5)
      cp(3,5)=-x1*(bb1/x6+ph3/x3)*ph5/x3
      cp(5,3)=cp(3,5)
```

```
      cp(1,6)=-x1*(bb1/x6+ph1/x3)*ph6/x3
      cp(6,1)=cp(1,6)
      cp(2,6)=-x1*(bb1/x6+ph2/x3)*ph6/x3
      cp(6,2)=cp(2,6)
      cp(3,6)=-x1*(bb1/x6+ph3/x3)*ph6/x3
      cp(6,3)=cp(3,6)
c
      cp(4,5)=-x1*(ph4*ph5/x3**2)
      cp(5,4)=cp(4,5)
      cp(4,6)=-x1*(ph4*ph6/x3**2)
      cp(6,4)=cp(4,6)
      cp(5,6)=-x1*(ph5*ph6/x3**2)
      cp(6,5)=cp(5,6)
c
      return
      end
c
      subroutine har(str,at,ym,xh,i)
      common/aux33/ix1(128),ix2(128),ix3(128),ix4(128),ix5(128),
     1             ix6(128),ix7(128),ix8(128),mxt(128),nmel
      dimension str(128),xh(128),at(1),stss(1,10),strn(1,10),
     1 sig(128),ym(128)
      mx=48*(mxt(i)-1)
      d99=0.99
      np=at(mx+31)
      sig(i)=str(i)
      do 10 j=1,np
      stss(i,j)=abs(at(mx+20+j))
      strn(i,j)=abs(at(mx+10+j))
10    continue
      do 20 j=1,np
      stss(i,j)=STSS(i,j)/(1.+strn(i,j))
      strn(i,J)=strn(i,j)*(1.+0.5*strn(i,j))
20    continue
      if(sig(I).le.stss(i,1)) goto 30
      do 40 kk=2,np
      nk=kk
      if(sig(i).ge.stss(i,kk-1).and.sig(i).lt.stss(i,kk)) goto 50
40    continue
      if(sig(i).ge.stss(i,np)) goto 60
      write(6,100)
      stop
50    continue
      range=stss(i,nk)-stss(i,nk-1)
```

```
      ratio=(stss(i,nk)-sig(i))/range
      if(ratio.le.0.1) nk=nk+1
      if(nk.gt.np) goto 60
      sss=(stss(i,nk)-stss(i,nk-1))/(strn(i,nk)-strn(i,nk-1))
      xh(i)=at(mx+1)*sss/(at(mx+1)-sss)
      goto 70
   60 continue
      xh(i)=0.
      goto 70
   30 sss=(stss(i,2)-stss(i,1))/(strn(i,2)-strn(i,1))
      xh(i)=at(mx+1)*sss/(at(mx+1)-sss)
   70 continue
  100 format(1h0, 37herror - effective stress out of range )
c
      return
      end
c
      subroutine zfail(s1,s2,s3,s4,s5,s6,alpha,beta,istat,sigc,a,
     1                 b,c,d,ps1,ps2,ps3,zzl,zzm,zzn,i,inel)
c
      dimension s1(128),s2(128),s3(128),s4(128),s5(128),s6(128),
     1 ss1(128),ss2(128),ss3(128),ss4(128),ss5(128),ss6(128),
     2 sita(128),ai1(128),aj2(128),aj3(128),as2(128),as3(128),
     3 aff(128),istat(128),beta(128),sigc(128),argi(128),
     4 zzl(128,3),zzm(128,3),zzn(128,3),dpres(128),dzcos(128),
     5 search(3),dzl(3),dzm(3),dzn(3),dzal(3),dzam(3),dzan(3),
     6 dp(3),ps1(128),ps2(128),ps3(128),a(128),b(128),
     7 c(128),d(128)
      data done/1.e0/,dtwo/2.e0/,dthree/3.e0/,dsmall/1.0e-5/
      dthird=done/dthree
      dr23r3=dthree*sqrt(dthree)/dtwo
      dr23=dthree/dtwo
      d99=0.9999999999999999E0
      pi=atan(1.)*4.0
c
c ... CALCULATION OF THE INVARIANTS OF THE STRESS TENSOR
c
      ai1(i)=s1(i)+s2(i)+s3(i)
      dpres(i)=ai1(i)/3.e0
      ss1(i)=s1(i)-ai1(i)*dthird
      ss2(i)=s2(i)-ai1(i)*dthird
      ss3(i)=s3(i)-ai1(i)*dthird
      ss4(i)=s4(i)
      ss5(i)=s5(i)
```

```
      ss6(i)=s6(i)
c
      as2(i)=0.5*(ss1(i)**2+ss2(i)**2+ss3(i)**2)+ss4(i)**2+ss5(i)**2+
     1        ss6(i)**2
      as3(i)=ss1(i)*(ss2(i)*ss3(i)-ss5(i)*ss5(i))-
     1        ss4(i)*(ss4(i)*ss3(i)-ss5(i)*ss6(i))+
     2        ss6(i)*(ss4(i)*ss5(i)-ss2(i)*ss6(i))
      if(abs(as2(i)).ge.dsmall)then
      argi(i)=dr23r3*as3(i)/(as2(i)**dr23)
      if(abs(argi(i)).gt.1.e0)argi(i)=sign(1.e0,argi(i))
      sita(i)=dthird*acos(argi(i))
      else
      sita(i)=0.
      endif
      aff(i)=-ai1(i)/(2.*1.732050808*sqrt(as2(i))*cos(sita(i)))
c
      if(aff(i)-done) 10,10,20
   10 beta(i)=done
      istat(i)=3
      goto 50
   20 if(aff(i)-alpha) 30,40,40
   30 beta(i)=aff(i)
      istat(i)=4
      goto 50
   40 beta(i)=dtwo
      istat(i)=5
   50 continue
c
      call prcos(s1,s2,s3,s4,s5,s6,ps1,ps2,ps3,zzl,
     1 zzm,zzn,sigc,a,b,c,d,ai1,as2,as3,sita,istat,i,inel)
c
      return
      end
c
      subroutine prcos(s1,s2,s3,s4,s5,s6,ps1,ps2,ps3,zzl,
     1 zzm,zzn,sigc,a,b,c,d,ai1,as2,as3,sita,istat,i,inel)
c
      dimension s1(128),s2(128),s3(128),s4(128),s5(128),s6(128),
     1 sita(128),ai1(128),aj2(128),aj3(128),as2(128),as3(128),
     2 zzl(128,3),zzm(128,3),zzn(128,3),dpres(128),dzcos(128),
     3 search(3),dzl(3),dzm(3),dzn(3),dzal(3),dzam(3),dzan(3),
     4 dp(3),ps1(128),ps2(128),ps3(128),sigc(128),a(128),b(128),
     5 c(128),d(128),istat(128)
      data done/1.e0/,dtwo/2.e0/,dthree/3.e0/,dsmall/1.0e-5/,
```

```
1      d99/0.99999999999/,
2      pi/3.14159265358979323846264338e0/
 dthird=done/dthree
 dr23r3=dthree*sqrt(dthree)/dtwo
 dr23=dthree/dtwo

 ai1(i)=s1(i)+s2(i)+s3(i)
 dpres(i)=ai1(i)/3.e0
 aj2(i)=s1(i)*s2(i)+s2(i)*s3(i)+
1       s3(i)*s1(i)-s4(i)*s4(i)-
2       s5(i)*s5(i)-s6(i)*s6(i)
 aj3(i)=s1(i)*s2(i)*s3(i)+
1       2.*s4(i)*s5(i)*s6(i)-s1(i)*s5(i)*s5(i)-
2       s2(i)*s6(i)*s6(i)-s3(i)*s4(i)*s4(i)
 as2(i)=dpres(i)*ai1(i)-aj2(i)
 if(as2(i).lt.dsmall) then
 as2(i)=d99*dsmall
 if(ai1(i).ge.d99*sigc(i)/d(i)) istat(i)=3
 goto 472
 endif
c
 as3(i)=aj3(i)-dpres(i)*aj2(i)+2.e0*dpres(i)*dpres(i)*dpres(i)
 dzcos(i)=2.598076211*as3(i)/(as2(i)**1.5e0)
 if(abs(dzcos(i)).gt.1.e0)dzcos(i)=sign(1.e0,dzcos(i))
c
c     TRIAXIAL STRESS
c     CALCULATE PRINCIPAL STRESSES
c
 if((abs(s4(i)).gt.dsmall).or.(abs(s5(i)).gt.dsmall)
1 .or.(abs(s6(i)).gt.dsmall)) goto 430
c
 search(1)=s1(i)
 search(2)=s2(i)
 search(3)=s3(i)
 imax=1
 imin=1
 do 409 jb=2,3
 if(search(jb).lt.search(imin))imin=jb
 if(search(jb).gt.search(imax))imax=jb
409 continue
 zzal=1.
 zzam=1.
 zzan=1.
 goto(410,411,412),imax
```

```
410 dp(1)=s1(i)
    dzl(1)=1.*sign(zzal,s1(i))
    dzm(1)=0.
    dzn(1)=0.
    zzal=1.
    goto 413
411 dp(1)=s2(i)
    dzl(1)=0.
    dzm(1)=1.*sign(zzam,s2(i))
    dzn(1)=0.
    zzam=1.
    goto 413
412 dp(1)=s3(i)
    dzl(1)=0.
    dzm(1)=0.
    dzn(1)=1.*sign(zzan,s3(i))
    zzan=1.
413 goto(414,415,416),imin
414 dp(3)=s1(i)
    dzl(3)=1.*sign(zzal,s1(i))
    dzm(3)=0.
    dzn(3)=0.
    zzal=1.
    goto 417
415 dp(3)=s2(i)
    dzl(3)=0.
    dzm(3)=1.*sign(zzam,s2(i))
    dzn(3)=0.
    zzam=1.
    goto 417
416 dp(3)=s3(i)
    dzl(3)=0.
    dzm(3)=0.
    dzn(3)=1.*sign(zzan,s3(i))
    zzan=1.
417 goto(418,419,420),imax+imin-2
418 dp(2)=s3(i)
    dzl(2)=0.
    dzm(2)=0.
    dzn(2)=1.*sign(zzan,s3(i))
    goto 474
419 dp(2)=s2(i)
    dzl(2)=0.
    dzm(2)=1.*sign(zzam,s2(i))
```

```
      dzn(2)=0.
      goto 474
420   dp(2)=s1(i)
      dzl(2)=1.*sign(zzal,s1(i))
      dzm(2)=0.
      dzn(2)=0.
      goto 474
430   if((abs(s4(i)).gt.1.0e-9).or.(abs(s6(i)).gt.1.0e-9))
     1 go to 439
      radius=sqrt(s5(i)*s5(i)+0.25*(s2(i)-s3(i))
     1 *(s2(i)-s3(i)))
      centre=0.5*(s2(i)+s3(i))
      search(1)=centre+radius
      search(2)=centre-radius
      search(3)=s1(i)
      imax=1
      imin=1
      do 429 jb=2,3
      if(search(jb).lt.search(imin))imin=jb
      if(search(jb).gt.search(imax))imax=jb
429   continue
      dp(1)=search(imax)
      dp(3)=search(imin)
      zzal=1.
      zzam=1.
      zzan=1.
      goto(431,432,465),imax+imin-2
431   dp(2)=s1(i)
      dzl(2)=1.*sign(zzal,s1(i))
      dzm(2)=0.
      dzn(2)=0.
      zzal=1.
      goto 433
432   dp(2)=search(2)
      goto 466
465   dp(2)=search(1)
466   temp1=(dp(2)-s2(i))/s5(i)
      dzl(2)=0.
      dzm(2)=sqrt(1./(1.+temp1*temp1))*sign(zzam,s5(i))
      dzn(2)=dzm(2)*temp1
      zzam=1.
433   goto(434,434,435),imax
434   temp1=(dp(1)-s2(i))/s5(i)
      dzl(1)=0.
```

```
      dzm(1)=sqrt(1./(1.+temp1*temp1))*sign(zzam,s5(i))
      dzn(1)=dzm(1)*temp1
      zzam=1.
      goto 436
  435 dzl(1)=1.*sign(zzal,s1(i))
      dzm(1)=0.
      dzn(1)=0.
      zzal=1.
  436 goto(437,437,438),imin
  437 temp1=(dp(3)-s2(i))/s5(i)
      dzl(3)=0.
      dzm(3)=sqrt(1./(1.+temp1*temp1))*sign(zzam,s5(i))
      dzn(3)=dzm(1)*temp1
      goto 474
  438 dzl(3)=1.*sign(zzal,s1(i))
      dzm(3)=0.
      dzn(3)=0.
      goto 474
  439 if((abs(s4(i)).gt.1.0e-9).or.(abs(s5(i)).gt.1.0e-9))
     1 go to 449
      radius=sqrt(s6(i)*s6(i)+0.25*(s3(i)-s1(i))
     1 *(s3(i)-s1(i)))
      centre=0.5*(s3(i)+s1(i))
      search(1)=centre+radius
      search(2)=centre-radius
      search(3)=s2(i)
      imax=1
      imin=1
      do 440 jb=2,3
      if(search(jb).lt.search(imin))imin=jb
      if(search(jb).gt.search(imax))imax=jb
  440 continue
      dp(1)=search(imax)
      dp(3)=search(imin)
      zzal=1.
      zzam=1.
      zzan=1.
      goto(441,442,467),imax+imin-2
  441 dp(2)=s2(i)
      dzl(2)=0.
      dzm(2)=1.*sign(zzam,s2(i))
      dzn(2)=0.
      zzam=1.
      goto 443
```

```
442 dp(2)=search(2)
    goto 468
467 dp(2)=search(1)
468 temp1=(dp(2)-s3(i))/s6(i)
    dzn(2)=sqrt(1./(1.+temp1*temp1))*sign(zzan,s6(i))
    dzm(2)=0.
    dzl(2)=dzn(2)*temp1
    zzan=1.
443 goto(444,444,445),imax
444 temp1=(dp(1)-s3(i))/s6(i)
    dzn(1)=sqrt(1./(1.+temp1*temp1))*sign(zzan,s6(i))
    dzm(1)=0.
    dzl(1)=dzn(1)*temp1
    zzan=1.
    goto 446
445 dzl(1)=0.
    dzm(1)=1.*sign(zzam,s2(i))
    dzn(1)=0.
    zzam=1.
446 goto(447,447,448),imin
447 temp1=(dp(3)-s3(i))/s6(i)
    dzn(3)=sqrt(1./(1.+temp1*temp1))*sign(zzal,s6(i))
    dzm(3)=0.
    dzl(3)=dzn(3)*temp1
    goto 474
448 dzl(3)=0.
    dzm(3)=1.*sign(zzam,s2(i))
    dzn(3)=0.
    goto 474
449 if((abs(s5(i)).gt.1.0e-9).or.(abs(s6(i)).gt.1.0e-9))
   1 go to 470
    radius=sqrt(s4(i)*s4(i)+0.25*(s1(i)-s2(i))
   1 *(s1(i)-s2(i)))
    centre=0.5*(s1(i)+s2(i))
    search(1)=centre+radius
    search(2)=centre-radius
    search(3)=s3(i)
    imax=1
    imin=1
    do 450 jb=2,3
    if(search(jb).lt.search(imin))imin=jb
    if(search(jb).gt.search(imax))imax=jb
450 continue
    dp(1)=search(imax)
```

```
      dp(3)=search(imin)
      zzal=1.
      zzam=1.
      zzan=1.
      goto(451,452,469),imax+imin-2
  451 dp(2)=s3(i)
      dzl(2)=0.
      dzm(2)=0.
      dzn(2)=1.*sign(zzan,s3(i))
      goto 453
  452 dp(2)=search(2)
      goto 475
  469 dp(2)=search(1)
  475 temp1=(dp(2)-s1(i))/s4(i)
      dzl(2)=sqrt(1./(1.+temp1*temp1))*sign(zzal,s4(i))
      dzm(2)=dzl(2)*temp1
      dzn(2)=0.
      zzal=1.
  453 goto(454,454,455),imax
  454 temp1=(dp(1)-s1(i))/s4(i)
      dzl(1)=sqrt(1./(1.+temp1*temp1))*sign(zzal,s4(i))
      dzm(1)=dzl(1)*temp1
      dzn(1)=0.
      zzal=1.
      goto 456
  455 dzl(1)=0.
      dzm(1)=0.
      dzn(1)=1.*sign(zzan,s3(i))
      zzan=1.
  456 goto(457,457,458),imin
  457 temp1=(dp(3)-s1(i))/s4(i)
      dzl(3)=sqrt(1./(1.+temp1*temp1))*sign(zzal,s4(i))
      dzm(3)=dzl(3)*temp1
      dzn(3)=0.
      goto 474
  458 dzl(3)=0.
      dzm(3)=0.
      dzn(3)=1.*sign(zzan,s3(i))
      goto 474
c
  470 darge=1.
c
c    CALCULATE OCTAHEDRAL SHEAR STRESS
c
```

```
      dtau=sqrt(2.e0/3.e0*as2(i))
      if(abs(dtau).le.dsmall)go t0 472
      drtau=1.e0/dtau
      darg=-1.414213562*as3(i)*drtau*drtau*drtau
      if(darg.gt.1.e0)darg=1.e0
      if(darg.lt.-1.e0)darg=-1.e0
      darge=1.e0*sign(darge,darg)
      droot=acos(abs(darg))/3.
      dp(1)=-darge*1.414213562*dtau*cos(droot)+dpres(i)
      dp(2)=darge*1.414213562*dtau*cos(pi/dthree+droot)+dpres(i)
      dp(3)=darge*1.414213562*dtau*cos(pi/dthree-droot)+dpres(i)
c
c  ORDER RESULTS
c
      search(1)=dp(1)
      search(2)=dp(2)
      search(3)=dp(3)
      imax=1
      imin=1
      do 460 jb=2,3
      if(search(jb).lt.search(imin))imin=jb
      if(search(jb).gt.search(imax))imax=jb
  460 continue
      dp(1)=search(imax)
      dp(3)=search(imin)
      goto(461,462,463),imax+imin-2
  461 dp(2)=search(3)
      goto 464
  462 dp(2)=search(2)
      goto 464
  463 dp(2)=search(1)
c
c  EVALUATE DIRECTION COSINES OF PRINCIPAL PLANES
c
  464 dt23=s2(i)*s3(i)
      dt31=s3(i)*s1(i)
      dt12=s1(i)*s2(i)
      dt64=s6(i)*s4(i)
      dt45=s4(i)*s5(i)
      dt56=s5(i)*s6(i)
c
      do 471 j=1,3
      dzal(j)=dt23-dp(j)*(s2(i)+s3(i))+(dp(j)+s5(i))
     1*(dp(j)-s5(i))
```

```
      dzam(j)=dt31-dp(j)*(s3(i)+s1(i))+(dp(j)+s6(i))
     1*(dp(j)-s6(i))
      dzan(j)=dt12-dp(j)*(s1(i)+s2(i))+(dp(j)+s4(i))
     1*(dp(j)-s4(i))
      if(abs(dzan(j)).gt.abs(dzal(j))) then
         if(abs(dzan(j)).gt.abs(dzam(j))) then
c           N HAS THE LARGEST DENOMINATOR
c
            dzam(j)=s5(i)*(dp(j)-s1(i))+dt64
            dzal(j)=s6(i)*(dp(j)-s2(i))+dt45
            dtemp1=dzal(j)+dzam(j)+dzan(j)
            dtemp2=dzal(j)*dzam(j)+dzam(j)*dzan(j)+dzan(j)*dzal(j)
            dzn(j)=dzan(j)/sqrt(dtemp1*dtemp1-2.e0*dtemp2)
            dzm(j)=dzn(j)*dzam(j)/dzan(j)
            dzl(j)=dzn(j)*dzal(j)/dzan(j)
         else
c           M HAS THE LARGEST DENOMINATOR
c
            dzan(j)=s5(i)*(dp(j)-s1(i))+dt64
            dzal(j)=s4(i)*(dp(j)-s3(i))+dt56
            dtemp1=dzal(j)+dzam(j)+dzan(j)
            dtemp2=dzal(j)*dzam(j)+dzam(j)*dzan(j)+dzan(j)*dzal(j)
            dzm(j)=dzam(j)/sqrt(dtemp1*dtemp1-2.e0*dtemp2)
            dzn(j)=dzm(j)*dzan(j)/dzam(j)
            dzl(j)=dzm(j)*dzal(j)/dzam(j)
         endiF
      else
         if(abs(dzal(j)).gt.abs(dzam(j))) then
c           L HAS THE LARGEST DENOMINATOR
c
            dzam(j)=s4(i)*(dp(j)-s3(i))+dt56
            dzan(j)=s6(i)*(dp(j)-s2(i))+dt45
            dtemp1=dzal(j)+dzam(j)+dzan(j)
            dtemp2=dzal(j)*dzam(j)+dzam(j)*dzan(j)+dzan(j)*dzal(j)
            dzl(j)=dzal(j)/sqrt(dtemp1*dtemp1-2.e0*dtemp2)
            dzm(j)=dzl(j)*dzam(j)/dzal(j)
            dzn(j)=dzl(j)*dzan(j)/dzal(j)
         else
c           M HAS THE LARGEST DENOMINATOR
c
            dzan(j)=s5(i)*(dp(j)-s1(i))+dt64
            dzal(j)=s4(i)*(dp(j)-s3(i))+dt56
            dtemp1=dzal(j)+dzam(j)+dzan(j)
            dtemp2=dzal(j)*dzam(j)+dzam(j)*dzan(j)+dzan(j)*dzal(j)
```

```
            dzm(j)=dzam(j)/sqrt(dtemp1*dtemp1-2.e0*dtemp2)
            dzn(j)=dzm(j)*dzan(j)/dzam(j)
            dzl(j)=dzm(j)*dzal(j)/dzam(j)
         endif
      endif
471   continue
      goto 474
472   do 473 j=1,3
      dp(j)=dpres(i)
         dzl(j)=0.577350269
         dzm(j)=0.577350269
473   dzn(j)=0.577350269
474   continue
c
         if(ai1(i).ge.d99*sigc(i)/d(i))then
         istat(i)=3
c
c  APPROACHING THE VERTEX OF THE FAILURE SURFACE CORRESPONDING TO
c  HYDROSTATIC TENSION.
c
         dp(1)=d99*dthird*sigc(i)/d(i)
         dp(2)=dp(1)
         dp(3)=dp(1)
         dscale=sigc(i)/(d(i)*ai1(i))
         do 489 j=1,3
         dzl(j)=0.577350269
         dzm(j)=0.577350269
489   dzn(j)=0.577350269
         goto 401
         endif
         dtau=sqrt(2.e0/3.e0*as2(i))
         if(abs(dtau).le.dsmall)go t0 472
         drtau=1.e0/dtau
         darg=-1.414213562*as3(i)*drtau*drtau*drtau
         if(darg.gt.1.e0)darg=1.e0
         if(darg.lt.-1.e0)darg=-1.e0
         darge=1.e0*sign(darge,darg)
         dlamda=b(i)+c(i)*darg/3.
         dqa=done
         dqb=dlamda*sigc(i)/a(i)
         dqc=(b(i)*sigc(i)*ai1(i)-sigc(i)*sigc(i))/a(i)
         dqroot=dqb*dqb-dtwo*dtwo*dqa*dqc
         if(dqroot.lt.0.0e0) goto 491
         dqroot=sqrt(dqroot)
```

```
      dqr1=(-dqb+dqroot)/(dtwo*dqa)
      dszs2d=dqr1
      if(dszs2d.lt.0.0e0) goto 490
      goto 481
  481 dscale=dszs2d/sqrt(as2(i))
      dp(1)=d99*(dscale*(dp(1)-dpres(i))+dpres(i))
      dp(2)=d99*(dscale*(dp(2)-dpres(i))+dpres(i))
      dp(3)=d99*(dscale*(dp(3)-dpres(i))+dpres(i))
       istat(i)=3
       goto 401
  490 write(6,497)inel
  497 format(' femse12: negative radius in element',i6)
      goto 495
  491 write(6,499)
  499 format(5x,'subroutine femse12 - sqrt of negative number')
  495 call adios(2)
  401 continue
c
c  REFORM CORRECTED CONCRETE STRESSES IN GLOBAL COORDINATES
c
       s1(i)=dp(1)*dzl(1)*dzl(1)+dp(2)*dzl(2)*dzl(2)
     1 +dp(3)*dzl(3)*dzl(3)
       s2(i)=dp(1)*dzm(1)*dzm(1)+dp(2)*dzm(2)*dzm(2)
     1 +dp(3)*dzm(3)*dzm(3)
       s3(i)=dp(1)*dzn(1)*dzn(1)+dp(2)*dzn(2)*dzn(2)
     1 +dp(3)*dzn(3)*dzn(3)
       s4(i)=dp(1)*dzl(1)*dzm(1)+dp(2)*dzl(2)*dzm(2)
     1 +dp(3)*dzl(3)*dzm(3)
       s5(i)=dp(1)*dzm(1)*dzn(1)+dp(2)*dzm(2)*dzn(2)
     1 +dp(3)*dzm(3)*dzn(3)
       s6(i)=dp(1)*dzn(1)*dzl(1)+dp(2)*dzn(2)*dzl(2)
     1 +dp(3)*dzn(3)*dzl(3)
c
       ps1(i)=dp(1)
       ps2(i)=dp(2)
       ps3(i)=dp(3)
c
       do 402 j=1,3
       zzl(i,j)=dzl(j)
       zzm(i,j)=dzm(j)
       zzn(i,j)=dzn(j)
  402 continue
c
       return
```

```
      end
```

D.7 LISTING OF ROUTINE SETS61

```
      subroutine sets61(cm)
c
c  CONCRETE MODEL - SET MATERIAL PARAMETERS.
c
      common/bk22/prop(48)
      dimension cm(1)
c
      do 1 i=1,48
    1 cm(i)=0.
      do 2 i=1,10
    2 cm(i)=prop(i)
      i1=9
      an=0.0
      do 3 i=11,20
      i1=i1+2
      j1=i1+1
      j=i+10
      cm(i)=-abs(prop(i1))
      if(cm(i).ne.0)an=an+1.0
    3 cm(j)=abs(prop(j1))
      cm(31)=an+0.1
c
c   EVALUATE THE CONSTANT OF THE FAILURE CRITERION
c
      call chenconst(ay,by,cy,dy)
      cm(36)=ay
      cm(37)=by
      cm(38)=cy
      cm(39)=dy
c
c   CALCULATE BULK AND SHEAR MODULII
c
      cm(40)=cm(1)/2./(1.+cm(2))
      cm(41)=cm(1)/3/(1.-2.*cm(2))
c
      return
      end
c
      subroutine chenconst(ac,bc,cc,dc)
```

```
c
c  THIS ROUTINE CALCULATES THE CONSTANTS OF THE FAILURE CRITERION
c
      common/bk22/prop(48)
      parameter(in=20)
      real a(in,in),u(in,in),b(in),x(in),xnew(in),ai1(in),ai2(in),
     1 aj2(in)
      integer row(in)
      data tol,its,n/1.e-03,10000,4/
      fc=-prop(3)
      ft=prop(4)
      do 1 i=1,n
c
c       UNIAXIAL COMPRESSIVE STRESS CONDITION
c
      if(i.eq.1) then
      s1=0.
      s2=0.
      s3=fc
      goto 2
      endif
c
      if(i.eq.2) then
c
c       UNIAXIAL TENSILE STRESS CONDITION
c
      s1=ft
      s2=0.
      s3=0.
      goto 2
      endif
c
      if(i.eq.3) then
c
c       BIAXIAL STRESS CONDITION
c
      s1=0.
      s2=1.15*fc
      s3=1.15*fc
      goto 2
      endif
c
      if(i.eq.4) then
c
```

```
c       TRIAXIAL STRESS CONDITION
c
        s1=0.8*fc
        s2=0.8*fc
        s3=4.2*fc
        goto 2
        endif
      2 continue
c
        ai1(i)=s1+s2+s3
        ai2(i)=0.5*(s1*s1+s2*s2+s3*s3)
        aj2(i)=ai2(i)-ai1(i)*ai1(i)/6
        a(i,1)=aj2(i)/(fc*fc)
        a(i,2)=sqrt(aj2(i))/fc
        a(i,3)=s1/fc
        a(i,4)=ai1(i)/fc
        b(i)=1
    1 continue
        call lupfac(a,in,n,row)
        call lupsol(a,in,b,x,n,row)
        ac=abs(x(1))
        bc=abs(x(2))
        cc=abs(x(3))
        dc=abs(x(4))
c
        return
        end
c
        subroutine lupfac(a,ia,n,row)
        real a(ia,*)
        integer row(*)
        do 1 i=1,n
      1 row(i)=i
        do 2 i=1,n-1
        ip=i
        pval=a(row(ip),ip)
        do 3 j=i+1,n
        if(abs(a(row(j),i)).gt.abs(pval)) then
        ip=j
        pval=a(row(j),i)
        endif
    3 continue
        if(abs(pval).lt.1.e-10)then
        write(6,1000)
```

```
      stop
      endif
      ih=row(ip)
      row(ip)=row(i)
      row(i)=ih
      do 4 j=i+1,n
      ie=row(j)
      pivot=a(ie,i)/pval
      a(ie,i)=pivot
        irow=row(i)
        do 5 k=i+1,n
        a(ie,k)=a(ie,k)-a(irow,k)*pivot
    5 continue
    4 continue
    2 continue
        if(abs(a(row(n),n)).lt.1.e-10)then
        write(6,1000)
        stop
        endif
 1000 format('singular equations detected in the calculation of
     1 A,B,C and D')
c
        return
        end
c
        subroutine lupsol(a,ia,b,sol,n,row)
        real a(ia,*),b(*),sol(*)
        integer row(*)
        do 1 i=1,n
        irow=row(I)
        sum=b(irow)
        if(i.gt.1) then
        do 2 j=1,i-1
        sum=sum-a(irow,j)*b(row(J))
      2 continue
        b(irow)=sum
        endif
      1 continue
        do 3 i=n,1,-1
        irow=row(i)
        sum=b(irow)
        if(i.lt.n) then
        do 4 j=i+1,n
        sum=sum-a(irow,j)*b(row(j))
```

```
    4 continue
      endif
      b(irow)=sum/a(irow,i)
    3 continue
      do 5 i=1,n
    5 sol(i)=b(row(i))
c
      return
      end
```

Bibliography

[1] CEB. *Concrete Structures Under Impact and Impulsive Loading.* Number 187 in Bultin d'information. 1988.

[2] Bangash M.Y.H. *Impact and Explosion Analysis and Design.* Blackwell Scientific Publications, 1993.

[3] Ugural A.C. and Fenster S.K. *Advanced Strength and Applied Elasticity.* Elsevier, London, 1987.

[4] Hughes G. and Speirs D.M. An investigation of the beam impact problem. Technical Report 546, Cement and Concrete Association, April 1982.

[5] Hughes G. and Beeby A.W. Investigation of the effect of impact loading on concrete beams. *Journal of the Structural Engineer*, 60B(3), September 1982.

[6] Bischoff P.H. Perry S.H. and Eibl J. Contact force calculations with a simple spring-mass model for hard impact: a case study using polystyrene aggregate concrete. *International Journal of Impact Engineering*, 1990.

[7] Hallquist J.O. *User's Manuals for DYNA3D.* University of California, Livermore National Laboratory, 1981.

[8] Hsu T.T.C. and Slate F.O. Tensile bond strength between aggregate and cement paste of mortar. *Journal of the American Concrete Institute*, 60(4), 1963.

[9] Shah S. and Chandra S. Critical stress, volume change, and microcracking of concrete. *Journal of the American Concrete Institute*, 65(9), September 1969.

[10] Peterson P.E. Crack growth and development of fracture zone in plain concrete and similar materials. *Report No. TVBM-1106, Division of Building Materials*, 1981. University of Lund, Lund, Sweden.

[11] Raiss M.E. and Dougill J.W. Development of fracture process zones in concrete. *Magazine of Concrete Research*, 42(153), 1990.

[12] Gerstle K.H. Linse D.L Bertacchi P. Kotsovos M.D. Strength of concrete under multiaxial stress states. *American Concrete Institute Special Publication S.P. 55-5*, 1976.

[13] Neville A.M. *Properties of Concrete.* Pitman, London, 1981.

[14] Sinha B.P. Gerstle K.H. and Tulin L.G. Stress-strain relations for concrete under cyclic loading. *Journal of the American Concrete Institute*, 61(2), February 1964.

[15] Hsu T.T.C. Slate F.O. Sturman G.M. and Winter G. Microcracking of plain concrete and the shape of the stress/strain curve. *Journal of the American Concrete Institute*, 60(2), 1963.

[16] ACI 318-77. Building code requirements for reinforced concrete. Technical report, American Concrete Institute Committee 318, Detroit, 1977.

[17] Hughes B.P. and Chapman G.P. The deformation of concrete and micro-concrete in compression and tension with particular reference to aggregate size. *Magazine of Concrete Research*, 18(64), 1966.

[18] Johnson R.D. *Structural Concrete.* McGraw Hill, London, 1969.

[19] Kupfer H.B. Hildorf H.K. and Rusch H. Behaviour of concrete under biaxial stresses. *Journal of the American Concrete Institute*, 66(8), August 1969.

[20] Tasuji M.E. Slate F.O. and Nilson A.H. Stress-strain response and gracture of concrete in biaxial loading. *Journal of the American Concrete Institute*, 75(7), July 1978.

[21] Rosenthal I. and Glucklich J. Strength of plain concrete under biaxial stresses. *Journal of the American Concrete Institute*, 67(11), November 1970.

[22] Nelissen L.J.M. Biaxial testing of normal concrete. *Heron*, 18(1), 1972.

[23] Krishnaswamy K.T. Strength and microcracking of plain concrete under triaxial compression. *Journal of the American Concrete Institute*, 65(10), October 1968.

[24] Mills L.L. and Zimmerman R.M. Compressive strength of plain concrete under multiaxial loading conditions. *Journal of the American Concrete Institute*, 69(10), October 1970.

[25] Launay P. and Gachon H. Strain and ultimate strength of concrete under triaxial stresses. *Special Publication SP-34, American Concrete Institute 1*, 1972.

[26] Van Mier J.G.M. and Vonk R.A. Fracture of concrete under multiaxial stress: Recent developements. *Materials and Structures*, 24, 1991.

[27] Chen W.F. *Plasticity in Reinforced Concrete.* McGraw-Hill, New York, 1982.

[28] Newman K. and Vile G.W.D. Strength of concrete under combined states of stress. *Civil Engineering Research Association*, (First Interim Research report RR8), 1967.

[29] Taylor S.J. Anchorage bearing stresses. *Proceedings of the Institution of Civil Engineers*, (21), 1967.

[30] Kotsovos M.D. Consideration of triaxial stress conditions in design: A necessity. *Journal of the American Concrete Institute*, June 1987.

[31] Atchely B.L. and Furr H.L. Strength and energy absorption capabilities of plain concrete under dynamic and static loadings. *Journal of the American Concrete Institute*, pages 745–756, 1967.

[32] Mainstone R.J. Properties of materials at high rate of straining or loading. *Matériaux et Constructions*, 8(44), 1975.

[33] Banthia N. and Pigeon M. *Dynamic Behaviour of Concrete and its Fibre Reinforced Composites: A review and Future Research Needs.* Elsevier CMP, Oxford, 1989.

[34] Bischoff P.H. and Perry S.H. Compressive strain rate effects of concrete. *Material Research Society Fall Symposium*, 1985.

[35] Bischoff P.H. and Perry S.H. Compressive behaviour of concrete at high strain rates. *Materials and Structures*, 24, 1991.

[36] Green H. Impact strength of concrete. *Proceedings of the Institution of Civil Engineers*, 28:383–396, 1964.

[37] Goldsmith W. Kenner V.H. and Ricketts T.E. Dynamic loading of several concrete like mixtures. *Journal of the Structural Division, Proceedings of ASCE*, (ST7), July 1968.

[38] Hughes B.P. and Gregory R. Concrete subjected to high rates of loading in compression. *Magazine of Concrete Research*, 24(78):25–36, 1972.

[39] Hughes B.P. and Bahramian B. Cube tests and uniaxial compressive strength of concrete. *Magazine of Concrete Research*, 17(53), 1965.

[40] Sparcks P.R. and Menzies J.B. The effect of rate of loading upon the static and fatigue strength of plain concrete in compression. *Magazine of Concrete Research*, 25(83), 1973.

[41] Hughes P.B. and Watson A.J. Compression strength and ultimate strain of concrete under impact loading. *Magazine of Concrete Research*, 30(105):189–199, 1978.

[42] Curbach M. and Eibl J. *Nonlinear Behaviour of Concrete Under High Compressive Loading Rates*, pages 20–22. Int. Conf. on Recent Developments in Fracture of Concrete and Rock. Elsevier Applied Science Press, University of Wales, College of Cardiff, UK, September 1989.

[43] Ahmed S. and Shah S.P. Behaviour of hoop confined concrete under high strain rates. *Journal of the American Concrete Institute*, October 1985.

[44] Sauris W. and Shah S.P. Properties of concrete subjected to impact. *Journal of Structural Engineering, ASCE*, 109(7), July 1983.

[45] Perry S.R. and Bischoff P.H. Measurement of the compressive impact strength of concrete using a thin loadcell. *Magazine of Concrete Research*, 42(151), 1990.

[46] Zielinski A.J. and Reinhardt H.W. Stress-strain behaviour of concrete and mortar at high rates of tensile loadings. *Cement and Concrete Research*, 12, 1982.

[47] Mlakar P.F. Vitaya-Udom K.P. and Cole R.A. Dynamic tensile-compression behaviour of concrete. *Journal of American Concrete Institute*, 1985.

[48] Zielinski A.J. *Concrete Under Biaxial Compressive Impact Tensile Loadings.* Fracture toughness and fracture energy of concrete (ed. F. H. Wittmann). The Netherlands, 1986.

[49] Takeda J. and Tachikawa H. Deformations and fracture of concrete subjected to dynamic load. In *Proc. of Int. Conf. on Mech. Behaviour of materials, IV, Concrete and Cement Paste, Glass and Ceramics*, Kyoto, Japan, August 1971.

[50] Takeda J. Tachikawa H. and Fujimoto L. *Mechanical properties of concrete and steel in reinforced concrete structures subjected to impact or impulsive loads.* Proc. of RILEM-CEB-IABSE-IASS-Interassociation Symposium. BAM, Berlin (West), June 1982.

[51] John R. Shah S.P. and Jenq Y. A fracture mechanics model to predict the rate sensitivity of mode i fracture of concrete. *Cement and Concrete Research*, 17(2), 1987.

[52] DiTommaso A. *Evaluation of concrete fracture.* Fracture mechanics of concrete: Material characterization and testing. Martinus Nijhoff, 1984.

[53] Chen W.F. and Han D.J. *Plasticity for structural engineers.* Springer-Verlag, London, 1988.

[54] Bazant Z. *Advanced topics in inelasticity and failure of concrete.* CBI Swedish Cement and Concrete Research Institute, Goteborg Sweden, 1977.

[55] Chen W.F. and Saleeb A.F. *Constitutive equations for engineering materials.* Wiley-Interscience, New York, 1982. Volume 1: Elasticity and Modelling.

[56] Chen W.F. and Ting E.C. Constitutive models for concrete structures. *Journal of the Engineering Mechanics Division, ASCE*, 106(EM1), 1980.

[57] ASCE Committee on Concrete and Masonry Structures. *A State of the Art report on Finite Element Analysis of Reinforced Concrete.* Task Committee on Finite Element Analysis of Reinforced Concrete structures, ASCE, Spec. publ., New York, 1981.

[58] Bazant Z.P., editor. *Constitutive relations for concrete and rock: Applications and extension of elasticity and plasticity theory*, volume 1 of *Mechanics of geomaterials rocks, concretes, soils.* A Wiley-Interscience Publication, 1984.

[59] Edwards A.D. *Advanced topic in mechanics of materials.* MSc in Structural Engineering, Heriot-Watt University, Edinburgh U.K, 1986.

[60] Nilson A.H. Nonlinear analysis of reinforced concrete by the finite element method. *Journal of the American Concrete Institute*, 65(55), September 1968.

[61] Saenz L.P. Discussion of equation of the stress-strain curve of concrete by desay and krishnan. *Journal of the American Concrete Institute*, 61, September 1964.

[62] Kupfer H.B. and Gerstle K.H. Behaviour of concrete under biaxial stresses. *Journal of the Engineering Mechanics Division, ASCE*, 99(EM4), August 1973.

[63] Cedolin L. Crutzen Y.R.J. and Dei Foli S. Triaxial stress-strain relationships for concrete. *Journal of Engineering Mechanics Division, ASCE*, 103(EM3, Proc. paper 12969), 1977.

[64] Bergan P.G. and Holland I. Nonlinear finite element analysis of concrete structures. *J. Comput. Meths. Appl. Mechs. Eng.*, 17 and 18, 1979.

[65] Lui T.C.Y. Nilson A.H. and Slate F.O. Biaxial stress-strain relations for concrete. *Journal of the Structural Division, ASCE*, 98(ST5, Proc. paper 8905), May 1972.

[66] Tasuji M.E. A.H. Nilson and Slate F.O. Biaxial stress-strain relationships for concrete. *Magazine of Concrete Research*, 31(109), December 1979.

[67] Darwin D. and Pecknold D.A. Nonlinear biaxial stress-strain laws for concrete. *Journal of the Engineering Mechanics Division, ASCE*, 103(EM2, Proc.. paper 12839), April 1977.

[68] Palaniswamy R. and Shah S.P. Fracture and stress-strain relationship of concrete under triaxial compression. *Journal of the Structural Division, ASCE*, 100(ST5 Proc.. paper 10547), May 1974.

[69] Phillips D.V. and Zienkiewicz O.C. Finite element nonlinear analysis of concrete structures. *Proceedings of Institution of Civil Engineers*, 61, March 1976. Part 2.

[70] Kotsovos M.D. and Newman J.B. Generalised stress-strain relation for concrete. *Journal of the Engineering Mechanics Division, ASCE*, 104(EM4), August 1978.

[71] Ottosen N.S. Constitutive model for short time loading of concrete. *Journal of the Engineering Mechanics Division, ASCE*, 105(EM1), February 1979.

[72] Gerstle H. Simple formulation of triaxial concrete behaviour. *Journal of the American Concrete Institute*, September 1981.

[73] Gerstle K.H. Linse D.L Bertacchi P. Kotsovos M.D. Behaviour of concrete under multiaxial stress state. *Journal of the Engineering Mechanics Division, ASCE*, 106(EM6), December 1980.

[74] Ottosen N.S. A failure criterion for concrete. *Journal of the Engineering Mechanics Division, ASCE*, 103(EM4), 1977.

[75] Berriaud C. Verpeaux P. and Jamet P. *Concrete Wall Perforation by Rigid Missile.* RILEM Symposium Concrete Structure Under Impact and Impulsive Loading. Berlin, June 1982.

[76] Gupta Y.M. and Seaman L. Local response of reinforced concrete to missile impacts. *Nuclear Engineering and Design*, 48, 1978.

[77] Gupta Y.M. and Seaman L. Local response of reinforced concrete to missile impacts. Technical report, Final Report EPRI NP-1217 Project 393-1 Palo Alto, 1979.

[78] Broadhouse B.J. and Neilson A.J. Modelling reinforced concrete structure in dyna3d. *UKAEA, Memorandum AEEW-M 2465*, October 1987.

[79] Fleischer C.C. Mistry N.S. and Weilch A.K. *Concrete Damage Assessment Under Blast Loading.* Elsevier CMP, Oxford, 1989.

[80] Valanis K.C. A theory of visco-plasticity without yield surface, part i, general theory. *Archives of Mechanics*, 23(4), 1971.

[81] Valanis K.C. A theory of visco-plasticity without yield surface, part ii, application to mechanical behaviour of metals. *Archives of Mechanics*, 23(4), 1971.

[82] Bazant Z.P. and Bhat P.D. Endochronic theory of inelastic and failure of concrete. *Journal of the Engineering Mechanics Division, ASCE*, 102(EM4), 1976. Proc. Paper 12360.

[83] Bazant Z.P. and Shieh H. Endochronic model for non-linear triaxial behaviour of concrete. *Nuclear Engineering and Design*, 47, 1978.

[84] Bangash M.Y.H. *Concrete and Concrete Structures: Numerical Modelling and Applications.* Elsevier Applied Science, 1989.

[85] Kotsovos M.D. Effect of testing techniques on the post-ultimate behaviour of concrete in compression. *Materials and Structures*, 15, 1983.

[86] Gonzalez Visdoza F. Kotsosvos M.D. and Pavlovic M.N. Three-dimensional non-linear finite-element model for structural concrete. part 1: main features and objectivity study. *Proceedings of the Institution of Civil Engineers*, 91:517–544, 1991.

[87] Van Mier J.G.M. *Complete Stress-Strain Behaviour and Damaging Status of Concrete Under Multiaxial Conditions*, volume 1 of *RILEM-CEB-CNRS, International Conference on Concrete Under Multiaxial Conditions.* Presses de l'Université Paul Sabatier, Toulous, France, 1984.

[88] Bresler B. and Pister K.S. Strength of concrete under combined stresses. *Journal of the American Concrete Institute*, 55, 1958.

[89] Chen A.C.T. and Chen W.F. Constitutive relations for concrete. *Journal of the Engineering Mechanics Division, ASCE*, 101(EM4), August 1975. Proc. paper 11529.

[90] Argyris J.H. Faust G. Szimmat J. Recent developments in the finite element analysis of prestressed reactor vessels. *Nuclear Engineering and Design*, 28, 1974.

[91] Hsieh S.S. Ting E.C. and Chen W. F. A plasticity fracture model for concrete. *International Journal of Solids and Structures*, 3, 1982.

[92] Willam K.J. and Warnke E.P. *Constitutive model for triaxial behaviour of concrete.* Number Paper III-1, IABSE Proc. 19 in International Association of Bridge and Structural Engineers. Seminar on Concrete Structures Subjected to Triaxial Stresses. Bergomo, Italy, May 1974.

[93] Axelsson K. and Samuelsson A. Finite element analysis of elastic-plastic material displaying mixed hardening. *International Journal for Numerical Methods in Engineering*, 14, 1979.

[94] Prager W. A new method of analysing stress and strain in work hardening solids. *Journal of Applied Mechanics, ASME*, 23, 1956.

[95] Ziegler H. A modification of prager's hardening rule. *Quarterly of Applied Mathematics*, 17, 1959.

[96] Owen R. and Figueiras J.A. *Ultimate load analysis of reinforced concrete plate and shell including geometric non-linear effect.* Finite Element Software for Plates and Shells. Pineridge Press, Swansea, U.K., 1984.

[97] Cervera M. and Hinton E. *Non-linear analysis of reinforced concrete plates and shells using three dimensional model.* Computational Modelling of Reinforced Concrete Structures. Pineridge Press, Swansea, U.K., June 1986.

[98] Chen E.Y.T. and Schnobrich W.C. Material modelling of plain concrete, advanced mechanics of reinforced concrete. 1981. IABSE Colloquium.

[99] Fardis M.N. Alibe B. and Tassoulas J. Monotonic and cyclic constitutive law for concrete. *Journal of the Engineering Mechanics Division, ASCE,* 109(EM2), 1983.

[100] Vermeer P.A. and De Brost R. Non-associated plasticity for soils, concrete and rocks. *Heron*, 29(3), 1984.

[101] Glemberg R. Oldenburg M. *A general constitutive model for concrete structures.* Computational Modelling of Reinforced Concrete Structures. Pineridge Press, Swansea, U.K., June 1986.

[102] Chen E.S. and Buyukosturk O. Constitutive model for concrete in cyclic compression. *Journal of the Engineering Mechanics Division, ASCE,* 111(EM6), 1985.

[103] Dougill J.W. and Rida M.A.M. Further consideration of progressively fracture solids. *Journal of the Engineering Mechanics Division, ASCE*, 106(EM5), October 1980.

[104] Dougill J.W. *Constitutive relations for concrete and rock: Applications and extension of elasticity and plasticity theory*, volume 1 of *Mechanics of geomaterials rocks, concretes, soils*. A Wiley-Interscience Publication, 1984.

[105] Bazant Z.P. and Kim S.S. Plastic-fracturing theory for concrete. *Journal of Engineering Mechanics Division ASCE*, 105(EM3), 1979.

[106] Labib F. *Nonlinear Analysis of the Bond and Crack Distribution in Reinforced Concrete Members*. PhD thesis, University of London, 1976.

[107] Taha M. *Reinforced Concrete Deep Beams with Web Openings*. PhD thesis, University of London, June 1976.

[108] Suziki W. and Chen W.F. Elastic-plastic fracture analysis of concrete structures. *Computers Structures*, 16, 1983.

[109] Bazant Z.P. and Cedolin L. Fracture mechanics of reinforced concrete. *Journal of the Engineering Mechanics Division, ASCE*, 106(EM6), 1980.

[110] ACI 226R-80:. Fracture mechanics of concrete: Concepts, models and determination of material properties. Technical report, American Concrete Institute Committee 446, December 1989.

[111] Bazant Z.P. and Cedolin L. Closure on discussion of reference [109]. *Journal of Engineering Mechanics Division ASCE*, 108(EM2), 1982.

[112] Lin C.S. and Scordelis A.C. Nonlinear analysis of reinforced concrete shell of general form. *Journal of the Structural Division, ASCE*, 101(ST3), 1975.

[113] Gilbert R.I. and Warner R.F. Tension stiffening in reinforced concrete slab. *Journal of the Structural Division, ASCE*, 104(ST3), 1978.

[114] Bathe K.J. and Sundberg J.A. *A concrete material model.* Computational Modelling of Reinforced Concrete Structures. Pineridge Press, Swansea, U.K., June 1986.

[115] Cope R.J. *Non-linear analysis of reinforced concrete slabs.* Computational Modelling of Reinforced Concrete Structures. Pineridge Press, Swansea, U.K., June 1986.

[116] Broadhouse B.J. *Drastic - A Computer Code for Dynamic Analysis of Stress Transients in Reinforced Concrete.* Winfrith UKAEA, 1986.

[117] Suidan M. and Schnobrich W.C. Finite element analysis of reinforced concrete. *Journal of the Structural Division, ASCE*, (ST10), October 1973.

[118] Millard S.G. and Johnson R.P. Shear transfer in cracked reinforced concrete. *Magazine of Concrete Research*, 36(130), 1985.

[119] Baker G. *A Numerical Parametric Study of Nonlinear Behaviour in Variable Depth Beams.* PhD thesis, Heriot-Watt University, 1987.

[120] Kotsovos M.D. Pavlovic M.N. and Arnaout S. *Nonlinear finite element analysis of concrete structures: a model based on fundamental material properties*, volume 2 of *Numerical Methods in Engineering: Theory and Application (NUMETA 85)*. Middleton and Pande, 1985.

[121] Ngo D. and Scordelis A.C. Finite element analysis of reinforced concrete beam. *Journal of the American Concrete Institute*, 64(3), March 1967.

[122] Zienkiewicz O.C. *Finite Element Method.* McGraw-Hill, London, third edition, 1977.

[123] Ingraffea A.R. Gerstle K.H. Gergley P. and Saouma V. Fracture mechanics of bond in reinforced concrete. *Journal of Structural Division ASCE*, 110(4), 1984.

[124] Gupta A.K. and Akbar H. A finite element for the analysis of reinforced concrete. *International Journal of Numerical Methods in Engineering*, 19, 1983.

[125] Baker G. and Edwards A.D. *Some parameters for monitoring the conditions of nonlinear solution process*, volume 1 of *Proc. Int. Conf. Accuracy estimates and adaptive refinement in finite element computations (ARFEC).* 1984.

[126] Crisfield M.A. *Some recent research on numerical techniques for structural analysis*, volume 2 of *Numerical Methods in Engineering: Theory and Application (NUMETA 85)*. Middleton and Pande, 1985.

[127] May I.M. and Al-Ramadhani N.S. *The effect of integration rules on the stability of cracked 8-nodded isoparametric elements*, volume 1 of *Numerical Methods in Engineering: Theory and Application (NUMETA 90)*. Middleton and Pande, 1990.

[128] Rots J.G. and De Bros R. Analysis of mixed-mode fracture in concrete. *Journal of the Engineering Mechanics Division, ASCE*, 1987.

[129] De Borst R. Stability and uniqueness in numerical modelling. *IABSE Colloquium*, 1987.

[130] McHenry D. A lattic analogy for the solution of plane stress problems. *Proceedings of the Institution of Civil Engineers*, (21), 1943.

[131] Hrenikoff A. Solution of problems of elasticity by framework method. *Journal of Applied Mechanics, ASME*, 8, 1943.

[132] Argyris J.H. and Kelsey S. Structural analysis by the matrix force method with applications to aircraft wings. *Wiss. Ges. Luftfahrt Jahrb.*, 1956.

[133] Turner M.J. Clough R.W. Martin H.C. and Topp L.J. Stiffness and deflection analysis of complex structures. *Journal of Aeronautical Society*, 23(9), 1956.

[134] Clough R.W. The finite element method in plane stress analysis. *Journal of the Structural Division, ASCE Proc. 2nd Conference on Electronic Computation*, 1960.

[135] Bathe K.J. *Finite Element Procedures In Engineering Analysis.* Prentice-Hall, New Jersey, 1982.

[136] Cook R.D. *Concepts and Application of Finite Element.* Wiley and Sons Inc., New York, 1974.

[137] Hinton E. and Owen R. *An introduction to the finite element computations.* Pineridge Press Limited, Swansea, 1979.

[138] Fjeld S.A. *Three dimensional theory of elasticity.* Finite element method in stress analysis, Editors Holand I. and Bell K. Tapir Trondheim, 1969.

[139] Clough R.W. Comparison of three-dimensional finite elements. *Proc. Symp. on Appl. of finite element method in Civil Engineering, ASCE*, 1969.

[140] Goudreau G.L. and Hallquist J.O. Recent developments in large scale finite element hydrocode technology. *J. Comput. Meths. Appl. Mechs. Eng.*, 30, 1982.

[141] Thabet A. *An analysis of prestressed concrete dams using infinite elements.* M.Sc thesis, Heriot-Watt University, Edinburgh, August 1987.

[142] Hansen R.J. and Liepins A.A. Behaviour of bond under dynamic loading. *Journal of the American Concrete Institute*, 59(4), 1962.

[143] Vos E. and Reinhardt H.W. *Bond stress-slip behaviour of deformed bars.* Plain bars and strands under impact loadings: Bond in concrete, ed. Bartos P. London, 1982.

[144] Hallquist J.O. Goudreau G.L. and Benson D.J. Sliding interface with contact-impact in large-scale lagrangian computations. *J. Comput. Meths. Appl. Mechs. Eng.*, 51, 1985.

[145] Rots J.G. and Nauta P. Smeared crack approach and fracture localization in concrete. *Heron*, 30(1), 1985.

[146] Hallquist J.O. *User's Manuals for TAURUS: An Interactive Post-Processor for the analysis code DYNA3D.* University of California, Livermore National Laboratory, 1981.

[147] Balfour A. and Marwick D.H. *Programming in standard FORTRAN 77.* Heinemann Educational Book, London, 1987.

[148] Hallquist J.O. and Stillman D.W. *User's Manuals for INGRID: A three-dimensional mesh generator for modeling non-linear systems.* University of California, Livermore National Laboratory, 1985.

[149] Sheridan A.J and Cowdery C.A. *An Analysis of Shear/Flexure Coupling Applied to the Failure of Reinforced Concrete Structures*, pages 189–197. Structures Under Shock and Impact II. CMP Thomas Telford, University of Wales, College of Cardiff, UK, June 1992.

[150] Watson A.J. and Ang T.H. *Reinforced Micro-concrete Beams under Impact Loading.* RILEM, Concrete Structures under Impact and Impulsive Loading. Berlin, June 1982.

[151] Eibl J. Block K. and Kreuser K. Vergleichende versuche an stoβbelasteten balken und platten mit bewehrung aus betonstahl 1100 bzw. herkömmlichen betonstählen. Technical report, Universität Karlsruhe, Oktober 1983.

[152] Drücker D.C and Prager W. Soil mechanics and plasticity analysis of limit design. *Quarterly of Applied Mathematics*, 10(2), 1952.